Boris M. Smirnov
R. Stephen Berry

SPRINGER SERIES IN ATOMIC, OPTICAL AND PLASMA PHYSICS 42

Phase Transitions of Simple Systems

Springer

Springer Series on
ATOMIC, OPTICAL, AND PLASMA PHYSICS 42

Springer Series on

ATOMIC, OPTICAL, AND PLASMA PHYSICS

The Springer Series on Atomic, Optical, and Plasma Physics covers in a comprehensive manner theory and experiment in the entire field of atoms and molecules and their interaction with electromagnetic radiation. Books in the series provide a rich source of new ideas and techniques with wide applications in fields such as chemistry, materials science, astrophysics, surface science, plasma technology, advanced optics, aeronomy, and engineering. Laser physics is a particular connecting theme that has provided much of the continuing impetus for new developments in the field. The purpose of the series is to cover the gap between standard undergraduate textbooks and the research literature with emphasis on the fundamental ideas, methods, techniques, and results in the field.

36 **Atom Tunneling Phenomena in Physics, Chemistry and Biology**
Editor: T. Miyazaki

37 **Charged Particle Traps**
Physics and Techniques of Charged Particle Field Confinement
By V.N. Gheorghe, F.G. Major, G. Werth

38 **Plasma Physics and Controlled Nuclear Fusion**
By K. Miyamoto

39 **Plasma-Material Interaction in Controlled Fusion**
By D. Naujoks

40 **Relativistic Quantum Theory of Atoms and Molecules**
Theory and Computation
By I.P. Grant

41 **Turbulent Particle-Laden Gas Flows**
By A.Y. Varaksin

42 **Phase Transitions of Simple Systems**
By B.M. Smirnov and S.R. Berry

43 **Collisions of Charged Particles with Molecules**
By Y. Itikawa

44 **Collisions of Charged Particles with Molecules**
Editors: T. Fujimoto and A. Iwamae

45 **Emergent Non-Linear Phenomena in Bose–Einstein Condensates**
Theory and Experiment
Editors: P.G. Kevrekidis, D.J. Frantzeskakis, and R. Carretero-González

46 **Angle and Spin Resolved Auger Emission**
Theory and Applications to Atoms and Molecules
By B. Lohmann

Vols. 10–35 of the former Springer Series on Atoms and Plasmas are listed at the end of the book

Boris M. Smirnov · R. Stephen Berry

Phase Transitions of Simple Systems

With 81 Figures and 32 Tables

Springer

Prof. Boris M. Smirnov
Russian Academy of Sciences
Institute of High Temperatures
Izhorskaya ul. 13/19
127412 Moscow, Russia

Prof. Dr. R. Stephen Berry
University of Chicago
Department of Chemistry
929 East 57th Street
Chicago, Illinois 60637
USA

ISSN 1615-5653

ISBN 978-3-540-71513-9 Springer Berlin Heidelberg New York

Library of Congress Control Number: 2007933847

Typesetting and prodcution: LE-TEX Jelonek, Schmidt & Vöckler GbR, Leipzig, Germany
Cover design: eStudio Calamar S.L., F. Steinen-Broo, Girona, Spain

Printed on acid-free paper SPIN: 11921653 57/3180/YL – 5 4 3 2 1 0

Preface

Thermodynamic concepts of aggregate states and their phase transitions developed during the 19th Century and are now the basis of our contemporary understanding of these phenomena. Thermodynamics gives an universal, macroscopic description of the equilibrium properties of phase transitions independent of the detailed nature of the substances. However understanding the nature of phase transitions at the microscopic level requires a different approach, one that takes into account the specifics of the interparticle interactions. In this book, we lay the groundwork that connects the microscopic phenomena underlying phase changes with the macroscopic picture, but in a somewhat restricted way. We deal only with systems in which electronic excitations are not important, only with atomic systems, and only with homogeneous systems. We also restrict our analysis to systems in which only pairwise interactions need be included, and, in many parts of the treatment, to systems in which one need consider only the interactions between nearest neighbor atoms. In establishing these restrictions, we can be guided by the solid and liquid states of inert gases and the phase transitions between them, although the subsequent analysis is relevant and applicable for a series of other physical systems.

To study the behavior of a system of many interacting identical particles, we work extensively with its potential energy surface (PES), a surface in a many-dimensional space whose independent variables are the monomer coordinates or some transformation thereof. A central property of any multidimensional PES is its large number of local minima. We can think of the evolution of a system described by this surface as the trajectory taken by the system as it passes from the neighborhood of one local minimum to another. At moderate and low temperatures, the system remains in each of these neighborhoods for a time long compared with the period of atomic oscillations. This allows us to distinguish two forms of the system's excitation: thermal or vibrational excitation corresponds to the energy of oscillations of individual atoms; configurational excitation is that associated with location and change of location among the neighborhoods of the local minima of the PES. From this

perspective, a phase transition corresponds to a change of the configurational excitations of the system.

The approach treats both bulk systems and small systems, and their differences and similarities. One can gain insights into the properties of bulk phase transitions by seeing how they evolve from the equilibria of phase-like forms of systems of only tens of atoms, for example. Some of the information comes from analysis of simple model systems; some comes from simulations, by molecular dynamics for example; some, especially for bulk systems, comes from experimental data.

One particularly illustrative phenomenon is the apparent paradox that, while bulk systems show sharp phase transitions and satisfy the Gibbs phase rule, with two phases in equilibrium at only one pressure if the temperature is fixed, atomic clusters can coexist in two or more phases over a range of temperatures and pressures. The analysis presented here shows how the behavior of bulk systems evolves from the behavior of very small systems, as the number of particles comprising the system grows larger. In the course of the analysis, one encounters surprises that resolve themselves when one comes to understand some of the tacit assumptions underlying traditional development of thermodynamics and kinetics for bulk systems. We learn, by examining microscopic behavior as well as traditional properties such as caloric curves, how the fundamentals of thermodynamics remain valid even when some of those tacit assumptions are not.

Much of the development is based on the model of a simple dense material consisting of particles and voids. We introduce the void as an elementary configurational excitation. In a lattice, a void is very much like a vacancy, but here, "void" implies that the neighbors of the vacancy can relax to a stable form. In an amorphous material, the void need not have a specified shape and may even change its size. The void concept, together with the distinction between configurational and vibrational degrees of freedom, opens the way to analytic and combinatorial approaches to elucidating the phase behavior of small and large systems alike. The liquid and solid, for example, differ in the density of their voids. In small systems, they can coexist over a range of conditions because the solid is stabilized by its low energy with few voids, and the liquid is stabilized by its high entropy with many voids.

This book, devoted as it is to various aspects of the nature of the phase transitions in simple systems, addresses some aspects of the kinetics of phase changes as well as their thermodynamics and equilibrium properties. We hope that this approach will enable colleagues to go further, to extend these ideas to more complex systems, and to apply them in the expanding field of nanoscale materials.

Chicago, R. Stephen Berry
Moscow, Boris M. Smirnov
August 2007

Contents

Introduction

To consider phase states and phase transitions, we must look first to thermodynamic concepts. According to classical thermodynamics, the phase or aggregate state of an ensemble of interacting atoms or molecules is a uniform spatial distribution of atoms or molecules that is restricted by boundaries. A transition between two phases of a macroscopic system has a stepwise character and results from variation of thermodynamic parameters, typically (but not necessarily) the temperature. Most commonly, the variable controlling the phase and phase change is an intensive variable. A thermodynamic description of phase transitions has advantages and disadvantages. The advantage of this description is its universal character; it is suitable for many kinds of systems with different interactions between atoms or molecules. But for this reason, a thermodynamic description of aggregate states and phase transitions is formal and does not allow one to exhibit the nature of phenomena under consideration at a microscopic level.

Computer simulation of clusters and bulk ensembles of interacting atoms opens the possibility for us to understand the nature of the phase transitions at that molecular level. But the microscopic character of this phenomenon depends on the form of interatomic interaction. In analyzing this phenomenon from the microscopic standpoint, we will consider ensembles of atoms interacting via a pairwise force; this corresponds to the simplest model and, apart from ionic materials such as alkali halide, represents the predominant interaction. This allows us to understand at a level deeper than the phenomenological that thermodynamics gives us, the nature of an aggregate state of an ensemble of interacting atoms. This approach provides a microscopic description to connect the true phase transition between equilibrium states with related phenomena, in particular, with the glass transition.

A real example of a system with pairwise interaction between atoms is a condensed inert gas. Indeed, because the atoms of inert gases have completed electron shells, the exchange interaction between such atoms and hence the short-range interatomic forces are repulsive in this case. Hence at equilibrium interatomic distances in condensed inert gases, the interaction potential of

two atoms is small in comparison with typical electronic energies. As a result, interactions between two atoms do not influence the interactions of these atoms with other atoms in condensed inert gases. In other words, two-body interactions dominate the behavior of such systems; we can neglect three-body and higher interactions and retain a reasonably accurate picture of the behavior of such systems.

Next, because the exchange interaction between two atoms is dominated by electron coordinates near the axis connecting the atoms, the pairwise character of interaction is conserved at high pressures, and is primarily a repulsive interaction. Therefore inert gases are objects that satisfy models based on a pairwise interaction. Consequently, in the following discussion, we make use of the properties of condensed inert gases in detail. We restrict our discussion only to the "heavy" inert gases Ne, Ar, Kr and Xe, whose atoms may be considered as classical particles under the conditions of phase changes. Ignoring quantum effects simplifies the analysis of an ensemble of identical particles yet retains the essential characteristics of such systems. The study of a bulk ensemble of classical atoms together with known properties of inert gases gives rich insights about these atomic systems and their phase transitions. Moreover we bring the properties of bulk systems into a common context with their very small counterparts, the nanoscale particles and clusters composed of the same inert gas atoms.

To study the phase changes of an ensemble of classical particles, one can separate excitations of such systems into two groups. The first group relates to thermal motion of particles, specifically their oscillations in the total system; the second group consists of configurational excitations, which include diffusion and translational motions because the high density of the systems require configurational excitation for translational motion to be possible. Phase transitions are closely related to configurational excitation of a particle ensemble, and therefore configurational excitation is the principal object of study of this book. At zero temperature the first, vibrational excitations disappear; hence it is convenient to study the configurational excitation of an ensemble of classical particles at zero (vibrational) temperature, to be free from thermal motion of particles. An effective way to characterize the behavior of such a system is to cast that behavior in terms of motions on its potential energy surface (PES) in a many-dimensional space of particle coordinates. The important property of the PES, that is the basis of understanding of the nature of configurational excitation, is that the PES has many local minima which are separated by barriers. Just this fact allows us to separate the thermal and configurational degrees of freedom. Indeed, assuming a typical barrier height is large compared to thermal energy, we find that an ensemble has many oscillations near a given local minimum of the PES before the transition to the neighboring minimum. The first kind of excitations are motions within the region of a single local minimum on the many-dimensional surface; the second kind correspond to motions from one local minimum to another.

Classical thermodynamics, being intrinsically phenomenological, does not allow us to understand phases and phase transitions at the microscopic level. Fortunately, it is possible to study a simple ensemble of classical particles with pairwise interaction to reach a level of understanding at that level. Indeed, we define a phase as a group states of configurational excitations with similar excitation energies if these excitations are realized with roughly similar probabilities. For the dense particle ensembles under consideration, in the present context we have only two phase states, the solid or ordered state and the liquid or disordered state. Of course, one can go to a more detailed description to recognize different solid structures as different phases, and, for small systems at least, distinguish liquid character or liquid-like phases in terms of the behavior of different shells. We shall study these problems in detail later.

By analyzing some phenomena exhibited by an ensemble of classical atoms from the standpoint of the local minima of the PES, we obtain a depend understanding of these phenomena. In reality, one can simplify the concept of the PES by introducing voids as elementary configurational excitations. If we assume individual voids to be identical, the void concept simplifies the understanding and description of the properties of the phase states.

It is convenient to start the void concept from formation of vacancies in a crystal structure of classical particles. Suppose the system contains n particles and v voids. Indeed, assume the number of classical particles of an ensemble $n+v$ is so large that surface particles of this particles give a negligible contribution to its parameters. In the ground configurational state these particle form a close-packed crystal structure, face-centered cubic or hexagonal, that follows from the pairwise interaction between the particles. Each internal particle of this structure has 12 nearest neighbors. In order to prepare a configurationally excited cluster consisting of n particles and v internal vacancies, v internal particles are removed to the outside. If newly-formed vacancies do not border one another (i. e. a number of vacancies $v < n/12$), this system is stable and its state corresponds to a local minimum of the PES. At large excitation ($v > n/12$) such a state is unstable; the system formed by removing atoms and creating site vacancies relaxes by shrinking under its own attractive van der Waals forces. As a result, vacancies are converted into voids. These are free spaces between particles that vary their shape and size in time. We consider and use average parameters of voids. Of course, during relaxation, vacancies can join into bubbles – large empty constituents inside a system of particles. However usually (and in any case, for condensed inert gases) vacancies convert into voids and not into large bubbles. Moreover, the number voids is equal approximately to the number of initial vacancies. This method of generation of voids inside a particle ensemble is convenient for the void analysis.

Describing the phase state of a system of identical classical particles within the framework of the void concept simplifies our understanding of various phenomena connected with configurational excitation and phase transitions. In

particular, displacement of elementary configurational excitations in terms of voids describes some key properties and phenomena in these systems. A void can transfer to a neighboring site; this is precisely the transition between two neighboring local minima of the PES. Because neighboring local minima of the PES are separated by barriers, this transition has an activation character, so it proceeds only slowly at low temperature. A sum of transitions between local minima of PES, each considered as the motion of independent voids, determine diffusion of voids inside the particle ensemble. Naturally the diffusion coefficient of voids decreases sharply with decreasing temperature. Hence at low temperatures, one can prepare an unstable configurational state of this system with voids frozen inside it. The transition into a stable configuration state consists of diffusion of voids to the boundaries, and since this time is long, these states are characterized by long lifetimes at low temperatures. These states are total analogous with glassy states, so we have a possibility to analyze the glassy states for simple systems.

Because the phase states of a system of classical particles differ by the presence or absence the voids inside the system, a phase transition is characterized by displacement of those voids. Hence, growth of nuclei of a new phase inside the system, the nucleation process, can be considered as a result of diffusion of voids in a space separated into two regions by the phase boundary. Considering the growth of nuclei of a new phase as a result of diffusion of voids allows us to analyze some aspects of this phenomenon in a simple manner.

Thus, this book is devoted the analysis of ensembles of classical particles with pairwise interaction between particles and configurational excitations of these ensembles which include the phase transitions and adjacent phenomena. Because we consider simple systems, ensembles of classical particles with pairwise interaction and not at low particle densities, this allows us to describe these phenomena in a simple manner that conserves the strictness of the analysis.

Part I

Thermodynamics of Ensembles of Classical Particles

1

Excitations in Simple Atomic Ensembles

1.1 Thermodynamics and Dynamics of Particle Ensembles

We consider systems of large numbers of identical particles. From the thermodynamic standpoint, this system can form an aggregate state or a phase. According to the definition [1–5], a phase is a uniform distribution of particles in a region restricted by a boundary. Thermodynamics determines stable, equilibrated aggregate states that correspond to the minima of an appropriate thermodynamic potential in accordance with external conditions [2, 4, 6–8]. In particular, if an ensemble of identical particles is in equilibrium at a certain temperature and pressure, a corresponding equilibrium volume per particle follows from the minimum of the Gibbs thermodynamic potential (or the Gibbs free energy). This means that if an initial volume per particle differs from the equilibrium one, the system will compress or expand until this equilibrium volume is attained.

An ensemble of simple particles, of atoms for example, can be in the solid or liquid state; these aggregate states are characterized by different thermodynamic parameters. At almost any given temperature, one of theses aggregate states is stable and the other one is metastable. The stable state is characterized by a lower Gibbs thermodynamic potential. However, at the melting point, the Gibbs thermodynamic potentials for these states are identical. If the distribution of particles differs from that in a stable aggregate state, the ensemble relaxes to a stable aggregate state. This means that parameters of the space and velocity particle distribution tend to those of aggregate states. The final state may be stable or metastable, depending on which locally stable atomic distribution is "closer", i. e. more kinetically accessible to the initial distribution.

In addition to the stable aggregate states or phases, the distribution of particles of many systems can form a glassy state. From the thermodynamic standpoint, a glassy state does not ordinarily correspond to the global minimum of a thermodynamic potential (i. e. it is not a stable aggregate state, according to our usage here), but the relaxation time for a glassy state is

very long compared to the relaxation time of vibrations. Because relaxation typically involves some activation step, the relaxation time increases dramatically with a temperature decrease, so glassy states are typically realized at low temperatures.

The thermodynamic description of aggregate and glassy states is universal and is valid for any ensemble of many identical particles. Therefore we use it below as a basis and will characterize these states by thermodynamic parameters. But for a deep understanding of the nature of these states when we include in consideration interaction between particles, the connection between the form of interaction between particles and aggregate or glassy states of a particle ensemble may depend on the nature of the interparticle interactions. Moreover, we must leave the realm of thermodynamics when we describe the process of relaxation of an ensemble of particles from a thermodynamically unstable state [9]. Indeed, first, relaxation of such states typically has a non-exponential character [10, 11] although at small deviation from equilibrium, this deviation varies in time in an exponential way. Second, the relaxation time $\tau_{\rm rel}$ typically has an Arrhenius temperature dependence,

$$\tau_{\rm rel} \sim \exp\left(\frac{E_{\rm a}}{T}\right) , \tag{1.1}$$

if the relaxation process proceeds from one local equilibrium state to another and occurs by transition over a barrier. Here $E_{\rm a}$ is the activation energy to cross the barrier, T is the temperature which, here and below, is expressed in energy units. Relaxation of glassy states may be non-Arrhenius [12–15]. Third, relaxation of glassy states may be non-linear [9], that is, the relaxation time need not be proportional to the degree of excitation. These all exhibit the complexity of this problem.

For this reason a large number of models exist to describe various aspects of phase and glassy transitions. Each model for change of a particle configuration can be connected with certain real objects and hence has a phenomenological character. Therefore although we have a strict thermodynamic description of equilibrium states for ensembles of identical particles, this description loses its universality when we move to discussing the evolution of non-equilibrium ensembles.

Dynamics of particle ensembles may be analyzed by methods of computer simulation for specified interactions between particles and external constraints. In each case, we deal with a specific landscape of the potential energy surface (PES) in a many-dimensional space of particle coordinates; evolution of the particle ensemble corresponds to motion of a point in this space along the PES. In this manner, one can describe dynamics of the particle ensemble. This approach is productive at low temperatures (or low kinetic energies of particles) when the character of the PES landscape is important for the evolution of the system. In the course of evolution, the configuration of the particles varies; simulation allows us to study transitions between different particle configurations.

The objects of our consideration are ensembles of classical atoms with simple interactions between them. In analyzing these ensembles, we will be guided by clusters and bulk systems of inert gases excluding helium, so the atoms can be treated as classical, and we apply the above general principles to these objects. We also treat model systems of particles that interact through Lennard-Jones potentials which have been analyzed widely by numerical methods of computer simulation. Because of its simplicity, various aspects of the phase and glassy transitions for these objects may be analyzed in simpler and more transparent assumptions than for very realistic representations of the rare gas atoms. This allows us to exhibit the essences of the nature of phenomena under consideration.

1.2 Interaction of Inert Gas Atoms

Because ensembles of inert gas atoms are the objects we are using as our guides, we consider interaction of inert gas atoms in detail. In all the cases under consideration, the interaction potential of two inert gas atoms is small compared to a typical value of any electronic excitation energy of the system, in particular, the ionization potentials of these atoms. Figure 1.1 gives the separation dependence of the interaction potential for two inert gas atoms, and Table 1.1 contains the parameters of the minimum of the interaction potential for two identical atoms of inert gases that are examined in this analysis [16–19]. The Table presents various data governing the interactions and collisions of inert gas atoms which are determined by their interaction potential. We note again that the depth of a typical attractive interatomic potential well D_e is small compared to the ionization potentials for inert gas atoms, and the equilibrium distance between two atoms in a diatomic molecule R_e exceeds considerably any typical atomic size a_o. Although the potential well depth D_e differs from the dissociation energy D_o of the corresponding diatomic molecule due to zero-point vibrations of the atoms, for a system of many interacting atoms the contribution of zero-point vibrations to the dissociation energy is small and we shall ignore this.

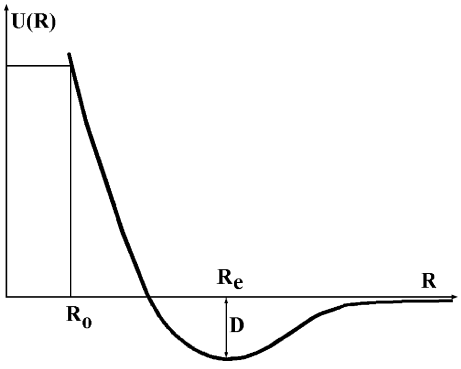

Fig. 1.1. A typical interaction potential between two atoms as a function of the distance between atoms, and the parameters of Table 1.1

Table 1.1. Parameters of the pair interaction potential for inert gas atoms. R_e, D_e are the parameters of the interaction potential minimum, $\gamma = \sqrt{2m_e I}/\hbar$, C is the parameter of the asymptotic expression (1.2) for the exchange interaction potential; parameters k, R_o [20] correspond to variables in the formula (1.3), where $U(R_o) = 0.3\,\text{eV}$, and the parameter k' are given by formula (1.4).

	Ne	Ar	Kr	Xe
R_e, Å	3.09	3.76	4.01	4.36
D_e, meV	3.64	12.3	17.3	24.4
D_e, K	42	143	200	278
γa_o	1.26	1.08	1.03	0.944
C	15	51	54	14
R_o, Å	2.07	2.85	2.99	3.18
k	7.6	8.1	7.7	5.9
$2R_o\gamma$	9.9	11.6	11.6	11.3
k'	7.1	9.4	9.2	8.6

At relatively large distances between atoms where the interaction potential is relatively small, the interaction can be represented as a sum of long-range and short-range interactions. A long-range interaction is a result of interaction of induced atomic dipoles (Fig. 1.2) and is determined by redistribution of electrons in the region around their parent atoms. One can consider this interaction as an electrostatic interaction of two polarizable charge distributions that leads to a small change in their mean spatial distributions.

The short-range, repulsive part of the interaction is due to the combination of the exchange interaction of the electrons and the Coulomb repulsion of the nuclei. The exchange interaction is determined by overlapping of the wave functions of valence electrons of the neighboring atoms. The exchange interaction effectively drives electrons away from the internuclear axis, unshielding the positive cores from one another and hence producing a repulsive force. As the internuclear distance is made smaller, that force grows, not at the rate given by Coulomb's law but by the rate at which the unshielding occurs. As a consequence, at moderate to large distances between interacting atoms, their exchange interaction $\Delta(R)$ is characterized by a dependence [21–24] $\Delta(R) \sim \exp(-2\gamma R)$, where $\hbar^2\gamma^2/(2m_e)$ is the atomic ionization potential, $\hbar$ is the Planck constant, and m_e is the electron mass. A more precise expres-

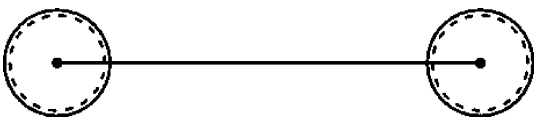

Fig. 1.2. The regions occupied by valence electrons in atoms (*solid circles*) and those responsible for the long-range interaction between atoms (*dotted circles*)

sion for the exchange interaction potential at those distances is [25, 26]

$$\Delta(R) = CR^{\frac{7}{2\gamma}-1} \exp(-2\gamma R) , \quad \gamma R \gg 1 . \tag{1.2}$$

Table 1.1 lists the parameters of this formula. Since the exchange interaction between two atoms is determined by the overlap of the wave functions of their valence electrons, it is generated predominantly in the region close to the internuclear axis, as shown in Fig. 1.3. The ratio of the volume of this region to the entire volume of valence electrons is $\sim (\gamma R)^2$.

The exchange interaction determines the interatomic repulsion over a range of distances R in which the repulsive interaction potential $U(R)$ is still small compared with the ionization potential I of the atoms, but is large compared with the dissociation energy of the weakly-bound diatomic molecule D_e of rare gas atoms,

$$D_\mathrm{e} \ll U(R) \ll I .$$

We can infer that the repulsive interaction potential of two inert gas atoms is $\sim 1\,\mathrm{eV}$ in the distance range of interest here from measurements of the differential cross section of scattering on small angles for incident atoms of KeV-energies. Because this interaction potential varies sharply with the distance R between atoms, it is convenient to approximate it by the relation

$$U(R) = U(R_\mathrm{o}) \left(\frac{R_\mathrm{o}}{R}\right)^k = \frac{A}{R^k} , \quad k \gg 1 , \tag{1.3}$$

and Table 1.1 contains parameters of this formula which are taken from the review [20]. Together with this, Table 1.1 contains the parameter

$$k' = 2\gamma R_\mathrm{o} - \left(\frac{7}{2\gamma} - 1\right) \tag{1.4}$$

that characterizes the exchange repulsion interaction potential at a separation R_o. As the data of Table 1.1 show, the asymptotic behavior of the repulsive interaction potential (1.2) corresponds also to a sharp increase of repulsion when atoms approach this range of interaction energies.

If several inert gas atoms partake in interaction, their potential energy is a sum of pair interaction potentials of the atoms, within the approximations we use here. Indeed, in the case of a long-range interaction, any

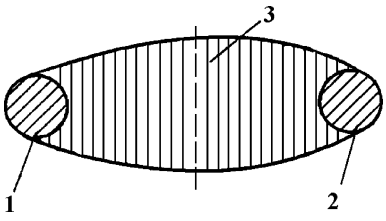

Fig. 1.3. The region occupied by valence electrons in atoms (*1,2*) and that responsible for the exchange interaction between those atoms (*3*)

induced dipole moment is relatively small, enough to justify our dropping three-body and higher multibody interaction terms. The exchange interaction potential that leads to repulsion and follows from the overlapping of wave functions of valence electrons is created mostly in a spatial region close to the axis that joins the atoms. Because of the small and very localized volume of the region of the overlapping wave functions (its ratio to the total valence electron volume is $\sim (R_o\gamma)^{-2}$), one can ignore three-body exchange interactions. Hence, the potential energy U of an ensemble of inert gas atoms can be represented as a sum of the pair interaction potentials for these atoms

$$U = \sum_{i,k} U\left(|\mathbf{R}_i - \mathbf{R}_k|\right) \ , \tag{1.5}$$

where $\mathbf{R}_i$, $\mathbf{R}_k$ are coordinates of the atoms of this ensemble. Moreover, since at longer ranges the pair interaction potential of inert gas atoms drops significantly with increasing interatomic distance, one can, for many purposes, restrict the discussion to interactions between neighboring atoms. Thus, in considering an ensemble of inert gas atoms, we deal with interaction between neighboring atoms only and this interaction has a pairwise form. (An exception that can serve as an example is determining the relative stabilities of the two close-packed lattice structures, the face-centered cubic or fcc and the hexagonal close-packed or hcp structures. To determine the relative energies of these correctly, one must include second- and third-nearest neighbor atoms.)

One more characteristic of the interaction of many inert gas atoms is large values of their electronic excitation energies; these exceed by orders of magnitude the typical energies of interatomic interaction. Hence transitions between electronic levels of a system of interacting inert gas atoms are not relevant to describing the course of evolution of the system; we need consider only the system in its ground electronic state. Thus the development of this system corresponds to its motion in a many-dimensional space of atomic coordinates along the potential energy surface of the ground electronic state. From another perspective, this system is a strong dielectric, a consideration that simplifies its analysis.

A strong and convenient method for analyzing ensembles with simple atomic interactions is based on the scaling or similarity law. The concept of the scaling law is based on composing a quantity of each dimensionality from three dimensional parameters [27–29]. Dimensionality or scaling analysis is used widely in hydrodynamics and gas dynamics [28, 30, 31]. In the case of inert gas systems, the three natural, basic parameters are the atomic mass m, the equilibrium distance between atoms $r_o = R_e$ and the well depth for the pair interaction potential of atoms $\varepsilon_o = D$. These parameters are given in Table 1.2 together with typical values of some quantities constructed from these parameters for inert gases [32]. One then uses the basic parameters to define new variables, scaled by these parameters, to derive relations that apply "universally" for an entire family of substances.

Table 1.2. Reduced parameters of an ensemble of interacting inert gas atoms ($1a.u.m. = 1.6606 \cdot 10^{-24} g$)

	Ne	Ar	Kr	Xe
r_o, Å	3.09	3.76	4.01	4.36
ε_o, meV	3.64	12.3	17.3	24.4
m, a.u.m.	20.18	39.95	83.80	131.3
$p_o = D/R_e^3$, MPa	20.2	37.1	43.0	47.1
$V_o = R_e^3$, cm^3/mol	17.8	32.0	38.8	49.9
$\rho_o = m\sqrt{2}/R_e^3$, g/cm^3	1.606	1.764	3.051	3.718

1.3 Similarity Law for Simple Atomic Ensembles

Note that the scaling analysis based on the parameters of Table 1.2 assumes that an analyzing parameter or process is determined mostly by attractive interaction of atoms in the range of their maximum attraction. The scaling analysis is effective for processes and phenomena that are determined by collective interaction of atoms when each atom interacts simultaneously with several surrounding atoms. In such cases, the parameter under consideration follows from many simultaneous interactions that would often create a difficulty when one must sum these interactions in an unscaled representation. In the scaling analysis, we effectively circumvent this summation by using the result of an experiment or computer simulation. Scaling makes it possible to use the result from one system to determine this parameter for other related ensembles. Because of the identical inherent character of their interactions, the parameters for two different systems are connected by the scaling law.

1.4 Evolution of Particle Ensembles

We now consider the evolution of an ensemble of classical particles, using systems of a finite number of inert gas atoms – clusters of inert gases – as our guide. The pair interaction between atoms dominates, and the basic interaction for a test atom is that with neighboring atoms (in contrast to electrolytes with their Coulomb interactions). The limiting case of this system is a cluster with a short-range interaction of a test atom with surrounding ones in which only nearest neighbors interact. In this case, the form of the interaction potential between nearest neighbors can have almost any form consistent with our assumptions.

The evolution of this ensemble of classical atoms is considered as motion of a point along the potential energy surface in a phase space of atomic coordinates. The potential energy surface for a cluster contains many minima separated by saddles; the number of these local minima increases sharply

with cluster size [33–38]. The number of geometrically distinct locally stable structures increases approximately exponentially, with the number n of particles, and the number of permutational isomers of each increases approximately as $n!$ [36, 38, 35]. Hence, one can describe the cluster's evolution as a result of transitions between local minima of the extremely complex potential energy surface. These motions correspond to saddle-crossing dynamics [38–42]. Within the framework of this description, a rare gas cluster remains near a given minimum of the potential energy surface for a relatively long time interval, since its average total kinetic energy is lower than typical saddle heights. By that, we can infer that the vibrational modes within the vicinity of the local minimum can come to thermal equilibrium [43].

The saddle character of the potential energy surface was first revealed in computer calculations of the cluster energy [33, 34]. In order to find the global minimum of a cluster's internal energy and the optimal configuration of its atoms, one can start from any atomic configuration, calculate the cluster's energy for this configuration, and then move to a new atomic configurations with lower energy. In this manner one can hope to reach the global minimum of the cluster's effective potential energy and the optimal atomic configuration at zero temperature. But this method is virtually impossible to realize because a typical cluster's PES has so many local minima. For example, the Lennard-Jones cluster of 13 atoms (a cluster with the Lennard-Jones interaction potential between atoms) was characterized by 988 local minima on its potential energy surface [33, 34]; a later, more detailed analysis [39] found 1478 local minima and 17,357 saddle points of the potential energy surface for this Lennard-Jones cluster of 13 atoms; still more recently, that number has reached 1509 [38]. The number of geometrically distinct local minima of the cluster PES increases roughly exponentially with increasing the number of cluster atoms [35, 36, 42].

Understanding the behavior of such a cluster is a natural subject for simulation by molecular dynamics or Monte Carlo methods. Evolution of this system consists of passage of classical particles from the vicinity of an initial local minima of the PES to any of its neighboring minima [37, 38, 42, 40, 44]. Studying the corresponding saddle-crossing dynamics [41] is a convenient method for analyzing cluster evolution. Figure 1.4 demonstrates the character of transitions between neighboring minima of the potential energy surface. In Fig. 1.4 schematic projections of a potential energy surface on planes are given in a space of atomic coordinates. Only one coordinate is used for each transition, the coordinate that corresponds to the lowest energy path connecting the two local minima of the potential energy surface for that given transition. These (curvilinear) coordinates are of course different for each transition. Energy levels for each well indicate an average atomic energy along a coordinate of the transition. Because this average energy is often significantly less than the barrier height, such transitions occur infrequently, only when the kinetic energy of atoms in the transition degree of freedom exceeds its average energy

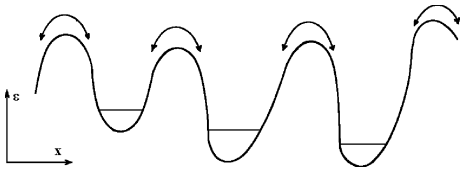

Fig. 1.4. Evolution of an ensemble of atoms in the ground electron state as propagation of a point in the multidimensional space of atomic coordinates, resulting from a transition between neighboring local minima of the potential energy surface. The x-coordinate lies along the axis joining the positions of two neighboring local minima of the potential energy surface; hence this direction is different for each pair of neighboring local minima

adequately. Of course having energy enough to cross a saddle is a necessary but not sufficient condition for a system to find its way across that saddle. If the saddle is very narrow and in some obscure corner of the surface, passage over it may occur extremely infrequently. Hence a cluster typically has many oscillations inside a given well until it passes to another local minimum of the potential energy surface. Then identifying a given local (but not global) minimum of the potential energy surface as a configurational excitation of a cluster, one can separate it from thermal motion associated with atomic oscillations.

We divide the cluster excitation into two parts, thermal and configurational, assuming those to be independent. We characterize a configurational state of this system by the local minimum of the potential energy surface around which the system vibrates. Assuming the dwell time of a system near one minimum of the potential surface is long compared with the period of atomic vibrations in that local minimum, one can separate the energy into two parts [43]. The first is the thermal energy of particle vibrational (and rotational) motion, and the second, configurational part is that of the local minimum of the potential surface in whose region the system resides. At zero temperature, the only energy of the system is the configurational energy of the system at its global minimum on the PES. Next, since the dwell time is high, thermodynamic equilibrium for thermal motion of atoms is established during cluster location in a given configuration state. This means that the thermal motion of the atoms can be characterized by a temperature. If a cluster is isolated, this temperature is dependent of the configurational state. Note that this temperature refers only to thermal motion of atoms, while the character of excitation of configurational states in general need not be connected with this temperature. This implies that one may well find a non-equilibrium distribution of configurational excitations in a thermodynamic analysis of atomic ensembles. This is of course particularly so if the system is undergoing any kind of relaxation.

Figure 1.5 shows the possibility of dividing degrees of freedom for cluster atoms into the configurational and vibrational, with a simple example of 13 atoms and a short-range interaction between atoms, i. e. the total potential

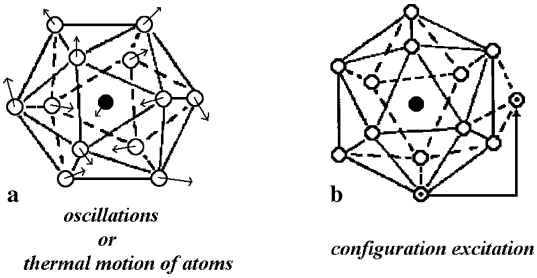

Fig. 1.5. Two types of cluster excitations: cluster oscillations due to thermal motion of atoms (**a**) and configurational excitation (**b**)

energy of the cluster is determined by interaction between nearest neighbors predominantly. In the lowest configurational state, the atoms of this cluster form an icosahedron with one central and 12 surface atoms, and all the surface atoms are equivalent. In addition, distances between neighboring surface atoms are equal also, so that joining of the centers of neighboring surface atoms gives a surface consisting of 20 equilateral triangles. Then if we exclude three degrees of freedom for motion of the cluster as a whole (its center-of-mass motion) and another three degrees of freedom associated with the rotation of the cluster about its center, we find 33 remaining vibrational degrees of freedom. These appear for each configurational cluster state. These vibrations or thermal motion of atoms are shown in Fig. 1.5a for the ground configurational state, the regular icosahedron.

As we see, the central atom of the icosahedral cluster forms 12 bonds with surface atoms. Each surface atom has 5 bonds with neighboring surface atoms and one bond with the central one. Hence, there are 30 bonds between surface atoms and the total number of bonds of this cluster is 42 for the ground configurational state. The lowest configurationally excited state corresponds to transition of one surface atom to a face of the cluster surface as shown in Fig. 1.5b. In this configurational state, the promoted atom has only 3 bonds with surface atoms, so the total number of bonds for this state is 39; this configurational excitation yields a loss of three bonds. Note that this state is separated by a barrier from the ground state in a space of atom coordinates. Indeed, exciting the cluster from the ground configuration into this excited one by promoting a surface atom, we can conserve at most only two of the bonds between this atom and its neighbors during the course of the transition, while in the final state this atom has three bonds. Hence the transition between these two configurations proceeds through any of the saddle points located on the top of a barrier or saddle that separates these configurational states.

One more peculiarity relates to this symmetric system. If we enumerate atoms, we have one ground configurational state when each atom occupies a certain position, and this configuration corresponds to a certain point in the many-dimensional space of the potential energy surface. In this case we obtain 180 equivalent points in this space that correspond to this lowest excited configurational state. Indeed, this excited state can be obtained by promoting any of the 12 surface atoms of the cluster, and this promoted atom can

occupy any of 15 position above the cluster surface when it forms bonds with three surface atoms. Hence, the lowest configurationally excited state of this symmetric cluster is characterized by a large statistical weight (or entropy). (Strictly, the configurational states in which the promoted atom is on a face neighboring the new vacancy differ from those in which that atom is removed from its former site in the full icosahedral shell.)

Thus this example demonstrates how it is that the potential energy surface has many local minima in a space of atomic coordinates, and these local minima are separated by barriers with saddle points in this space. Therefore excited configurational states are locally stable states, and a cluster can remain enough long in a specific excited configurational state to equilibrate its vibrations. Hence, if the ground configuration state is the basis for the solid cluster state, we can anticipate that configurationally excited states can be a basis for the liquid aggregate state.

1.5 Voids as Elementary Configurational Excitations

One can consider the example just given of a configurational excitation of a cluster of 13 atoms as an elementary configurational excitation. In this case a vacancy or hole is formed in the surface cluster shell, and this vacancy is deformed due to interaction of surrounding atoms. Let us widen this example and consider a very large regular surface whose configurational excitation results in passage of some atoms from the surface layer to positions on the surface. In contrast to the previous example of the 13-atom cluster, several or many elementary configurational excitations of this kind can characterize the total configurational excitation. In the same manner, one can consider internal excitations of a large or bulk crystal if internal atoms are removed onto the surface of this crystal. So long as we remove only atoms which do not neighbor one another, the total energy of this configurational excitation is simply a sum of the excitation energies for individual vacancies. In this way, representing the total configurational excitation as a sum of elementary configurational excitations, we pass from a dynamic description of the system to its statistical description.

So long as vacancies do not border one another, the energy of formation of an elementary vacancy is determined by the number of bonds for a removed atom. Because we consider atomic ensembles in which interaction between nearest neighbors is dominant, this number of bonds equals 12. When this condition is not fulfilled, we take a void [45] or empty internal space as an elementary configurational excitation of an ensemble of bound classical particles, considering a void as a perturbed (or relaxed) vacancy. But in contrast to a vacancy in a bulk solid, a void has an indefinite volume and shape that change in time. Therefore from the standpoint of saddle-crossing dynamics, each configurationally excited state corresponds to a certain number of voids which are identical on average.

Note that configuration excitation in the case of a large cluster or bulk crystal means formation of an additional empty space inside the crystal, and in principle one can introduce an elementary configurational excitation in an arbitrary way. In order to escape this ambiguity, we introduce the number of voids inside the system as the number of atoms initially removed from the crystal [46, 48, 49], and a given configurationally excited state is formed after fast relaxation of such a system. This allows us to define the elementary configurational excitation – a void – unambiguously.

One can generalize this operation for the case with a number of vacancies that is not so small, $12v \sim n$, so that neighboring vacancies could border. Then the crystalline lattice structure is lost, and vacancies are transformed in voids whose shape and volume may vary in time, in contrast to vacancies. Voids are elementary configurational excitations that occur when the total number of configuration excitations is not so small, and a certain number of internal voids v are connected with a certain configurational excitation of a body composed of n bound particles. Moreover, in considering an atomic ensemble with a given number of particles n and of internal voids v, we prepare it from a crystalline particle of $n + v$ particles and remove from it v particles to the outside. A newly formed ensemble of n particles and v internal voids relaxes, resulting in its compression. We assume that this process leads to formation of v voids; this is the basic assumption of our treatment here.

In developing the void concept, we note that each configuration of atoms and voids corresponds to a certain stable atomic configuration, which, in turn, corresponds to a certain local minimum of the PES for this system. In addition, such a configurationally excited state includes a specific number of voids that characterizes the elemental configurational excitations, the voids themselves. Such a configurationally excited state is not stable for a long time interval, since voids can go to the cluster boundary and disappear there. But the process of transition between two neighboring local minima of the PES results in void transport and has an activation character, i. e. at low temperatures it is slow, and these configurationally excited states are stable on a short time scale. Therefore, this configurationally excited state is a non-equilibrium state, but its lifetime is enough at low temperatures for it to be characterized and perhaps detected in an observation. Hence we consider this state during time intervals short compared with a time for its transport to the boundary or from it. Of course the entropy associated with voids ensures that the state of thermodynamic equilibrium of the system at any but quite low temperatures will have some vacancies or voids, whose number necessarily increases with temperature.

We use above the assumption of equality of the numbers of initial vacancies and final voids in developing a simple method for preparing a configurationally excited state for a system of many bound classical particles. Indeed, as a result of relaxation of an initial system of particles, vacancies are converted into voids during times comparable to the periods of particle oscillations ($\sim 1/\omega_{\mathrm{D}}$),

but from this it does not follow that the numbers of vacancies and voids are equal if we consider a void literally as a perturbed vacancy. But our approach is rough enough to neglect this problem; we simply assume only that a configurationally excited state resulting from relaxation of a state with a given number of vacancies contains the same number of voids. Moreover, although we characterize a void by certain parameters such as its volume, entropy and energy of formation, these parameters are intended to be averages. An individual void as a empty space inside the system "breathes" in time, and its parameters oscillate. Therefore the void concept is useful in a statistical description of a situation with many elementary excitations or a few of such excitations during a long time interval.

Thus, the concept of an average void is useful when configurational excitation can be separated from the vibrational excitation associated with an increase of the kinetic energy of the atoms. Then we define the cluster's aggregate state as a sum of its accessible configurations in the multidimensional space of atomic coordinates near the relevant local minima of the PES, with their nearby excitation energies. This is a generalized definition of the aggregate state in comparison with that of traditional thermodynamics, in which the phase or aggregate state is characterized by a uniform (mean) spatial distribution of atoms, i. e. an excited aggregate thermodynamic state includes many elementary configurational excitations. In the cluster case, the liquid aggregate state can contain even one elementary excitation, as takes place for the Lennard-Jones cluster of 13 atoms [50, 51]. Hence uniformity is not a requirement for the cluster aggregate state.

In essence, by defining the aggregate state in this way, we introduce a time scale on which our thermodynamic variables are defined. The accessible volume that defines the spatial contribution to the entropy of a system in traditional thermodynamics is the space accessible on an arbitrarily long time scale. The approach here is much more akin to the approach used for flow systems, for example, in which one defines "local thermal equilibrium", or "LTE", the effective thermodynamic equilibrium attained in a small but macroscopic region of space in which the system resides for some time period. It is implicit in the approach used here that it would be possible to make experimental observations, e. g. with picosecond or femtosecond spectroscopy or scattering, of the system in one or a small set of configurations.

The void concept simplifies understanding and description of phenomena involving ensembles of many interacting atoms, and we use it next to analyze the aggregate and glassy states and also to describe the phase and glassy transitions. Of course, the basis of such a description must rest on the parameters of elementary configurational excitations, the voids, and we take them both from experimental data and from computer simulations of clusters.

2

Structures of Ensembles of Interacting Particles

2.1 Close-Packed Structures

In considering an ensemble of atoms with pairwise interactions, we take the pair interaction potential in a typical form, as given in Fig. 1.1. This interaction potential is characterized by two parameters, the equilibrium distance between atoms R_e at which the interaction potential $U(R)$ as a function of a distance R between atoms has a minimum $[U'(R_e) = 0]$ and the depth of this potential well D $[U(R_e) = -D]$. On the basis of this we have a potential energy of the ensemble of interacting atoms that at zero temperature coincides with the total ensemble energy E

$$E = \frac{1}{2} \sum_{i,k} U(r_{ik}) \, . \tag{2.1}$$

Here $U(r)$ is the pair interaction potential for a distance r between atoms, r_{ik} is a distance between i-th and k-th atoms, and the factor $1/2$ takes into account that two atoms partake in each bond.

Let us introduce the sublimation energy ε_{sub} of a macroscopic ensemble of atoms as the average binding energy per atom

$$\varepsilon_{sub} = -\frac{E}{n} \, , \tag{2.2}$$

where $n \to \infty$ is the number of atoms. At low temperatures for close-packed structures (for fcc and hexagonal structures) the distance between nearest atoms a corresponds to the equilibrium distance between nuclei of a diatomic molecule R_e, neglecting the long-range interaction, i. e. ignoring the interaction between non-nearest atoms. Correspondingly, the energy per bond for nearest neighbors is equal to the dissociation energy D of a diatomic molecule. Because each internal atom of a close packed structure has 12 nearest neighbors, the sublimation energy, i. e. the energy of release of one atom of this structure, is $\varepsilon_{sub} = 6D$.

At low temperatures the ensemble of atoms can form a crystal lattice due to attractive interaction. We divide interaction between atoms into two parts, a short-range interaction that includes interaction between neighboring atoms, and a long-range interaction that takes into account interaction between non-nearest neighbors. Being guided by condensed inert gases and similar systems of interacting atoms, we will assume that the short-range interaction gives the dominant contribution to the total interaction in atomic ensembles under consideration. Atoms of an ensemble, for which a short-range interaction between atoms is essential or dominates, form a crystal lattice at low temperatures with the maximum number of nearest neighbors for an internal atom. Such lattices correspond to structures of close packing where each internal atom has 12 nearest neighbors. These structures include two types of crystal lattices [52–55], face-centered cubic (fcc) and hexagonal close-packed. One can model these lattices from hard balls such that the distance between neighboring balls is a given value a, the lattice constant.

We first place balls compactly on a plane, so that each ball touches 6 nearest ones, as shown in Fig. 2.1 [56]. The distance between neighboring balls is equal to the lattice constant a. Then we construct the second plane of balls by placing the balls in the holes between the balls of the previous layer. The centers of these balls are located at a distance $b = a\sqrt{3}/2$ from the previous plane of atomic centers. Lines joining centers of nearest atoms are shifted with respect to analogous lines of the previous plane by $a/2$. One can construct the third plane of balls of the close packed structure in two ways, and then balls form either the hexagonal or the fcc structure. Indeed,

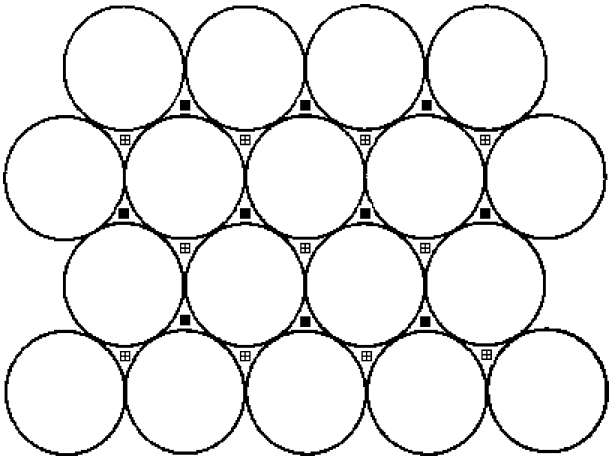

Fig. 2.1. Crystal lattices of close packed structures. *Circles* correspond to positions of atoms or balls of a given layer. *Crosses* are the positions of atomic centers of the layer beneath. *Open squares* are the positions of atomic centers of the upper layer for the hexagonal structure of the crystal lattice, and *filled squares* are those for the face-centered cubic lattice

for the hexagonal structure the projections of balls of the third and first layers coincide, whereas for the fcc structure they are different (see Fig. 2.1). In this manner we obtain two structures with close packing.

In order to describe the lattice symmetry, we reduce it to usual frame of axes. We will characterize the planes where atoms are located by so called Miller indices [54] which denote the coordinates of a vector drawn from the origin perpendicular to a given plane. In particular, if the Miller indices of a given plane, whose notation is $\{k_1k_2k_3\}$, indicate that the vector $\mathbf{b} = k_1\mathbf{i} + k_2\mathbf{j} + k_3\mathbf{k}$ is perpendicular to a given plane. Above we take as a basis the plane $\{111\}$. One can see the symmetry for the Miller indices that admits both their permutation and a sign change. The latter corresponds to reflection with respect to main plane of the axis frame. The symmetry indicates that there are 8 planes of directions $\{111\}$.

Until now the above procedure has related to the construction of both hexagonal and fcc-lattices. Placing balls of the third plane in the hollows of the second plane, one can obtain two types of ball positions (see Fig. 2.1 [56]). If the projections of the balls of the first and third planes coincide, a hexagonal lattice is formed. The other possibility of location of atoms of the third layer leads to the formation of an fcc-lattice. One can see that the number density of balls for both structures of close packing is equal to $\sqrt{2}/a^3$. Thus, there are two structures of close packing, the face-centered cubic and hexagonal. We can denote the first layer as A, the second as B, and, in the fcc structure, the third as C. This way, the hexagonal lattice has the layer pattern ABAB ... and the fcc, the layer pattern ABCABC ... (It is striking that one does not find structures with random patterns in the sequence of their layers.) From the standpoint of interactions in the system, the difference of these structures is weak. Below we evaluate the binding energy for these structures for certain pair interaction potentials. Comparison of real parameters of rare gases with calculated ones will allow us to determine the character of atom interaction in real solid inert gases.

The fcc structure has the higher symmetry. One can construct the fcc lattice as a sum of two interpenetrating simple cubic lattices. Atoms are placed on parallel planes, forming a square net of side a, and the distance between neighboring planes of directions $\{100\}$ is $a/\sqrt{2}$. An elementary cell of this lattice is a face-centered cube. Directing the x, y, z axes along sides of this cell and taking as an origin of the frame of axis the position of any atom or the middle of an elementary cell, we find the cubic symmetry [57] $\mathbf{O_h}$ of the fcc lattice that is conserved as a result of the following transformations

$$x \longleftrightarrow -x\,, \quad y \longleftrightarrow -y\,, \quad z \longleftrightarrow -z\,; \quad x \longleftrightarrow y \longleftrightarrow z\,. \tag{2.3}$$

In the case of the hexagonal structure, the geometric figure has a lower symmetry, whose atomic configuration is conserved as a result of transformation

$$z \leftrightarrow -z\,; \quad \Phi \to \Phi \pm \frac{\pi}{3}\,. \tag{2.4}$$

Here we take a plane {111}, in which each atom has 6 nearest neighbors, as a basis of the hexagonal lattice. The z-axis is directed perpendicular to this plane, and Φ is the polar angle with respect to that z axis. According to this symmetry, the maximum number of atoms of one shell is equal to $2 \cdot 6 = 12$ for a cluster with hexagonal structure, as with the fcc structure. Optimal configurations of atoms in solid hexagonal clusters may be found by the same method [58, 59], as we described above for the fcc solid clusters.

2.2 Shells in Close-Packed Structures

In order to evaluate energetic parameters of a close packed lattice, it is convenient to consider first the planes which restrict this structure. In the case of the fcc structure, there are three types of planes, {100}, {110} and {111}. We use standard notation for these planes [54] expressed as the coordinates of a line through the origin perpendicular to this plane. There are 6 different planes of {100}-type, 12 planes of {110}-type, and 8 planes of {111}-type. Thus, the maximum number of simple, low-order plane facets of an fcc crystalline particle is 26. This determines the variety of geometric figures for clusters of the fcc symmetry. The planes of the fcc crystal lattice are given in Fig. 2.2 [48, 56]. Correspondingly, the growth of clusters of fcc structure results from filling of facets of the three directions {100}, {110} and {111}.

Let us evaluate the number of nearest neighbors for a surface atom of each plane of the fcc structure. Each surface atom of a {100}-plane has 4 nearest neighbors from the surface layer and 4 nearest neighbors from the next, more interior one, i. e. a surface atom of a {100) plane has 8 nearest neighbors. In the same manner we find that each surface atom of a {110} plane has 7 nearest neighbors, and each surface atom of a {111} plane has 9 nearest neighbors. From this it follows that geometric figures with surface facets of directions {111} and {100} are the energetically more stable for bulk fcc crystalline particles with pair interactions.

If we construct a macroscopic crystal structure, it is convenient to take a test atom as an origin of this structure. Then because of the symmetry of the structure, surrounding atoms of an infinite crystal lattice form a shell, so that the distances of atoms of one shell from a test atom are identical and atoms of one shell are transformed into one another as a result of the symmetry transformations of this lattice. The higher is the lattice symmetry, the greater is the number of atoms of each shell.

Thus, taking a test atom as an origin, we distribute other atoms of the solid system on shells, so that Table 2.1 contains parameters of atomic shells for the face-centered cubic structure, and Table 2.2 gives the shell parameters for the hexagonal structure [48, 58].

The sublimation energy of an infinite crystal ε_{sub}, i. e. the binding energy per atom at zero temperature, for an infinite crystal lattice with a pair

Table 2.1. Parameters of shells of the crystal fcc-structure, so that r_k is the shell distance from a test atom, a is the distance between nearest neighbors, n_k is a number of shell atoms [48, 58]

Shell	r_k^2/a^2	n_k	Shell	r_k^2/a^2	n_k
011	1	12	044	16	12
002	2	6	334	17	24
112	3	24	035	17	24
022	4	12	006	18	6
013	5	24	244	18	24
222	6	8	116	19	24
123	7	48	235	19	48
004	8	6	026	20	24
114	9	24	145	21	48
033	9	12	226	22	24
024	10	24	136	23	48
233	11	24	444	24	8
224	12	24	055	25	12
015	13	24	017	25	24
134	13	48	345	25	48
125	15	48	046	26	24

Table 2.2. Parameters of shells of the hexagonal structure. r_k is the distance of atoms of k-th shell from a test atom, a is the distance between nearest neighbors, n_k is the number of atoms of this shell [48, 58]

Layer	r_k^2/a^2	n_k	Layer	r_k^2/a^2	n_k
0	1	6	1	9	6
1	1	6	2	29/3	24
1	2	6	1	10	12
2	8/3	2	3	31/3	12
0	3	6	4	32/3	2
1	3	12	1	11	12
2	11/3	12	3	34/3	6
0	4	6	2	35/3	12
1	5	12	4	35/3	12
2	17/3	12	0	12	6
1	6	6	3	37/3	12
3	19/3	6	0	13	12
2	20/3	12	1	13	12
0	7	12	4	41/3	12
1	7	12	3	43/3	6
3	22/3	6	2	44/3	12
3	25/3	12	4	44/3	12
0	9	6	1	15	12

interaction between atoms is given by [48, 56, 61]

$$\varepsilon_{\text{sub}} = \frac{1}{2} \sum_k n_k U(r_k) \ , \tag{2.5}$$

where $U(r_k)$ is the interaction potential for an atom of k-th shell with a test atom, and the factor $1/2$ accounts for the fact that each bond relates to two atoms. In this limit of low temperatures we ignore any contribution of the atomic kinetic energy to the total lattice energy.

This formula gives a simple result in the case in which a long-range interaction is absent in an infinite close packed lattice, i. e. one in which only nearest neighbors interact. Then the distance between nearest neighbors a coincides with the equilibrium distance R_{e} for the pair interaction potential, and the binding energy per bond coincides with the dissociation energy D formed by

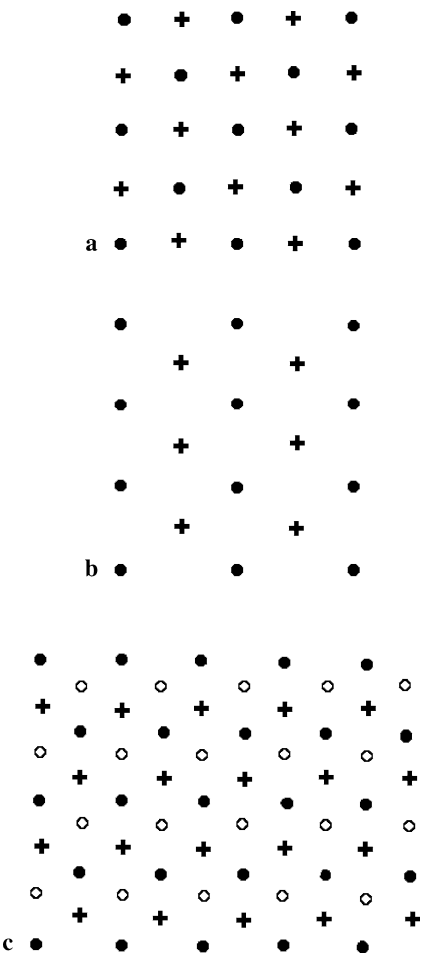

Fig. 2.2. The planes formed from bound atoms of the face-centered cubic structure. *Filled circles* – atoms of the basic layer, *crosses* – atoms of the upper layer, *light circles* – atoms of the previous layer. **a** {100}-plane, **b** {110}-plane, **c** {111}-plane

two classical atoms. Because each internal atom of an infinite crystal lattice has 12 nearest neighbors, the sublimation energy, i. e. the binding energy per atom is equal to $\varepsilon_{\rm sub} = 6D$ in this case. In the presence of a long-range interaction the lattice constant a differs from $R_{\rm e}$, and interaction with non-nearest atoms gives a contribution to the sublimation energy, so that connection between parameters of the crystal lattice and pair interaction potential become more complex. We consider below this connection for simple interaction potentials.

2.3 Lennard-Jones Crystal

We now determine parameters of the infinite crystal lattices of close packed structures with the pairwise Lennard-Jones interaction potential with the form [62, 63]

$$U_{\rm LD}(R) = D \cdot \left[\left(\frac{R_{\rm e}}{R} \right)^{12} - 2 \cdot \left(\frac{R_{\rm e}}{R} \right)^{6} \right] , \tag{2.6}$$

where R is the distance between atoms. The Lennard-Jones is a popular interaction potential that is used for modelling of solid inert gases [55, 64]. Our goal is to analyze the role of a long-range interaction in formation of real crystals. In addition, such an analysis reveals an inherent error in using this interaction potential for solid inert gases.

Formula (2.6) together with formulas (2.1) and (2.2) gives for the crystal sublimation energy [55]

$$\frac{\varepsilon_{\rm sub}}{D} = -\frac{C_1}{2} \left(\frac{R_{\rm e}}{a} \right)^{12} + C_2 \left(\frac{R_{\rm e}}{a} \right)^{6} , \quad C_1 = \sum_k n_k \left(\frac{R_{\rm e}}{r_k} \right)^{12} ,$$
$$C_2 = \sum_k n_k \left(\frac{R_{\rm e}}{r_k} \right)^{6} . \tag{2.7}$$

Replacing summation in formula (2.6) by integration for $R \geq r_{\rm o}$ we have the contribution to the constants C_1, C_2 from a range where $r_k > r_{\rm o}$

$$\Delta C_1 = \frac{1}{2} \sum_{R \geq r_{\rm o}} \frac{n_k}{r_k^{12}} = \frac{1}{2} \int\limits_{r_{\rm o}}^{\infty} \frac{\sqrt{2}}{a^3} \frac{4\pi r^2 \, {\rm d}r}{r^{12}} = \frac{4\pi\sqrt{2}}{9 r_{\rm o}^9} ,$$

$$\Delta C_2 = \sum_{R \geq r_{\rm o}} \frac{n_k}{r_k^{6}} = \int\limits_{r_{\rm o}}^{\infty} \frac{\sqrt{2}}{a^3} \frac{4\pi r^2 \, {\rm d}r}{r^{6}} = \frac{4\pi\sqrt{2}}{3 r_{\rm o}^3} .$$

We account for the fact that the average number density of atoms for a close packed structure is $\sqrt{2}/a^3$. Taking $r_{\rm o}^2$ to be between 26 and 27 [32], we get for the face-centered cubic structure of the crystal on the basis of the Table 2.1 data [55]

$$C_1 = 12.131 , \quad C_2 = 14.454 \pm 0.002 ,$$

and the error indicated is determined by the choice of the lower limit of integration. In expressions for $\Delta C_1, \Delta C_2$ we take k_o such that $r_\mathrm{o}^2 = 26$. This gives for parameters of the face-centered cubic form of the Lennard-Jones crystal

$$a = R_e \left(\frac{C_1}{C_2}\right)^{1/6} 0.971 R_\mathrm{e} \,, \quad \varepsilon_\mathrm{sub} = \frac{C_2^2 D}{2C_1} = 8.61 D \,. \tag{2.8}$$

Comparison with the case of a short-range interaction of atoms, for which $\varepsilon_\mathrm{sub} = 6D$, shows that a short-range interaction gives a contribution of approximately 70% to the energy of the Lennard-Jones crystal with the face-center cubic structure.

It is convenient to separate the specific binding energy in three parts [65]

$$\varepsilon_\mathrm{sub} = \varepsilon_{nn}(R_\mathrm{e}) + \varepsilon_{nnn}(R_\mathrm{e}) + \varepsilon_\mathrm{str} \,, \tag{2.9}$$

where $\varepsilon_{nn}(R_\mathrm{e})$, and $\varepsilon_{nnn}(R_\mathrm{e})$ are the interaction energies between nearest neighbors and non-nearest neighbors, respectively, and the strain energy is given by

$$\varepsilon_\mathrm{str} = \varepsilon_\mathrm{sub}(a) - \varepsilon_\mathrm{sub}(R_\mathrm{e}) \,, \tag{2.10}$$

where a is the optimal distance between nearest neighbors that corresponds to the maximum binding energy of the crystal. For the structures of close packing $\varepsilon_{nn}(R_\mathrm{e}) = 6D$. In the case of a short-range interaction between atoms, if only nearest neighbors interact, we have $\varepsilon_{nn}(R_\mathrm{e}) = 6D$, $\varepsilon_{nnn} = \varepsilon_\mathrm{str} = 0$, and as we found above $\varepsilon_\mathrm{sub} = 6D$, $a = R_\mathrm{e}$.

For the face-centered cubic Lennard-Jones crystal we have for terms of formula (2.9)

$$\begin{aligned} &\varepsilon_{nn}(R_\mathrm{e}) = 6D \,, \quad \varepsilon_{nnn}(R_\mathrm{e}) = \left(C_2 - \frac{C_1}{2} - 6\right) D = 2.39D \,, \\ &\varepsilon_\mathrm{str} = \frac{(C_2 - C_1)^2}{2C_1} D = 0.22D \,. \end{aligned} \tag{2.11}$$

Repeating the above operations for the hexagonal lattice, we obtain, on the basis of the data of Table 2.2,

$$C_1 = 12.132 \,; \quad C_2 = 14.454 \pm 0.002 \,.$$

As we see, within the limits of the accuracy used, the energetic parameters of the Lennard-Jones crystal coincide for the fcc and hexagonal structures. Although a more accurate calculation shows the advantage of the hexagonal structure [66], this fact has no practical significance. Correspondingly, the parameters for the face-center cubic and hexagonal structures of the Lennard-Jones crystal effectively coincide.

2.4 Morse Crystal

A second, widely-used form of the interaction potential allows us to vary the ratio between the short-range and long-range parts of the interaction potential. We now consider a crystal consisting of atoms with the Morse interaction potential which has the form [67]

$$U(R) = D\left[\mathrm{e}^{2\alpha(R-R_\mathrm{e})} - 2\,\mathrm{e}^{\alpha(R-R_\mathrm{e})}\right] . \tag{2.12}$$

This pair interaction potential has a minimum at $R = R_\mathrm{e}$. On the basis of formulas (2.1), (2.2) and (2.12) we have for the crystal sublimation energy [68, 69]

$$\varepsilon_\mathrm{sub} = D\left[\mathrm{e}^{\alpha R_\mathrm{e}} F(\alpha a) - \frac{1}{2}\,\mathrm{e}^{2\alpha R_\mathrm{e}} F(2\alpha a)\right] , \quad F(\alpha a) = \sum_k n_k \exp(-\alpha r_k) . \tag{2.13}$$

Here r_k is the distance between a test atom and atoms of k-th shell, n_k is the number of atoms of this shell, and a is the distance between nearest neighbors of the lattice. Values of the function $F(\alpha a)$ are evaluated on the basis of the data of Table 2.1 for the face-centered cubic lattice and are given in Table 2.3. In addition, Table 2.3 contains an effective number of atoms $F(\alpha a)\exp(\alpha a)$ that partake in the interaction with a test atom, and the derivative of the function under consideration is given by

$$F'(\alpha a) = \frac{\mathrm{d}F(\alpha a)}{\mathrm{d}(\alpha a)} = -\sum_k \frac{n_k r_k}{a} \exp(-\alpha r_k) . \tag{2.14}$$

Note that the value $F(\alpha a)\exp(\alpha a)$ tends at large αa to 12, the number of nearest neighbors.

Formula (2.13) establishes the connection between the equilibrium distance between atoms of the diatomic molecule R_e and the distance between nearest neighbors of the crystal a. This connection takes the form

$$\exp(\alpha R_\mathrm{e}) = f(\alpha a) = \frac{F'(\alpha a)}{F'(2\alpha a)} , \tag{2.15}$$

and the optimal specific binding energy of the crystal is given by

$$\frac{\varepsilon_\mathrm{sub}}{D} = f(\alpha a)F(\alpha a) - \frac{1}{2} f^2(\alpha a)F(2\alpha a) . \tag{2.16}$$

These parameters for the lattice of the fcc structure are given in Table 2.3.

Note that in contrast to the Lennard-Jones interaction potential, the single variable parameter α of the Morse interaction potential allows us to change continuously the specific binding energy of atoms. In particular, the specific binding energy of the Lennard-Jones interaction potential (2.6) $\varepsilon_\mathrm{sub} = 8.61D$ is realized at the value $\alpha a = 4.17$ for the Morse interaction potential. This corresponds to $\alpha R_\mathrm{e} = 4.46$, i. e., $a = 0.935 R_\mathrm{e}$. Thus the Morse crystal at this Morse parameter is more compressed than the Lennard-Jones. In addition,

Table 2.3. Parameters of the face-centered cubic crystal lattice in the case of the Morse interaction potential between atoms [48, 69]

αa	$\alpha R_{\rm e}$	$F(\alpha a)$	$-\,{\rm d}F(\alpha a)/{\rm d}(\alpha a)$	$F(\alpha a)\exp(\alpha a)$	$\varepsilon_{\rm sub}/D$
2	3.03	3.87	6.47	28.6	21.3
3	3.57	0.910	1.17	18.3	12.2
4	4.31	0.274	0.311	14.9	8.94
5	5.17	0.0911	0.0975	13.5	7.52
6	6.10	0.0318	0.0330	12.8	6.84
7	7.06	0.0114	0.0116	12.5	6.47
8	8.03	0.00412	0.00417	12.3	6.29
9	9.02	0.001503	0.001514	12.2	6.18
10	10.01	$5.499 \cdot 10^{-4}$	$5.523 \cdot 10^{-4}$	12.1	6.11

in this case the terms of formula (2.9) for the Morse interaction potential of atoms are

$$\varepsilon_{nn}(R_{\rm e}) = 6D\ , \quad \varepsilon_{nnn}(R_{\rm e}) = 2.136D\ , \quad \varepsilon_{\rm str} = 0.474D\ . \tag{2.17}$$

The contributions to the total binding energy from interactions between non-nearest neighbors and from the strain energy for the Morse crystal with $k = 6$ are equal to 25% and 5.5% correspondingly. For the Lennard-Jones crystal these values according to formula (2.11) are equal to 28% and 2.6%. From this fact and crystal compression one can conclude that the crystal parameters depend on the form of the interaction potential between atoms.

Another alternative for relating Morse and Lennard-Jones potentials is based on the value of $\alpha R_{\rm e} = 6$, for which the curvature at the energy minima is the same for the two potentials. This, too, gives significant differences between other properties of the two forms of potential.

2.5 Surface Energy of Lennard-Jones and Morse Crystals

We now determine the specific energy of the surface of a face-centered cubic crystal with the above interaction potentials. Three types of the crystal surfaces of the fcc-structure are given in Fig. 2.2. Let us take an infinite fcc-crystal and divide it in two parts by a {100} or {111} plane. The specific surface energy corresponds to the interaction potential of these open facets, per unit area. Let us denote the interaction energy of a test surface atom with all the atoms of k-th layer by ε_k (this test atom is located in the zero-th layer). Then the specific surface energy is given by

$$\sigma = \sum_{k=1}^{\infty} k\varepsilon_k / s\ , \tag{2.18}$$

where s is the area per one atom and we take into account that each bond relates to two atoms. From this formula we have in the case of the Lennard-Jones interaction potential for the specific surface energy of a solid

$$\frac{\sigma}{D} = \frac{1}{s}\left(B_6\frac{R_\mathrm{e}^6}{a^6} - B_{12}\frac{R_\mathrm{e}^{12}}{2a^{12}}\right) , \tag{2.19}$$

where D is the dissociation energy of the diatomic molecule, a is the distance between nearest neighbors, R_e is the equilibrium distance for diatomic, s is the surface area per atom, and

$$B_6 = \sum_{i,k} kn_{ik}\frac{a^6}{r_{ik}^6} , \quad B_{12} = \sum_{i,k} kn_{ik}\frac{a^{12}}{r_{ik}^{12}} . \tag{2.20}$$

Here r_{ik} is a distance from a test atom to i-th atom of k-th layer, and n_{ik} is a number of such atoms.

First we consider the {100} surface. The area per atom of this surface is $s = a^2$, and the distance between neighboring layers is $a/\sqrt{2}$. Table 2.4 gives the numbers of atoms whose distance in units of a from a test atom is $r_{ik}^2 \le 12$, and their locations in the layers. We take the sum in formulas (2.20) up to $r_{ik}^2 = 12$, and for $r_{ik}^2 > 12$ we replace the sum by integration both for atoms of first four layers and for atoms of subsequent layers. Correspondingly, the sums (2.20) are represented in the form of three terms

$$B_6^{100} = 5.35 + 10a^6\int\limits_{r_\mathrm{o}}^{\infty}\frac{2\pi\rho\,\mathrm{d}\rho\,\mathrm{d}z}{(\rho^2+z^2)^3} + \sum_{k=5}^{\infty} ka^4\int\limits_{ka/\sqrt{2}}^{\infty}\frac{2\pi\rho\,\mathrm{d}\rho}{(\rho^2+k^2a^2)^3} = 5.39 , \tag{2.21}$$

where we take $r_\mathrm{o}^2 = 13$. In the same way we get $B_{12}^{100} = 4.06$.

Table 2.4. Distances of nearest atoms for a test atom of {100}-surface of the fcc-structure [48, 69]

r_{ik}^2/a^2	first layer	second layer	third layer	forth layer
1	4	–	–	–
2	–	1	–	–
3	8	4	–	–
4	–	4	–	–
5	4	–	4	–
6	–	4	–	–
7	8	8	8	–
8	–	–	–	1
9	8	–	4	4
10	–	4	–	4
11	–	–	8	–
12	–	8	–	4

We use the same method for the {111} surface. Table 2.5 lists positions of nearest atoms for a test atom of this surface. In this case we get

$$B_6^{111} = 4.116 + \frac{10\pi}{\sqrt{3}} \cdot \frac{a^4}{r_o^4} + \frac{3\sqrt{3}\pi}{8k_o^2} = 4.44\,, \quad B_{12}^{111} = 3.07\,, \tag{2.22}$$

where $k_o = 5$.

Let us take the distance between nearest neighbors of the surface as it is in the Lennard-Jones crystal, $a = 0.975R_e$. Then, taking into account that for the {100}-surface the area per atom is $s = a^2$, and that for the {111}-surface is $s = a^2\sqrt{3}/2$, we get from formula (2.20) for the specific surface energy of these surfaces in the case of the Lennard-Jones interaction potential

$$\sigma_{100} = \frac{3.66D}{a^2}\,, \quad \sigma_{111} = \frac{3.59D}{a^2} \tag{2.23}$$

In the case of the Morse potential (2.12), the specific surface energies of the face-centered cubic lattice are given by

$$\sigma = D\left[\mathrm{e}^{\alpha R_e}G(\alpha a) - \frac{1}{2}\mathrm{e}^{2\alpha R_e}G(2\alpha a)\right]\,, \quad G(\alpha a) = \sum_k kn_{ik}\exp(-\alpha r_{ik})/s\,. \tag{2.24}$$

Here k is the number of a layer, i is the number of an atom in this layer, n_{ik} is a number of such atoms, r_{ik} is the distance from a test surface atom to this one, and s is the area per atom in the layer of the corresponding direction. The first terms of this series for the {100} and {111} surface planes have the form

$$G_{100} = 4\mathrm{e}^{-\alpha a} + 2\mathrm{e}^{-\alpha a\sqrt{2}} + 16\mathrm{e}^{-\alpha a\sqrt{3}} + 8\mathrm{e}^{-2\alpha a} + 16^{-2\alpha a\sqrt{5}}\,,$$
$$G_{111} = 3\mathrm{e}^{-\alpha a} + 3\mathrm{e}^{-\alpha a\sqrt{2}} + 12\mathrm{e}^{-\alpha a\sqrt{3}} + 6\mathrm{e}^{-2\alpha a} + 18\mathrm{e}^{-\alpha a\sqrt{5}}\,,$$

Table 2.5. Distances of nearest atoms for a test atom of the {111}-surface of the fcc-structure [48, 69]

r_{ik}^2/a^2	first layer	second layer	third layer	forth layer
1	3	–	–	–
2	3	–	–	–
3	6	3	–	–
4	–	3	–	–
5	6	6	–	–
6	3	–	1	–
7	6	6	6	–
8	–	3	–	–
9	3	6	6	–
10	6	–	–	–
11	6	3	6	3
12	–	6	3	3

Table 2.6. Parameters of a bulk crystalline of the fcc-structure for the Morse interaction potential between atoms [48, 69]

αa	αR_e	G_{100}	G_{111}	g_{100}	g_{111}	A	δ_{opt}
2	3.03	2.00	1.70	37.6	32.1	155	0.30
3	3.57	0.387	0.321	11.3	9.52	46.4	0.33
4	4.31	0.103	0.0832	5.53	4.57	22.4	0.35
5	5.17	0.0322	0.0255	3.64	2.94	14.5	0.39
6	6.10	0.0109	0.0^2850	2.85	2.28	11.3	0.41
7	7.06	0.0^2384	0.0^2296	2.48	1.95	9.69	0.43
8	8.03	0.0^2138	0.0^2106	2.25	1.74	8.71	0.45
10	10.01	0.0^3184	0.0^3139	2.08	1.59	7.96	0.48
12	12.00	0.0^4247	0.0^4186	2.02	1.52	7.66	0.49

and the first term of each expansion corresponds to a short-range interaction, i. e., it accounts for the interaction between nearest neighbors only.

The results of numerical calculations are given in Table 2.6 where the above sum is restricted by $r_{ik}^2 \leq 12$. In order to estimate the accuracy of this operation when we neglect the interaction between a test and further atoms, we compare the contribution of further atoms in the sum for ΔG with that from nearest neighbors of the first layer $G_{nn} = n_1 \exp(-\alpha a)$, where n_1 is the number of nearest neighbors of a test surface atom in the first layer. This value is $n_1 = 4$ for the $\{100\}$ plane and $n_1 = 3$ for the $\{111\}$ surface plane. We have in the case $\alpha r_o \gg 1$

$$\frac{\Delta G}{G_{nn}} = \frac{231}{\beta \alpha n_1} \exp\left(-2.6 \alpha a\right)$$

for $r_o = \sqrt{13}$. In particular, for $\alpha a = 3$ and for the $\{111\}$ surface plane this ratio is 0.01. Because we are guided by $\alpha a \geq 3$, below we neglect ΔG.

From this one can find the optimal specific energy per surface atom g, given in Table 2.6,

$$g(\alpha a) = \exp(\alpha R_e) G(\alpha a) - \frac{1}{2} \exp(2\alpha R_e) G(2\alpha a) \ , \quad \sigma(\alpha a) = \frac{D g(\alpha a)}{s} \ , \ (2.25)$$

where s is the surface area per atom.

2.6 Solid and Liquid Inert Gases Near the Triple Point

Ensembles of atoms of inert gases are the simplest systems whose properties are determined predominantly by interactions between nearest neighbors. Since one can treat atoms in these ensembles (apart from helium, of course) as classical, these systems obey the scaling law [32], so that specific (i. e. scaled) parameters of all these systems are identical and are expressed through the

parameters of the pair interaction potential given in Table 1.1. Next, all the solid inert gases have face-centered crystal lattices [52–55]. However they may exhibit the hexagonal close-packed structure in films formed on a special substrate [70–72].

Because a variable of any dimensionality may be constructed from three dimensional parameters (for example, [27, 29, 31]), we use the parameters D, R_e and m for inert gas atoms as given in Table 2.7 in order to construct their parameters. This Table is based on measured parameters of solid inert gases [73–79], and the degree of coincidence of their reduced values [32, 47, 61, 80] confirms the validity of the similarity law for these systems. Now we turn to examining the triple points and surface properties of these systems. In Table 2.7, a is the distance between nearest neighbors of the crystal lattice at zero temperature, $\rho_o = \sqrt{2}m/R_e^3$, m is the atomic mass, $\rho(0)$ is the crystal density at zero temperature, ρ_{sol} is the density of the solid inert gas at its triple point, ε_{sub} is the binding energy per atom for the solid inert gas at the melting point, V_{sol} is the volume per atom for a solid inert gas at the melting point. In addition, Table 2.7 contains the atomic binding energy in the crystal ε_{sol} determined on the basis of the Clausius-Clapeyron formula [4, 6], according to which the equilibrium pressure of saturated vapor $p_{sat}(T)$ over a plane solid surface is given by

$$p_{sat}(T) = p_o \exp\left(-\frac{\varepsilon_{sol}}{T}\right) \tag{2.26}$$

at a temperature T.

It follows from the data of Table 2.7 that the similarity law holds true for solid inert gases, with their fcc crystal lattices, within the accuracy of

Table 2.7. Parameters of solid inert gases and their reduced parameters near the triple point

	Ne	Ar	Kr	Xe	Average
a, Å	3.156	3.755	3.992	4.335	–
a/R_e	1.02	1.00	0.99	1.01	1.005 ± 0.013
$\rho(0)/\rho_o$	1.06	1.00	0.99	0.98	1.01 ± 0.04
ρ_{sol}, g/cm^3	1.444	1.623	2.826	3.540	
ρ_{sol}/ρ_o	0.899	0.920	0.926	0.952	0.92 ± 0.02
V_{sol}, cm^3/mol	14.0	24.6	29.6	37.1	
V_{sol}/R_e^3	0.77	0.77	0.76	0.74	0.76 ± 0.01
ε_{sub}, meV	22	80	116	164	
ε_{sol}, meV	22.5	80.2	112	152	
ε_{sub}/D	6.1	6.5	6.7	6.7	6.5 ± 0.3
ε_{sol}/D	6.2	6.5	6.5	6.5	6.4 ± 0.2
$\varepsilon_{sub}/\varepsilon_{sol}$	0.98	1.00	1.04	1.04	1.02 ± 0.03
p_{sol}, MPa	1800	4600	5600	4900	
$p_{sol}R_e^3/D$	89	124	130	104	110 ± 20

several percent. On the basis of these data one can choose the most suitable form to represent the interaction between atoms. Indeed, in the case of a short-range interaction that includes only nearest-neighbor interactions, we have $a = R_e$, $\varepsilon_{sub} = 6D$, whereas in the case of the Lennard-Jones interaction these parameters are equal to $a = 0.971R_e$, $\varepsilon_{sub} = 8.61D$ according to formula (2.8). One can see that solid inert gases are described better by a short-range interaction potential, and that a long-range interaction only influences the lattice parameters weakly. Hence the Lennard-Jones interaction potential that is used often for modelling condensed inert gases is not the best choice for this goal. It is better to use the truncated Lennard-Jones interaction potential in which interaction between remote atoms is ignored.

If we approximate the interaction potential of inert gas atoms by the Morse potential (2.12), in order to obtain the sublimation energy and the distance between nearest neighbors in accordance with the data of Table 2.7, it is necessary to take the Morse parameter $\alpha R_e = 8 \pm 1$. In this case the contribution of interaction of non-nearest neighbors to the total crystal energy is less than 10%. Thus, comparing parameters of the crystal of the close packed structure with those of real inert gas solids, one can conclude that interaction in solid inert gases is close to a short-range one.

We now determine the surface tension for solid inert gases assuming a short-range interaction between atoms. Then on the basis of the data of Table 2.6, we have $g_{100} = 2$ for $\{100\}$-surface plane and $g_{111} = 3/2$ for $\{111\}$-surface plane, and because the surface area per atom is a^2 for the $\{100\}$ plane and is $a^2\sqrt{3}/2$ for the $\{111\}$ plane, we obtain the surface tension for these planes

$$\sigma_{100} = \frac{2D}{a^2}\,, \quad \sigma_{111} = \frac{D\sqrt{3}}{a^2}\,,$$

In this case the distance between nearest neighbors a coincides with the equilibrium distance R_e for the diatomic molecule. On the basis of these formulas we get approximately for the surface tension of a face-centered cubic solid with a random direction of the surface

$$\sigma_{fcc} = \frac{1.9D}{a^2}\,, \tag{2.27}$$

with an accuracy of about 10%. This is approximately one half of that of the Lennard-Jones crystal according to formulas (2.23).

Thus the analysis of various model interaction potentials of atoms and their application for solid inert gases shows the validity of a short-range interaction for describing solid inert gases, in contrast to a widespread supposition that properties of dense and condensed rare gases are determined accurately by the Lennard-Jones interaction potential. Next, the use of the scaling law allows us to understand more deeply the nature of these systems, and can give additional

parameters for models. We will demonstrate this below, in the analysis of liquid and gaseous states of inert gases.

Table 2.8 contains some parameters of the solid and liquid inert gases near the triple point. Namely, $T_{\rm tr}$, $p_{\rm tr}$ are the temperature and pressure at the triple point, $\rho_{\rm liq}$ is the density of a liquid inert gas at its triple point, $\varepsilon_{\rm sub}$ is the binding energy per atom for the solid rare gas at the melting point, $V_{\rm liq}$ is the volume of a liquid inert gas per atom at the triple point, $\Delta S_{\rm fus}$ is the entropy variation per atom as a result of melting at the triple point, $\Delta H_{\rm fus} = T_{\rm tr}\Delta S_{\rm fus}$ is the fusion energy, $\Delta V = V_{\rm liq} - V_{\rm sol}$ is the specific volume variation resulted from the melting. As these data show, the mechanical energy $p_{\rm tr}\Delta V$ during melting is small comparison to the fusion energy $\Delta H_{\rm fus}$. This allows us to consider the phase transition of rare gases as a thermodynamical process which depends on just one variable. The parameter $T_{\rm tr}/(p_{\rm tr}V_{\rm sol})$ shows that the solid state of an inert gas differs significantly from its gaseous state for which this parameter is one.

One can approximate the phase curve of melting which separates the solid and liquid states near the triple point by the Simon equation [81, 82]

$$\frac{p - p_{\rm tr}}{P} = \left(\frac{T}{T_{\rm tr}}\right)^c - 1 \,, \tag{2.28}$$

where $p_{\rm tr}$, $T_{\rm tr}$ are the parameters of the triple point, and the parameters of this equation [82] are given in Table 2.8. Table 2.8 gives also the temperature

Table 2.8. Parameters of melting of inert gases near the triple point

	Ne	Ar	Kr	Xe	Average
$\rho_{\rm liq}$, g/cm^3	1.247	1.418	2.441	3.076	
$\rho_{\rm liq}/\rho_{\rm o}$	0.776	0.804	0.800	0.827	0.80 ± 0.02
$\rho_{\rm sol}(0)/\rho_{\rm liq} - 1$	0.159	0.144	0.157	0.151	0.153 ± 0.006
$T_{\rm tr}$, K	24.54	83.78	115.8	161.4	
$T_{\rm tr}/D$	0.581	0.587	0.578	0.570	0.579 ± 0.007
$p_{\rm tr}$, kPa	43.3	68.8	73.1	81.6	
$p_{\rm tr}/p_{\rm o}$, 10^{-3}	2.2	1.9	1.7	1.7	1.9 ± 0.2
$V_{\rm liq}$, cm^3/mol	16.2	28.2	34.3	42.7	
$V_{\rm liq}/R_{\rm e}^3$	0.911	0.879	0.884	0.855	0.88 ± 0.02
$T_{\rm tr}/(p_{\rm tr}V_{\rm sol})$	340	400	450	450	410 ± 50
$\Delta H_{\rm fus}/D$	0.955	0.990	0.980	0.977	0.98 ± 0.02
$\Delta S_{\rm fus}$	1.64	1.69	1.70	1.71	1.68 ± 0.03
$p_{\rm tr}\Delta V/\Delta H_{\rm fus}$, 10^{-4}	2.8	2.1	2.1	2.0	2.2 ± 0.4
P, MPa	102	209	235	258	
c	1.600	1.593	1.617	1.589	1.60 ± 0.01
$P/p_{\rm o}$	5.14	5.70	5.52	5.52	5.5 ± 0.2
$R_{\rm e}^3\,{\rm d}p/\,{\rm d}T$	13.2	15.0	14.0	15.1	14.3 ± 0.9
$(T_{\rm m} - T_{\rm o})/D$, 10^{-4}	1.7	1.3	1.2	1.1	1.3 ± 0.2

T_o that characterizes the melting curve at $p = 0$ and the reduced derivative that is large; that is, $R_e^3 \, dp/dT \gg 1$.

One can compare some reduced parameters of inert gases near the triple point with those for the Lennard-Jones system [36, 83]. The reduced temperature of the Lennard-Jones system at the triple point is $T_{tr}/D = 0.695$, the reduced density of the liquid Lennard-Jones system is $\rho_{liq}/\rho_o = 0.85$ at the triple point. These parameters for the Lennard-Jones interaction potential of atoms differ from those of inert gases, falling outside the accuracy limits of the Table 2.8 data.

In conclusion, we note that the scaling law is valid for solid and liquid inert gases near the triple point, with accuracy better than 10%. This shows the similar character of atomic interactions in such systems and these interactions are pairwise. Next, from the analysis of solid inert gases, it follows that interaction has a short-range character, i. e. nearest neighbors dominate the interactions. This fact allows as to use the properties of condensed inert gases as systems with short-range interaction so that the interaction of non-nearest neighbors may be ignored. Such a simple character of interaction gives us the possibility to use condensed inert gases for the analysis of other properties of atomic ensembles.

3

Thermodynamics of Dense Gases and Liquids

3.1 Equation of State for an Ensemble of Randomly Distributed Particles

Figure 3.1 gives the phase diagram for a macroscopic ensemble of particles. In this simple case we have three aggregate states of this system. We consider first the gas, liquid and transition regions of the phase diagram. In these forms, particles have random distributions in space, and in the limit of low particle density, the ideal gas equation of state holds true

$$p = NT \,, \tag{3.1}$$

where p is the gas pressure, T is the temperature, $N = 1/V$ is the particle number density, so that V is the volume per particle. Usually in chemistry when the total volume of the system V is included in this equation, it has the form

$$pV = nRT \,, \tag{3.2}$$

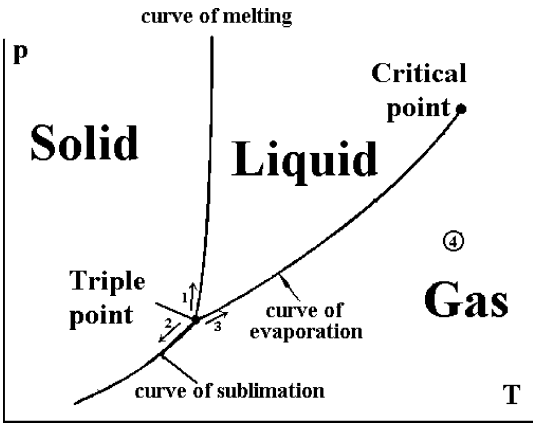

Fig. 3.1. The phase diagram of simple atomic systems. *1* – the melting curve, *2* – the sublimation curve, *3* – the evaporation curve

where n is the quantity of gas measured in mol, R is the gas constant given by

$$R = 82.06 \frac{\mathrm{cm}^3}{\mathrm{mol}} \frac{\mathrm{atm}}{\mathrm{K}} = 8.314 \frac{\mathrm{cm}^3}{\mathrm{mol}} \frac{\mathrm{MPa}}{\mathrm{K}} .$$

Below for simplicity we deal with the specific volume V that relates to one particle, for which the ideal gas equation of state has the form (3.1).

In situations in which nearest-neighbor interactions dominate, this characteristic can be incorporated into the equation of state. The popular and convenient equation of state for a dense gas or liquid in which particles are distributed randomly is the van der Waals equation [84–88] whose form in our notation is

$$\left(p + \frac{a}{V^2}\right)(V - b) = T . \tag{3.3}$$

Here a, b are the van der Waals constants, whose values for inert gases are given in Table 3.1. There are more accurate equations of state for gases [82, 86, 89, 90], but the van der Waals equation is used often due to its simplicity. It is very important that the van der Waals describes simultaneously the gaseous and liquid states and includes the critical point [91] in the gas-liquid behavior. A scaling analysis allows one to estimate the accuracy of this equation. Indeed, on the basis of this equation, one can determine parameters of the critical point beyond which the liquid and gaseous states are not distinguished. At the critical point we have [6, 88, 92]

$$\left(\frac{\partial p}{\partial V}\right)_T = 0 , \quad \left(\frac{\partial^2 p}{\partial V^2}\right)_T = 0 . \tag{3.4}$$

According to the van der Waals equation (3.3), the parameters of the critical point V_{cr}, p_{cr} T_{cr} are expressed through the parameters of this equation as

$$V_{\mathrm{cr}} = 3b , \quad p_{\mathrm{cr}} = \frac{a}{27b^2} , \quad T_{\mathrm{cr}} = \frac{8a}{27b} . \tag{3.5}$$

In particular, this leads to a simple relation between parameters at the critical point

$$\frac{T_{\mathrm{cr}}}{V_{\mathrm{cr}} p_{\mathrm{cr}}} = \frac{8}{3} . \tag{3.6}$$

The critical phenomena for a bulk ensemble of interacting atoms are determined by the character of atomic interaction [75, 76, 86, 93–98], and critical parameters in turn characterize the interactions between atoms. Table 3.2 contains the critical parameters of inert gases [79]. We use also the scaling law for critical parameters of inert gases assuming that these parameters are determined by atomic interactions in the attraction range of interaction as it is for the crystal latices of inert gases. The validity of the scaling law means also that the main contribution to these parameters follows from interaction of nearest neighbors. One can see that the accuracy of the scaling law for

Table 3.1. Parameters of van der Waals equation for rare gases [79] and their reduced values

	Ne	Ar	Kr	Xe	
a, 10^5 MPa $\cdot$ cm^6/mol^2	0.208	1.35	2.32	4.19	–
b, cm^3/mol	16.72	32.01	39.6	51.56	–
$a/(DR_e^3)$	3.27	3.57	3.59	3.57	3.50 ± 0.15
b/R_e^3	0.941	1.000	1.020	1.033	1.00 ± 0.04
V_{liq}/b	0.97	0.88	0.87	0.83	0.89 ± 0.06

Table 3.2. Critical parameters of inert gases [79] and their reduced values

	Ne	Ar	Kr	Xe	Average
T_{cr}, K	44.4	150.9	209.4	289.7	
p_{cr}, MPa	2.76	4.90	5.50	5.84	
V_{cr}, cm^3/mol	42	75	91	118	
ρ_{cr}/ρ_o	0.283	0.302	0.302	0.300	0.297 ± 0.009
φ_{cr}	0.209	0.224	0.224	0.222	0.220 ± 0.007
T_{cr}/D	1.05	1.06	1.04	1.02	1.04 ± 0.02
$p_{cr}R_e^3/D$	0.137	0.132	0.128	0.124	0.130 ± 0.006
V_{cr}/R_e^3	2.50	2.34	2.34	2.36	2.38 ± 0.08
$T_{cr}/(p_{cr}V_{cr})$	3.4	3.5	3.2	3.5	3.4 ± 0.1

interacting inert gas atoms yields uncertainties and errors of approximately several percent. According to the data of Table 3.2, the ratio $T_{cr}/p_{cr}V_{cr}$ is equal, on average, to 3.4 ± 0.1. Comparing this with formula (3.6), one can conclude that the accuracy of the van der Waals equation of gas state is characterized by the accuracy of tens of percent in the range in which interatomic interaction is significant.

The van der Waals equation (3.3) is the simplest equation of state for a simple ensemble of interacting particles with a random spatial distribution. The parameter a in this equation accounts for an additional contribution to the total pressure, compared with that of an ideal gas of point particles. This additional pressure is created by interactions with surrounding particles. The parameter b takes into account that the volume occupied by the gaseous particles themselves is inaccessible to the centers of mass of the gas atoms. In this way interaction between particles is included in the state equation for interacting articles with random spatal distribution.

In order to improve the accuracy of this equation near the critical point, we modify the van der Waals equation slightly, representing it in the form

$$\left[p + \frac{a}{(V + \Delta)^2}\right](V - b] = T\,. \tag{3.7}$$

In order to satisfy the relation $T_{\rm cr}/p_{\rm cr}V_{\rm cr} = 3.4$ at the critical point, we take $\Delta = 11b/6 = 11V_{\rm cr}/18$. In this form the modified van der Waals equation conserves its form for a gas when $V \gg \Delta$. Correspondingly, the definitions of the parameters a, b are preserved from the usual gas equation when gaseous conditions hold true. But near the critical point, this form brings in some corrections, and the connection between critical parameters with the parameters of the van der Waals equation is now

$$V_{\rm cr} = 6.67b\,, \quad T_{\rm cr} = 0.105\frac{a}{b}\,, p_{\rm cr} = 0.0046\frac{a}{b^2}\,. \tag{3.8}$$

Thus, the equation of state (3.7) describes inert gases and other gases with a short range interparticle interaction both in the dilute gaseous state and in the vicinity of the critical point.

Note that in the case of the Lennard-Jones interaction (2.6), the reduced parameters at the critical point are $V_{\rm cr}/R_{\rm e}^3 = 2.33$, $T_{\rm cr}/D = 1.316$, $p_{\rm cr}R_{\rm e}^3/D = 0.184$ according to [36, 83] and are equal to $V_{\rm cr}/R_{\rm e}^3 = 2.9 \pm 0.2$, $T_{\rm cr}/D = 1.34 \pm 0.02$ according to [99, 100]. As we can see, the above parameters, apart from the critical volume, differ from those of Table 3.2 for inert gases. In addition, the ratio $T_{\rm cr}/(p_{\rm cr}V_{\rm cr})$ is 3.1 for the Lennard-Jones system, which differs from 3.4 ± 0.1 (Table 3.2) for inert gases.

3.2 Equilibrium of Gas and Condensed States

If a gas is located above the solid or liquid surface and is in equilibrium with its solid or liquid, the equilibrium pressure of saturated vapor $p_{\rm sat}(T)$ over a plane solid and liquid surface is determined by the Clausius-Clapeyron formula that has the form [4, 6]

$$p_{\rm sat}(T) = p_{\rm sol}\exp\left(-\frac{\varepsilon_{\rm sol}}{T}\right)\,, \quad p_{\rm sat}(T) = p_{\rm liq}\exp\left(-\frac{\varepsilon_{\rm liq}}{T}\right)\,, \tag{3.9}$$

at a temperature T for the solid and liquid states correspondingly. The parameters $\varepsilon_{\rm sol}$ and $\varepsilon_{\rm liq}$ are the binding energies of surface atoms within accuracy up to thermal energy. Figure 3.2 represents the temperature dependence of the saturated vapor pressure of inert gases over a solid plane surface, constructed on the basis of [76, 79, 101, 102]. Table 3.3 gives the parameters of formula (3.9) for solid and liquid inert gases near the melting point. Together with this, Table 3.3 contains the energy $\varepsilon_{\rm ev}$ that is consumed on evaporation of one atom from the liquid surface at the boiling point $T_{\rm b}$. Because all these parameters are determined by the pair interaction potential between atoms, the reduced parameters coincide, within the accuracy of validity of the similarity law ($\sim 10\%$).

Note that the parameters $\varepsilon_{\rm sol}$ and $\varepsilon_{\rm sub}$, which are effectively the atomic binding energies for the solid state, must be almost identical, and the comparison in Table 3.3 confirms this. The same relates to the parameters $\varepsilon_{\rm liq}$

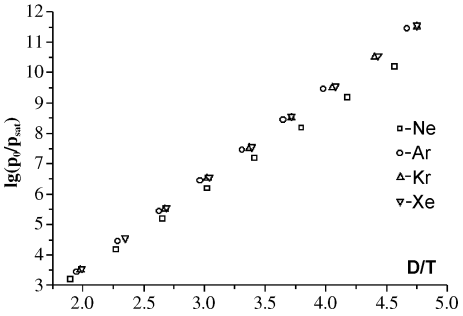

Fig. 3.2. The reduced saturated vapor pressure over a plane surface for inert gases in the solid aggregate state, according to experimental data.

Table 3.3. Parameters of saturated inert gases over plane solid and liquid surfaces near the melting point

	Ne	Ar	Kr	Xe	Average
$\varepsilon_{\rm liq}$, meV	19.4	69.6	95.6	134	
$\varepsilon_{\rm ev}$, meV	18.6	68	95	132	
$p_{\rm liq}$, MPa	410	1060	1030	1270	
$\varepsilon_{\rm liq}/D$	5.3	5.7	5.5	5.5	5.5 ± 0.1
$\varepsilon_{\rm ev}/D$	5.1	5.5	5.5	5.4	5.4 ± 0.2
$\varepsilon_{\rm ev}/\varepsilon_{\rm liq}$	0.96	0.98	0.99	0.98	0.98 ± 0.012
$p_{\rm liq}R_{\rm e}^3/D$	20	29	24	27	25 ± 4
$\varepsilon_{\rm sol}$, meV	22.5	80.2	112	158	
$\varepsilon_{\rm sol}/D$	6.2	6.5	6.5	6.5	6.4 ± 0.2
$\varepsilon_{\rm sub}/\varepsilon_{\rm sol}$	0.98	1.00	1.04	1.04	1.02 ± 0.03
$p_{\rm sol}$, MPa	1800	4600	5600	4900	
$p_{\rm sol}R_{\rm e}^3/D$	89	124	130	104	110 ± 20
$T_{\rm b}$, K	27.05	87.28	120.1	165.1	
$T_{\rm b}/D$	0.640	0.610	0.601	0.594	0.61 ± 0.02

and $\varepsilon_{\rm ev}$ which must be identical with the accuracy up to a thermal energy, though the value $\varepsilon_{\rm liq}$ is taken at the triple point, and the specific evaporation energy $\varepsilon_{\rm ev}$ is measured at the boiling point. It should be noted that all the reduced parameters of inert gases relate to an atomic system with short-range interaction.

Table 3.3 contains also the boiling point $T_{\rm b}$ for rare gases, i. e. the temperature at which the saturated vapor pressure is equal to 1 atm. It is necessary to recognize that the boiling point is not a parameter which must satisfy the scaling law. It is more appropriate to compare temperatures at which the saturated vapor pressure is proportional to a typical value $p_{\rm o}$ of this system; these are given in Table 2.2 for inert gases. Comparing the boiling points of various inert gases as temperatures corresponding to different reduced pressures, we get an error in the scaling law which is estimated to lie within the limits of several percent. This error corresponds to the Table 3.3 data.

According to the physical sense of the above energetic parameters, we have the following relation along the phase coexistence curve between the binding

energies per atom $\varepsilon_{\rm sol}$ (or $\varepsilon_{\rm sub}$) and $\varepsilon_{\rm liq}$ (or $\varepsilon_{\rm ev}$) for the solid and liquid states on the melting line

$$\varepsilon_{\rm sol} = \varepsilon_{\rm liq} + \Delta H_{\rm fus} \; ; \tag{3.10}$$

this is the definition of the fusion energy $\Delta H_{\rm fus}$. Table 3.4 contains the ratio $(\varepsilon_{\rm ev} + \Delta H_{\rm fus})/\varepsilon_{\rm sub}$, which is equal to one if the value $\varepsilon_{\rm ev}$ coincides with the atomic binding energy $\varepsilon_{\rm liq}$ for the liquid state.

One can adjust the difference of the parameters of the solid and liquid states near the triple point with the void model [45] of the liquid state, so that it differs from the solid state by formation internal voids. We simplify this model for a system of atoms with short-range interaction, taking the liquid state as a result of formation of internal vacancies inside the crystal lattice. Formation of internal vacancies leads simultaneously to a decrease of the atomic density and the binding energy per atom. From here, we now evaluate the relative number of internal vacancies that leads to the observed values of the liquid density and the binding energy of atoms in the liquid state.

Let us introduce the effective number q of nearest neighbors for the liquid state, a number equal to 12 for the solid state. This value is equal to [48, 80]

$$q = 24 - \frac{12\rho_{\rm sol}}{\rho_{\rm liq}} \tag{3.11}$$

within the framework of this model, where $\rho_{\rm sol}$, $\rho_{\rm liq}$ are the densities for the solid and liquid states.

Alternatively, one can find the number of nearest neighbors q' of an internal atom, or the coordination number, from the fusion energy under the assumption of a short-range interaction in this system, i. e. with range short enough that only nearest neighbors interact. Then we obtain for the average number of nearest neighbors

$$q' = \frac{12\varepsilon_{\rm liq}}{\varepsilon_{\rm sol}} = \frac{12}{1 + \frac{\Delta H_{\rm fus}}{\varepsilon_{\rm liq}}} \; , \tag{3.12}$$

where $\varepsilon_{\rm sub}, \varepsilon_{\rm liq}$ are the binding energies per atom for the solid and liquid states, and $\Delta H_{\rm fus}$ is the specific fusion energy.

Table 3.4 contains the numbers of nearest neighbors q and q' for liquid rare gases based, respectively, on density and on energy, in accordance with

Table 3.4. Parameters of liquid inert gases

	Ne	Ar	Kr	Xe	Average
$(\varepsilon_{\rm ev} + \Delta H_{\rm fus})/\varepsilon_{\rm sub}$	1.00	1.00	1.00	0.96	0.99 ± 0.02
q	10.10	10.27	10.11	10.19	10.17 ± 0.08
q'	10.07	10.15	10.14	10.19	10.14 ± 0.04

formulas (3.11) and (3.12). For this calculation we replace the atomic binding energy in the liquid state $\varepsilon_{\rm liq}$ at the melting point by the atomic binding energy $\varepsilon_{\rm ev}(T_{\rm b})$ at the boiling point, which leads to some increase of q. The data of Table 3.4 show that both methods give close values of numbers of nearest neighbors for liquid inert gases, confirming the validity of this rough model. Averaging over the various inert gases and the methods of its determination, we obtain the result $q = 10.15 \pm 0.06$. In addition, from these data it follows that one effective vacancy of a liquid inert gas at the melting point relates to 5.6 ± 0.2 atoms [80].

Thus, the melting process leads to simultaneous change of the atomic density and the binding energy per atom. This simple model in which formation of the liquid state from the solid is attributed to formation of effective vacancies – voids – inside the system, is thus justified by the data for melting of inert gases.

3.3 Liquid Surface Parameters

In contrast to the solid state, the random distribution of particles and their motion allows us to say that a macroscopic liquid is isotropic. Let us consider a spherical liquid drop consisting of $n \gg 1$ atoms. One can characterize atoms in this drop by the Wigner–Seitz radius

$$r_{\rm W} = \left(\frac{3m}{4\pi\rho}\right)^{1/3} , \tag{3.13}$$

where m is the atomic mass, and ρ is the bulk density. The average volume per atom is $4\pi r_{\rm W}^3/3$ in this case. Table 3.5 gives the values of the Wigner–Seitz radius for liquid inert gases near the triple point. Though the Wigner–Seitz radius (3.13) is defined for a bulk liquid, it can be used for a liquid cluster under assumption that the liquid drop density is independent of the cluster's size.

The surface energetic characteristic is the surface tension that is defined by formula (2.18) $\sigma = E_{\rm sur}/S$. It is determined by the character of atom–atom interaction in the surface layer of the liquid and the surface tension

Table 3.5. Parameters of liquid inert gas surfaces

	Ne	Ar	Kr	Xe	Average
$r_{\rm W}/R_{\rm e}$	0.654	0.639	0.641	0.627	0.64 ± 0.01
σ, erg/cm^2	5.65	13.55	16.33	18.83	
$\sigma R_{\rm e}^2/D$	0.93	0.97	0.95	0.95	0.94 ± 0.02
A, meV	18.1	61.4	84.8	111	
A/D	4.98	5.00	4.90	4.53	4.9 ± 0.2

follows from interaction of surface atoms with internal ones [89, 96, 103–106]. Figure 3.3 gives the dependence of the surface tension of liquid inert gases [105, 106] as a temperature function along the liquid-vapor equilibrium (or evaporation) curve, and Table 3.5 contains the surface tension of liquid inert gases near the triple point [105, 106]. The specific surface tension in Fig. 3.3 is given both on the basis of the surface tension at the triple point, and as constructed from three scaling parameters which are given for interacting inert gas atoms in Table 1.2.

Note that at the triple point the surface tension of liquid macroscopic atomic ensembles with short-range interatomic interaction (Table 3.5) which we ascribe to inert gases, is approximately one half of that for the solid state, that is given by formula (2.27). Next, according to the definition, the surface tension is zero at the critical point. Hence, the temperature dependence for the liquid surface tension along the evaporation curve of the phase diagram (Fig. 3.1) has the simple form seen in Fig. 3.3.

It is convenient to introduce the specific surface energy of a bulk liquid drop consisting of n atoms if we represent the total binding energy E of atoms of this drop in the form of expansion in powers of a small parameter $n^{-1/3}$. Then we have [107]

$$E = \varepsilon_{\rm o} \cdot n - An^{2/3} \,, \tag{3.14}$$

where the parameter $\varepsilon_{\rm o}$ is the binding energy of a bulk liquid per atom, and the parameter A is the specific surface energy of this drop. Evidently, for the liquid state, the value $\varepsilon_{\rm o}$ of formula (3.14) is close to the parameters $\varepsilon_{\rm liq}, \varepsilon_{\rm ev}$ given in Table 3.3. The specific surface energy A is connected with the surface tension σ, so that by definition the surface energy of a surface having an area S is equal to $E_{\rm sur} = \sigma S$. Comparing this relation with the definition for the surface energy of the liquid drop of radius r, we have

$$A = \frac{4\pi r^2 \sigma}{n^{2/3}} = 4\pi r_{\rm W}^2 \sigma \,, \tag{3.15}$$

Table 3.5 gives the specific surface energy A for the liquid state of inert gases near the triple point.

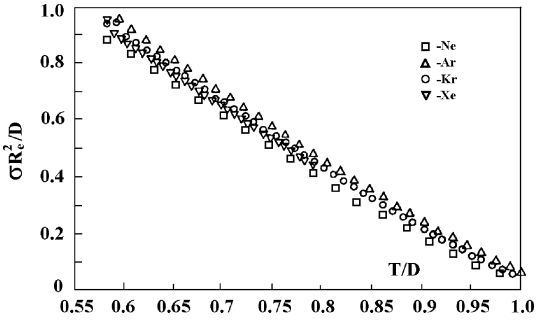

Fig. 3.3. The temperature dependence for the reduced surface tension of liquid inert gases according to measurements

3.4 Peculiarities of Similarity for Inert Gases

The scaling law for inert gases is a tool to find the parameters of macroscopic atomic ensembles with short-range atomic interaction. The scaling law is valid only within some limiting accuracy; we now give factors which determine this error. First, we assume the character of atom-atom interaction in dense and condensed systems does not depend on the overall form of the pair interaction potential but it is determined only by the parameters of that potential near the well bottom. Second, we ignore the contribution of long-range contributions to parameters under consideration. Third, we neglect all quantum effects. Fourth, we assume three-body interactions are unimportant for these systems. Evidently, these assumptions are valid within the accuracy of the scaling laws, i. e. within a few percent, for the rare gas systems.

One can decrease this error by increasing the number of parameters of the same dimensionality as those already introduced. Table 3.6 contains the ratios of such parameters. For the scaling analysis, we used the following parameters with the dimension of energy: $T_{\rm tr}, T_{\rm b}, T_{\rm cr}, \varepsilon_{\rm ev}$, and $\varepsilon_{\rm sub}$ (the notations are given above). The parameters $V_{\rm liq}, V_{\rm cr}, b$ have the dimension of the volume, and the parameters with dimension of pressure are $p_{\rm tr}, p_{\rm cr}$ and the constant a of the van der Waals equation. We do not include in this list the values $\varepsilon_{\rm liq}$, $\varepsilon_{\rm sol}$ assuming them to be identical to $\varepsilon_{\rm ev}, \varepsilon_{\rm sub}$, and the values $p_{\rm liq}, p_{\rm sol}$ which by definition correspond to a typical atomic number density and are characterized by a large error. The variety of physical parameters under consideration improves the scaling analysis and excludes occasional errors in this analysis.

Figure 3.1 gives the phase diagram of inert gases. We indicate on this diagram the information used for the scaling analysis. We take the parameters of the triple point $(T_{\rm tr}, p_{\rm tr}, V_{\rm sol}, V_{\rm liq})$ and the critical point $(T_{\rm cr}, p_{\rm cr}, V_{\rm cr})$. Next, we use the parameters of the three curves of phase coexistence, which are:

Table 3.6. Ratios of inert gas parameters of identical dimensionality at the critical and triple points

Ratio	Ne	Ar	Kr	Xe	Average
$T_{\rm b}/T_{\rm tr}$	1.808	1.801	1.805	1.795	1.802 ± 0.006
$T_{\rm cr}/T_{\rm b}$	1.64	1.73	1.75	1.76	1.72 ± 0.05
$\varepsilon_{\rm liq}/T_{\rm tr}$	9.2	9.6	9.6	9.6	9.5 ± 0.2
$\varepsilon_{\rm sol}/T_{\rm tr}$	10.6	11.2	11.3	11.4	11.1 ± 0.4
$V_{\rm cr}/V_{\rm liq}$	2.74	2.66	2.65	2.76	2.70 ± 0.06
$p_{\rm cr}/p_{\rm tr}$	64	71	75	72	70 ± 5
$\varepsilon_{\rm sol}/T_{\rm cr}$	5.9	6.2	6.2	6.3	6.2 ± 0.2
$\varepsilon_{\rm liq}/T_{\rm cr}$	5.1	5.4	5.3	5.4	5.3 ± 0.1
$\varepsilon_{\rm ev}/T_{\rm cr}$	4.9	5.2	5.3	5.3	5.2 ± 0.2
$\varepsilon_{\rm ev}/\varepsilon_{\rm liq}$	0.96	0.98	0.99	0.98	0.98 ± 0.01
$V_{\rm cr}/V_{\rm liq}$	2.74	2.66	2.65	2.76	2.70 ± 0.06
$V_{\rm cr}/b$	2.51	2.34	2.30	2.29	2.36 ± 0.10

P, c, the parameters of the Simon equation (2.28) for the solid-liquid phase transition, the parameters $\varepsilon_{\rm sol}$ and $\varepsilon_{\rm liq}$ for the solid-gas and liquid-gas phase transitions. The binding energies per atom $\varepsilon_{\rm sub}$ and $\varepsilon_{\rm ev}$ for the solid and liquid states are assumed to be close to the values $\varepsilon_{\rm sol}$ and $\varepsilon_{\rm liq}$ respectively. In addition, we use the parameters a and b of the van der Waals equation which describe the behavior of a gas of weakly interacting atoms. It is essential that the number of parameters used here is well over three – the minimum number of parameters on which basis one can construct a system of units. The variety of physical parameters under consideration improves the reliability of the above scaling analysis and effectively eliminates occasional errors in this analysis. This fact allows us also to determine that its accuracy is several percent. Table 3.6 contains the ratios of parameters of the same dimensionality.

The advantage of the scaling law is twofold. First, we obtain various parameters for an atomic ensemble with short-range interaction on the basis of the corresponding data for inert gases. Second, this allows us to find some parameters of macroscopic systems on the basis of these parameters for inert gases. The latter is demonstrated by the radon case. Indeed, on the basis of some parameters of macroscopic radon follow from the parameters of the pair interaction potential of the other rare gases [32]

$$D = 30.2 \pm 0.4\,\text{meV}\ , \quad R_{\rm e} = 4.68 \pm 0.04\,\text{Å}\ . \tag{3.16}$$

This allows us to find unknown parameters of radon systems on the basis of the scaling law [32].

From the analysis of the scaling law for condensed inert gases it follows that the actual interaction in these systems is close to that of a short-range interatomic interaction, in which nearest neighbor interactions dominate the behavior. One more important result of scaling near the triple point is the insensitivity of the pressure term for the solid-liquid phase transition (see Table 3.5). This allows us to account for the entropy contribution to the thermodynamical potentials, simplifying the analysis.

3.5 Scaling Law for Molecular Systems

One can expand the scaling analysis to some molecular systems. An example of such a system is a bound collection of fullerene molecules C_{60} [108]. The fullerene molecule has the form of a soccer ball, essentially a truncated icosahedron; the molecule's surface consists of 12 pentagons and 8 hexagons [109, 110]. When these molecules form a crystal, they interact primarily through the atoms of facing pentagons which allows us to consider the interaction between fullerene molecules through a pair interaction potential. This leads to the analogy with inert gas systems and makes it possible to determine the parameters of fullerene systems on the basis of the scaling analysis [108].

The same scheme may be used for systems of other "round" molecules such as SF_6 or CH_4 if interaction between these molecules depends only weakly on

molecule orientations. This is generally a situation found at temperatures high enough that the molecules can rotate freely in a dense system, solid or liquid. Table 3.7 contains parameters of dense and condensed systems of tetrafluoride molecules which are examples of "round" molecules. The values determined via the scaling law are given in parentheses. Although the scaling law is not as accurate in this case as it is for dense and condensed rare gases, it is nonetheless estimated at about 10%. This is the accuracy of restoring parameters. In addition, the ratios of values of parameters of the same dimensionality for these molecular systems can differ from those of rare gas systems.

The dissociation energies of the bonds within the molecules play no role in this analysis and do not appear. However the fact that molecules have internal vibrations that change with temperature can make the scaling parameters for molecules more temperature-dependent than those of atomic systems.

One more peculiarity of molecular systems relates to the boiling point which is defined as the temperature at which the saturated vapor pressure is 1 atm, an arbitrary value rather than a special one, in terms of basic physical properties. But the reduced pressure should depend on fundamental physical parameters of the system. Therefore using the boiling point as a scaling parameter of the system is problematic at best, and can be considered inap-

Table 3.7. Parameters of dense and condensed systems of AF_6 molecules [32]. Values in parentheses are determined on the basis of the scaling law

Molecule	MoF_6	SF_6	UF_6	WF_6	IrF_6	ReF_6	Average
T_g, K	291	223	338	276	317	292	
T_b, K	307	209	330	290	327	307	
T_{cr}, K	473	319	506	444	(500)	(470)	
ε_{ev}, meV	282	236	394	268	316	293	
ε_{liq}, meV	350	247	442	274	357	364	
ΔH_{fus}, meV	45	52	200	42	87	–	
p_{cr}, MPa	4.75	3.77	4.66	4.34	(8)	(4.6)	
V_{cr}, cm^3/mol	226	199	250	233	(140)	(240)	
a, 10^5 MPa $\cdot$ cm^6/mol^2	(13)	7.86	16.0	13.2	(9)	(14)	
b, cm^3/mol	(100)	88	113	106	(63)	(110)	
ρ_{liq}, g/cm^3	2.6	1.9	4.7	3.4	6.0	3.6	
V_{liq}, cm^3/mol	81	77	75	88	51	83	
T_{cr}/T_m	1.62	1.43	1.50	1.61	(1.58)	(1.61)	1.54 ± 0.09
T_{cr}/T_b	1.54	1.52	1.53	1.53	(1.53)	(1.53)	1.53 ± 0.01
ε_{ev}/T_b	10.7	13.1	13.8	10.7	11.2	11.1	12 ± 1
$\varepsilon_{ev}/\varepsilon_{liq}$	0.81	0.96	0.89	0.98	0.88	0.80	0.89 ± 0.07
ε_{ev}/T_{cr}	6.9	8.6	9.0	7.0	–	–	8 ± 1
$T_{cr}/(p_{cr}V_{cr})$	3.66	3.53	3.61	3.65	–	–	3.6 ± 0.1
V_{liq}/b	–	0.87	0.85	0.83	–	–	0.85 ± 0.02
V_{cr}/b	–	2.26	2.21	2.20	–	–	2.22 ± 0.03
V_{cr}/V_{liq}	2.8	2.6	3.3	2.7	–	–	2.8 ± 0.3
$\Delta H_{fus}/\varepsilon_{ev}$	0.16	0.22	0.51	0.16	0.27	–	0.26 ± 0.14

propriate. In the case of rare gases it is justifiable because the triple point pressure is significantly less than 1 atm. In the case of molecular gases this can be violated. Moreover, in the cases of SF_6 and UF_6, the melting point is higher than the boiling point, that is, the vapor pressure reaches 1 atm when the material is in the solid phase. Note also the absence of scaling for the fusion energy $\Delta H_{\rm fus}$ of these systems. This indicates a different character of the phase transition for systems under consideration.

We demonstrate this with the examples of macroscopic systems of tetrafluoride molecules [32]. Because they are "round" molecules, systems consisting of these molecules might be taken to be very similar to systems of rare gas atoms. But the scaling analysis shows only a partial identity between parameters of macroscopic inert gases and these molecular systems. In particular, we see the similarity in that the ratio $V_{\rm cr}/V_{\rm liq} = 2.70 \pm 0.06$ for rare gas systems corresponds to $V_{\rm cr}/V_{\rm liq} = 2.8 \pm 0.1$ for systems of tetrafluoride molecules, and the combination $T_{\rm cr}/(p_{\rm cr}V_{\rm cr}) = 3.4 \pm 0.1$ for rare gas systems coincides with the value $T_{\rm cr}/(p_{\rm cr}V_{\rm cr}) = 3.6 \pm 0.1$ for systems of tetrafluoride molecules. These are within the limits of the accuracy of these values, estimated as 10%. This means that expansion of the systems in the course of the transition from the triple point to the critical point is effectively identical for these atomic and molecular systems. However the ratio $\varepsilon_{\rm ev}/T_{\rm cr}$ is different for these systems indicating a different character of interaction for these phenomena. Note that the data used in Table 3.7 have only limited accuracy that increases the error in the scaling analysis.

4

Clusters with Short-Range Interaction

4.1 Configurations of Solid Clusters with Pairwise Atomic Interactions

In considering a cluster as a system of bound atoms, we base our approach on the concept that we can distinguish two types of cluster excitations, configurational and vibrational. Indeed, each local minimum of the potential energy surface of this cluster in a space of atomic coordinates corresponds to a specific, locally stable atomic configuration, i. e. to a certain configurational state of the cluster, with its own excitation energy and vibrational spectrum, up to energies that allow the cluster to move to other minima. Within this configurational characterization, the amount of vibrational motion around each local minimum characterizes the degree of thermal excitation of the cluster atoms. We assume that each configurational state establishes a thermal equilibrium for the degrees of freedom of the small-amplitude vibrations. This means that thermal equilibrium is established rapidly compared with transition from one local minimum to another on the cluster's potential energy surface. Thus, we suppose we can separate the configurational and vibrational excitations and characterize the latter by a definite temperature.

In the following discussion, we focus on pairwise interaction between atoms as the simplest form of interactions between bound atoms. In this case one can express the cluster's energy parameters in terms of parameters of the interaction potential of two isolated atoms. If we go to the limit of zero temperature in the sense of zero energy of thermal excitation, only configurational excitation of the cluster takes place; we analyze configurational excitation of the cluster in this manner. In considering clusters with pair interactions between atoms, we will be guided by clusters of inert gases for which the interaction potential between neighboring atoms is small compared to a typical energy of electronic excitation. Because of the weakness of interaction between these atoms, we ignore three-body and many-body interactions. This simplifies the problem and allows one to ascertain the role of short-range and long-range interactions for properties of a system of many bound atoms.

At zero and low temperatures clusters form regular structures, some of which can be found in bulk crystalline solids – but many others have structures that do not form lattices. One can construct clusters with lattice-based structures by cutting them out of a bulk crystal. There are 230 groups of symmetry for crystalline lattices [54], and hence such clusters can have any one of these depending on the character of interaction inside the system. Other clusters have structures based on polyhedra that do not form lattices. The most common for the systems we discuss here are icosahedra. These clusters have symmetries described by point groups, rather than by space groups. Clusters have greatest stability at sizes corresponding to completed structures composed of "magic numbers" of atoms. Magic numbers of solid clusters may be recognized from local maxima in mass spectra of clusters [111–117]. The optimal cluster structures themselves for these magic numbers have been determined from electron diffraction experiments [118–123], although the interpretation of electron diffraction spectra of clusters is associated with some challenges [124, 125]. Magic numbers reveal themselves through other cluster properties, e. g. ionization spectra [126–128]. Magic numbers are important in the way they influence various cluster properties; the binding energy of a surface atom, the ionization potential, the electron affinity and other cluster parameters have local maxima at magic numbers of atoms at which a cluster has the greatest stability. Magic numbers disappear in the liquid aggregate states because the parameters of these exhibit monotonic dependence on their size. This effect is sometimes used to determine the cluster melting point [129, 130].(We speak here of structural magic numbers; metal clusters can have magic numbers based on electronic shells; we do not consider these here.)As a demonstration of the size dependence of cluster mass spectra, Fig. 4.1 shows the mass spectra

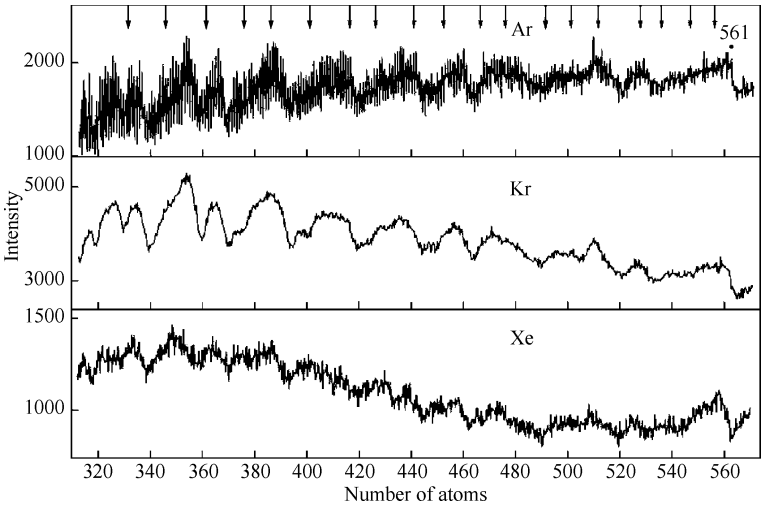

Fig. 4.1. Mass spectra of inert gas clusters resulting from free jet expansion [117]

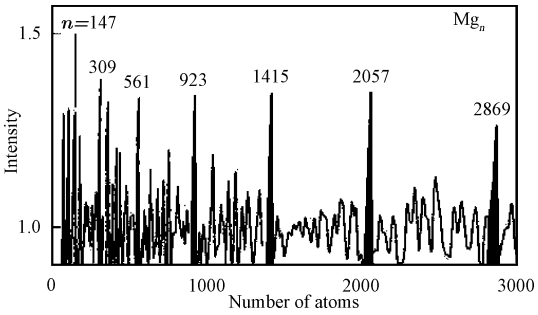

Fig. 4.2. Mass spectra of charged Mg clusters resulting from photoionization of a beam of neutral clusters [131]

of inert gas clusters produced by a free jet expansion of these gases through a nozzle [117]. In addition, Fig. 4.2 contains the mass spectrum of charged magnesium clusters formed as a result of photoionization of a beam of neutral clusters [131].

Below we restrict our discussion to two close-packed crystal structures that result from a pair interaction potential when the short-range interaction dominates a system of many bound atoms. These are of course the face-centered cubic and hexagonal crystal lattices. In these, each internal atom of the lattice has 12 nearest neighbors, the maximal possible number of nearest neighbors. We now examine these structures and analyze their energetic parameters.

4.2 Peculiarities of Close-Packed Clusters with Short-Range Interaction

We now consider ensembles of a finite number of bound atoms – clusters. At low temperatures one can ignore the kinetic energy of atoms, and therefore the total atomic energy of solid clusters is determined by their interaction. If the interatomic interaction is short-range, then in a close-packed structure, the distance between nearest atoms coincides with the equilibrium distance R_e, so that the binding energy of cluster atoms at zero temperature E_b is simply proportional to the total number Q of bonds between nearest neighbors and is thus

$$E_b = QD \,, \tag{4.1}$$

where D is the energy required to break one bond. Since the total energy of such a cluster is $E = -E_b$, one can introduce the surface energy of a cluster consisting of n atoms as

$$E_{sur} = E + 6nD \,,$$

since an internal atom of a close packed structure has 12 nearest neighbors, and each bond connects two atoms. In the limit of large clusters with $n \to \infty$, the cluster surface energy is proportional to the cluster surface that, in turn,

is proportional to $n^{2/3}$. In this limit, formula (3.14) has the asymptotic form

$$E = -6nD + E_{\rm sur} \ , \quad E_{\rm sur} = An^{2/3} \ , \tag{4.2}$$

where A is the specific surface energy that is connected to the change of unit area da_0 by the surface tension σ, whose values for liquid inert gases are given in Table 3.4.

$$dA = \sigma da_0 \ .$$

In reality, $E(n)$ has a nonmonotonic dependence on n due to the varying structures of incomplete cluster shells. One can ascribe this to the surface energy and define in this manner the function $A(n)$ as a nonregular function in accordance with formula (3.3). With such a definition, we have

$$A(n) = \frac{\varepsilon_{\rm o} n + E}{n^{2/3}} \ . \tag{4.3}$$

Like crystalline particles, whose optimal shape is determined by the character of atomic interactions, the configuration of cluster atoms is determined by parameters of the pair interaction potential in the case we consider. Atoms of a solid cluster are distributed over cluster shells or layers, and joining new atoms to a cluster proceeds through filling such shells or layers. In contrast to bulk particles, edge and vertex atoms give a non-negligible contribution to the cluster energy. Optimal atomic configurations correspond to complete cluster shells, layers or facets; these configurations of atoms correspond to magic numbers of atoms.

In the case of solid clusters or crystalline particles with an interaction of range short enough that we need consider only nearest neighbors, then, beyond formula (4.3), one can use one more expression for the surface energy based just on the number of nearest neighbors of each atom. Indeed, taking n_k as a number of atoms with k nearest neighbors, we obtain from formula (4.1) for the total binding energy of atoms [61]

$$E_{\rm sur} = \sum_k \left(6 - \frac{k}{2}\right) n_k \ . \tag{4.4}$$

Internal atoms have $k = 12$ nearest neighbors and do not give a contribution to the cluster surface energy; that is determined just by the surface atoms.

4.3 Constructing fcc-Clusters with Short-Range Interaction

Clusters of a chosen structure can be cut off from a crystal lattice of this structure – provided we choose a lattice, and not some other structure, such

as a polyhedron. Choosing a cluster with face-centered cubic (fcc) structure, we use as a basis the fcc crystal lattice. If we take either an atom of the fcc lattice or the middle of an elementary cell as the origin of the reference frame and place some atoms on axes of this reference frame, then, apart from the periodicity of the full lattice, the fcc crystal satisfies the corresponding symmetry, the reflections, rotations and inversions, so that this crystal lattice is in a sense conserved as a result of transformations (2.3). Note that we have two kinds of fcc crystal lattice, depending on the position of the reference frame origin. The origin can be placed either in the center of an elemental cell or at an atom of the lattice. Thus, there are two types of fcc-clusters, with and without a central atom.

Taking planes {100} as the planes of the reference frame, we obtain the 12 nearest neighbors of a test atom with coordinates xyz, whose coordinates are

$$x, y \pm \frac{a}{\sqrt{2}}, z \pm \frac{a}{\sqrt{2}}; \quad \text{or} \quad x \pm \frac{a}{\sqrt{2}}, y, z \pm \frac{a}{\sqrt{2}}\ ; \quad \text{or} \quad x \pm \frac{a}{\sqrt{2}}, y \pm \frac{a}{\sqrt{2}}, z\ , \tag{4.5}$$

where a is the distance between nearest neighbors. It is convenient to introduce reduced values for atomic coordinates expressing them in units $a/\sqrt{2}$. Then the coordinates xyz of each atom are whole numbers, and the 12 nearest neighbors of an atom with coordinates xyz have the following reduced coordinates

$$x \pm 1, y \pm 1, z\ ; \quad x \pm 1, y, z \pm 1\ ; \quad x, y \pm 1, z \pm 1 \tag{4.6}$$

by analogy with macroscopic systems, we define a cluster shell of a system of atoms whose positions are transformed into one another as a result of symmetry transformations (2.3). Then the coordinates of atoms of one shell differ by the sign of one or some coordinates and by transposition of coordinates zxy. We see that the maximum number of atoms in one shell is equal to $3 \cdot 2 \cdot 2 \cdot 2 = 48$. Next, a shell is completed if any transformation (2.3) transfers a test atom into an initially occupied position. The number of atoms that gives a cluster a completed outer atomic shell is a magic number.

Let us formulate the method to construct a cluster of fcc structure with a short-range interaction between atoms that allows one to find the cluster structure with the maximum binding energy for a given number of cluster atoms [56, 58, 61]. The optimal configuration of atoms corresponds to a maximum number of bonds according to formula (4.1). Determining the optimal configuration of cluster atoms by computer simulation can be a serious challenge because of the large number of local minima on the potential surface, but for clusters with short-range interaction, a simple algorithm allows one to find the optimal atomic configuration by comparing the cluster energies for a restricted number of favorable configurations. It is clear that the maximum number of bonds corresponds to compact atomic configurations and filled atomic shells. Therefore the favorable atomic configurations are based on a spherical core with completed shells and additive atoms outside these

Table 4.1. Nearest neighbors of adjoining atoms in the course of cluster growth [48, 56, 58, 61]. Nearest neighbors from previous shells are indicated in *bold* text, and nearest neighbors from the filling shell are indicated in *italic*

Shell	Nearest neighbors	Binding energy
222	**211 121 112** 213 123 132 231 321 312 233 323 332	3
123	**112 022 013** 114 024 033 *132* **222** *213* 134 224 233	4–6

shells, so that the optimal atomic configuration follows from comparison of the cluster energies at different positions of a subsidiary atom. This method gives both the most favorable configuration for a given number of atoms and the sequence of filling of atomic shells.

We demonstrate this method in Table 4.1 where the addition of new atoms to the cluster with completed shells is analyzed. The cluster core is the cuboctahedral cluster of 55 atoms with a central atom that is grown by addition of atoms in shells 222 and 123 so that atoms of these shells are located at distances $\sqrt{1}2$ and $\sqrt{1}4$ from the cluster center. The shell 222 contains 8 atoms, and the shell 123 consists of 48 atoms. From Table 4.1 it follows that the optimal way of cluster growth consists in addition of blocks of 7 atoms, so that each block includes 1 atom in the 222 shell and 6 atoms in the 123 shell. This character of cluster growth provides the maximum number of bonds for a cluster of a given size with incomplete atomic shells.

This method of cluster construction is not rigorous, but is pragmatic, since its basis is a concept that the structure of a cluster with the maximum number of bonds for a given size and a short-range atomic interaction is characterized by a compact distribution of atoms. This allows us to compare a restricted number of cluster configurations in the course of cluster construction by addition of one atom at a time.

4.4 Growth of fcc Clusters with Short-Range Atomic Interaction

We use the above method to construct a cluster of fcc-structure with short-range interaction between atoms. We take as a basis of the cluster an elementary cell of the fcc crystal lattice and add atoms to this cell to maximize the number of bonds. We thus carry out the construction in accordance with the above scheme whose demonstration is given in Table 4.1. But the initial cell

may be chosen in two ways. In the first case we take an atom of the fcc crystal lattice as the origin of the frame so the elementary cell is formed by this atom and its 12 nearest neighbors, i. e. the elementary cell is a cuboctahedron that consists of 13 atoms including one central one. Subsequent growth of the fcc-cluster results from addition of atoms that become nearest neighbors for surface atoms.

In the other way to construct a cluster, we take an elementary cell as an octahedron consisting of 6 atoms and add atoms to be nearest neighbors of these atoms. In this manner we use two methods to construct a fcc-cluster, with the central atom and without it. Thus we have two series of fcc-clusters with the optimal binding energy of atoms for each of them. Comparing the number of bonds for each series, one can choose the optimal structure from these two rows, for a given number of cluster atoms. The results of this operation are represented in Table 4.2 and 4.3 for fcc-clusters with the central atoms and without it.

Analyzing the data of Tables 4.2, 4.3, we conclude that the optimal cluster configurations in the course of cluster growth proceeds by adding blocks consisting of atoms of different shells. Comparing energies of structures with a central atom and without it allows us to choose the energetically optimal structure for a given size of fcc-clusters. The data of Tables 4.2 and 4.3 that the additive cluster blocks in the course of cluster growth are elements of plane facets. Magic numbers of clusters correspond to addition of individual blocks to a spherical core.

Table 4.2. The sequence of growth of fcc-clusters with a central atom for a short-range interaction of atoms [48, 56, 58, 61]

Filling shells	n	E_{sur}	Filling block
011	2–13	–	–
002(4)	13–19	42–54	–
112(3–5)+022(5)	19–55	54–114	110
013(4)	55–79	114–138	100
222(3)+123(4–6)	79–135	138–210	111
035(5)+004(4)+114(5)+024(6)	135–201	210–258	100
233(3–5)+224(5)+134(5–6)	201–297	258–354	111
015(4–6)+125(5–6)	297–369	354–402	100
044(5)+035(6)	369–405	402–414	110
006(4)+116(5)+026(6)	405–459	414–450	100
334(3–5)+244(5)+235(5–6)+ +145(5–6)+226(5)+136(6)	459–675	450–594	111
055(5)+046(6)	675–711	594–606	110
017(4–6)+127(5–6)+037(6)	711–807	606–654	100
008(4)+118(5)+028(6)	807–861	654–690	100
444(3)+345(4–6)+255(5)+336(5)+ +246(6)+156(5–6)+237(5–6)+147(6)	861–1157	690–858	111

Table 4.3. The sequence of growth of fcc-clusters without a central atom for a short-range interaction of atoms [48]

Filling shells	n	E_{sur}	Filling block
001	1–6	–	–
111(3)	6–14	24–48	111
012(3–6)	14–38	48–84	110
003(4)	38–44	84–96	100
122(3–5)+113(5)+023(5–6)	44–116	96–180	110
014(4–6)	116–140	180–204	100
223(3–5)+133(5)+124(5–6)+034(5–6)	140–260	204–312	111
005(4)+115(5)+025(6)	260–314	312–348	100
016(4–6)	314–338	348–372	100
333(3)+234(4–6)+225(5)+			
+144(5)+135(6)+126(5–6)	338–538	372–516	111
045(5–6)+036(6)	538–586	516–528	110
007(4)+117(5)+027(6)	586–640	528–564	100
018(4–6)	640–664	564–588	100
344(3–5)+335(5)+245(5–6)+236(5–6)+			
+155(5)+146(6)++227(5)+137(6)	664–952	588–756	111
056(5–6)+047(6)	952–1000	756–768	110

Thus, one can formulate the method of assembling of a fcc-cluster with short-range interaction. The main goal of this cluster construction is to analyze compact atomic configurations and to choose, for a given number of atoms, the configuration that corresponds to the maximum number of bonds between nearest neighbors. Because such an idealized growing cluster has almost spherical form, the number of filling shells is restricted for moderately large clusters. In reality, growth of a fcc-cluster with short-range interaction proceeds through growth of individual facets, and magic numbers correspond to filling of each cluster facet. The same method of cluster construction may be used if a long-range interaction is present. However this additional interaction can change intermediate magic cluster numbers.

In Tables 4.2 and 4.3, we use the surface cluster energy as the energetic cluster parameter, in accordance with formula (4.2), taking into account that the maximum binding energy corresponds to the minimum surface energy. One can introduce the specific surface energy on the basis of formula (4.3). Then the minimum values of the specific surface energy corresponds to magic numbers of cluster atoms. According to the data of Tables 4.2 and 4.3, the magic numbers of cluster atoms correspond to filling of each atomic block.

4.5 Regular Clusters of Close-Packed Structures

Bulk particles and clusters of a given crystalline structure can form different geometric figures. The optimal structure depends on the parameters of the pair interaction. Energy parameters of a cluster with incomplete shells are sensitive to the filling of certain shells or layers. The optimal cluster structure results from competition of various cluster shapes even when only one crystalline structure is realized. The competition of cluster shapes for structures of close packing is the object of this analysis.

In the course of growth, a cluster passes through completed structures; now we consider the geometric figures that can be realized for clusters with pairwise interactions. Regular figures of close-packed structures can have either fcc or hexagonal structures. In the case of the fcc structure, the corresponding geometric figure has cubic symmetry $\mathbf{O_h}$. This means that any transformation (2.3) transfers a test atom of this cluster to a position that is occupied by another atom (or by this one). In the case of the hexagonal structure, the geometric figure has a lower symmetry, whose atomic configuration is conserved as a result of transformation (2.4).

If we take a {111} plane, in which each atom has 6 nearest neighbors as a basis of the hexagonal lattice, the z axis is directed perpendicular to this plane, and Φ is the polar angle for the polar axis z. According to this symmetry, the maximum number of atoms of one shell is equal to $2 \cdot 6 = 12$ for a cluster with hexagonal structure. Optimal configurations of atoms in solid hexagonal clusters may be found by the same method we used for the fcc solid clusters.

In order to construct geometric figures of solid clusters that are restricted by plane facets, we consider first planes which can be formed for a close-packed structure. In the case of the fcc structure, there are three types of planes, {100}, {110} and {111}. There are 6 different planes of {100}-type, 12 planes of {110}-type, and 8 planes of {111}-type. (We of course consider parallel planes as equivalent here.) Thus, the maximum number of plane facets of a crystalline particle of the fcc-structure is 26. This determines the variety of geometric figures for clusters of the fcc symmetry. The planes of the fcc crystal lattice are given in Fig. 2.2.

Let us evaluate the number of nearest neighbors for a surface atom of each plane of the fcc structure. Each surface atom of a {100}-plane has 4 nearest neighbors from the surface layer and 4 nearest neighbors from the previous one, i. e. a surface atom of a {100) plane has 8 nearest neighbors. In the same manner we find that each surface atom of a {110} plane has 7 nearest neighbors, and each surface atom of a {111} plane has 9 nearest neighbors. From this it follows that geometric figures with surface facets of directions {111} and {100} are energetically more favorable for fcc particles with pair interactions. Hence below we restrict ourselves to geometric figures whose facets are directed along these planes (see Fig. 2.2).

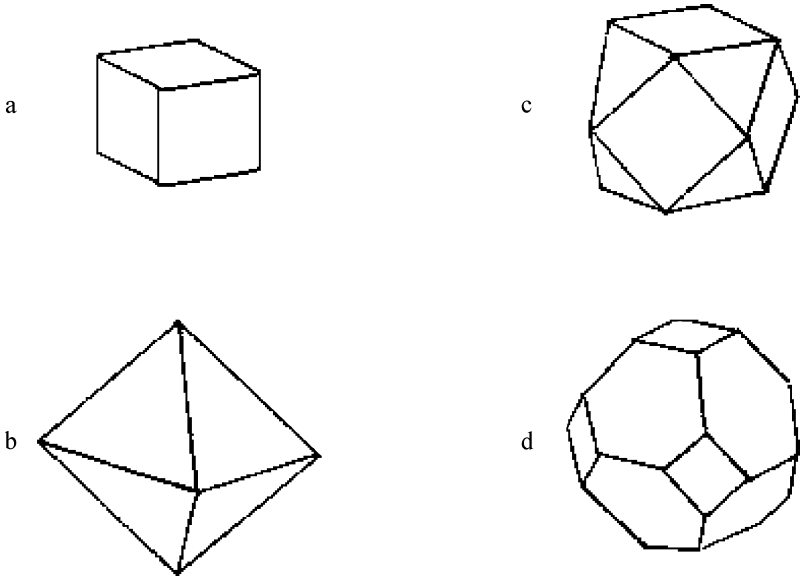

Fig. 4.3. Regular geometric figures formed by bound atoms: **a** – cube; **b** – octahedron; **c** – cuboctahedron; **d** – truncated octahedron. All the last figures can be formed from the cube by cutting off regular pyramids near the cube vertices

One can construct families of identical figures which differ by size. Some spread cluster figures are given in Fig. 4.3. Taking the edge length of a geometric cluster figure to be ma, where a is the distance between nearest neighbors, we call m as the figure number in the series. One can express the energetic cluster parameters for a given family through a number m of the cluster in

Table 4.4. Parameters of the families for geometric figures of clusters of close packed structures with a short-range interaction between atoms [48, 132, 133]

Figure	n	$E_{\rm sur}/D$	$E_{\rm b}/D$	A_∞/D
Octahedron	$\frac{2}{3}m^3+2m^2$ $+\frac{7}{3}m+1$	$6m^2+12m+6$	$4m^3+6m^2+2m$	7.86
Cuboctahedron	$\frac{10}{3}m^3+5m^2$ $+\frac{11}{3}m+1$	$18m^2+18m+6$	$20m^3+12m^2+4m$	8.07
Trunc. octahedron	$n^{\rm oct}$ $-k(k+1)(2k+1)$	$E_{\rm sur}^{\rm oct}-6k(k+1)$	$E_{\rm b}^{\rm oct}-12k^2(k+1)$	–
Reg. trunc. octahed.	$16k^3+15k^2$ $+6k+1$	$48k^2+30k+6$	$6k(16k^2+7k+1)$	7.56
Hexahedron	$4m^3+6m^2$ $+4m-7$	$21m^2$ $+21m-12$	$24m^3+15m^2$ $+3m+5$	8.33
Trunc. hexahedron	$28m^3+21m^2$ $+6m+1$	$72m^2+36m+6$	$168m^3+90m^2$	7.81

this family. We start from the octahedral cluster (Fig. 4.3a) whose surface consists of 8 regular triangles. An octahedral cluster can be either centered or non-centered. The 8 vertex atoms of such a cluster have the coordinate $0, 0, m$ or can be obtained from this as a result of transformations (2.3). Table 4.4 contains the numbers of atoms for this cluster depending on a number m of the series, the surface energy E_{sur} of the cluster, and the total binding energy E_{b}. The total cluster energy is connected with its surface energy by formula (4.2). The surface of the cuboctahedral figure (Fig. 4.3b) consists of 6 squares and 8 equilateral triangles. Table 4.4 gives its parameters for a short-range interaction. In contrast to octahedral clusters, all the cuboctahedral clusters have a central atom.

The truncated octahedral structure is formed from the octahedral one by cutting off 6 regular square pyramids near its vertices. A cluster so formed is characterized by the index m, the number of the octahedron in its family and by the index k, the number of atoms on each pyramid's basal edge. Parameters of this cluster figure for a short-range interaction are given in Table 4.4 [48, 61, 132, 134], and the parameters n^{oct}, $E_{\text{sur}}^{\text{oct}}$, $E_{\text{b}}^{\text{oct}}$ refer to the octahedral cluster of the m-th series. The regular truncated octahedron is the optimal structure for a short-range interaction. Its surface consists of 8 regular hexagons and 6 squares and contains 36 edges of identical size. For the family of regular truncated octahedrons we have $m = 3k$ [48, 61, 132, 135], and the parameters of this figure are given in Tables 4.2, 4.3.

Favorable structures of fcc clusters with a short-range interaction have the structure of a truncated octahedron, and Table 3.7 gives completed structures of such fcc clusters in the course of their growth. Almost all these structures consisting of hundreds atoms are truncated octahedrons. The regular truncated octahedron is an optimal cluster structure also if long-range interaction is important. Note that the specific surface energy A given by formulas (3.15), (4.3) is the energetic characteristic of a solid cluster. For optimal structures this quantity has minimal values. This parameter is given in Table 4.4 for infinite clusters of the structures under consideration. For the truncated octahedron this value is equal to [48]

$$A_\infty = 3 \cdot (18)^{1/3} * \frac{(1 - k^2/m^2)}{(1 - 3k^3/m^3)^{2/3}} \,. \tag{4.7}$$

As follows from Table 4.5, the regular truncated octahedron is the optimal figure for large clusters with fcc structure.

The hexagonal structure is the other close-packed structure in which each internal atom of the lattice has 12 nearest neighbors. This structure may be analyzed for clusters in the same manner as we did for clusters of the fcc structure. We illustrate this structure constructing the cuboctahedral cluster of 13 atoms. Indeed, taking a plane in the direction $\{111\}$ as a base of this cluster, we place a regular hexagon of atoms with a central atom on this plane. The edge of this pentagon is a, the equilibrium distance for a pair atomic interaction. Next, three atoms are located in a layer parallel to and

Table 4.5. Parameters of filled structures of fcc-clusters with a short-range interatomic interaction within the framework of the structure of a truncated octahedron. The *asterisk* marks the minimum of $A(n)$ as a function of magic numbers

n	A	m,k	n	A	m,k
201*)	7.519	6,2	1000	7.680	–
260	7.659	7,3	1072*)	7.561	11,3
314*)	7.533	7,2	1126	7.650	11,2
338	7.666	7,1	1139	7.647	12,5
369	7.814	–	1157	7.785	–
405	7.563	8,3	1289*)	7.548	12,4
459*)	7.562	8,2	1385	7.581	12,3
538	7.801	–	1504	7.587	13,5
586*)	7.540	9,3	1654*)	7.550	13,4
640	7.594	9,2	1750	7.602	13,3
664	7.699	9,1	1804	7.693	13,2
675	7.719	–	1865	7.643	–
711	7.607	10,4	1925	7.561	14,5
807*)	7.545	10,3	2075*)	7.561	14,4
861	7.624	10,2	2171	7.622	14,3
885	7.746	10,1	2190	7.614	15,6
952	7.812	–	2225	7.710	14,2
976	7.561	11,4	2406*)	7.552	15,5

located above and at a distance $a\sqrt{2/3}$ from the original plane, and then the same kind of layer is constructed below the basic layer. Atoms are placed in these layers in hollows of triangles and form regular triangles such that atoms of new layers form a regular triangle whose edge equals a. There are two possibilities for the relative location of atoms of the upper and lower layers. If the projections of atoms of the upper and lower layers onto the central layer plane do not coincide, these atoms form a cuboctahedron. This cluster has the fcc structure and is conserved as a result of transformations (2.3). If the atomic projections coincide, the figure formed is a hexahedron. This cluster has hexagonal symmetry and is conserved under transformations (2.3). Figure 4.4 shows the difference between the cuboctahedral and hexagonal structures for a cluster consisting of 13 atoms.

Clusters with hexagonal structure contain a central atom in a basic layer and a system of regular hexagons is formed around a common center located at the central atom. Atoms of subsequent layers are located in the hollows of triangles formed by atoms of preceding layers, and the distance between nearest layers is $a\sqrt{2/3}$, as in the above case of the simplest hexagonal cluster of 13 atoms. Taking a system of regular hexagons in the base layer and placing atoms of a new layer in hollows between three atoms of the previous layer, one can obtain a hexahedron that is conserved under transformations (2.3) and find its energetic parameters for a short-range interaction of atoms [58, 48, 59].

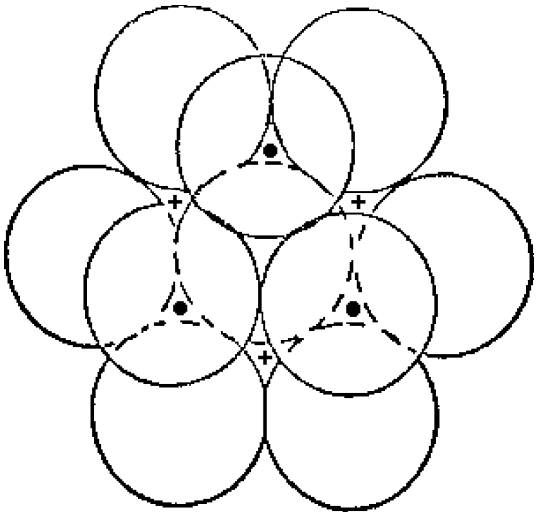

Fig. 4.4. Close-packed structures of a cluster consisting of 13 atoms with the base plane in the {111} direction. If projections of atoms of the upper and lower layers onto the basic plane coincide (atoms of the lowest layer are *dark circles*), the hexahedron is formed as a result of joining centers of nearest-neighbor surface atoms. This figure shows the hexagonal structure. If the above projections are different (atoms of the lowest layer are *crosses*), the cuboctahedron is formed as a result of joining centers of nearest surface atoms. This figure is an elementary cell of the face-centered cubic lattice

Parameters of the family of hexahedrons are given in Table 4.4. We construct also a truncated hexahedron by removing some layers of the hexahedron. For parameters of Table 4.4 we take a $2m$-th hexahedron and remove m upper and lower layers. From this, a large truncated hexahedron is a more favorable figure, but the energetics of large hexagonal clusters are worse than those of fcc clusters because of the former's lower symmetry. Next, in contrast to fcc clusters in which all the surface atoms are located on plane facets, atoms of lateral sides of hexagonal clusters do not form planes.

Thus, the hexagonal cluster structure competes with the fcc structure for small clusters [136], but for these systems, the icosahedral structure is more favorable than either of the close-packed lattice structures, and therefore the competition of fcc and hexagonal cluster structures is not significant [48, 59]. Because of its higher symmetry, the fcc cluster surface is more favorable for large cluster sizes than the hexagonal, and therefore large clusters of the fcc structure are characterized by a higher atomic binding energy than hexagonal clusters. The competition of the hexagonal and fcc structures becomes stronger for bulk clusters or crystals when surface effects are not dominant and the competition depends on the character of atomic interactions. In particular, in the case of the Lennard-Jones crystal, the hexagonal structure is favorable, but the difference of the sublimation energies

per atom is small ($\sim 0.2\%$) [66]. In reality, inert gas crystals have the fcc structure.

One interesting puzzle that we discuss again at the end of this chapter is this. If we think of growing a close-packed structure by adding layer after layer to the original basal plane with its close-packed array, then might not the layers sometimes add in a random fashion? Call the first, basal layer A, and the next layer B, with its atoms in the interstices of the first layer. We have just seen that the hexagonal structure corresponds to a set of planes ABAB ..., while the fcc structure needs a third arrangement that we call C, so the fcc pattern is ABACABAC ... The puzzle is this: Under what circumstances may we see a random arrangement, e. g. ABABACABACAC ...? The structure would be close-packed but would not be a conventional lattice, of course. In addition, if we conserve this order of planes in this direction, there are some lattice defects in other direction of 8 possible directions of 111-planes.

4.6 Icosahedral Clusters

The number of ordered cluster structures is greater than the number of types of crystal lattices. Clusters with a pair interaction of atoms, including clusters of inert gas atoms, demonstrate this fact vividly. Indeed, clusters with short-range interaction, like bulk systems of bound atoms, can have a close-packed structure that corresponds to the fcc or hexagonal crystal lattices, but such clusters also admit the icosahedral structure that cannot be realized for bulk crystals because it does not admit the translational symmetry required for a lattice. Thus, clusters with pair interactions give a convenient example for understanding the structural and energetic parameters of clusters of some kinds of real atoms.

The icosahedral cluster structure (see Fig. 4.5) can be related to close-packed structures because each internal atom has 12 nearest neighbors. But in the close-packed lattice structures, all the distances between nearest neighbors of a bulk system are identical, whereas in the case of the icosahedral structure there may be two different distances between nearest neighbors. Therefore the icosahedral structure cannot compete with the close-packed structures at the limit of a bulk atomic system, and, as we just noted, this structure cannot be realized in a bulk crystal lattice. But this structure is compact enough because all 20 surface triangles of the completed icosahedral cluster are {111} planes with the maximum number of nearest neighbors for surface atoms. Hence the icosahedral structure is favorable for moderate sizes of clusters, up to thousands of atoms in the case of the rare gas clusters.

An icosahedral cluster as a geometric figure [137] has 12 vertices located at identical distances from the center. The icosahedron has a high symmetry $\mathbf{Y_h}$ [57] characterized by 6 five-fold axes passing through the icosahedron

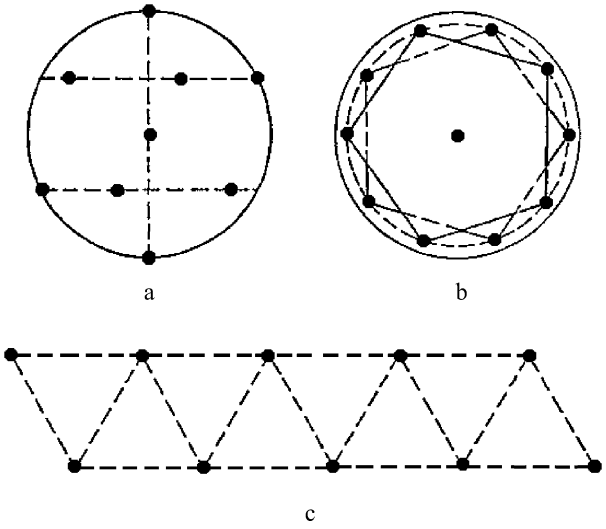

Fig. 4.5. The icosahedral figure. **a** – a side view, **b** – a view from above, **c** – a developing view

center and two opposite vertices located on a sphere; rotation of the icosahedron by angle $2\pi/5$ around any symmetry axis conserves this figure. Along with this, the icosahedron is conserved as a result of rotation by the angle $\pi/5$ around one of these axes and reflection with respect to the plane perpendicular to the axis and passing through the icosahedron center. Another symmetry of the icosahedron corresponds to the inversion operation $x \longleftrightarrow -x; y \longleftrightarrow -y; z \longleftrightarrow -z$. Finally, the icosahedron has symmetry of reflection with respect to the planes that pass through any given symmetry axis and two vertices of pentagons. This also is valid for any axis of the icosahedron. Thus the icosahedron is a geometric figure of high symmetry.

In order to construct the simplest icosahedral cluster consisting of 13 atoms, we place one atom in the center and construct around this atom a sphere of a radius R where the other 12 atoms are located in the following way. Two atoms are placed at the sphere's poles, so that they are connected by a line that passes through the center. The other 10 atoms form two pentagons whose planes are perpendicular to this line. The pentagons are inscribed in circles that are sections of planes and the sphere, and the pentagon's vertices are rotated by an angle of $\pi/5$ with respect to each other. These circles form a cylinder whose axis is the icosahedral axis. Joining the nearest vertices of the icosahedron, we obtain 20 equivalent equilateral surface triangles. This means that the distances between nearest neighbors on the sphere are identical, and each surface atom has 5 nearest neighbors on the sphere. Nearest neighbors of polar atoms on the sphere are atoms of the nearest pentagon, and each atom of a pentagon has as nearest neighbors on the sphere one atom of the nearest pole, two nearest atoms of its own pentagon, and two atoms of the neighboring pentagon. The distance, R_o, between nearest neighbors on the

sphere and the distance, R, from the center to surface atoms are connected by the relation

$$R = \sqrt{\frac{\sqrt{5}}{8}(1+\sqrt{5})} = 0.951 R_{\rm o} \; . \tag{4.8}$$

All the atoms on the surface of this cluster are equivalent; only central atom is unique. Let us find the specific binding energy of atoms for a bulk icosahedral cluster with only nearest-neighbor interactions. The method of determining the cluster binding energy takes into account that the equilibrium distance $R_{\rm e}$ for the pair interaction potential is close to distances between cluster nearest neighbors $R_{\rm o}$ and R, so that the total binding energy can be expanded in powers of a corresponding small parameter. This allows us to find the total binding energy of atoms in the icosahedral cluster on the basis of this expansion. Indeed, let the number of bonds between nearest-neighbor atoms of different shells to be a and of nearest-neighbor atoms of the same shell to be b. Assuming the distance between atoms of these groups to be R and $R_{\rm o}$, respectively, for clusters with completed shells, we have for the total binding energy $E_{\rm b}$ of cluster atoms

$$\begin{aligned} E_{\rm b} &= -aU(R) - bU(R_{\rm o}) \\ &= (a+b)D - \frac{1}{2}U''(R_{\rm e})\left[a(R-R_{\rm e})^2 + b(R_{\rm o}-R_{\rm e})^2\right] \; , \end{aligned}$$

where $U(R)$ is the pair interaction potential of atoms in the cluster, and $R_{\rm e}$ is the optimal distance that corresponds to the pair binding energy maximum. The latter leads to the equation for the optimal distance

$$a(R-R_{\rm e})\frac{\partial R}{\partial R_{\rm o}} + b(R_{\rm o}-R_{\rm e}) = 0 \; ,$$

that gives [80]

$$\frac{R_{\rm e}}{R_{\rm o}} = \frac{0.904a+b}{0.951a+b} \; , \quad E_{\rm b} = (a+b)D - 0.012U''(R_{\rm e})\frac{abR_{\rm e}^2}{0.904a+b} \; . \tag{4.9}$$

This method, based on the close values of distances R and $R_{\rm e}$ between nearest neighbors in the icosahedral cluster, allows us to analyze the cases of incomplete cluster shells [138, 136]. We will demonstrate this method for a bulk icosahedral cluster with interaction between nearest neighbors only, when the cluster binding energy per internal atom is given by

$$\varepsilon = -3U(R) - 3U(R_{\rm o}) \; , \tag{4.10}$$

where $U(r)$ is the interaction potential of two atoms at a distance r between them. We use the relation that each internal atom has 6 nearest neighbors of the same layer at a distance $R_{\rm o}$, 3 nearest neighbors of the previous layer and 3 nearest neighbors of the following layer at a distance $R = 0.951 R_{\rm o}$. We

take into account that each bond is shared between two atoms. Expanding this specific energy near the equilibrium distance R_e, we obtain from formula (4.10)

$$\varepsilon = 6D - \frac{1}{2}U''(R_e) \cdot \left[(R_e - R)^2 + (R_e - R_o)^2\right] ,$$

and, optimizing this energy, we have

$$R_e - R + \frac{\partial R}{\partial R_o}(R_e - R_o) = 0 .$$

From the last relation it follows that $R = 0.975R_e$, and $R_o = 1.025R_e$, so that the asymptotic expression for the specific binding energy has the form

$$\varepsilon_o = 6D - 0.00189U''(R_e) . \tag{4.11}$$

The surface energy per atom for a short-range interaction is $\varepsilon_{sur} = -\frac{3}{2}U(R)$. The number of surface atoms of an icosahedral cluster is $10m^2$, where m is the number of filled layers of the completed icosahedral cluster, and the total number of cluster atoms in this approximation is $n = 10m^3/3$. From this we obtain the cluster surface energy

$$E_{sur} = -15m^2U(R) = -15 \cdot (0.3n)^{2/3}U(R) . \tag{4.12}$$

This gives the cluster specific surface energy

$$A = 15 \cdot (0.3)^{2/3}\left[D - \frac{1}{2}(R - R_e)^2U''\right] = 6.72D - 0.0022U'' . \tag{4.13}$$

4.7 Competition of Icosahedral and Close-Packed Structures

Thus, since two distances between nearest neighbors are realized in an icosahedral cluster, its energetic parameters depend also on the shape of the interaction potential between atoms – nearest neighbors. Because these two distances are very similar, they are close also to the equilibrium distance of the pair interaction potential. The difference between these values leads to an additional term in the expression of the binding energy of cluster atoms, a term proportional to the second derivative of the pair interaction potential, whereas the leading term is proportional to the total number of bonds in this cluster. Let us use as the pair interaction potential the Lennard-Jones interaction potential, the popular potential that is given by formula (2.6). It is convenient to use the truncated Lennard-Jones interaction potential as a short-range interaction potential; this interaction potential is given by formula (2.6), if two atoms are nearest neighbors, and it is zero for two atoms that are non-nearest neighbors. In the case of the truncated Lennard-Jones

interaction potential we have for a bulk icosahedral cluster with completed layers from formulas (4.11), (4.13)

$$\varepsilon_{\rm o} = 5.86D\,, \quad A = 6.56D\,. \tag{4.14}$$

Let us compare these parameters with parameters of the optimal fcc structure and regular truncated hexahedron, for which we have in the limit $n \to \infty$ according the Table 4.4 data $\varepsilon_{\rm o} = 6D$, $A = 7.55D$. This comparison shows that for very large clusters the fcc structure is more favorable, whereas the optimal cluster structure is the icosahedral for not very large clusters. The transition between these structures occurs in the range of several hundreds of atoms, and there is indeed a range of size for this transition, in which increasing the cluster size by one atom in this range may change the most favorable structure.

In comparing the icosahedral and fcc structures of clusters, we note that the total binding energy of atoms is close for different interaction potentials between atoms. Hence, the optimal structure is determined by the form of the pair interaction potential and is sensitive to this. The most evaluations of binding energies in clusters have been made for the Lennard-Jones pair interaction potential (2.6) both for clusters with completed shells [122, 139–142] and small clusters with incomplete shells up to $n = 147$ [139]. Because the distances between nearest neighbors of the icosahedral cluster are nearly identical, and an icosahedral cluster is more compact than clusters with close lattice packing, the icosahedral structure can be more favorable for small and medium-size but not very large clusters. Let us demonstrate this for the Lennard-Jones cluster consisting of 13 atoms. Accounting for the cluster structure, we represent the total binding energy of atoms in the following form by analogy with formula (2.7) [55]

$$\frac{E_{\rm b}}{D} = 2C_6 \left(\frac{R_{\rm e}}{R}\right)^6 - C_{12} \left(\frac{R_{\rm e}}{R}\right)^{12} .$$

Table 4.6 lists the parameters of this formula for the cuboctahedral, hexahedral and icosahedral Lennard-Jones clusters, where k is the total number of bonds between nearest neighbors, a is the optimal distance between nearest neighbors, $E_{\rm b}$ is the total binding energy of atoms at the optimal atomic configuration, and these parameters are given by formulas

$$a = R_{\rm e} \left(\frac{C_{12}}{C_6}\right)^{1/6} , \quad E_{\rm b} = \frac{C_6^2}{C_{12}} .$$

It follows from Table 4.6 that the icosahedral cluster structure is preferable for a 13-atom cluster over the close-packed structures because of its larger number of bonds between nearest neighbors. In addition, the icosahedral Lennard-Jones cluster shrinks more than the cuboctahedral or hexahedral structures under a long-range attractive interaction. The interaction between nearest

neighbors gives the main contribution to the total binding energy of clusters in all these cases. Comparing close-packed structures, one can see that the hexahedral structure is favorable, but the distinction between the two close-packed structures is small.

Comparison of the energies of the cuboctahedral and icosahedral structures is convenient because these structures are characterized by the same number of atoms in their completed geometric figures, and therefore such a comparison is convenient for the analysis of competition of the fcc and icosahedral structures [122, 140–142]. This comparison of completed structures with the Lennard-Jones interaction potential shows that the cuboctahedral structure becomes more stable for sizes starting from about 10^4 atoms in a cluster. But the cuboctahedral structure is not optimal among the fcc structures, and hence comparison of the energies of the cuboctahedral and icosahedral structures does not allow us to draw conclusions about competition of the fcc and icosahedral structures. Nevertheless, on the basis of comparison of the atomic binding energies for the cuboctahedral and icosahedral structures, one can ascertain the character of interaction of these structures. In particular, in the case of the truncated Lennard-Jones interaction potential, we have, for the total binding energies of a cuboctahedral and an icosahedral cluster, the corresponding values $7476D$ and $7474D$ [48], if these clusters have 7 layers or 1415 atoms. (D is the binding energy per bond.) In the case of 8 layers or 2057 atoms in the cluster, these values are $11040D$ and $11005D$ correspondingly, whereas for clusters containing 6 layers or 923 atoms, these total binding energies of atoms at zero temperature are $4776D$ and $4793D$ for the cuboctahedral and icosahedral clusters (see [48]). One can see a weak dependence, a small increase, of the mean binding energy per atom on the number of cluster atoms. We add to this that the difference of the binding energies of two structures is a nonmonotonic function of the number of atoms, so one can infer that there is a wide range of competition among these structures. In particular, this is demonstrated in [68, 69] by the competition of the fcc and icosahedral cluster structures for the Morse interaction potential between atoms for which the binding energies of cluster atoms and the optimal cluster structure depend on the Morse parameter value. Figure 4.6a contains values of the specific surface energies for fcc clusters with a short-range interaction of atoms, and Fig.4.6b gives the same value for icosahedral clusters with a truncated Lennard-Jones

Table 4.6. Energy parameters for different structures of the Lennard-Jones clusters of 13 atoms

Structure	k	C_6	C_{12}	E_b/D	a/R_e
Cuboctahedron	36	38.48	36.22	40.88	0.990
Hexahedron	36	38.56	36.23	41.04	0.990
Icosahedron	42	35.59	28.57	44.34	0.964

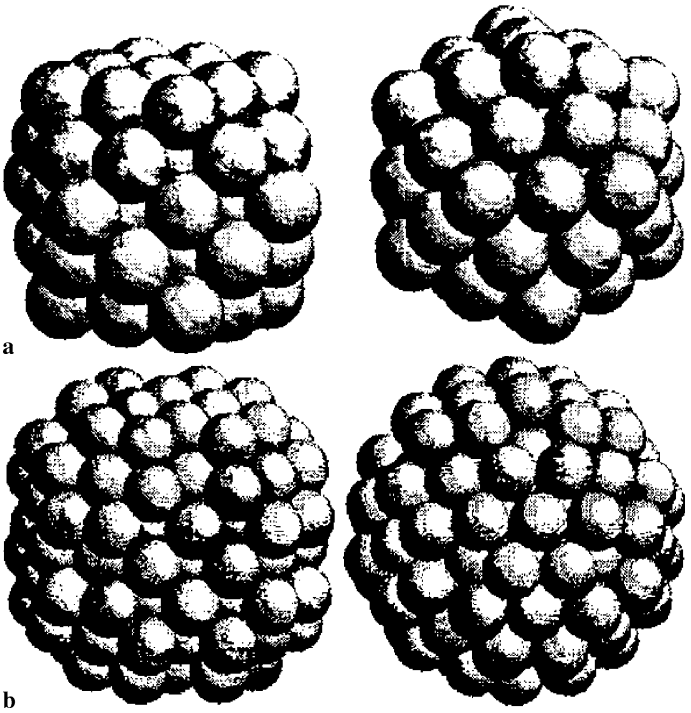

Fig. 4.6. Clusters of the fcc (*left*) and icosahedral (*right*) structures consisting of 55 (**a**) and 147 atoms (**b**) [148]

interaction potential when only nearest neighbors interact. These data testify to the competition of these cluster structures.

Comparison of the cuboctahedral and icosahedral filled cluster structures is useful also in order to ascertain the role of a long-range interaction. For the full, untruncated Lennard-Jones interaction potential, the binding energies of atoms in clusters of these structures consisting of 1415 atoms (or 7 completed layers) are $10309D$ and $10232D$ for the icosahedral and cuboctahedral structures correspondingly [140, 142]. Comparing them with those for the truncated Lennard-Jones pair interaction potential, when nearest neighbors interact only, for which the values are $7474D$ and $7476D$ respectively, we find that the character of the structure competition depends on the shape of the pair interaction potential. Indeed, the structure is determined primarily by the number of bonds between nearest neighbors, but the difference of these values for competing structures is relatively small in the range of competition. Hence the smaller contributions, notably from non-nearest neighbors, can play a determining role in the competition. For example, the number of bonds between nearest neighbors is 4902 for the icosahedral cluster consisting of 923 atoms, whereas the optimal fcc cluster of this size contains 4814 bonds between nearest neighbors [143, 144], and the number of these bonds is 4776

for the corresponding cuboctahedral cluster. Therefore the favorable structure is sensitive to the shape of the pair interaction potential in the competition range [65, 69]. In addition, the number of bonds between nearest neighbors varies in an irregular manner with increasing number of atoms for the icosahedral structure as a cluster layer is filled [138, 136], a consideration that intensifies the structure competition. This fact follows also from the energy calculations [139] for the icosahedral Lennard-Jones clusters in the course of increasing the atom number up to $n = 147$. This leads to expansion of the range of structure competition. We note also that the hexagonal structure is not important in the structure competition. Indeed, at small cluster sizes where fcc and hexagonal structures compete, the icosahedral structure is favorable, whereas at moderate and large cluster sizes, where the icosahedral and fcc structures compete, the hexagonal structure is not favorable [48, 59].

A general conclusion from competition of the icosahedral and fcc cluster structures is that small clusters prefer the icosahedral structure, whereas the fcc structure of large clusters with a given character of interaction is more probable. In particular, the Lennard-Jones solid clusters containing fewer than 100 atoms have the icosahedral structure except clusters consisting of 38, 75, 76 and 77 atoms [145–147]. The reason is that the icosahedral clusters are characterized by a greater number of bonds between nearest atoms than the fcc clusters, and they have more nearly round surfaces. In particular, this is illustrated in Fig. 4.6 [148].

Still another peculiarity of the competition of cluster structures consists in structure mixing. In the case of close-packed structures, the mixed structure of the crystal lattice may simultaneously contain elements of face-centered cubic and hexagonal structures that results in dislocations and twinning (for example, [61, 149]). Such structural defects can be important for transitional structures of clusters [125]. The mixing structure of the crystal lattice of the close packed structure may simultaneously contain elements of face-centered cubic and hexagonal structures. A simple version of twinning results in alternation of the fcc and hexagonal structures and is given in Fig. 4.7.

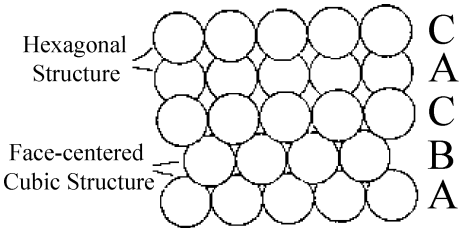

Fig. 4.7. Twinning as a result of alternation of the hexagonal and fcc structures in a crystal lattice [61]. A, B, C are three possible distributions of atoms on the {111} plane. The hexagonal structure corresponds to alternation of the type $ACACA$ with repetition of the layer structure through one layer, and the fcc structure corresponds to the $ABCABCABC$ layer sequence

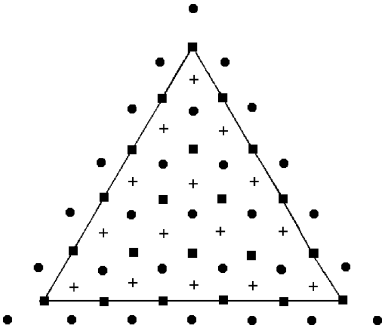

Fig. 4.8. Projections of surface atoms of the icosahedral cluster on the plane of surface triangles. *Dark squares* show positions of atoms of the filled layer and the *solid lines* join boundary atoms. *Dark circles* correspond to positions of atoms of the next layer's filling for the icosahedral structure, and *crosses* correspond to the fcc-structure of a new layer

In clusters with a pair interaction, new possibilities of mixing of structures arise due to competition of the icosahedral and fcc structures. The most important mixing of these structures [120, 121, 139] relates to filling of cluster layers when the icosahedral structure is favored, so that a growing cluster has an icosahedral core. In the first stage of filling, the new layers have the fcc structure, but this then transforms into the icosahedral [138] as it is shown in Fig. 4.8. Indeed, a joining atom goes onto the cluster surface in a hollow between three surface atoms, and the number of such positions for the surface of a fcc-structure is greater than that for the icosahedral structure, which requires places for edge atoms. For the cluster with m filled layers, the number of positions above each triangle is $m(m-1)/2$ for the fcc layer structure and is only $(m-1)(m-2)/2$ for the icosahedral layer structure. Comparison of these surface structures shows [138] that at the first stage of filling of a new layer, the fcc structure of that new layer is favored. However, after filling 8 surface triangles, the icosahedral structure of the filling layer provides the maximum binding energy of cluster atoms.

Thus, the analysis of clusters with a pair interaction of atoms exhibits the variety of cluster structures that can be realized. Even for this simple character of interaction, clusters can have face-centered cubic, hexagonal or icosahedral structures, or their mixture, and each structure gives different cluster shapes. At low temperatures, when a cluster is solid, one can find the optimal configuration of cluster atoms that leads to the maximum binding energy of cluster atoms. Even for large clusters one can observe a size range with alternation, with cluster size, of optimal structures, so that a change of the number of cluster atoms by one can change the optimal cluster structure. In addition, the optimal configuration of cluster atoms in a range of competition can contain elements of different structures.

We now use the above results to determine the surface energy of solids with face-centered cubic structure. A figure of such structure with the maximum binding energy of atoms has plane facets with directions {111} and {100} (the definition of such planes are shown in Fig. 2.2), i. e. this figure has 8 facets – hexagons of the direction {111} and 6 facets – squares of the direction {100}. This figure is represented in Fig. 4.9 [132].

One can introduce the total binding energy of atoms E in this system on the basis of formula (4.2). An optimal shape of the crystalline particle of Fig. 4.9 is characterized by the maximum binding energy for a given num-

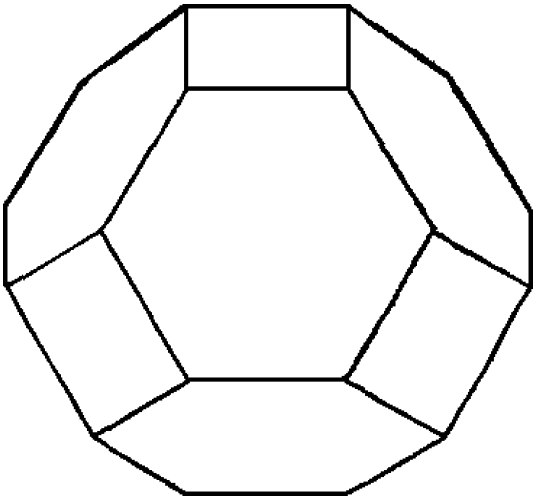

Fig. 4.9. An optimal completed geometric figure for bound atoms in a cluster of the fcc structure [132]

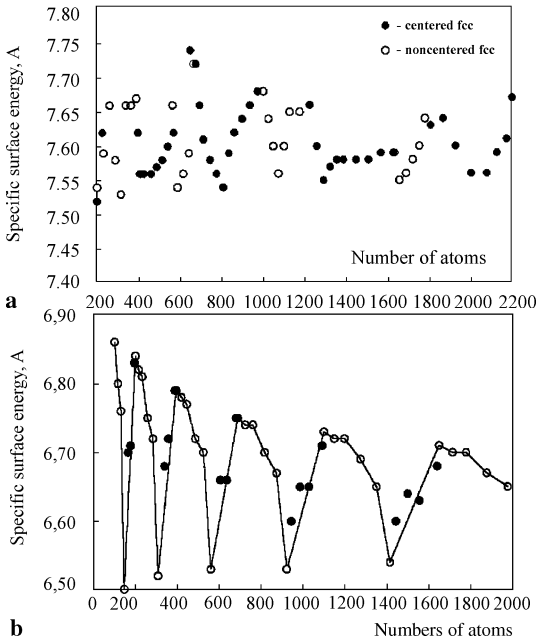

Fig. 4.10. The specific surface energy for optimal atomic configurations of fcc-clusters (**a**) and icosahedral clusters (**b**) [48]. In the case of fcc-clusters, *dark circles* correspond to clusters with a central atom and *open circles* respect to noncentered clusters

ber n of atoms, and hence by the minimal surface energy. In the case of a short-range interaction of atoms the optimal figure is the regular truncated octahedron [135] that can be formed from the octahedron by cutting off 6 regular pyramids near its vertices such that the pyramid edge length is one third of the edge length of the initial octahedron. The surface of the resulting regular truncated octahedron contain facets consisting of 6 squares and 8 regular hexagons. The specific surface energy is $A = 7.56$ [61, 138] in the case of an infinite cluster. Constructing a truncated octahedron in a general case [132], one can characterize it by the parameter

$$\delta = \frac{l_6}{l_4 + l_6} \,, \tag{4.15}$$

where l_4 is the length of a general side of surface squares and hexagons, and l_6 is the length of other sides of hexagons. The geometric figure under consideration (Fig. 4.9) with surface squares and hexagons is realized if $0 < \delta < 1$ [132]. Table 2.6 contains the optimal values of δ and A for the crystalline particle with the Morse interaction potential of atoms [69]. Note that the connection between the near-neighbor distance a and the equilibrium distance R_e of the diatomic molecule is given in Table 2.3 in accordance with formula (2.15). One can see that a decrease of the Morse parameter which leads to an increase of the role of interaction of non-nearest neighbors to the total particle energy is accompanied by an increase both an asymmetry of the particle shape and its surface energy. For the Lennard-Jones crystalline particle the above parameters are $\delta = 0.3$, $A = 15.1$ [48, 69]. Thus the specific surface energy is twice that of the Lennard-Jones case in comparison with that of a short-range interaction of atoms.

Thus, depending on the shape of the pair interaction potential between atoms, competition between the fcc and icosahedral cluster structures is realized in some range of sizes, so that the favorable structure in this range depends non-monotonically on cluster size. This occurs because of the strong dependence of energetic parameters on the extent of shell filling for the icosahedral clusters in comparison with fcc. This is demonstrated in Fig. 4.10 where the size dependence is given for the specific surface energy of clusters with short-range interaction. This dependence is given for magic numbers of cluster atoms when, for the icosahedral structure, some facets of the cluster surface are filled. Because of the oscillatory character of this dependence, the structure competition is realized over a rather wide range of sizes.

5

Ensembles of Classical Particles with Repulsion

5.1 Thermodynamics of Ensembles of Repelling Particles

We now consider the properties of an ensemble of repelling classical particles. In contrast to a system of bound particles that can be stable in the absence of external forces, external fields are necessary to support particles close enough to each other that they repel. External fields that keep an ensemble of repelling particles in a restricted space region may be considered as boundary conditions and are represented in Table 5.1 for various systems. In spite of different boundary conditions, these systems are similar and some of their properties are identical. In addition, as follows from computer simulations and measurements [150–153], this system has two aggregate states, the solid and liquid. But in spite of its simplicity, its properties do not follow from general considerations. Here, we analyze the properties of such systems.

If an ensemble of atoms or particles with a pair interaction between them is governed by an interaction potential given by Fig. 1.1 and is supported by a high external pressure or external field, typical distances between atoms become less than the equilibrium one. In this distance range the interaction of neighboring atoms corresponds to repulsion, and the interaction potential between nearest neighbors is given by formula (1.3). Systems of many particles with a repulsive interaction potential are simple and are characterized by

Table 5.1. Ensembles of repelling particles and boundary conditions that allow one to concentrate the particles in a restricted spatial region

Ensemble of particles	Boundary conditions
Inert gases under high pressure	External pressure
Hard spheres in a box	Pressure under weight of upper particles
Colloid solutions	External pressure
Dusty plasma	Electric traps

two aggregate states, the solid and liquid, similar to the ensembles of bound atoms. One can expect that like bound atoms, the liquid state of repelling particles corresponds to a random spatial distribution of particles, whereas in the solid state the particles form a close-packed crystal lattice i. e. particles form the face-centered cubic or hexagonal structure discussed earlier, in which each internal particle has 12 nearest neighbors. However, in reality this condition does not hold and an ensemble of repelling particles in the solid state has a polycrystalline structure, i. e. long range order is not realized for such systems. This compels us to study in detail the solid aggregate state of various ensembles of particles with repulsion.

Let us consider an inert gas at high pressure. Then the repulsive part of the interaction potential (Fig. 1.1) determines the distribution of atoms, and some parameters of this potential are given in Table 1.1. Since the exchange interaction potential of atoms at small distances is determined by the extent of overlap of their electron shells, it has a sharp exponential dependence on the distance between atoms. In this case interaction of two atoms acts along the axis joining these two atoms, and if this interaction is relatively small, interaction of each pair of atoms is independent of other interactions, i. e. the pair character of interactions is realized now. Next, since the pair interaction potential of atoms varies sharply with separation between atoms, the model of hard spheres describes the system of repelling atoms. We below are guided by inert gases at high pressure, for which the pair interaction potential of particles is given by (1.3)

$$U(R) = U(R_\mathrm{o}) \left(\frac{R_\mathrm{o}}{R} \right)^k ,$$

and the steepness of the repulsive interaction is exemplified by its satisfying the criterion

$$k = \frac{d \ln U}{d \ln R} \gg 1 . \tag{5.1}$$

Therefore this interaction is very similar to the model of hard spheres that portrays the particles as hard balls. In particular, the criterion (5.1) is fulfilled for interactions of inert gas atoms at small distances between them, as follows from the data of Table 1.1.

Note that the system of repelling atoms at high pressures is governed by a pair interaction between atoms, since repulsion of interacting atoms is determined by overlapping of the wave functions of valence electrons. Consequently this interaction is created by the electron distribution near the axis joined interacting atoms, and the exchange interaction potential of two atoms does not depend on positions of other atoms. Next, the interaction potential of two atoms is small compared to a typical value of an electronic excitation or ionization of an atom (the atom ionization potential) that restricts the range of pressures for which the foregoing discussion is valid. In particular, for xenon, metallization is expected at pressures of about 150 GPa [154–156]. Hence the pressure range under consideration here lies below this limit; for

other inert gases this transition occurs at higher pressures. The absence of a stable crystal lattice for a system of repelling atoms does not mean the absence of two aggregate states similar to the solid and liquid aggregate states for a system of bound particles. We next consider these two aggregate states.

Thus, as demonstrated by modelling an ensemble of repelling atoms by hard balls filled a container [153, 157–159], and by computer simulation of the system of hard, repelling spheres [160–162], the system of strongly repelling atoms does not form a crystalline lattice at high pressures and low temperatures. Information about a system of repelling atoms is also available from X-ray diffraction investigations of compressed inert gases at low temperatures. If we start from the crystalline state of an inert gas and increase the pressure, a stacking instability [163, 164] occurs in some pressure range that is reported to induce a transition from the face-centered lattice to the hexagonal lattice. In particular, for xenon at low temperatures, a stacking disorder starts to appear at a pressure of about 4 GPa ($p \approx 100 p_\mathrm{o}$). At pressures above 70 ± 5 GPa ($p \approx 2000 p_\mathrm{o}$ for Xe), high-resolution X-ray diffraction studies show the presence of only the hexagonal close-packed structure for the system of repelling atoms [165]. But such measurements give only one aspect of the atomic structure, namely, that the correlation in positions of nearby atoms corresponds to the hexagonal structure. Simultaneously, a pressure increase reduces the long-range order of the structure, even while nearby atoms remain correlated. This results in some resonance-like maxima in the high-resolution X-ray diffraction pattern, but nevertheless the correlation length drops to be comparable with the distance between nearest atoms. Hence the atoms may form hexagonal arrays over, for example, several interparticle distances, yet have enough disorder that one cannot say the structure corresponds to a true, regular lattice.

5.2 A System of Hard Spheres

In the limit when the criterion (5.1) holds true, the analysis of the system of repulsed particles is simplified. Such a system is described by the model of hard spheres [26, 166, 167], and it is convenient to introduce the packing parameter φ of the system according to the formula

$$\varphi = \frac{4\pi}{3n} r^3 N \tag{5.2}$$

as a characteristic of the particle ensemble. Here r is the radius of a sphere whose volume encloses the particle ensemble, N is the number density of hard spherical particles, n is a number of atoms inside the sphere. The packing parameter φ is the fraction of the space occupied by hard balls. Evidently, the maximum value of this parameter for hard balls of a radius r_o corresponds to a close-packed crystal lattice whose number density of atoms-balls is $N =$

$\sqrt{2}/a^3$, where $a = 2r_o$ is the distance between nearest atoms, and the packing parameter is [153]

$$\varphi_{cr} = \frac{\pi\sqrt{2}}{6} = 0.74 \, . \tag{5.3}$$

Note that the hard sphere model for a particle ensemble means that the particle interaction potential is zero if particles do not touch with each other, and a strong, formally infinite repulsion between particles takes place during their contact. Hence, an ensemble of repelling particles has features of a gas with almost non-interacting (but space-filling) particles and those of a condensed particle system with a strong interaction. This results in certain properties of such systems. In particular, the state equation of an ensemble of repelling particles has the form [168–170] analogous to the gaseous (3.1) and van der Waals (3.3) state equations.

The hard sphere model for an ensemble of repelling particles is a basis for computer simulations [151, 160–162, 170] which allow one to study various aspects of the behavior of this ensemble. The packing parameter φ of such an ensemble follows from simple experiments based on filling a container with hard balls and from computer simulations with hard spheres. In particular, Fig. 5.1 gives the dependence of the packing density on the container volume that is determined by surface effects near the container boundary. In the limit of a large container volume, we have for the packing parameter $\varphi_d = 0.64$ that agrees with a more precise value from the above-cited computer simulations

$$\varphi_d = 0.644 \pm 0.005 \, . \tag{5.4}$$

One can assume an average number of nearest neighbors q is proportional to the packing parameter φ of the particle distribution. The average number q of nearest neighbors for an ensemble of repelling particles with density ρ for a given distribution can be related easily to the crystal density ρ_{cr}:

$$q = 12\frac{\rho_{cr}}{\rho} \, . \tag{5.5}$$

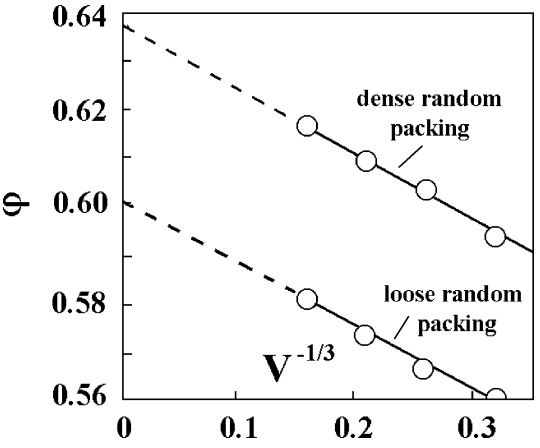

Fig. 5.1. The dependence of the packing density on the reciprocal container size (V is the container volume), when this volume is occupied by balls of identical radius for two methods of filling, with shaking and without it [158]

With $q = 12$ for the close packed structure, we have, on the basis of (5.2) and (5.3),

$$q = 12\frac{\varphi}{\varphi_{\rm cr}} = 16.2\varphi\,, \tag{5.6}$$

and formulas (5.4) and (5.6) give $q = 10.4 \pm 0.1$, close to the coordination number of liquid inert gases at low pressures, in which atoms are bonded by attractive forces, and for which $q = 10.1 \pm 0.1$.

Thus, a bulk ensemble of atoms with a repulsive pair interaction that models inert gases at high pressures, has a structure other than that of a crystal of bound atoms with a short-range attractive interaction even at low temperatures. But this structure is not amorphous – it does have short-range order, and confirmation of this fact is the phase transition for this ensemble that occurs at higher temperatures. One can introduce the solid (s) and liquid (l) aggregate states of the system of repelling particles by analogy with the solid and liquid aggregate states for an ensemble of bound particles. The phase transition of first order [171] between these states leads to the following values of the packing density at the melting curve

$$\varphi_{\rm s} = 0.545\,, \quad \varphi_{\rm l} = 0.494\,. \tag{5.7}$$

From formula (5.7) it follows for the number of nearest neighbors of a test atom in the solid state at the melting curve $q_{\rm s} = 8.8$ and $q_{\rm l} = 8.0$ for the liquid state. From general considerations one can assume a partial order in the solid state, whereas the liquid state is random. These values for the packing parameter and the average number of nearest atoms lead to a domain structure of the solid state, when the atom distribution consists of individual domains – close-packed clusters (fcc or hexagonal). The average number of nearest neighbors for this system relates to volumes which include many domains – clusters. Thus, the optimal structure of a simple ensemble of atoms described by the hard sphere model, even at low temperatures with almost zero kinetic energy, is not simple.

The model of hard spheres allows one to describe the behavior of systems consisting of repelling classical particles. Briefly, this behavior is such [160, 170, 172] that at the packing parameter $\varphi < \varphi_{\rm f}$ this system is found in the liquid (or fluid) state, at $\varphi_{\rm f} < \varphi < \varphi_{\rm d}$ it consists of a mix of solid and liquid regions, and at $\varphi > \varphi_{\rm d}$ the solid (polycrystal) state is thermodynamically stable. The solid state is composed of crystal particles, i. e. it has the polycrystalline structure. Such a structure can remain for long intervals, so the metastable state of Fig. 5.2 with its random distribution of atoms is favorable. This glassy state is the more probable, the higher is the packing parameter at $\varphi < \varphi_{\rm d}$.

Thus, in spite of the apparent simplicity of a system of repelling particles, the character of particle distribution is not so simple as might follow from intuition. Figure 5.2 gives the phase diagrams for the ensemble of repelling particles which are compared with the phase diagrams for systems of atoms with a short-range interaction (or ensembles of bound inert gas atoms)

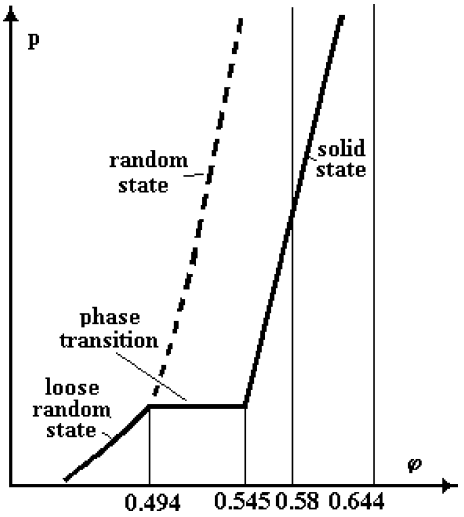

Fig. 5.2. Schematic diagrams for an ensemble of hard balls

near the triple point. From this it follows that a bulk ensemble of atoms with a purely repulsive pair interaction does not form a crystal lattice as do atoms bound by a short-range attractive interaction. Even at low temperatures, repulsive atoms do not form a crystal lattice, so that the number q of nearest neighbors for a test internal atom of this system differs from the close-packing value of 12. Because the exchange interaction potential between atoms at small distances is determined by the extent of overlap of their electron shells, it is frequently represented by a sharp exponential dependence on the distance between atoms. Alternatively, a model of hard spheres can be used effectively to describe the system of repelling atoms that is valid if $k \gg 1$ in formula (1.3).

5.3 Colloid Suspensions as Systems of Repelling Particles

The hard sphere model describes correctly colloid suspensions which consist of insoluble particles of almost identical size that are suspended in a liquid. A typical means to create such a suspension uses particles with polymethylmethacrylate (PMMA) cores stabilized by a thin layer (10 – 15 nm) of polyhydroxystearic acid that prevents particle aggregation. These PMMA particles are stable and are not charged; hence they are suitable as monomers in suspensions – which we may also call solutions [173–176]. As a liquid solvent, one often uses a mixture of decaline and carbon disulfide or cycloheptilbromide. Under these conditions the particles do not aggregate. A standard polydispersity of PMMA particles is 5%, and their size varies in a wide range in different experiments. In particular, the mean particle radius was 0.170 μm in experiment [177], between 0.254 μm and 0.259 μm in experiment [178],

1.18 μm in experiment [179], 1.26 μm in experiment [180], and 0.225 μm in experiment [176].

Since sizes of repelling colloid particles in these experiments are comparable with the wavelength of visible light, the processes in such colloid solutions, in particular, crystallization of an ensemble of colloid particles, can be studied by light scattering (for example [177, 181, 182]). Light scattering allows one to detect formation of particle structures.

The colloid solutions (or suspensions) exhibit the properties which follow from the hard sphere model. Indeed, for the packing parameter $\varphi < \varphi_{\mathrm{f}}$, one observes a random distribution of colloid particles that corresponds to the liquid aggregate state, whereas at $\varphi > \varphi_{\mathrm{m}} = 0.545$ the colloid solution consists of a large number of randomly directed crystallites, each of them including a large number of colloidal particles. In an intermediate range of packing parameters the colloid solution consists of amorphous and polycrystal phases which are separated by sharp boundaries [177, 181]. For example, an experiment [177] shows the colloid solution consisting of a large number of randomly directed crystallites of size $\sim 100\,\mu\mathrm{m}$. The density of individual crystallites exceeds $10^6\,\mathrm{cm}^{-3}$ [177], corresponding to a number of monomers in an individual crystallite of order of 4×10^7.

It is surprising that the crystal shape differs from spherical, and the ratio of the shortest and longest ellipsoid axes is 0.65 ± 0.15 according to measurements [180]. In addition, along with non-spherical shape, the surface of an individual crystal particle is irregular and is similar to that of a fractal aggregate. The fractal dimension for the crystallite in the colloid case is 2.35 ± 0.15 [180].

Next, the time required for crystallization is long enough under real conditions and the crystallization time increases with an increase of the packing parameter. For example, in experiment [177] the crystallization time was 1 hour at the freezing point ($\varphi = \varphi_{\mathrm{f}}$) and several days at $\varphi = 0.58$. This process exceeds 1 year at any still higher value of the packing parameter $\varphi = 0.619$ under normal gravity conditions of the experiment [178], while in shuttle flight experiments this process lasts approximately 4 days. This exhibits the role of gravitational forces in this process that testifies to a difference, under these experimental conditions, from the hard sphere model.

Note that study of kinetics of the crystallization process allows one to determine the interfacial interaction between the crystal and fluid phase. Then the interfacial free energy between a crystal and melt surface per unit of area within the framework of the hard-sphere model, as follows from the theory [183–185] and experiment [178, 186–188] is approximately

$$F = \frac{0.6T}{d^2}\ , \tag{5.8}$$

where d is the diameter of particles.

The phase diagram of Fig. 5.2 for a system of repelling particles contains two branches above the freezing point $\varphi_{\mathrm{f}} = 0.494$. The metastable phase with

a random distribution of particles (the random close-packing state) terminates at $\varphi_c = 0.64$ [189]. The end of the thermodynamically stable phase of the phase diagram relates to the maximum value of the packing parameter $\varphi_{cr} = 0.74$. The solid state in the packing parameter range $\varphi > \varphi_f$ has a polycrystalline structure with a close packed structure of individual crystal particles. In the course of growth of these particles, competition takes place between the fcc and hexagonal structures, but these structures are characterized by similar free energies. Indeed, the difference of the free energies per particle for the fcc and hexagonal structure is less than $0.002T$ [190–193]. A correct calculation [194] of the entropy difference near the densest packing $\varphi \approx \varphi_{cr}$ shows the relative difference of the entropies for these states is also very small, approximately 0.001, and the hexagonal structure is favored. So small a difference has no practical meaning because of many other weak perturbations in a real system. Therefore solids composed of colloid particles are considered to have a stacking structure [178, 177, 195, 196].

The study of colloid particles in solutions is particularly stimulated by possibility to the fact that one can prepare such a solution with particles of a specific size (more precisely, with a narrow dispersity of sizes), governed by the solution acidity. One can accelerate or stop the growth of individual particles in the solution and obtain in this manner solid particles of a nearly identical size with a standard deviation in size of 5%.

Thus, colloid solutions of repelling particles exhibit properties that resemble those of the hard-sphere system. Hence, study of such colloid solutions allows one to study some properties of an ensemble of repelling atoms. On the other hand, these colloid solutions have specific properties due to fine interactions between particles. In particular, the rate of crystallization, as well as other details of this process, depend on external conditions. As a result, study of colloid solutions give a deeper understanding of the behavior of ensembles of repulsed particles.

Until now, in this section we have considered particles covered by a thin, charged film that prevents colloid particles from adhering, so that the colloid solution is a system of repelling particles. One can create other conditions in which particles can stick together. This occurs in a colloid solution of solid particles of gold, in which the particles exhibit aggregation. In this case solid monomers can form fractal aggregates [197–203], and this method allows one to study such processes.

5.4 Virial Theorem and Instability of Crystal Structure

Additional understanding regarding the structure of an ensemble of repelling particles follows from the virial theorem [89] that allows one to find the connection between an external pressure at zero temperature and the particle density at a given pair interaction potential [166, 204]. Clearly the previous results imply that the solid states of such systems observed in simulations and

experiments are not regular, crystalline solids. Here we show that the crystalline aggregate state of the system of repelling atoms is not the most stable thermodynamically, relative to a disordered aggregation of clusters. We will base the results on the virial theorem for a system of repelling atoms with pair interactions between them. Let us represent the equation of state for atoms interacting through the potential (1.3) by invoking the virial theorem, yielding the form

$$T = pV - \frac{k}{3}\overline{U} \,, \tag{5.9}$$

where V is the volume per atom, and $\overline{U}$ is the average interaction potential per atom. We have, in the mean field approximation,

$$V = \frac{a^3}{\sqrt{2}} \cdot \frac{12}{q} \,, \quad \overline{U} = \frac{q}{2} U(a) \,, \tag{5.10}$$

where a is the distance between nearest neighbors, and the pair interaction potential $U(a)$ is given by formula (1.3). In the limiting case (5.1) we have $pV \gg T$, i. e. equation (5.9) allows one to estimate the pressure from just its second term, as

$$p = 2\sqrt{2}k \left(\frac{q}{12}\right)^2 \frac{U(a)}{a^3} \,. \tag{5.11}$$

We demonstrate below the validity of this formula in the case of a close-packed crystal lattice. Let us draw a plane parallel to a symmetry plane of this lattice, so that the pressure is the force per unit area between atoms located on different sides of the crossing plane. Then the pressure is

$$p = \frac{mf_x}{s} = \frac{mf\cos\theta}{s} \,, \tag{5.12}$$

where m is the number of nearest neighbors of a test surface atom that lie above and below the separation plane, s is the surface area per atom, and f_x is the force projection onto the perpendicular to the separation plane, so that this force acts between a test atom and its nearest neighbor outside the separation plane, f is this force, and θ is an angle between the line connecting interacting atoms and the perpendicular to the separation plane. From this we have for the $\{100\}$ separation plane, with $m = 4, s = a^2, \cos\theta = 1/\sqrt{2}$,

$$p = \frac{4f(a)}{\sqrt{2}a^2} = \frac{2\sqrt{2}}{a^2} \left|\frac{\mathrm{d}U(a)}{\mathrm{d}a}\right| = \frac{2\sqrt{2}}{a^3} kU(a) \,. \tag{5.13}$$

In the case of the $\{111\}$ direction of the separation plane we have $m = 3, s = \sqrt{3}a^2/2$, $\cos\theta = \sqrt{2/3}$, so

$$p = \frac{3f(a)}{\frac{\sqrt{3}}{2}a^2}\sqrt{\frac{2}{3}} = \frac{2\sqrt{2}}{a^2} \left|\frac{\mathrm{d}U(a)}{\mathrm{d}a}\right| = \frac{2\sqrt{2}}{a^3} kU(a) \,. \tag{5.14}$$

As we see, formulas (5.13) and (5.14) are transformed into formula (5.11) in the case $q = 12$.

These formulas allow us to compare the crystalline state of the repelling atoms with a random distribution of the same atoms characterized by a mean coordination number q. We analyze the possibility of a phase transition between these states when the total number of repelling atoms, the pressure and the temperature are conserved. Then the condition we apply here for equilibrium of the two phases is the equality of the Helmholtz free energies of two phases, $\Delta F = \Delta E - T\Delta S = 0$, and ΔE and ΔS are the differences of the internal energies and entropies of the two phases. (Strictly, at constant pressure, one should use the Gibbs free energy difference, $\Delta G = \Delta H - T\Delta S$, but the difference can be neglected here.) In order to ascertain the stability of the crystalline state of the system repelling atoms, we take into account that the transition from the crystal to a disordered state corresponds to an increase of the entropy. Because $p = \text{const}$, we have

$$\Delta E = n\left(\Delta\overline{U} + p\Delta v\right) \ , \tag{5.15}$$

where $\overline{U}$ is the average interaction energy per atom and v is the volume per atom. From formula (5.14) it follows for the transition from the crystalline state with $q = 12$ to another state characterized by a coordination number q that

$$\begin{aligned}\frac{\Delta E}{n} &= \left(1+\frac{k}{3}\right)\left(\overline{U}_{\rm cr} - \overline{U}_{\rm r}\right) = \left(1+\frac{k}{3}\right)\left[6U(a_{\rm cr}) - \frac{q}{2}U(a_{\rm r})\right] \\ &= 6U(a_{\rm cr})\left(1+\frac{k}{3}\right)\left[1 - \frac{q}{12}\frac{U(a_{\rm r})}{U(a_{\rm cr})}\right] \ ,\end{aligned}$$

where $U(a)$ is the pair interaction potential (1.3) at the distance a between interacting atoms, and $a_{\rm cr}$ and $a_{\rm r}$ are, respectively, the (mean) distances between nearest neighbors in the crystalline state and in the state with randomly distributed atoms. In the mean field approach, the average interaction potential per atom is $\overline{U}_{\rm cr} = 6U(a_{\rm cr})$ and $\overline{U}_{\rm r} = qU(a_{\rm r})/2$. The condition $p(a_{\rm cr}) = p(a_{\rm r})$ gives

$$\frac{\Delta E}{n} = 6U(a_{\rm cr})\left(1+\frac{k}{3}\right)\left[1 - \left(\frac{12}{q}\right)^{\frac{k-3}{k+3}}\right] \ . \tag{5.16}$$

Only the final factor is negative, so that a transition from the crystalline state to any random state of the system of repelling atoms with a lower density or an increase in the mean distance of nearest neighbors corresponds to energetic stabilization, i. e. to $\Delta E < 0$. Clearly, so long as $T > 0$, $\Delta S > 0$ for any transition from the crystalline (ordered) state of atoms to any disordered (random) state. (We introduce the temperature constraint to avoid any issues of the third law of thermodynamics.) Hence the crystalline state of a system of atoms with a steeply varying repulsive interaction potential ($k > 3$) is not stable thermodynamically with respect to a state with a random distribution of atoms. Hence, the crystalline state of such a system is not realized under conditions of thermodynamical equilibrium, so long as the random state has

any local stability under the same conditions. In the present case, that stability is due to the externally-applied pressure.

Generalizing, we use the analogy of formula (5.16) to find the change of the internal energy of the system ΔE between states with coordination numbers q_1 and q_2:

$$\frac{\Delta E(q_1 \to q_2)}{n} = \frac{q_1}{2} U(a_1) \left(1 + \frac{k}{3}\right) \left[1 - \left(\frac{q_1}{q_2}\right)^{\frac{k-3}{k+3}}\right] . \qquad (5.17)$$

This gives $\Delta E(q_1 \to q_2) < 0$ if $q_1 > q_2$, a natural consequence of relieving the repulsive force. For this transition, the entropy change ΔS per atom can have either sign. If the transition is accompanied by a volume decrease, then it must also exhibit an entropy decrease if the transition takes place between two disordered states with random distributions of atoms. Hence, in principle, a phase transition is possible between random states. Note that in the limit $k \to \infty$, formula (5.17) gives $\Delta E/n = p\Delta V$, where ΔV is the volume change per atom. In this limit, we have $p\Delta V = T\Delta S$, where ΔS is the entropy change per atom, and if this phase transition corresponds to a decrease of the coordination number q, this implies an increase of the specific volume V and a decrease of the specific entropy S. (One kind of exception can arise in unusual cases. It can happen that the state of lower density is a state of greater order; the one obvious example is water. The denser liquid water obviously has a higher entropy than the less dense ice crystal.)

We obtain, on the one hand, that an ensemble of repelling particles with their uniform distribution in a space cannot form an infinite crystal structure as it follows from the virial theorem. On the other hand, this ensemble of repelling particles can form two aggregate states. It is clear that one of these states is the liquid and hence, the other is characterized by the polycrystalline structure [204].

Thus, in spite of the simplicity of the representation of the interaction we used initially, the structure of solid systems of repelling atoms is not so simple as one might expect from that convenient but limited model. In considering the ensemble of repelling atoms, we assume it to be sustained under external pressure, and that the transition between two aggregate states proceeds at a constant pressure. Under these conditions, the crystal lattice is not formed at low temperatures, but the sizes of crystallites or crystal regions may vary, depending on external conditions. In particular, this conclusion does not hold true for a dusty plasma, in which charged particles of micron size may be captured by a trap made of a gas discharge, as was observed from experiments [205–208] and was analyzed in some reviews (for example [209–213]). This electric trap for charged particles may be the near-cathode region of a high-frequency discharge or striations of a glow discharge; there, the charged macroscopic particles interact with each other through the Yukawa interaction potential. The Yukawa potential consists of short-range repulsive interactions and long-range screened Coulomb interactions; with the strong screening of charges in a plasma (or large distances between nearest particles), the long-

range part makes a small contribution to the total particle interaction, so an ensemble of micron particles in a plasma trap becomes virtually identical to a system of hard particles. Under certain conditions this ensemble is analogous to saturated solutions of charged colloidal particles.

In contrast to an ensemble of repelling atoms, the particles of a dusty plasma can form a crystal lattice under some conditions. Moreover, the phase transition between the solid and liquid states in a dusty plasma can proceed in the form of a wave [214], whereas in usual ensembles of interacting particles the phase transition results from the growth of nuclei of a new phase inside an old one [153]. One can explain roughly the difference in behavior of these systems in terms of the conditions under which they are found. The ensembles of repelling atoms under consideration here are under constant pressure, whereas an ensemble of charged particles in a dusty plasma is best described as being in a potential well created by an external source, whose parameters are determined partially by the self-consistent field of charged particles. Hence, in the latter case, we have more complicated boundary conditions, which may allow the pressure to change in the course of the phase transition. As for the phase transition wave, it can occur under a high degree of metastability (overcooling of a liquid or overheating of a solid) that is possible in a dusty plasma.

We note also the distinction between the aggregate states at low temperatures for the ensemble of hard spheres and for a system of particles interacting through the Yukawa potential. The latter [215–221] can have crystal structures at low temperatures and small screening length, although in this limit one might expect the behavior of the system of Yukawa particles to be similar to that of the ensemble of hard spheres. Possibly this contradiction follows from experiments with a small number of particles in a dusty plasma. This could be resolved by computer simulation simultaneously for both interaction potentials.

Thus, both a dusty plasma and a collection of Yukawa particles can be considered as representatives of simple ensembles of interacting particles, and the analysis of their aggregate states together with transitions between these aggregate states may be joined in a general scheme. The apparent contradictions or paradoxes just described can be overcome with more detailed analyses that will deepen our understanding of the physics of aggregate states.

Thus, from the virial theorem it follows that the crystalline system of repelling atoms with a uniform spatial distribution of particles is unstable with respect to a decrease of the mean coordination number. A nonregular distribution of atoms is characterized by a lower interatomic repulsive energy, and because the entropy of a nonregular atomic distribution is higher than that of a crystal lattice, we conclude that the ordered state of this system is unfavorable thermodynamically. This analysis does not allow us to find the optimal mean coordination number of an atomic distribution, because we cannot determine the entropies of distributions with a given coordination number. Nonetheless, it demonstrates the thermodynamic instability of the crystalline state of an ensemble of repelling atoms.

Hence one can suggest that the system of repelling atoms at high pressures consists of individual domains – solid clusters of fcc and hexagonal structure (or one of these structures). These clusters are presumably oriented randomly, with neighboring clusters connected by fixed "bonds". Voids or vacancies on the boundaries between neighboring clusters lower the average number of nearest neighbors q in comparison with that for the close-packed crystal for which $q = 12$. At high pressures the average number of nearest neighbors is $q = 10.4$ at very low temperatures. This picture is not consistent with one set of computer simulations by molecular dynamics of xenon at high pressures [222]; however for those calculations, a regular, body-centered cubic structure was assumed. Since the number of nearest neighbors is precisely $q = 8$ for a body-centered crystal, the assumption of this structure is in disagreement with our results and seems incompatible with the evidence now available. Whether a bcc structure would have enough local stability to be observed is an open question at this time.

The domain structure of an ensemble of repelling atoms at high pressures that follows from computer simulation, experiments, and the behavior of hard balls in a container, means that some degree of order with hexagonal structure, probably with some long-range character, is established, at least temporarily, for each test atom. In order to estimate the length of this correlation at high pressure, we compare this structure with an ensemble of noninteracting clusters with hexagonal structure, for which the magic number of atoms $n = 946$ for the optimal hexagonal structure – a truncated hexahedron corresponding to the average coordination number $q = 10.5$ [48, 61]. This coincides with the coordination number $q = 10.4$ of nearest neighbors for an ensemble of repelling atoms at high pressures. Hence, the number of correlating atoms on a line that links a test atom with its neighbors, is 4–5, and the total number of correlating atoms, we can infer, is several hundreds.

Thus, one can describe the character of evolution of the structure of solid inert gases resulting from compression in the following way. At low pressures $p \ll p_o = D/R_e^3$, the crystal has fcc structure ($q = 12$); an increase of the external pressure leads to a stacking instability which starts from $p \sim p_o$. As a result of this instability, regions of hexagonal structure develop inside the crystal, at first for layers, and later for domains or small clusters. The random distribution of cluster orientations produces a decrease of the packing density φ and of the mean coordination number q of this system due to formation of voids on boundaries of structured clusters. Together with this development of separate crystalline clusters, pairwise interactions fix neighboring clusters. As a result, at high pressures solid inert gases consist of small solid domains – clusters – so that a bulk solid containing a large number of such domains has an amorphous structure, in the sense of having no long range order. Since interaction of adjacent domains may be determined in significant part by interaction of non-nearest atoms (depending on the specific interatomic potential), their structure can be sensitive to the details of that interaction potential. Consequently the parameters of strongly compressed

rare gases at low temperatures can be very different for different inert gases. Hence, the solid system of strongly repelling atoms is characterized by order on the scale of typical sizes of individual clusters, but is amorphous on large scales. Thus, in spite of the simple character of the approximate model for interaction, the structure of solid systems of repelling atoms is not so simple as one might expect from general, simplistic considerations.

5.5 Phase Transition for an Ensemble of Repelling Atoms

The solid–liquid phase transition of a simple system of bound atoms near the triple point that was considered previously results from the attractive forces between atoms. For macroscopic systems with a short-range atomic interaction the triple point pressure $p_{\rm tr}$ is low compared to a typical pressure in this system $p_{\rm o} = D/R_{\rm e}^3$ due to interaction of atoms, where $D, R_{\rm e}$ are the parameters of the attractive interaction potential in Fig. 1.1. This allowed us to ignore the volume change in this phase transition. If we move along the melting curve with increasing pressure, which increases the role of repulsion in atom interaction, the role of the pressure term becomes important in the thermodynamic potential. Starting from pressures $p \sim p_{\rm o}$, one can support the solid-liquid phase transition only by an external pressure, and repulsion of atoms is of importance in this case.

We now consider another limiting case,

$$p \gg p_{\rm o} = \frac{D}{R_{\rm e}^3} \ , \tag{5.18}$$

for which the state equation for the system of atoms is dominated by the repulsive part of the interaction potential. We assume the pair character of atom interaction and take the interaction potential (1.3) of two atoms $U(R)$ at a distance R between them with parameters of Table 1.1 for inert gas atoms. Using the similarity law, one can introduce a parameter with dimensionality of length, which is equal to

$$d = \left(\frac{C}{T}\right)^{1/k} \ , \tag{5.19}$$

where T is a temperature on the melting line. Introducing the pressure p, the specific volume jump ΔV as a result of melting, and the volume $V_{\rm sol}, V_{\rm liq}$ per atom for the solid and liquid states correspondingly on the melting curve, we obtain the following scaling law on the melting curve

$$p \sim \frac{T}{d^3} \ , \quad \Delta V \sim V_{\rm sol} \sim V_{\rm liq} \sim d^3 \ , \quad N_{\rm sol} \sim \frac{1}{V} \sim \frac{1}{d^3} \ , \tag{5.20}$$

and the entropy jump $\Delta S \sim 1$. Table 5.2 gives the parameters on the melting curve for a system of atomic particles with the interaction potential (1.3)

Table 5.2. Parameters of a system of repulsing atoms with the interaction potential (1.3) on the melting line [151]

k	4	6	8	12	∞
$pV_{\rm sol}/T$	90	38	28	19	11
pd^3/T	16.2	17.2	20.4	15.9	10.6
$V_{\rm sol}\sqrt{2}/d^3$	0.254	0.641	1.030	1.185	1.359
$V_{\rm liq}\sqrt{2}/d^3$	0.255	0.649	1.060	1.230	1.499
$\Delta V/V_{\rm sol}$	0.005	0.013	0.030	0.038	0.103
$p\Delta V/T$	0.45	0.50	0.63	0.72	1.16
ΔS	0.80	0.75	0.84	0.90	1.16

for different k. The relation between the pressure p and temperature T on the melting curve gives the state equation for the melting curve. According to these data, the mechanical work during melting $p\Delta V$ is comparable with the melting heat or the fusion enthalpy $\Delta H = T\Delta S$. Moreover, in the limit $k \to \infty$ the melting becomes a reversible process, so that the fusion energy is compensated by the energy which is consumed on compression at the phase transition. Note that according to the data of Table 5.2, the mechanical work $p_{\rm tr}\Delta V_{\rm tr}$ as a result of melting near the triple point ($p_{\rm tr}$ is the triple point pressure, and $\Delta V_{\rm tr}$ is the volume jump at the triple point) differs from the enthalpy change $\Delta H_{\rm fus}$ at melting by almost four orders of magnitude. In the case of a system of repulsing particles these values are comparable.

In the limiting case $k \to \infty$, interaction of atomic particles is determined by their contact. We take $\varphi = 4\pi r_{\rm o}^3 N/3 = \pi d^3 N/6$ as the packing parameter for a given state of an ensemble of repelling particles, where $r_{\rm o} = d/2$ is the particle radius and N is the number density of particles. This parameter characterizes the volume fraction occupied by particles. For the close-packed crystal structures of close packing when in which each particle touches 12 nearest neighbors, this parameter is equal to $\varphi_{\rm cr} = \pi\sqrt{2}/6 = 0.7405$, the maximum possible value for this parameter. On the melting curve for the solid and liquid states this parameter is

$$\varphi_{\rm sol} = \frac{\pi d^3}{6V_{\rm sol}} = 0.545\,, \quad \varphi_{\rm liq} = \frac{\pi d^3}{6V_{\rm liq}} = 0.494\,, \tag{5.21}$$

as follows from Table 5.2 in the limiting case $k \to \infty$. Again, each particle has 12 nearest neighbors in the crystal state, but only 6 nearest neighbors in the fluid. In addition, the packing density $\varphi = 0.64$ for the solid state in the limit $k \to \infty$, with the pressure going to infinity at a temperature consistent with the state equation for the limit of high pressures

$$\frac{pV_{\rm sol}}{T} = 9.4\,, \tag{5.22}$$

where $V_{\rm sol}$ is the volume per atom in this limit for the solid state, and the packing parameter is $\varphi = 0.64$ in this case.

5.6 Phase Transitions in Inert Gases under High Pressure

Inert gases under high pressures are an example of a bulk ensemble of repelling atoms. At low pressures and low temperatures all the inert gases form fcc crystal lattices. This structure is destroyed at sufficiently high pressure and elements of the hexagonal or icosahedral structures appear in solid inert gases at pressures above p_o. Recall that alternation of crystal layers in the fcc-structure is $ABCABCABC$, while for the hexagonal structure this alternation is $ACACAC$. Hence, in the latter structure, an atom of the third layer is projected on the corresponding atom of the first layer. This correlation in atomic positions is not observed for solid inert gases at low pressures but occurs at intermediate pressures, as shown by X-ray diagnostics. The same correlation also holds for the icosahedral structure. Thus, at high pressure but below metallization, solid inert gases have a domain or polycrystalline structure and contain many bound clusters of the hexagonal or icosahedral structure.

Experimental methods of constructing the melting curve for inert gases at high pressures are based on the diamond-anvil cell containing an inert gas compressed by a laser beam. The laser beam heats the inert gas inside the diamond cell through its metal substratum, and is used to measure the inert gas pressure and temperature in the course of its heating. The melting point is found from a change of optical properties of the compressed condensed inert gas. This method allows us to analyze the pressures up to 100 GPa, two orders of magnitude higher than those available by classical methods of gas compression (for example, [152, 223–226] in the argon case).

Even at the highest pressures, the kinetic energy of atoms on the melting curve is small compared to the electronic excitation energy or the ionization potential of these atoms. Hence, thermal electronic excitation and ionization of atoms on the melting curve is negligible and does not influence on the phase transition. At very high pressures, however, compression of inert gases creates such strong overlap of the wave functions of valence electrons that it can induce a transition from the dielectric state to the metallic state. This effect is especially strong for xenon for which the transition to the metallic conductivity is expected at 130 – 150 GPa [154–156]. In reality, this transition proceeds over a wide pressure range and evidently depends on the temperature. This effect can of course affect the behavior of the melting curve. Moreover, one can expect that the observed decline of the melting curve $T(p)$ for xenon at pressures above 15 GPa and for krypton at the pressures above 25 GPa can be attributed to this effect.

The phase transition in inert gases at high pressures corresponds to transition from a polycrystalline structure to the liquid aggregate state with a random distribution of atoms, a distribution without short-range order. Because the exchange interaction potential of two inert gas atoms is a repulsive interaction potential varying sharply with distance (see Table 1.1), melting of inert

gases at high pressure is described moderately well by the hard sphere model. This is valid in a restricted pressure range, between the low range specified by the criterion (5.18) and the upper limit set by the onset of metallization. In reality, when the pressure is very high indeed, the electron bands of the ground and excited states approach as the pressure increases. When these bands become close enough that metallic conductivity begins, electronic processes become important, and this scheme terminates.

Indeed, we assume the ensemble of atoms is described by one potential energy surface for interacting atoms in their ground electronic states. This potential energy surface is separated by a large energetic gap from the next state that corresponds to electronically excited atoms. But compression of an inert gas, on the one hand, decreases the energetic gap between the ground and excited electron bands of this system, and on the other hand, increases the melting temperature. As a result, the probability of electronic excitation by compression increases with increasing pressure, as does the conductivity. Finally, compressed enough, inert gases take on metallic properties, and their description in terms of repelling atoms loses its validity. Indeed, electron shells of neighboring atoms are overlapped under these pressure, and atoms lost their individuality. The applicable range of this model for xenon lies between $p_{\rm o} = 47\,\text{MPa}$ and approximately 150 GPa, a range of three orders of magnitude. Even at the highest pressures, the kinetic energy of atoms on the melting curve is small compared to the electronic excitation energy or the ionization potential of these atoms. Hence, thermal electronic excitation and ionization of atoms on the melting curve under consideration is small and does not influence on the phase transition.

As a demonstration of this discussion, Fig. 5.3 gives the melting curve for compressed argon when parameters of criterion (5.18) are $p_{\rm o} = 37\,\text{MPa}$, $D = 12.3\,\text{meV} = 143\,\text{K}$. Filled signs are the results of experiments; the melting curve is constructed on the basis of the experimental data [163, 227, 228], which are approximated by the following expression for the argon melting curve

$$\frac{\mathrm{d}p}{\mathrm{d}T} = 4 + a\left[\left(\frac{T}{T_{\rm tr}}\right)^{\alpha} - 1\right] . \tag{5.23}$$

In this formula the derivative $\mathrm{d}p/\,\mathrm{d}T$ is measured in MPa/K, and $T_{\rm tr} = 83.8\,\text{K}$ is the argon triple point. We take this derivative at $T_{\rm tr}$ to be 4 MPa/K, as follows from the Clausius-Clapeyron and Simon equations for argon. The parameters of formula (5.23) are $a = 2.1, \alpha = 0.78$. One can see that this derivative varies by one order of magnitude (from 4 MPa/K up to 37 MPa/K) when the temperature along the melting curve varies over the temperature (or pressure) range under consideration, from $T_{\rm m}$ up to 3400 K. The melting curve for argon, given in Fig. 5.3 at high pressures, is constructed from data of Table 5.2. We see that this theoretical curve is located above and close to the melting curve that approximates experimental results.

Thus, the phase transition in a bulk ensemble of repelling inert gas atoms is similar to the phase transition in a condensed system of bound atoms, i. e.

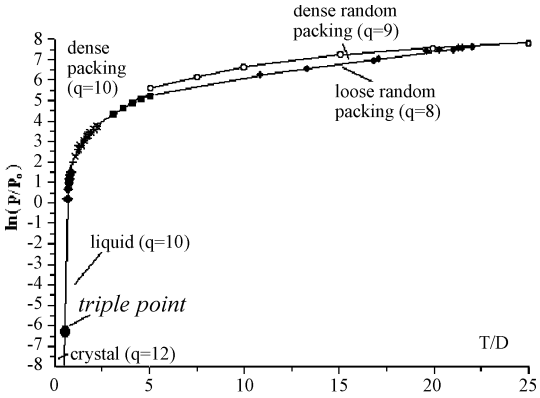

Fig. 5.3. The melting curve for condensed argon. *Solid signs* are experimental data which are joined by the experimental melting curve, q is the number of nearest neighbors for an internal atom for the corresponding aggregate states. *Open circles* correspond to evaluations based on data of Table 5.2 with the pair interaction potential as given in to Table 1.1, corresponding to the parameters $p_\mathrm{o} = 37\,\mathrm{MPa}$ and $D = 143\,\mathrm{K}$ for argon

an order–disorder or solid–liquid transition. But in contrast to the latter, the phase transition in a bulk ensemble of repelling atoms proceeds between two random distributions of atoms. In addition, according to experiments and computer simulations, a general Stishov statement [152] is fulfilled that the melting curve on the pressure–temperature phase diagram for a bulk ensemble of repelling atoms need not terminate at a critical point, but may continue up to high temperatures and pressures, until other phenomena determine the properties of the system.

One can construct the state equation of inert gases on the basis of the data of Table 5.2 and parameters of the pair interaction potential (1.3). Then for $k \gg 1$ we have on the melting curve

$$\frac{pR_\mathrm{o}^3}{T} = 10.6\,, \tag{5.24}$$

where a typical size R_o is determined by the relation

$$U(R_\mathrm{o}) = 6T\,. \tag{5.25}$$

The argon melting point evaluated on the basis of this formula with the data of Table 2.5 for parameters of the repulsion interaction potential for two argon atoms is given in Fig. 5.3 by open circles, and their joining gives us the theoretical melting curve, that lying above the experimental one. The solid state above the melting curve has a domain structure, whereas the liquid state below the melting curve is characterized by a random distribution of atoms. Next, the melting of a compressed inert gas changes the average number of nearest neighbors for a test internal atom from approximately $q = 9$ to $q = 8$,

but this number tends to $q = 10$ if the temperature of the solid aggregate state tends to zero.

One can summarize the character of evolution of the structure of solid inert gases resulting from compression in the following way. At low pressures $p \ll p_o = D/R_e^3$, the crystal has fcc structure ($q = 12$); an increase of the external pressure leads to a stacking instability which starts from $p \sim p_o$. As a result of this instability, regions of hexagonal structure develop inside the crystal, at first for layers, and later for domains or small clusters. The random distribution of cluster orientations produces a decrease of the packing density φ and of the mean coordination number q of this system due to formation of voids on boundaries of structured clusters. Together with this, pairwise interactions fix neighboring clusters. As a result, at high pressures solid inert gases consist of small solid domains – clusters – so that a bulk solid containing a large number of such domains has an amorphous structure on a long-range scale. Since interaction of adjacent domains may be determined in significant part by interaction of non-nearest atoms (depending on the specific interatomic potential), their structure can be sensitive to the details of that interaction potential. Consequently the parameters of strongly compressed rare gases at low temperatures can be very different for different inert gases. Hence, the solid system of strongly repelling atoms is characterized by order on the scale of typical sizes of individual clusters, but is amorphous on large scales.

This character of evolution of the structure of solid inert gases is substantiated by X-ray diffraction investigations of compressed inert gases at low temperatures. If we start from the crystalline state of an inert gas and increase the pressure, a stacking instability occurs in some pressure range that is reported to induce a transition from the face-centered lattice to the hexagonal lattice. In particular, for xenon at low temperatures, a stacking disorder starts to appear at a pressure of about 4 GPa ($p \approx 100 p_o$). At pressures above 70 GPa ($p \approx 2000 p_o$), high-resolution X-ray diffraction studies show the presence of only the hexagonal close-packed structure for the system of repelling atoms. But such measurements give only one aspect of the atomic structure, namely, that the correlation in positions of nearby atoms corresponds to the hexagonal structure. Simultaneously, a pressure increase reduces the long-range order of the structure, even while nearby atoms remain correlated. This results in some resonance-like maxima in the high-resolution X-ray diffraction pattern, but nevertheless the correlation length is comparable to the distance between nearest atoms. Hence this does not prove that atoms form a regular hexagonal crystal lattice.

The structure of the solid state of inert gases at high pressures is determined by the growth behavior of crystal regions as temperature decreases, or by the structure change under a pressure increase. The latter is determined by the stacking instability [163, 164] that corresponds to displacement of layers and leads to transition from fcc-lattice to the hexagonal structure for atoms of nearest layers. Since the displacement of layers becomes difficult after layers in other directions are displaced, this method to prepare the solid can lead

to an atomic density higher than one that begins from an amorphous atomic distribution. In that case, the creation of small crystallites results from diffusion of vacancies and voids outside the system. In the same manner, one can conclude that the final density for the second method depends on the rate of cooling since the final density is determined by diffusion of atoms and voids.

5.7 Structures of an Ensemble of Repelling Particles at Low Temperatures

One can expect that a size of individual domain-clusters of the ensemble solid aggregate state at low temperatures depends both on the sharpness k of the pair interaction potential (1.3) and boundary conditions (Table 5.1) which keep the particles in a restricted region. We will make rough estimations of this size for the system of hard spheres ($k \to \infty$) in formula (1.3) when the solid aggregate state is characterized by the packing parameter $\varphi = 0.64$ according to formula (5.4) or the average number of nearest neighbors $q = 10.4$ that follows from formula (5.6). We take the solid state of a bulk ensemble of repelling particles as a system of noninteracting clusters with hexagonal structure, assuming the stable clusters to be characterized by magic numbers of atoms. Note that the magic number $n = 946$ for the optimal hexagonal structure – a truncated hexahedron corresponds to the average coordination number $q = 10.5$, close to the average number $q = 10.4$ of nearest neighbors for an ensemble of repelling atoms at high pressures. Hence, within the framework of the above assumptions we infer, for an ensemble of hard balls, that the number of correlating particles on a line linking a test atom with its neighbors, is 4–5, and the total number of correlating particles is $\sim 10^3$.

Our experience is limited for the sizes of domain-clusters in different systems of repelling atoms in Table 5.1. In the case of hard balls in a container, it is $\sim 10^2$–10^3, more or less coinciding with our estimate for an ensemble of hard balls under pressure. In the case of a dusty plasma, in which charged particles of micron size may be captured by a gas discharge trap, all the particles may go into a single crystal, although the total number of particles is restricted to 10^4–10^5. In this case, charged particles of micron size are captured in the near-cathode region of a high-frequency discharge or in striations of a glow discharge. These charged macroscopic particles interact with each other through the Yukawa interaction potential; as indicated previously, with the strong screening of charges in a plasma (or large distances between nearest particles), the long-range part of the potential makes only a small contribution to the total particle interaction, so an ensemble of micron particles in a plasma trap becomes virtually identical to a system of hard particles.

Under certain conditions an ensemble of particles in a dusty plasma is analogous to saturated colloidal solutions of charged colloidal particles whose sizes are smaller by one or two orders of magnitude. With strong screening, the Yukawa interaction potential is transformed into a short-range repulsive

interaction potential that behaves much like the hard-sphere model. Hence, a system of charged dusty particles or of charged colloidal particles can be identical to an ensemble of repelling particles.

Thus, at low temperature the solid state of an ensemble of repelling particles has a polycrystalline structure, but the sizes of individual crystallites depend both on the parameters of the pair interaction potential (1.3) of repelling particles, and on the boundary conditions which compel the particles to locate in a restricted region. This analysis shows that simple systems – ensembles of repelling classical particles – demonstrate a nonsimple kind of behavior.

Part II

Configurational Excitations and Aggregate States of Ensembles of Classical Particles

6

Configurational Excitation and Voids in Ensembles of Bound Classical Atoms

6.1 Separation of Thermal and Configurational Degrees of Freedom of Clusters

Let us consider the evolution of a classical cluster, an ensemble of a finite number of bound classical atoms, as motion in the space defined by the atomic coordinates and the internal potential energy of the atomic interactions. We assume we are dealing with clusters whose ground electronic state is well separated from electronically excited states. We assume also that we need consider only pair interactions between atoms. The typical potential energy surface for a cluster contains many minima separated by barriers; evolution of a classical cluster consists of occasional transitions between neighboring local minima on that surface, followed by rapid equilibration of the relatively fast atomic vibrations, via coupling of the internal vibrational modes.

Figure 1.4 demonstrates the character of transitions between neighboring minima of the potential energy surface. In Fig. 1.4 schematic projections of a potential energy surface on planes are given in a space of atomic coordinates, and only one coordinate is used for each transition; this is a schematic representation of motion from one minimum to the next, represented by an axis connecting the two local minima. These axes are of course unique for each transition. The use of a schematic representation allows us to avoid specifying the precise path the system takes as it goes from one minimum to the next. Energy levels for each well indicate an average internal energy along a coordinate of the transition. Because this energy is often significantly less than the barrier height, such transitions proceed seldom, only when the kinetic energy of atoms in the transition degree of freedom exceeds its average energy adequately. Hence a cluster has many oscillations inside a given well until it transfers to another local minimum of the potential energy surface. We identify each local minimum above the global minimum, together with the local well around it, as a configurational excitation of a cluster. In so doing, one can separate the structural contribution to the total internal energy from thermal motion associated with atomic oscillations (see Fig. 1.5).

Thus, describing cluster evolution as transitions between neighboring local minima of the potential energy surface, we divide cluster excitation in two parts, thermal and configurational. We can safely assume those to be independent and characterize each configurational state of this system by its own local minimum. This will be the basis of a subsequent analysis of aggregate states and phase transitions between them. Indeed, just configurational excitation is responsible for formation the aggregate state. We shall apply these concepts to some simple examples. In addition, we will justify that a typical time of passage between neighboring local minima is long enough that equilibrium among the vibrational degrees of freedom occurs faster than a typical change of configurational state. This allows us to characterize thermal (or vibrational) motion of atoms in a cluster by a certain temperature.

6.2 Lattice Model for the Order–Disorder Phase Transition

The nature of the phase transition between two aggregate states of a condensed system of atoms has been interpreted on the basis of the lattice model [229–232]. Within the framework of this model, we place atoms in sites of a crystal lattice, as shown for the square lattice in Fig. 6.1. Denoting by n_1 the number of atoms in lattice sites and by n the total number of sites, we consider the limit of a large number of atoms $n_1 \longrightarrow \infty$; the concentration of atoms is $c = n_1/n$. We consider the Bragg–Williams approximation [229, 230, 232–234], a simple version of the lattice model, assuming interaction of nearest neighbors only. In the limit under consideration $n \longrightarrow \infty$ one can extract two types of atomic distributions over the lattice sites, so that in the first the binding energy is maximal; a random distribution with higher entropy corresponds to the second type. In the first case, for a compact atomic distribution, we obtain the total binding energy of the system to be $kn_1\varepsilon_o/2$, where ε_o is the binding energy per bond, and k is the number of nearest neighbors for an internal atom.

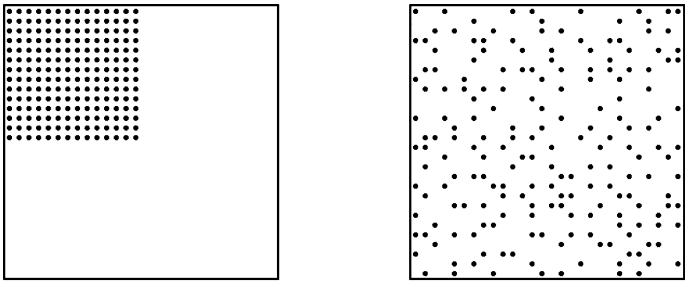

Fig. 6.1. The distribution of atoms over the sites of a square lattice for the ordered (**a**) and disordered (**b**) aggregate states of an atomic ensemble

Analyzing the random distribution of atoms over the sites, we obtain the average number of nearest neighbors for a test atom to be kc, and the average binding energy is $kcn_1\varepsilon_o/2 = knc^2\varepsilon_o/2$. Therefore, the energy change as a result of transition from the compact or ordered distribution of atoms to a random distribution is

$$\Delta E = \frac{k}{2}nc\varepsilon_o - \frac{k}{2}nc^2\varepsilon_o = \frac{q\varepsilon_o}{2}nc(1-c)\ . \tag{6.1}$$

The entropy of the random distribution of atoms is

$$S = \ln\frac{n!}{n_1!(n-n_1)!} = -n[c\ln c + (1-c)\ln(1-c)]\ , \tag{6.2}$$

and we take the entropy of the completely ordered lattice as 0. The change of the free energy ΔF as a result of transition between the ordered and disordered states is thus

$$\Delta F = \Delta E - TS = \frac{k\varepsilon_o}{2}nc(1-c) + Tn[c\ln c + (1-c)\ln(1-c)]\ , \tag{6.3}$$

where we use the Stirling formula and the condition $n_{1,2} \gg 1$. This gives the temperature T_c of the phase transition according to the relation $\Delta F(T_c) = 0$

$$T_c = \frac{k\varepsilon_o}{2\left(\dfrac{\ln\frac{1}{c}}{1-c} + \dfrac{\ln\frac{1}{1-c}}{c}\right)}\ . \tag{6.4}$$

We note that in this treatment the atomic concentration c is fixed, but the number of unoccupied sites is a free parameter of the problem. Since this parameter is not connected with any specific properties of an ensemble of bound atoms, the lattice model allows us to make qualitative, general conclusions about the nature of the phase transition. Indeed, we have two distributions of bound atoms in a loosely confined space, a compact (or ordered) distribution of atoms with a large total binding energy and a random distribution with a large entropy (or statistical weight). Competition between these two forms leads the system to equilibrate to the more thermodynamically stable state. From this it follows that the phase transition from compact to the less ordered state is possible only under conditions in which the aggregate state with the lower binding energy has a large statistical weight. From this standpoint one can analyze and contrast atoms (and small molecules) and clusters. Both systems have shell structures, but the excited states of atoms and small molecules are sparse, so the statistical weights of their excited states are not large, and therefore phase transitions are impossible in such systems. This contrasts with the cluster case. (It is possible, however, that ensembles of heavy atoms with open electronic shells could show order–disorder transitions at temperatures high enough to produce a variety of excited electronic states.)

One more conclusion from this treatment is the stepwise character of the phase transition for an ensemble of many bound atoms. Indeed, the ratio of the

probabilities for the ensemble to be found in the disordered and ordered state is characterized by the factor $\exp\left(-\frac{\Delta F}{T}\right)$, where T is a current temperature, and ΔF is the free energy difference for the ordered and disordered aggregate states. A temperature range in which the ordered and disordered states coexist in observable quantities, i. e. the probabilities for these states are comparable, is

$$\frac{\delta T}{T_\mathrm{c}} \sim \frac{T_\mathrm{c}}{\Delta E} \sim \frac{1}{n} \,. \tag{6.5}$$

Thus the width of the range of observable coexistence in thermal equilibrium is inversely proportional to the number of atoms. In the limit $n \to \infty$ we obtain a stepwise transition. In fact, the transition is effectively stepwise for any macroscopic assembly of atoms or molecules.

We now go on to use the lattice model to describe condensed inert gases near their triple point. Recall that the vacancy concentration c is a free parameter of the model; we found it previously for liquid inert gases from the lattice model (Table 3.5), and from the enthalpy and density change at the triple point. This gave the average value of the number of nearest neighbors (3.11) and (3.12) within the framework of the lattice model to be $q = 10.15 \pm 0.06$, corresponding to the concentration of atoms in the close-packed crystal lattice of $c = q/12 = 0.846 \pm 0.005$. From this we obtain the melting point according to formula (6.4) $T_\mathrm{m} = 1.82 \pm 0.01$, which differs significantly from its real value $T_\mathrm{m} = 0.58$ (Table 2.8).

Thus the lattice model is able to describe the phase transition only qualitatively. Indeed, the subsequent analysis will show the role of thermal motion of atoms in the phase transition, while the lattice model ignores this. Next, the lattice model describes phase transitions of second order, whereas the melting of solid inert gases, like all melting, is first order. Nevertheless, this model is useful because it gives the concept of the order–disorder phase transition in a simple, qualitatively correct form.

6.3 Chemical Equilibria and Phase Transitions

The order–disorder phase transition in a bulk ensemble of atoms involves a stepwise change of the internal energy so is a phase transition of first order in a bulk system, sharp and stepwise as the temperature passes through the melting point. This leads to the infinite heat capacity of this atomic system. But a strong increase of the heat capacity is observed in some chemical transformations; we now compare phase transitions of the first type with chemical transformations. A strong increase of the heat capacity takes place as a chemical transformation takes place for transitions between discrete and continuous states, in particular, for ionization and dissociation equilibria. Let us use as an example the ionization equilibrium associated with an electron–atom collision

$$A + e \longleftrightarrow A^+ + 2e \,. \tag{6.6}$$

We have an analogy of the ionization equilibrium and the order–disorder phase transition because atomic ionization requires an energy that exceeds the atomic ionization potential, but the right-hand continuum state is characterized by a statistical weight much larger than that on the left, and hence the transition from the ground atom state into the ionized state proceeds with a very large entropy change. Thus, one can see a formal analogy between the phase transition and the ionization transition in a gas [235]. We shall consider this analogy in detail, to obtain a principal difference between phase transitions and chemical transformations.

Let us introduce a test atom in a gas; it may be in either the bound or ionized with probabilities w_a and w_e, respectively. Since we allow only these two states, we have $w_\mathrm{e} + w_\mathrm{a} = 1$. The relation between these probabilities is given by the Saha equation [4, 167]

$$\frac{w_\mathrm{e}^2}{w_\mathrm{a}} = g \exp\left(-\frac{J}{T_\mathrm{e}}\right) . \tag{6.7}$$

Here J is the atomic ionization potential, T_e is the electron temperature, and $g \gg 1$ is the statistical weight of the continuous spectrum state. The statistical weight of continuous spectrum is roughly the ratio of the volume per atom in the container to a typical atomic volume (more exactly, to the volume per electron when the gaseous criterion for electrons is violated), and therefore it is large. Hence, the transition from neutral to ionized gas occurs at a relatively low temperature T_* compared to the ionization potential J. We define the transition temperature T_* from the relation $w_\mathrm{e}(T_*) = w_\mathrm{a}(T_*) = 1/2$. Next, a large statistical weight provides a narrow temperature range ΔT for the transition from the ionization to neutral state which is

$$\Delta T \sim \frac{T_*}{\ln g} . \tag{6.8}$$

Therefore, the heat capacity of ionized gas becomes large in the transition range. As an example, we give in Fig. 6.2 the heat capacity of ionizing sodium vapor in the temperature range in which the ionizing transition occurs.

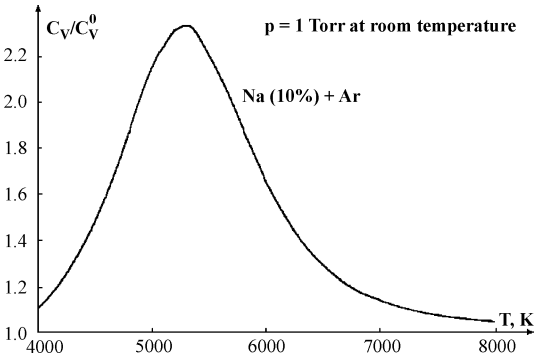

Fig. 6.2. The heat capacity of the mixture of 10% sodium atoms in argon at the total density that corresponds to the pressure of 1 Torr at room temperature

Let us construct the partition function for the ionized and neutral states. Taking the total number of nuclei in the system to be n, and the number of ionized atoms to be m, we determine the probability of this event by the Poisson formula

$$W_{nm} = C_n^m w_{\mathrm{e}}^m w_{\mathrm{a}}^{n-m} = C_n^m w_{\mathrm{e}}^m (1 - w_{\mathrm{e}})^{n-m} \; .$$

The partition function Z_{nm} of the system with a given number of free and bound electrons is proportional to the value of W_{nm}. Note that formation of m free electrons in this system corresponds to the excitation energy $m(J + 3T_{\mathrm{e}}/2) \approx mJ$. In the case of a large number of free and bound electrons in the system $m \gg 1, n \gg 1$, the partition function Z_{nm} as a function of m has a sharp maximum, and near the maximum $m = m_{\mathrm{o}}$ it has the form

$$Z_{nm} = Z_{\mathrm{o}} \exp\left[-\alpha(m - m_{\mathrm{o}})^2\right] \; , \tag{6.9}$$

and according to the above relations we have

$$m_{\mathrm{o}} = n w_{\mathrm{e}} \; ; \quad \alpha = \frac{1}{2m_{\mathrm{o}}} \cdot \frac{n}{n - m_{\mathrm{o}}} \; . \tag{6.10}$$

Thus the partition function has a narrow maximum in a specific range of the number of ionized electrons $\Delta m \sim \sqrt{n}$, if $m_{\mathrm{o}} \sim n$, and the relative maximum width $\Delta m/m_{\mathrm{o}}$ tends to zero as $\sim 1/\sqrt{n}$, when the total number of free and bound electrons tends to infinity.

Comparing the partition function of the disordered aggregate state in the order–disorder transition with that of the ionized state in the case of ionization equilibrium reveals the analogy in their structure. Moreover, in both cases the transition energy is proportional to the number of transferring particles. The partition function of the disordered aggregate state is summed over bonds between particles. Evidently, this partition function is a sharp function of the number of bonds, similar to the partition function of an ionized gas with respect to a number of free electrons. Hence we have an analogy between the partition functions of the disordered aggregate state of interacting atoms and of an ionized gas, based on the number of broken bonds in the first case and the number of ionized atoms in the second case. But in the case of the order–disorder phase transition the ordered aggregate state is characterized by a local maximum at a relatively small number of broken bonds. We characterize the first as a phase transition, evaluating the partition functions of both forms separately, so that each form has its own maximum, each at a different value of the excitation energy (see Fig. 6.2). We treat the ionization case as a chemical equilibrium and thus compute the partition function for the entire system, so the value of the partition function determines the relative amounts of each form, neutral and ionized, at equilibrium at any chosen temperature. From this approach, the partition function exhibits only one single maximum, corresponding to a system in which both states exist together. Hence, in the case of chemical equilibrium the transition between limiting chemical states proceeds in a continuous way, as the temperature varies and the partition

function maximum drifts. The order–disorder phase transition corresponds to passage between two maxima of the partition function. Thus, the phase transitions and chemical transformations have a different nature [235].

6.4 Internal Voids in a System of Identical Particles

We now consider a configurationally excited state of a system of many classical particles from the standpoint of void formation inside this system. Consider a void or empty internal space as an elementary configurational excitation of an ensemble of bound classical particles; In this way, we consider a void as a relaxed, and hence transformed vacancy. But in contrast to a vacancy in an ordered solid, a void has an indefinite volume and shape that change in time. Therefore from the standpoint of saddle-crossing dynamics, each configurationally excited state corresponds to a certain number of voids which we can take to be identical on average. The concept of an average void is useful when configurational excitation can be separated from the vibrational excitation associated with an increase of the kinetic energy of the atoms. Then we define the cluster's aggregate state as a sum of its accessible configurations in the multidimensional space of atomic coordinates near the relevant local minima of PES, with their nearby excitation energies. This is a generalized definition of the aggregate state (and, by implication, of the configurational entropy) in contrast to that of traditional thermodynamics, in which the phase or aggregate state is characterized by a uniform (mean) spatial distribution of atoms, i. e. an excited aggregate thermodynamic state includes many elementary configurational excitations. For clusters, the liquid aggregate state can contain even as few as one elementary excitation, as in the case of the Lennard-Jones cluster of 13 atoms. Hence uniformity of the kind invoked for a bulk phase is not a requirement for the aggregate state of a cluster. One could, for example, differentiate between an aggregate state whose voids are all in a surface layer from one in which the same number of voids could be anywhere in the cluster.

The void concept is convenient also for the analysis of condensed inert gases for which the scaling law is valid and nearest-neighbor interactions give the main contributions to the parameters. Within the framework of the void concept, one can describe coexistence of the solid and liquid phases in a cluster as a result of formation and decay of voids [236, 237]. Hence, the hierarchy of times for establishment of thermal equilibrium, the lifetimes of aggregate states and typical times of cluster interaction with an environment must be included in analyzing cluster phase transitions.

It is convenient to construct a configurationally excited state of a system of bound particles by starting from the crystalline distribution (or polyhedral, for clusters) of particles and creating vacancies inside the system. An internal vacancy is an elemental configurational excitation in this case. In order to construct a cluster consisting of n particles and v vacancies, we take at the beginning a cluster consisting of $n + v$ particles in the ground configuration

state, with no internal vacancies, and remove v particles to the outside. If $n > 12v$, we can assume that the internal vacancies do not border each other. Then each specific configuration of vacancies corresponds to a certain local minimum of the PES for this particle ensemble, and neighboring local minima are separated by barriers. Assuming the particles to be identical, we obtain the number of configurations in this case to be equal to the number of particle and vacancy combinations C^v_{n+v}. From this we determine statistical parameters of such a particle configuration. Indeed, the entropy of this configuration excitation $S_{\rm con}$ and the excitation energy E are

$$\begin{aligned} S_{\rm con} &= \ln C^v_{n+v} = \frac{\ln(n+v)!}{\ln n! \ln v!} = (n+v)\ln(n+v) - n\ln n - v\ln v \ , \\ E &= v\varepsilon_{\rm v} \ , \quad \frac{n}{12} > v \gg 1 \ . \end{aligned} \tag{6.11}$$

Here $\varepsilon_{\rm v}$ is the energy of formation of an individual vacancy. In this manner we use parameters of classical thermodynamics to describe a system of bound particles.

One can generalize this operation for the case with a larger number of vacancies, $12v \sim n$, if neighboring vacancies can border. By taking into account the effect of vacancies on the vibrational frequencies of the component atoms and of the lattice, one finds that the system stabilizes when vacancies do neighbor [236]. The reason, of course, is that the more vacancies that neighbor, the lower are the vibrational frequencies associated with that region, so the density of states and the entropy increase, and the energy drops because the zero-point energy drops.

But vacancies, particularly when they border other vacancies, no longer remain as empty lattice sites. They undergo a relaxation process that typically involves some (small) shrinkage of the volume or increase of density. Then the particle's crystal structure is lost, and vacancies transform in voids whose shape and volume vary in time, in contrast to vacancies. Voids are elementary configurational excitations that involve more than minimal configurational excitations. Any specific number of internal voids v can be identified with a specific configurational excitation of of the n bound particles.

Moreover, to generate an atomic ensemble with a given number of particles n and internal voids v, we start with a crystalline particle of $n+v$ particles and remove from it v particles. A newly-formed system of n particles and v internal voids relaxes, resulting in its compression. We assume that this process leads to formation of v voids; this is the basic assumption of our treatment. In other words, each configuration of n particles and v voids leads to formation of a certain stable particle configuration that corresponds to a certain local minimum of PES for this ensemble of classical particles.

In this manner we associate each configurationally excited state of a system of n bound particles with a stable configuration of particles, i. e. it corresponds to a certain local minimum of the PES. From a more coarse-grained viewpoint, this configurationally excited state includes a specific set of voids, determined

by their number and approximate location. That is, we ascribe configurational excitation to relaxed elemental configurational excitations. Such a configurationally excited state of a system is not necessarily stable in the thermodynamic sense, since voids can go to the cluster boundary and disappear there. However entropy alone can make such a state more stable than the void-free state, at sufficiently high temperatures; real solids do have defects, including voids.

The process of transition between two neighboring local minima of the PES results from void transport and has an activation character, so that at low temperatures, that process is slow. Therefore this configurationally excited state may be a nonequilibrium state, but its lifetime is typically long enough at low temperatures that we can observe it for time intervals long enough to ascribe quasistationary state properties to it, yet brief compared with a time for transport of its voids to the boundary or from it. Thus we have three time scales in this analysis: the shortest, corresponding to vibrational relaxation of a specific configuration; the intermediate, corresponding to the process of configurational excitation, and the longest (which we do not use here) that corresponds to the system reaching its "ultimate" thermal equilibrium state, and achieving ergodicity [237].

We use the assumption of equal numbers of initial vacancies and final voids to develop a simple method to create a configurationally excited state for our system of classical particles. Indeed, the relaxation of an system initially with voids among its particles converts vacancies into voids in times comparable to particle oscillation periods ($\sim 1/\omega_{\mathrm{D}}$), but this does not imply that the numbers of vacancies and voids are precisely equal. Nevertheless, one can find limiting values for the number of voids after relaxation of the system that begins with vacancies. First, because the system shrinks during its relaxation, the number of voids does not exceed the number of initial vacancies. This rationalizes the assumption that the number of initial vacancies is equal to the number of final voids, a relation valid in the limit of small void concentrations c given by

$$c = \frac{v}{n} \, . \tag{6.12}$$

Second, compression or shrinkage of the system leads to an increase of the average number of nearest neighbors for each internal atom. Therefore, the empty volume V_{v} per void does not exceed the volume per vacancy (if the vacancies do not join into bubbles).

Now we define the aggregate state as the set of all the configurational states with similar excitation energies and correspondingly with approximately the same density or number of voids. We can evaluate the probability of this set of configuration states comprising this aggregate state and use it to assign an entropy to the aggregate state. For a given n and void concentration c, the total statistical weight, and of course the entropy, increase with an increase of the void concentration c, because increasing c increases the volume where a particle can be located. Hence, in considering this configurational excitation,

we introduce the statistical weight $g_{\rm v}$ of a void that accounts for this effect. In addition, we take the energy of formation of an elemental void $\varepsilon_{\rm v}$ to be a function of the void concentration c. The expansion of the system as a result of configurational excitation is small, and hence makes only a small contribution to the cluster's free energy. Then the free energy for configuration excited state of this particle ensemble is

$$F = -TS_{\rm con} - Tv \ln g_{\rm v} + v\varepsilon_{\rm v} \; . \tag{6.13}$$

Here we neglect the pressure term, being guided by the behavior of inert gases near their triple points, where this term is small. From this we find the entropy variation per void as a result of the phase transition

$$\Delta s = \frac{S_{\rm con}}{v} + \ln g_{\rm v} = \frac{1}{c} \ln(1+c) + \ln\left(1 + \frac{1}{c}\right) + \ln g_{\rm v} \; . \tag{6.14}$$

The last term accounts for the different compactness of the solid and liquid states, and the first terms include the contribution of the number of different atomic configurations for a given configurationally excited state at a given temperature. In the case when two aggregate states exist the dependence of the partition function of the particle ensemble on a void number is given in Fig. 6.3 [46], and maxima of the partition function correspond to aggregate states.

Strictly, for any given problem, one must specify what set of voids define each aggregate state. For small systems, this does not arise, but for clusters of moderate to large size, say n of about 50 or more, one has a choice. As mentioned previously, one can define one aggregate state for each specific number v of voids, or one can define one aggregate state in which all the voids are confined to the system's surface and another in which the voids are in the interior. If the void density and temperature are high enough, these would correspond to surface-melted and liquid states, respectively. Another arbitrary distinction one may make is in the choice of distinguishing aggregate states strictly by the number of voids, or by the energy band in which a set

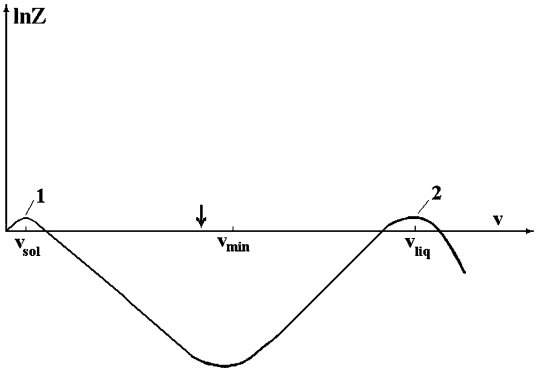

Fig. 6.3. The logarithm of the partition function for an ensemble of bound atoms with a pairwise atomic interaction depending on the energy of configurational excitation at the melting point [46]. The group of states 1 corresponds to the solid aggregate state, the group of states 2, to the liquid aggregate state

of configurationally excited states lies. The choice in situations of these kinds should obviously be based one what kind of observation one is trying to describe, and to the energy and time resolution of that observation. In practice, we do not foresee any serious difficulties in choosing how to define aggregate states suitable to a given investigation.

6.5 Void Formation in Two Dimensions

The first step of this method to prepare a configurationally excited state is generating the desired set of internal vacancies for the two-dimensional particle distribution. In the second stage, the excited ensemble relaxes, and vacancies evolve into relaxed voids, causing the system to shrink. Of course, the relaxation and shrinkage are weak if the initial concentration of vacancies is small, $c < 1/12$, so no vacancy has another vacancy as a nearest neighbor. In the more concentrated situation, $c > 1/12$, when vacancies become voids, one can still assume, guided by the liquid aggregate state of inert gases, that the number of final voids is roughly equal to the number of initial vacancies. Thus we suppose that vacancies do not join into bubbles. Even if some effective attractive forces do bring voids together to some extent, we can still suppose that the fully relaxed void space is approximately that of the sum of the separate, isolated voids [236]. In the cases of ensembles of repulsive particles, c.f. Table 5.1, it is useful to use the model of hard spheres for particles [153, 160–162] with each particle modelled by a hard ball. We start from the two-dimensional case with hard disks filling an area [238].

Thus, we model the two-dimensional case with circles of radius a. At the beginning, we take an element of the hexagonal lattice consisting of 16 particles, as shown in Fig. 6.4. The centers of circles are sites of the hexagonal lattice and each internal atom has 6 nearest neighbors. Configurational excitation may be described as a result of removal of some circles and formation of vacancies in positions from which circles are removed. So long as the number of these vacancies is relatively small and these vacancies do not border each other, such an excited state is stable.

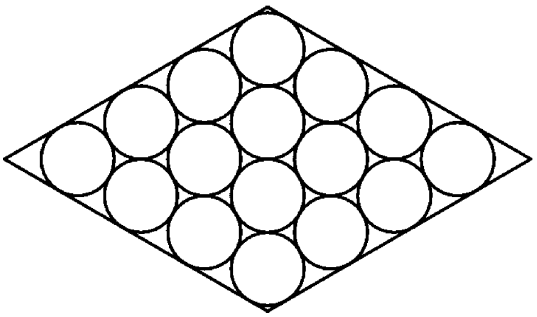

Fig. 6.4. An element of 16 particles-disks which form a compact hexagonal structure and are located in a rhombic box that provides the maximum density of particles in it [238]

After relaxation, an element of the hexagonal lattice with vacancies produced by removal of one (Fig. 6.5) or two (Fig. 6.6) neighboring particles (circles) shrinks, and surrounding atoms move to fill some of the empty space. After this shrinkage, two pentagons may be formed (Fig. 6.7), and the original empty space is partially filled. This leads to a decrease of the area of this element as well as to internal voids. For simplicity, we consider only symmetric configurations of particles that can be formed after relaxation. As a result of compression of the element under consideration, the total system's volume shrinks, and dislocations with tensions are formed inside and on boundaries of this element. In addition, the number of nearest neighbors for some particles decreases from that of the initial configuration, and the average empty space for each surrounding particle increases.

In analyzing an ensemble of hard disks, we introduce the packing parameter φ by analogy with the three-dimensional case (5.2), that is, that measures the fraction of the total area occupied by disks. Taking an element of an area S that includes k identical disks of a radius a, we define the packing parameter as [153]

$$\varphi = k\frac{\pi a^2}{S} \; . \tag{6.15}$$

Then the maximum value of the packing parameter corresponds to the hexagonal crystal lattice and is equal to

$$\varphi_{\rm hex} = \frac{\pi}{2\sqrt{3}} = 0.907 \; . \tag{6.16}$$

We will be guided by this value as the maximum packing parameter.

We now analyze the case when 16 particles or disks are located in a rhombic box and attach to its edges (Fig. 6.4). This element may be cut out of the hexagonal crystal lattice. The angles between rhombus sides are $\pi/3$ and $2\pi/3$, and the side length is $(6 + 4/\sqrt{3})a = 8.309a$. The packing parameter for this system is less than that for a bulk hexagonal lattice and is equal to

$$\varphi_{16} = \frac{8\pi\sqrt{3}}{(3\sqrt{3}+2)^2} = 0.841 \; . \tag{6.17}$$

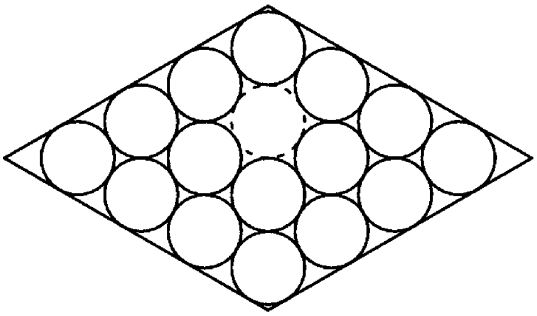

Fig. 6.5. An element of a compact hexagonal structure consisting of 16 particles-disks in a rhombic box with one vacancy [238]

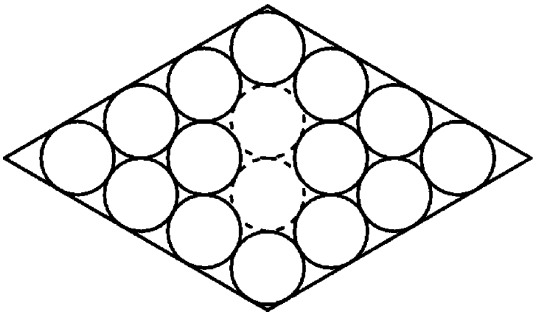

Fig. 6.6. An element of a compact hexagonal structure consisting of 16 particles-disks in a rhombic box with two vacancies [238]

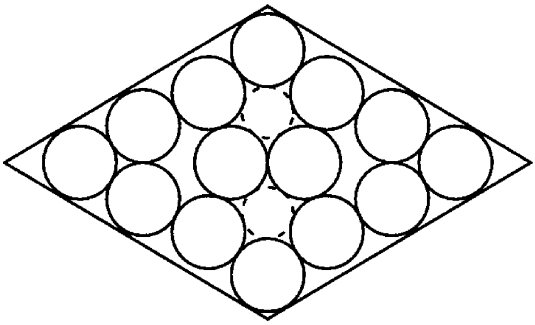

Fig. 6.7. The character of transformation of vacancies into voids for a compact hexagonal structure in a rhombic box [238]

From this one can construct ensembles of particles in a box with one vacancy (Fig. 6.5) and two vacancies (Fig. 6.6), by removal of one and two atoms from an element of Fig. 6.4. The packing parameters in these cases are given by

$$\varphi_{15} = \frac{15}{16}\varphi_{16} = 0.788\,, \quad \varphi_{14} = \frac{14}{16}\varphi_{16} = 0.736\,. \tag{6.18}$$

In the latter case two vacancies may transform into two voids, as shown in Fig. 6.7 for a symmetric configuration of the particles and voids. In contrast to vacancies, voids can change their shape and size.

But too dense a packing does not allow particles (and vacancies) to change their positions. Indeed, particle 1 of Fig. 6.8 can transfer to the position 2 if the distance between two neighboring particles 3 and 4 exceeds $4a$, whereas it is $2a + a\sqrt{3}$ for the close-packed particles in the rhombic box. This particle transition becomes possible if we increase a box size.

Let us introduce the parameter r, so that a rhombus side for the box is

$$l = \left(6 + \frac{4}{\sqrt{3}}\right) r\,. \tag{6.19}$$

Under conditions of Fig. 6.4 we have $r = a$; the case $\Delta r = r - a \ll a$ in which relative positions of particles change only slightly. The distance AB of Fig. 6.8 is equal to $(3\sqrt{3}+2)a$ and becomes $(3\sqrt{3}+2)r$ after the box is enlarged. For particle 1 to pass into a new position, the initial value AB must increase at

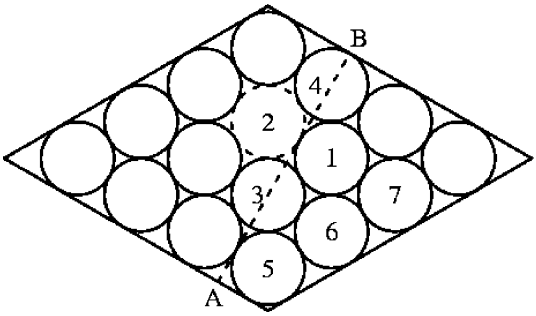

Fig. 6.8. The character of the transition of a particle in the box of particles, when this transition changes the particle configuration [238]

least by $(2-\sqrt{3})a$; this value exceeds $(4+2\sqrt{3})a$. Thus, particle 1 of Fig. 6.9 may transfer to position 2 when the criterion $r-a \geq 0.037a$ is fulfilled, as it is under conditions

$$(3\sqrt{3}+2)r \geq (4+2\sqrt{3})a \tag{6.20}$$

or $r \geq 1.037a$. This corresponds to the packing parameter

$$\varphi \geq \left(\frac{a}{r}\right)^2 \varphi_{15} = 0.732\,. \tag{6.21}$$

This value is approximately that of the packing parameter for formation of two vacancies as given in Fig. 6.6. Note that the critical packing parameter for particle transition depends on the box shape.

In the same manner one can find the minimum packing parameter required for a particle to move between positions 6 and 1 of Fig. 6.8. On the basis of the above consideration, we obtain again the relation (6.20) for the packing parameter in this case. Next, let us consider a transition between positions 5 and 6 of Fig. 6.8 or between positions 5 and 3, when one of these positions is located in a box angle and, of course, one of transition positions is free. This transition is possible if the length AB is increased by $(2-\sqrt{3})a$, which allows transfer of a particle in an obtuse angle, or of another particle to an obtuse angle site. We obtain the minimal packing parameter for particle transfer in this case also in accordance with formula (6.20).

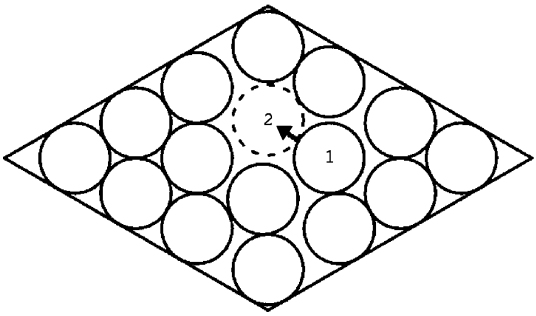

Fig. 6.9. Particles-disks in a rhombic box at the density that ensures transition of particles and voids to other positions [238]

Thus, we find the critical value of the packing parameter above which transitions of particles and vacancies are possible in a box under the conditions given above. This consideration is based on conservation of the particle configuration when the box is enlarged; i. e. it requires that the criterion $\Delta r = r - a \ll a$ holds true. The criterion gives $\Delta r \geq 0.037a$; this requirement must be fulfilled for site-to-site passage to occur. Up to the critical value of the packing parameter, the diffusion coefficient for particles in a box due to their thermal motion is zero; it increases with a decrease of the packing parameter. For small numbers of particles, the diffusion coefficient in a box depends also on the box shape.

Note that the structure of 2 regular pentagons (Fig. 6.6) is not stable, i. e. the atoms are subject to the action of tensions. Nevertheless, the two voids, one centered in each pentagon, are conserved during particle motion, although both the area of each void and its shape vary in the course of particle motion. These voids can change their positions and even join with each other, but this requires specific positions of surrounding particles since voids are locked by particles. Hence such diffusive transitions are activation processes. In considering simple configurations of disks, we note that in contrast to Figs. 6.6 and 6.7, in reality the gap between two neighboring circles changes shape continually; this facilitates displacement of voids and decreases tensions inside the system. Thus, within the framework of the scheme of void generation through formation of a specified number of vacancies in a crystal lattice, we find that the equality between a number of initial vacancies and final voids is entirely plausible.

6.6 The Cell Model for Disk Particles

The cell model for an ensemble of particles [239–241] assumes that disk-like particles can occupy positions inside certain cells which are given in Fig. 6.10 in the two-dimensional space. We will determine the partition function for an ensemble of disk-particles as a function of the packing parameter (5.2). Starting from the hexagonal structure of disks with the packing parameter $\varphi_{\text{hex}} = 0.907$, we will decrease the packing parameter. Within the framework of the cell model, this involves two phenomena: an increase of the radius r of an individual cell beyond that of the disk radius a, and formation of vacancies.

Suppose the initial area contains $n + v$ cells, and n of them are occupied by particles. Thus v empty cell are vacancies. Then the packing parameter is

$$\varphi = \varphi_{\text{hex}} \cdot \frac{n}{n+v} \cdot \left(\frac{a}{r}\right)^2 . \tag{6.22}$$

The partition function of this system with an accuracy up to a constant factor is

$$Z = C_{n+v}^{n} \cdot \left(\frac{r^2 - a^2}{a^2}\right)^n . \tag{6.23}$$

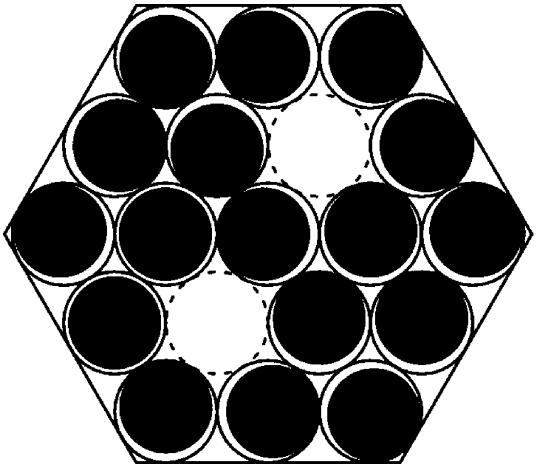

Fig. 6.10. The cell model, in which disk-particles (*solid circles*) are located in their cells (*open circles*) [238]

We take the partition function of an individual particle in its cell to be proportional to an area $\pi(r^2 - a^2)$ that is available to the particle in its cell. The first factor of this formula takes into account permutations of particles and cells. In order to obtain a thermodynamically stable state, it is necessary to optimize the entropy $S = \ln Z$ with respect to the number of vacancies at a given value of the packing parameter φ. For large values of n and v we have

$$\begin{aligned} S = \ln Z &= \ln C_{n+v}^{n} + n \ln \left(\frac{r^2 - a^2}{a^2} \right) \\ &= n \ln \left(1 + \frac{v}{n} \right) + v \ln \left(1 + \frac{n}{v} \right) + n \ln \left(\frac{r^2 - a^2}{a^2} \right) \ . \end{aligned} \tag{6.24}$$

Expressing the cell radius from formula (6.22) and substituting it into formula (6.24), we find for the entropy per particle ($s = S/n$)

$$s = c \ln \left(1 + \frac{1}{c} \right) + \ln(c_{\max} - c) \ , \tag{6.25}$$

where the vacancy concentration is introduced as $c = v/n$, and its maximum value at a given packing parameter φ is attained when the cell radius is equal to the particle radius ($r = a$) and is

$$c_{\max} = \left(\frac{\varphi_{\text{hex}} - \varphi}{\varphi} \right) \ . \tag{6.26}$$

To derive formula (6.26), we take the cell radius r at a given packing parameter φ from formula (6.22) and substitute it into formula (6.24). Note that the entropy per particle s is defined only up to a constant.

To optimize the cell and particle distributions, we find the vacancy concentration c_{o} that corresponds to the maximum entropy. If $\varphi \sim \varphi_{\text{hex}}$, this

corresponds to a low value of the optimal vacancy concentration given approximately by

$$c_{\rm o} = \exp\left(-\frac{1+c_{\max}}{c_{\max}}\right) . \tag{6.27}$$

This value varies from 0.012 up to 0.12, if $c_{\max}$ varies from 0.2 up to 0.6, corresponding to variation of the packing parameter from 0.76 to 0.57. Thus, within the framework of the disk model for particles, a decrease of the packing parameter leads mostly to increase the cell radius, while only a small part of the increase of area per particle goes to formation of new vacancies.

Note that an ensemble of disk particles is, in a sense, a dense gas, since interactions between particles occur only when they touch with each other. Hence the interaction time for colliding particles is effectively infinitesimal; essentially the particles are free except during those instantaneous collisions. In contrast, in a real condensed system of repelling particles, a test particle interacts with nearest neighbors strongly, i. e. at all times, the interaction potential of a test particle with its neighbors is comparable to its kinetic energy. In order to understand the role of interparticle interactions in establishing their optimal spatial distributions, we analyze how the interactions between particles affect the entropy of the particle ensemble. The entropy for the cell model when particles are at cell centers, essentially its average, has the form [238]

$$S = \ln Z = \ln C_{n+v}^{n} + n \ln\left(\frac{r^2-a^2}{a^2}\right) - qn\frac{U(r)}{T} , \tag{6.28}$$

where $q = 6 - c$ is the average number of nearest neighbors for a test particle, $U(r)$ is the pair interaction potential at a distance r between particles, and we scale the interaction potential between nearest particles by that at an average distance between particles. The temperature T is expressed in energetic units. This gives for the entropy variation [238]

$$\mathrm{d}s = \mathrm{d}c\left[\ln\left(1+\frac{1}{c}\right) - \frac{1-c_{\max}}{(1+c)(c_{\max}-c)} + \frac{U(r)}{T} - \frac{qk}{2}\cdot\frac{U(r)}{T}\frac{1}{1+c}\right] . \tag{6.29}$$

According to this formula, the entropy decreases with the decreasing cell radius due to terms proportional to $U(r)/T$. Hence the optimal conditions for the particle concentration correspond to a lower vacancy concentration c than that for the hard disk model [238].

6.7 Peculiarities of Configurational Excitation for Bulk Atomic Systems

In considering the solid–liquid phase transition for a bulk system of bound atoms and their clusters in terms of thermodynamics, we characterize each aggregate state of this system by thermodynamic parameters and use the

two-state approximation for aggregate states. We assume there are only two aggregate states for a system of bound atoms, namely the solid and liquid states. Although a thermodynamic description of the aggregate states is universal, it is phenomenological, and we encounter questions connected with the microscopic nature of these states and require introducing the character of atom–atom interactions. For example, one question is, "Why does the phase transition have a stepwise character, while excitation of a large system is typically continuous?" In addition, "Why, for a bulk system, can we postulate existence of only two aggregate states, rather than just one or several?" In order to answer these questions, we must turn to the microscopic description of the particle ensemble.

Restricting our model to a pair interaction between atoms, we assume the interaction of a test atom with any atom to be independent of its interaction with other atoms. This is valid if the interaction potential between two atoms is small compared to a typical electronic excitation energy. This holds for inert gas atoms and many kinds of gaseous molecules, notably i. e. when these molecules found in a gaseous state under normal conditions. Therefore we use as our guides ensembles of inert gas atoms as systems with a pair interaction between atoms. In addition, we assume atomic motion in these systems to be classical, and hence ensembles of helium atoms are not included in our considerations.

The nature of the order–disorder phase transition follows from the lattice model (see Chap. 2). The ordered state is a compact distribution of atoms which leads to a maximum number of bonds between nearest-neighbor atoms, while the disordered state with a random distribution of atoms corresponds to a maximum entropy and to a loss of some of the bonds between nearest neighbors. The phase transition between these states proceeds at some temperature with stepwise changes of the mean binding energy of the atoms and the entropy of the optimal distributions of atoms. The order–disorder phase transition models the solid–liquid phase transition for an ensemble of bound atoms; the ordered state corresponds, of course, to the solid state, and the disordered state, to the liquid. Since this phase transition leads to a change of the atomic configuration, it results from configuration excitation [237]. Considering the phase transition within the framework of the multidimensional potential energy surface, we connect each local minimum with a certain configurational excitation of the atomic ensemble. Then neighboring local minima are separated by saddle points of the potential energy, so that evolution of a cluster can be envisioned as motion in a many-dimensional space of atomic coordinates, proceeding as illustrated schematically in Fig. 1.4.

We now turn to a much larger macroscopic ensemble with an infinite number of atoms, or at least so many that the surface atoms are completely negligible and the configurational excitations correspond only to the movement of internal atoms. By analogy with clusters, one can introduce an elementary configurational excitation, a void. But in contrast to clusters, for which

a void is a perturbed vacancy, a void in a macroscopic system is more complex and is a dynamic concept because the volume and shape of an individual void varies in time [236]. Moreover, parameters of an individual void depend on the void number density. Therefore introducing a void as an elementary configurational excitation in a macroscopic system, we will use average void parameters: the average energy of its formation, the average entropy, the average volume, etc.

Analyzing configurational excitation of a cluster, we recognized that it is a collective process with many atoms partake simultaneously. Strictly, this itself is an interesting issue because the effective number of particles that move in any single well-to-well passage depends on the nature of the interaction potential [242]. Systems with short-range potentials involve movement of only a few particles in each passage; systems with long-range potentials, such as Coulomb interactions, the longest range, have many particles moving in almost all interwell movements. This is completely consistent, of course, with one's intuition, which would say that the further each interaction reaches, the more particles it must influence.

As a consequence of this many-body correlation of motions, simple one-atomic models are not valid in this case. Our cluster results were based on data from computer simulations, in order to establish some parameters of voids. In macroscopic ensembles, this task is more complex since the difference between an elementary vacancy in a crystal and a void in a corresponding liquid is more than that for clusters. Nevertheless, we have an additional source of information for bulk systems. We recognized in Chap. 2 that inert gases are close to atomic systems with short-range interaction; the scaling law for condensed inert gases validates this statement. Therefore when using parameters of liquid inert gases, one can adopt parameters of an elementary configurational excitation for atoms with short-range interaction. We will carry this out.

6.8 Two-State Approximation for Aggregate States

A cluster consisting of bound atoms has many configurationally excited states. It is convenient to join them in groups, so that excited states with similar excitation energies are joined in one group. Often in this manner one can obtain two or more groups of configurationally excited states, even to the extent of the groups falling into well-defined energy bands [243]. As a consequence, the probability of finding a cluster located in one or the other of these states dominates the character of the population distribution. We next consider this form of the cluster distribution function, assuming just two cluster aggregate states; that is, we assume that the probability to find of finding other configurational excitations is small with our cluster parameters. In this simple picture, either there are enough voids to make the system liquid, or there are so few that all the accessible states we would call solid have about the same

energy. This two-state approximation [235] is useful in the range of phase coexistence when a cluster is found in the solid state part of the time and is otherwise in the liquid state, in a dynamic equilibrium of the two forms. Then cluster parameters are determined by averages over the two aggregate states.

Let us consider an isothermal case in which the ensemble of clusters is in a thermostat. This can be achieved experimentally by having the clusters in a bath of helium atoms that collide with clusters, in a chamber with metallic walls maintained at a desired temperature, as carried out in experiments [244, 245]. In this way, the wall temperature becomes the cluster temperature. Next, guided by the behavior of inert gases near their triple points where the solid and liquid states are close to coexistence, we recognize that the mechanical work resulted from the phase transition is small. This allows us to ignore pressure effects; an ordinary external pressure is small compared to a typical effective pressure due to the force of interaction between neighboring atoms. Then examining the phenomenon in thermodynamic terms, we restrict the changes in the phase transition that we consider to the internal energy change ΔE and the entropy change $\Delta S = \ln g$. All other thermodynamic parameters of the phase transition follow from these.

Taking the partition function of the solid $Z_{\rm sol}$ and liquid $Z_{\rm liq}$ states, we introduce their ratio as the parameter precisely analogous to a chemical equilibrium constant for species in dynamical chemical equilibrium:

$$p = \frac{Z_{\rm liq}}{Z_{\rm sol}} = \exp\left(\frac{-\Delta F}{T}\right) = \exp\left(\Delta S - \frac{\Delta E}{T}\right) , \tag{6.30}$$

that characterizes the relative probability of each aggregate state. Here ΔF, ΔE, and ΔS are the change of the free energy, energy and entropy of the system of n bound atoms as a result of the phase transition; T is the configurational temperature that governs the distribution over configurational states. Restricting the system to a narrow temperature range near the melting point, we first neglect the temperature dependence of these quantities. Taking these cluster parameters to be additive functions of its atoms, we have, for a large cluster of n atoms ($n \gg 1$)

$$\Delta E = n\Delta H_{\rm fus} , \quad \Delta S = n\Delta s_{\rm fus} , \tag{6.31}$$

where $\Delta H_{\rm fus}$ is the fusion energy per atom, and $\Delta s_{\rm fus}$ is the entropy jump per atom.

The probabilities for a cluster to be found in the solid $w_{\rm sol}$ and liquid aggregate $w_{\rm liq}$ states are expressed through the parameter (6.30) as [48, 80, 235]

$$\begin{gathered} w_{\rm sol} = \frac{Z_{\rm sol}}{Z} = \frac{1}{1+p} , \quad w_{\rm liq} = \frac{Z_{\rm liq}}{Z} = \frac{p}{1+p} , \\ p = g \exp\left(-\frac{\Delta E}{T}\right) = \exp\left(-\frac{\Delta F}{T}\right) , \end{gathered} \tag{6.32}$$

where g is the relative statistical weight of the liquid state $g = \exp \Delta S$. Evidently, the melting point is defined by the relation $w_{\mathrm{liq}}(T_{\mathrm{m}}) = w_{\mathrm{sol}}(T_{\mathrm{m}})$, or

$$p(T_{\mathrm{m}}) = g \exp\left(-\frac{\Delta E}{T_{\mathrm{m}}}\right) = 1 \,. \tag{6.33}$$

From formulas (6.32), (6.33) it follows that the melting point does not depend on n for a large cluster when surface effects are negligible and cluster thermodynamic parameters are proportional to a number of atoms a large cluster

$$T_{\mathrm{m}} = \frac{\Delta H_{\mathrm{fus}}}{\Delta s_{\mathrm{fus}}} \,. \tag{6.34}$$

Of course, the two-state approach is useful for describing coexistence of the solid and liquid aggregate states in a system consisting of a finite number of bound atoms in a temperature range near the melting point. Coexistence of phases means that for some time intervals, the cluster lives in the solid state, and the rest of the time, it is found in the liquid state [40, 50, 246–248]. The formalism of the two-state approach allows us to describe cluster thermodynamics in the range of phase coexistence.

7

Configurational Cluster Excitation with Pairwise Interactions

7.1 Peculiarities of Configurational Excitation of Clusters

We consider evolution of a cluster as motion of a point along a multidimensional potential energy surface in a phase space of atomic coordinates. The potential energy surface for a cluster contains many minima separated by saddles; the number of local minima increases sharply with cluster size [33–36, 237]. These include both the minima corresponding to geometrically-distinct structures, which typically increase at least exponentially with the number of particles n, and the permutational isomers, which increase approximately as $n!$. Hence, one can (in principle) describe the cluster's evolution as a result of transitions between local minima of the potential energy surface, passages that correspond to saddle-crossing dynamics [39–42]. Within the framework of this description, the cluster remains near a given minimum of the potential energy surface relatively long, since its average total kinetic energy is lower than typical saddle heights. We may characterize a configurational state of this system by the local minimum near which the cluster is found for a time long compared with a typical oscillation period near this minimum. Because the dwell times around local minima are typically long compared with vibrational periods and even with vibrational relaxation times, we may suppose that the configurational cluster state is independent of the atomic (vibrational) kinetic energy. In other words, one can separate the configurational and vibrational cluster excitations as independent degrees of freedom. (In a case in which the vibrational kinetic energy is higher than the barrier between two minima, we consider the accessible region containing both these minima as a single but nonrigid configurational state.)

This is the basis of our treatment in which we divide cluster excitation into configuration and vibration parts and assume these parts to be independent. (Of course they are ultimately coupled on sufficiently long time scales.) Next, to simplify the description of configurational excitation, we again introduce a void as an elementary configurational excitation, so that any configurational

excitation results from formation of one or more voids. Then one can express the parameters of the phase transition and other cluster properties through parameters associated with forming voids. Therefore our task in this chapter is to find the void parameters and to express through them the parameters of the cluster phase transition.

Assuming the motion of cluster atoms to be classical, we represent the energy E of a cluster consisting of n atoms with a pair interaction between them in the form

$$E = U + K = \sum_{i,j} u(r_{ij}) + \frac{m}{2} \sum_{i} \left(\frac{\mathrm{d}\mathbf{r}_i}{\mathrm{d}t} \right)^2 . \tag{7.1}$$

Here U is the total potential energy, K is the total kinetic energy of atoms, and $u(\mathbf{r}_{ij})$ is the pair interaction potential between atoms at a distance $\mathbf{r}_{ij} = \mathbf{r}_i - \mathbf{r}_j$, so that $\mathbf{r}_i, \mathbf{r}_j$ are the atomic coordinates, and m is the atomic mass. This formula is the basis for the analysis of computer simulations of clusters. Let us consider the properties of two terms of this formula, taking into account that the vibrations come to thermal equilibrium rapidly. We first approximate the vibrations as harmonic oscillators. In particular, in the limit of high temperatures, when a typical atomic kinetic energy significantly exceeds a typical small-amplitude vibrational energy (or the Debye temperature), the Dulong-Petit law is valid, according to which

$$K = \frac{3}{2}(n-6)T \, , \tag{7.2}$$

where n is the number of cluster atoms. We will focus on the large-system limiting case, $n \gg 1$. The global minimum of the complex potential energy surface corresponds to the cluster's ground state, its equilibrium state at zero temperature. Transitions from the global minimum to other local minima, corresponding to configurational excitations of the cluster, are responsible for a phase transition, whether from one solid form to another or from solid to liquid.

We note that even for an isolated ensemble of bound classical atoms, whose total energy does not change in time, the kinetic K and potential U energies of this ensemble oscillate in time. Because the system is large, we safely assume that the fluctuations of these energies relatively small, and this assumption is valid for large atomic ensembles.

We use the results of computer simulations of the Lennard-Jones cluster of 13 atoms [50] to guide our analysis. The simulated cluster is considered as a member of a microcanonical ensemble [6], i. e. it is isolated from any heat source and the total cluster energy is conserved during the cluster's evolution. There is a range of temperature and pressure, or of energy, in which the distribution of short-term-average total kinetic energy values of the cluster exhibits a bimodal distribution (see Fig. 7.1). In that range, one can treat the results of computer simulation [50] in terms of a dynamic equilibrium of two aggregate states. Such a treatment was fulfilled partially in several studies [48, 80, 235, 249]; here, we give the results of this treatment.

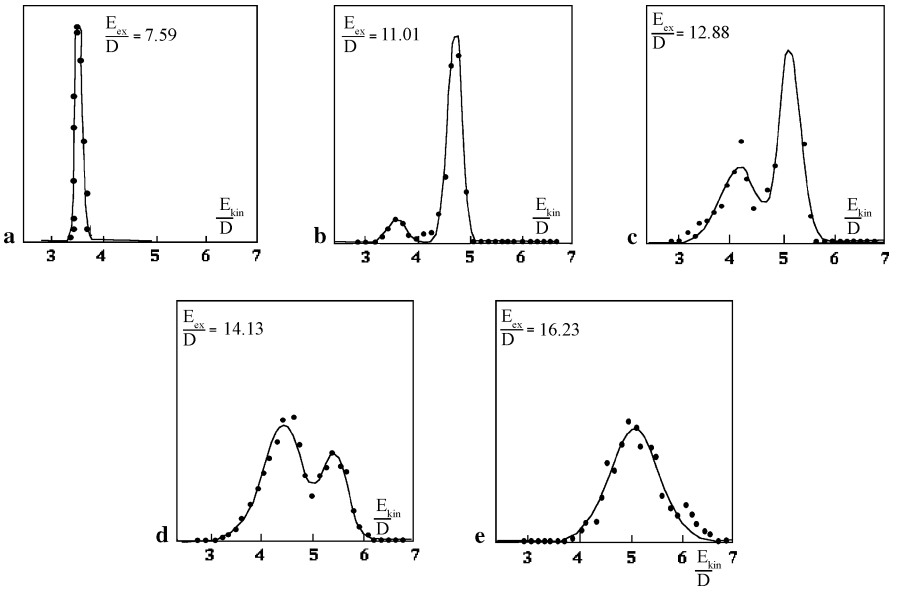

Fig. 7.1. The distribution function of the total kinetic energy of atoms for the 13-atom Lennard-Jones cluster. A range near the left maximum corresponds to the liquid aggregate state; the region near the right maximum relates to the solid aggregate state. $E_{\rm ex}$ is the excitation energy, $E_{\rm kin}$ is the total kinetic energy of atoms, and D is the energy required to break one bond [50]

The structure of the ground state of this cluster [250] at zero temperature and the character of its lowest configurational excitations are shown in Fig. 1.5. The simplest configurational excitation corresponds to promotion of one atom from the shell of 12 onto the hollow between three atoms on the cluster surface, as shown in Fig. 1.5; configurations for the lowest stable states arising from such a transition are given in Fig. 7.2. For this transition an atom must overcome a barrier. The atomic configurations for saddle points of the 13-atom icosahedral cluster are given in Fig. 7.3. Figure 7.4 gives the energies of the states for one-atom transitions at zero temperature and the values of barriers which separate them [51]. Increasing the energy facilitates transitions between different stable positions on the cluster surface, as well as exchanges between states of a configurationally excited cluster. All the configurationally excited states of this cluster in the liquid state are connected via single-atom transitions, so that the system may find all permutations among the atoms.

Let us represent formula (7.1) in the form

$$E - E_{\rm o} = E_{\rm ex} = U'_{\rm sol} + K_{\rm sol} = \Delta E + U'_{\rm liq} + K_{\rm liq}\,, \qquad (7.3)$$

where $E_{\rm o}$ is the atomic binding energy in the ground configurational state at zero temperature, $E_{\rm ex}$ is the total excitation energy, $K_{\rm sol}$ and $K_{\rm liq}$ are the

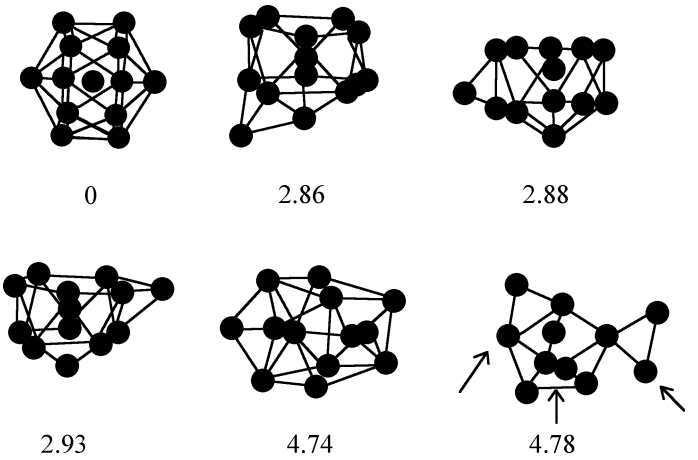

Fig. 7.2. Structures of the lowest configurationally stable states for the 13-atom Lennard-Jones cluster at zero temperature [51]. *Arrows* indicate atoms with identical projections, and excitation energies are expressed in the energy D to break one bond

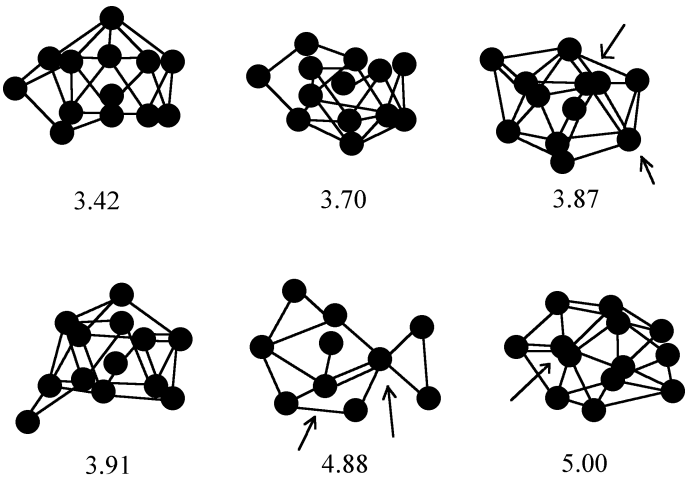

Fig. 7.3. Structures of saddle points between the two lowest configurationally stable states for the 13-atom Lennard-Jones cluster at zero temperature [51]. *Arrows* indicate atoms with identical projections, and excitation energies of saddle points are expressed in the energy D of one bond

total kinetic energies of atoms for the solid and liquid cluster states, $U'_{\rm sol}$ and $U'_{\rm liq}$ are the average potential energies of the cluster for each aggregate state, and ΔE is an average excitation energy to produce the liquid aggregate state. Within the framework of this formulation, we join nearby local minima of the potential energy surface into one aggregate state, whenever transitions between those local minima are faster than those between states of different

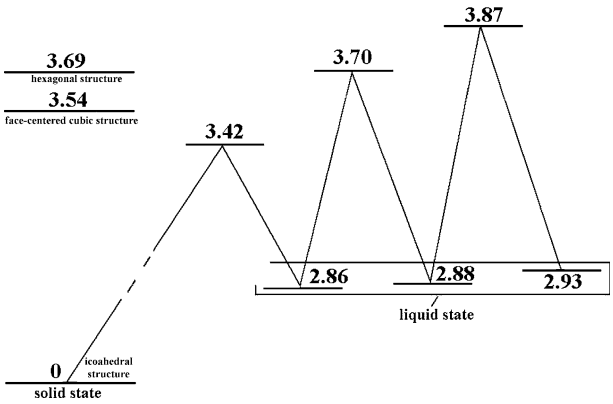

Fig. 7.4. The excitation energies and barrier energies for the lowest configurational excitations of the 13-atom Lennard-Jones cluster, according to [51]

aggregate states. That is, we suppose that it is easier to move a void from one site to another than to create or destroy a void.

One can introduce the effective temperature for each aggregate state of the cluster on the basis of the mean kinetic energy per degree of freedom, (formula (7.2)

$$T = \frac{2}{3n-6}K \ . \tag{7.4}$$

In particular, for a cluster consisting of $n = 13$ atoms this formula has the form

$$T = \frac{2K}{33} \ . \tag{7.5}$$

In addition to the temperatures $T_{\rm sol}$ and $T_{\rm liq}$ for the cluster solid and liquid aggregate states, one can formally introduce the effective cluster temperature of configurational excitation $T_{\rm con}$ based on the equilibrium population ratio of the solid and liquid cluster states, from the formula

$$p \equiv \frac{w_{\rm liq}}{w_{\rm sol}} = \exp\left(-\frac{\Delta F}{T_{\rm con}}\right) = \exp\left(-\frac{\Delta E}{T_{\rm con}} + \Delta S\right) \ , \tag{7.6}$$

where $w_{\rm sol}$ and $w_{\rm liq}$ are the probabilities for the cluster to be found in the solid and liquid states, respectively, and ΔF is the free energy jump at melting. We give in Fig. 7.5 the temperatures of the isolated Lennard-Jones cluster consisting of 13 atoms. The temperatures of the solid $T_{\rm sol}$ and liquid $T_{\rm liq}$ aggregate states of Fig. 7.5 are defined by formula (7.4) and follow from the results of computer simulation [50] given in Fig. 7.1. The transversal cluster temperature tends to the solid temperature $T_{\rm sol}$ in the limit of low temperatures, and to the liquid temperature $T_{\rm liq}$ in the limit of high temperatures. The configurational temperature is evaluated on the basis of populations of the solid and liquid aggregate states for the Lennard-Jones cluster consisting of 13 atoms in the range of coexistence of these states; the population of the liquid state is given in Fig. 7.6 [80, 133, 249]. Note that for a bulk atomic ensemble the dependence of the liquid state population on the excitation energy has a stepwise character, whereas for a cluster this shift of phase is smooth, over a range

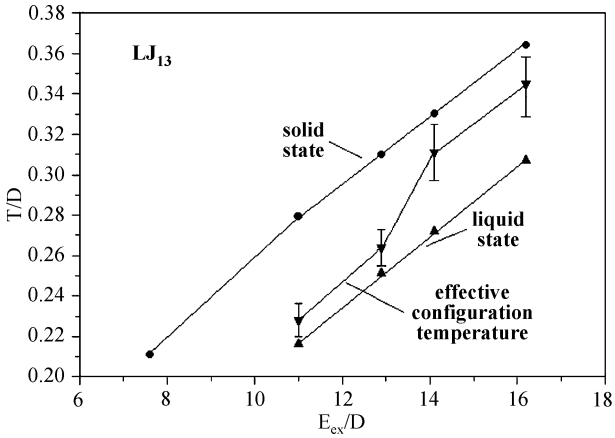

Fig. 7.5. The temperatures of atoms of the 13-atom Lennard-Jones cluster, constructed on the basis of data from Fig. 7.1. The three curves show the temperature for the solid, the liquid and the configurational temperature of this cluster.

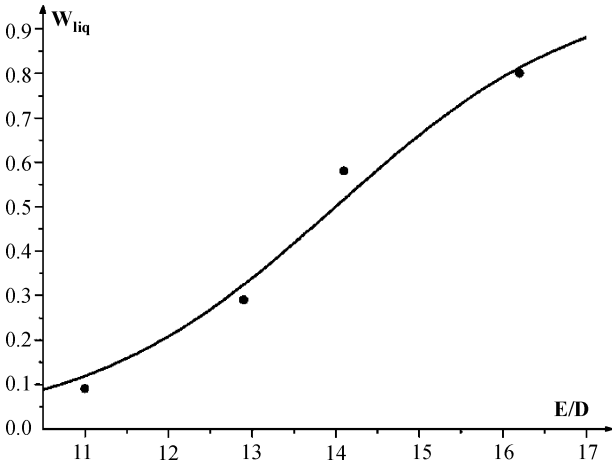

Fig. 7.6. The probability w_{liq} of the liquid aggregate state for the 13-atom Lennard-Jones cluster [80, 249] on the basis of computer simulation [50]. The *solid curve* corresponds to approximation according to formula (7.7)

of temperatures. In particular, in the case of the 13-particle Lennard-Jones cluster, dynamic coexistence of the solid and liquid states takes place over the range of the excitation energies 10D–16D.

The ratio of the liquid and solid state populations p depends on the excitation energy E for an isolated cluster, and it is convenient to approximate

the dependence $p(E)$ for an isolated cluster as

$$p(E) = \exp\left(-\frac{E - E_{\rm m}}{\delta E}\right) , \tag{7.7}$$

where $E_{\rm m}$ is the excitation energy of melting, at which $p = 1$. In particular, for the isolated 13-atom Lennard-Jones cluster, these parameters are $E_{\rm m} = (13.9 \pm 0.2)D$ and $\delta E = (1.5 \pm 0.2)D$, as follows from treatment of the Fig. 7.1 data [50]. Figure 7.6 includes this approximation (7.7) for the population of the liquid aggregate state $w_{\rm liq}$ together with that obtained from the simulation data of this cluster [50].

7.2 Structural Phase Transition in a Solid Cluster

The lattice model exhibits the character of a phase transition between two states, in which the higher-energy state invariably has the larger statistical weight or greater entropy at temperatures at which it is accessible. Consequently at a certain temperature an excited state becomes thermodynamically favorable, and then the phase transition proceeds, sharply in macroscopic systems, smoothly in small clusters. Since a large statistical weight of a high-energy form is required for the phase transition, this process of a phase change requires enough complexity to provide that statistical weight. Typically, that comes from there being at least a moderate number of particles in the system, and also at least a moderately high density of available states. For these reasons, atoms do not exhibit phase changes, because each atomic shell contains relatively few electrons, and the densities of their accessible states are low. However phase changes are possible for large or even moderate-sized clusters, in which many atoms can be located on a shell or layer.

The simplest phase transition takes place between two solid cluster structures. In particular, we consider here the structural transition between the face-centered cubic structure and the icosahedral structure of clusters with pairwise interaction between atoms. Previously we analyzed the general basis for the competition of these structures and established that for large clusters any of these structures may be thermodynamically favorable depending on the pair interaction potential and cluster size.

Let us consider such a cluster for which the binding energies of cluster atoms are close for these two structures at zero temperature, and the lower-energy structure is characterized by its completed atomic shells. In this treatment we will be guided by a cluster of 923 atoms whose lower-energy state has icosahedral structure with a complete outer shell, and the excitation energy to reach the fcc structure is comparable to the binding energy of one atom. Because the fcc cluster of this size has incomplete shells, it has a large statistical weight; specifically $g_{\rm o} = 5544$ at zero temperature for the fcc cluster of 923 atoms [68, 69]. This is just the number of places the surface vacancies can be. The pairwise binding energies of the two cluster structures are similar. For

example, let us use Morse interactions between atoms, i. e. the pair interaction potential of atoms is [67]

$$U(R) = D\left[\mathrm{e}^{2\alpha(R-R_\mathrm{e})} - \mathrm{e}^{\alpha(R-R_\mathrm{e})}\right] , \tag{7.8}$$

where R_e is the equilibrium distance, and α is the Morse parameter that sets a scale for the range of the interaction. Then the energies of the close-packed and icosahedral structures coincide at $\alpha R_\mathrm{e} = 7.1$ [68, 69]. Hence in the case under consideration $\alpha R_\mathrm{e} \leq 7.1$, so that in this range the icosahedral structure generally has lower energy, but the energy gap between structures is not large, and a transition between these structures occurs at temperatures well below the melting point, i. e. $T_\mathrm{m} = 0.44D$ [251]. Variation of αR_e allows us to analyze the character of this cluster's structural phase change and use it to help us understand structural phase transitions in solids.

When two structures compete, one can construct the cluster's partition function Z on the basis of these two structures

$$Z = Z_\mathrm{ico} + Z_\mathrm{fcc} , \tag{7.9}$$

where Z_ico and Z_fcc are the partition functions for the icosahedral and fcc structures, respectively. Taking the statistical weight of the lower icosahedral state to be one, we have the connection between these partition functions

$$Z_\mathrm{fcc} = Z_\mathrm{ico} g \exp\left(-\frac{\Delta}{T}\right) , \tag{7.10}$$

where Δ is the difference of the ground state energies for these structures, and g is the statistical weight of the fcc cluster. The temperature at which the two phases have equal free energies, which is the precise analog of the temperature of the bulk phase transition T_tr between the two solid structures, is determined by the condition of equality of the partition functions of the two phases $Z_\mathrm{fcc} = Z_\mathrm{ico}$. If the energy difference for the ground states of these structures Δ is small enough, the statistical weight g corresponds to the ground configuration state of the fcc cluster and is $g = 5544$. In this limiting case the transition temperature has the form for the cluster of 923 atoms (we take $Z_\mathrm{fcc} = Z_\mathrm{ico} = Z/2$)

$$T_\mathrm{tr} = \frac{\Delta}{\ln g + \ln Z_\mathrm{fcc}/Z_\mathrm{ico}} = 0.104\Delta . \tag{7.11}$$

Let us find the dependence of the structural transition on thermodynamic parameters of the cluster. We concentrate on the cluster's heat capacity under conditions that the configurational excitation is in equilibrium with thermal vibrations of the cluster, i. e. these degrees of freedom are characterized by the identical temperature T. Evidently, the configurational part of the cluster's heat capacity has a resonant-like structure, that is, it exhibits a maximum. We will focus on this aspect, relating the partition function (7.9) to configurational excitation and representing it in the form

$$Z = \sum_i g_i \exp\left(-\frac{\varepsilon_i}{T}\right) , \tag{7.12}$$

where ε_i and g_i are the excitation energy and statistical weight of a given configurational excitation of the cluster, and the configurational part of the heat capacity is

$$C = \frac{\partial E}{\partial T} = \frac{\partial}{\partial T}\left(\frac{1}{Z}\sum_i \varepsilon_i Z_i\right) = \frac{\overline{E^2}}{T^2} - \left(\frac{\overline{E}}{T}\right)^2 . \tag{7.13}$$

Here $\overline{E}$ and $\overline{E^2}$ are the average and mean square values of the configurational excitation energy of a cluster. Separating configurational excitation for the icosahedral and fcc structures and substituting formula (7.12) in formula (7.13), we represent the cluster's heat capacity in the form [143, 144]

$$C = \frac{Z_{\rm ico}}{Z}C_{\rm ico} + \frac{Z_{\rm fcc}}{Z}C_{\rm fcc} + \frac{1}{T^2}\frac{Z_{\rm ico}Z_{\rm fcc}}{Z^2}\left(\overline{\varepsilon_{\rm ico}} - \overline{\varepsilon_{\rm fcc}} - \Delta\right)^2 . \tag{7.14}$$

Here $Z_{\rm ico}$ and $Z_{\rm fcc}$ are the total partition functions for the corresponding cluster structures, Z is the total partition function according to (7.9), and $C_{\rm ico}$ and $C_{\rm fcc}$ are the heat capacities for each cluster structure when the other cluster structure is absent. In the last term, $\overline{\varepsilon_{\rm ico}}$ and $\overline{\varepsilon_{\rm fcc}}$ are the average excitation energies for a given cluster structure in which the ground configuration of this structure corresponds to zero energy. The last term has a resonant structure near the transition temperature (7.11) at which formula (7.14) has the form

$$C = \frac{1}{2}(C_{\rm ico}+C_{\rm fcc}) + \left(\frac{\Delta}{2T_{\rm tr}}\right)^2 \exp\left[-\alpha(T-T_{\rm tr})^2\right] , \quad \alpha = \left(\frac{\Delta}{2T_{\rm tr}^2}\right)^2 , \tag{7.15}$$

and the "resonance" corresponds to $Z_{\rm ico} = Z_{\rm fcc} = Z/2$. Defining the resonance width as $\Delta T = (1/\alpha)^{1/2}$, we obtain

$$\Delta T \equiv \frac{2T_{\rm tr}^2}{\Delta} , \tag{7.16}$$

where the temperature $T_{\rm tr}$ that corresponds to the heat capacity maximum is given by

$$p(T_{\rm tr}) = g\exp\left(-\frac{\Delta}{T_{\rm tr}}\right) = 1 ,$$

and $p(T)$ is the probability of the excited aggregate state at a given temperature T. In particular, for the cluster of 923 atoms and a small difference between the energies of the two structures Δ, we obtain $\Delta/T_{\rm tr} = 0.2$.

Near the maximum, the resonance shape of the heat capacity is approximated as

$$C = \left(\frac{\ln g}{2}\right)^2 \exp\left[-\frac{\ln^2 g}{4T_{\rm tr}^2}(T-T_{\rm tr})^2\right] = \frac{\Delta S^2}{4}\exp\left[-\frac{\Delta S^2}{4}\frac{(T-T_{\rm tr})^2}{T_{\rm tr}^2}\right] , \tag{7.17}$$

where $\Delta S = n\Delta s \gg 1$ for large clusters $n \gg 1$. A small parameter which determines the narrowness of the transition range is

$$\frac{1}{\Delta S} = \frac{1}{\ln g} \ll 1 \, .$$

Although we are guided here by small Δ when the maximum in the heat capacity appears at low temperature, one can spread it for larger Δ, but to do that, we must take into account configurationally excited cluster states for each structure. This step was made in [143, 144]. Figure 7.7 exhibits the behavior of the configurational heat capacity in the temperature range below the melting point [143]. In this temperature range a restricted number of cluster configurations is excited. Clearly, the maximum heat capacity increases with an increase of Δ.

The structural transition also influences other thermodynamic properties of the cluster. In particular, we can estimate the entropy change required for the phase change. Let us return to the case of a cluster of 923 atoms with a small energy gap between its two relevant structures; the entropy jump as a result of the transition from the icosahedral cluster structure to the fcc structure is $\Delta S = \ln g = 8.6$. This entropy jump must increase with an increase of the energy gap Δ, but its order of magnitude is conserved, i. e. $\Delta S \sim 10$.

Thus we find that the structural transition leads to a maximum in the cluster's heat capacity and to a jump in the cluster's entropy. Of course, corresponding changes occur in the other thermodynamic parameters as well. Let us compare these changes with the thermodynamic parameters due to atomic vibrations in the cluster. In particular, in the Debye approximation, the cluster entropy at moderate temperatures is given by [4]

$$S_{\mathrm{vib}} = 3n \left(\ln \frac{T}{\hbar \omega_{\mathrm{D}}} - 1 \right) \, , \tag{7.18}$$

where ω_{D} is the Debye frequency (the maximum or cut-off frequency in the model), and n is again the number of cluster atoms. In particular, for a cluster of 923 atoms, this formula gives $S_{\mathrm{vib}} \sim 1000$. One can see that this value significantly exceeds the jump due to structural transition. However the vibrational entropy does not change very much at all with the transition, typically increasing only slightly as a few modes drop in frequency as the system goes to the high-temperature phase, due to void spaces that soften local vibrational modes. This is a general result for large clusters. It is the *changing* part of the entropy that underlies the phase change, not the largest contribution to the total entropy. Any phase transition in a cluster influences its thermodynamic parameters through the appearance of resonance-like maxima and, in large systems, jumps at the phase transition temperature. It is important here to look at the configurational contributions directly associated with the transition process, and not at the contribution from the thermal motion of atoms; the changes of the cluster's thermodynamic parameters responsible for

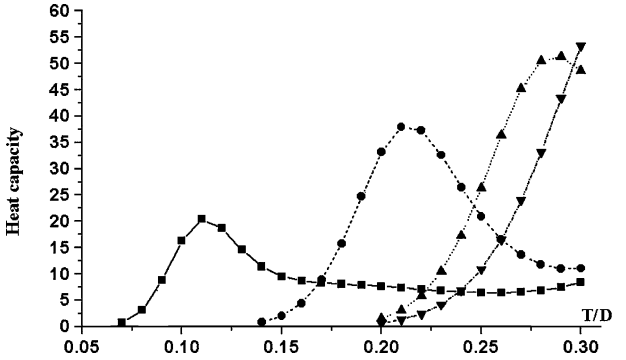

Fig. 7.7. The heat capacity of a solid cluster consisting of 923 atoms as a function of the temperature [143, 144]. The ground state of this cluster at zero temperature has a completed icosahedral structure, and Δ, the excitation energy to the ground state of the fcc structure, is equal, in units of one bond energy, to: *squares* $\Delta = 1$; *circles* $\Delta = 2$; *triangles* $\Delta = 3$; *inverted triangles* $\Delta = 4$

the phase transition are small in comparison with their total values arising primarily from thermal motion of the atoms, but that contribution undergoes very small changes while the configurational part changes significantly. The analysis of the structural transition in a cluster consisting of 923 atoms [143, 144] confirms this statement.

The importance of the particular icosahedral-to-fcc structural transition in large clusters decreases with cluster size because the larger systems cannot sustain icosahedral structures. From a more general perspective, structural transitions of atomic aggregates with pairwise interactions are rarely important. However for systems with more complex interactions, such as metallic or semiconductor systems, structural transitions of atomic aggregates can be quite important.

7.3 Configurational Excitation of the Icosahedral Cluster of 13 Atoms

Considering a general concept of cluster configurational excitation as a result of formation of voids, we start from the simplest cluster with completed shells, 13 atoms with icosahedral structure [250]. In the ground configuration, its first (and only) shell is filled. Configurational excitation of this cluster consists in transition of one atom from the surface shell to the cluster surface as is shown in Fig. 1.5b. After the vacancy forms in the cluster shell, the atoms around the vacancy are distributed over a larger space due to thermal motion, and the promoted atom moves about on the cluster surface more freely than any of the other atoms. Hence the lowest configurational excitation of this cluster at zero temperature is characterized by one vacancy and one atom above the

initially completed shell. At finite temperatures for thermal motion of atoms the vacancy expands and is converted into a void.

A cluster of 13 atoms is a convenient object for the analysis of configurational excitation. In spite of its small size, this cluster is characterized by a large number of local minima (well over 1000), and since excitations due to promotion of one and two atoms are well separated in energy, one can show that local minima of the potential energy surface are separated by barriers and tend to fall into rather distinct energy bands. Indeed, the lowest-energy excitations correspond to a single atom transition from the 13-atom shell onto the hollow between three atoms on the cluster surface. In the case of a short-range interaction between atoms, a surface atom in the ground cluster state has 6 bonds, i. e. its binding energy is close to $6D$, where D is the energy to break one bond, and on the cluster surface this atom has three bonds, so that its binding energy is equal to $3D$ roughly. We assume atoms to be classical, and hence the depth of the potential well D for two-atom interaction coincides with the dissociation energy of a diatomic molecule. When a surface atom is transferred to a neighboring position on the cluster surface, it retains two bonds between nearest neighbors as it makes the transition between neighboring hollows on the cluster surface. Hence, for this transition an atom must overcome a barrier whose magnitude is roughly $1D$.

Figures 7.2 and 7.3 show atomic structures for the lowest configurational excitations of the 13-atom cluster and saddles at such transitions [51]. The values indicated correspond to the Lennard-Jones cluster, i. e. to the case of the Lennard-Jones interaction potential (2.6). The energies of excitation for the lowest configurationally excited cluster states are given in Fig. 7.4 for zero temperatures. At higher temperatures, these states may be joined in the liquid aggregate state. This occurs when thermal motion allows passage among the different configurational states at rates high enough to compare with the frequencies of the slower vibrational modes. One can characterize the lowest excited cluster state which we would identify with the liquid aggregate state, by a large statistical weight g. At zero temperature the statistical weight g of the excited state and correspondingly the entropy jump ΔS_{o} of configuration transition are equal to

$$g = 12 * 15 = 180\,, \quad \Delta S_{\mathrm{o}} = \ln g = 5.2\,. \tag{7.19}$$

Here the value 12 is the number of shell atoms, any of which can be promoted, and 15 is the number of positions for a promoted atom if it is not in a site bordering the new vacancy. It is important that thermal motion gives a contribution to these values near the melting point because of the free motion of bound atoms in this configurationally excited state.

The special peculiarity of cluster configurational excitation is a consequence of its finite statistical weight so that the probabilities for a cluster to be located in the ground and configurationally excited states are comparable in some range of excitation energies. This leads to coexistence of phases

in this range of excitation energies. Because of this comparability, both aggregate states may be realized in observable quantities over finite ranges of temperature at a fixed pressure. Hence coexistence of phases for clusters appears to be vastly different from the case of macroscopic objects, with its sharp boundary defining the range of coexistence. The two cases are, however, simply related because the range of observable coexistence of the two phases trends to zero when the number of atoms tends to infinity. The relative amounts of the two phases can be expressed in terms of the so-called equilibrium constant, $K_{\mathrm{eq}} = \Delta F/kT$, where ΔF is the difference in free energies of the two species. In a large system, e. g. 10^{20} particles, if the free energy per atom differs even a very small amount, e. g. 10^{-10} in units of kT, then the unfavored phase is so unfavored as to be unobservable. The equilibrium ratio of the two phases in this case is $\mathrm{e}^{10^{10}}$. However if the number of particles n is of order 100 or 1000 or even 1,000,000, then the ratio of equilibrium amounts of the two phases can well be of order unity over an observable temperature range.

Figure 7.1 gives the probability that the Lennard-Jones cluster of 13 atoms has a given total kinetic energy [50]. The bimodal character of this distribution at intermediate excitation energies testifies to the existence of two aggregate states, the solid and the liquid, which are found in dynamic equilibrium. At low excitation energies only the solid aggregate state is realized, whereas at high excitation energies only the liquid aggregate state exists. Of course, the total atomic kinetic energy is averaged over times long compared with vibrational periods. However the time of such averaging must be brief compared to a typical time interval for transitions between aggregate states. This choice allows us to separate and distinguish cluster aggregate states. For clusters in the size range of roughly 10 to several hundred atoms, averaging over many tens of vibrational periods accomplishes this and separates the time scales for thermal equilibration very conveniently from that for passage between aggregate states. Dynamic coexistence of aggregate states for intermediate excitation energies is simply the phenomenon that part of time a cluster is found in one aggregate state, and the rest of the observation time, in another aggregate state. Clusters of many kinds exhibit the bimodal character shown in Fig. 7.1, i. e. residence times in each phase long enough to establish properties we normally identify with a bulk phase, such as the diffusion coefficient and pair correlation function.

Note that some clusters, e. g. Ar_{15}, pass between the phase-like forms too rapidly to develop such characteristic properties; these would appear in experiments to behave as a sort of slush in what would otherwise be the region of phase coexistence. This latter class of clusters has not yet been studied in depth. In addition, clusters may exhibit dynamic coexistence of more than two phases [252, 253]. This means that several configurationally excited states may be resolved [252, 253]. These states, in some cases, correspond to melting of different cluster shells. As the cluster size increases, only two liquid aggregate states remain distinguishable, the surface and volume liquid aggregate

states. Because of the difference in the binding energies for the internal and surface atoms, these liquid states may be separated and distinguished experimentally [254, 255]. Previously we restricted ourselves to the volume liquid state of bulk inert gases, while below we consider excited cluster states in which the liquid or amorphous character is restricted to the outermost shell. In this context, the surface melting proceeds at lower temperatures than the volume melting because of lower binding energies for surface atoms. This is proved experimentally [256], and one can expect the melting point for surface melting is lower that for the volume melting by 20 – 40%.

7.4 The Cluster as a Microcanonical Ensemble of Bound Atoms

There are two scenarios of cluster excitation, as shown in Fig. 7.8. In the first case, when a cluster is itself a microcanonical ensemble of atoms or is a member of a Gibbsian microcanonical ensemble, it is isolated, and its state is characterized by the total energy E that is conserved during transitions between aggregate states. In the second case, when a cluster is itself a canonical ensemble of atoms or is a member of a canonical ensemble of clusters, the temperature of cluster atoms corresponds to the fixed temperature of a thermostat in which the cluster or Gibbsian ensemble is located. Experimentally, helium gas is typically used as this thermostat, so that collisions of helium atoms with this cluster and metallic walls supported at a chosen temperature, establish thermal equilibrium between cluster, helium bath and the walls.

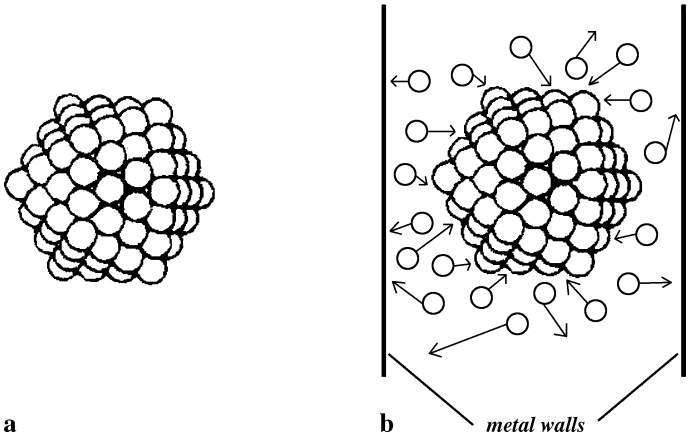

Fig. 7.8. Interaction of a cluster with an environment when it is a microcanonical (**a**) or canonical (**b**) ensemble of bound atoms

Let us introduce the parameter measuring the anharmonicity η that relates to the kinetic energy of atoms for each aggregate cluster state according to the formulas

$$\eta_{\rm sol} = \frac{K_{\rm sol}}{E_{\rm ex}} , \quad \eta_{\rm liq} = \frac{K_{\rm liq}}{E_{\rm ex} - \Delta E} . \tag{7.20}$$

If atomic motion is representable as a combination of harmonic oscillators, we have $\eta = 0.5$. Anharmonicity that softens the vibrations, as in stretching modes, typically leads to a decrease of this value, and $\eta(E_{\rm ex})$ decreases with an increase of $E_{\rm ex}$. Figure 7.9 gives this dependence which was obtained [80, 249] on the basis of computer simulation [50] for an isolated 13-atom cluster.

Note that $\eta_{\rm sol}(E_{\rm ex}) = \eta_{\rm liq}(E_{\rm ex})$ within the limits of their accuracy, while, strictly, this quantity has different values for the solid and liquid states at identical temperatures. This is because the value of η can be supposed first to be $\eta(E_{\rm ex} = 0) = 0.5$ if the system were to be described in terms of harmonic oscillators, but in a real system, it decreases monotonically with increasing excitation energy because of the increasing role of anharmonicity. Hence the parameter η characterizes influence of the anharmonicity in atomic motion of an isolated cluster as the excitation energy increases. Let us approximate $\eta(E_{\rm ex})$ of Fig. 7.9 by the dependence

$$\eta(E_{\rm ex}) = 0.5 \left[1 - \left(\frac{E_{\rm ex}}{E_*} \right)^k \right] . \tag{7.21}$$

Treatment of the data of Fig. 7.9 gives for the parameter E_* of this formula

$$k = 1.7 , \quad E_* = 51 \pm 3 . \tag{7.22}$$

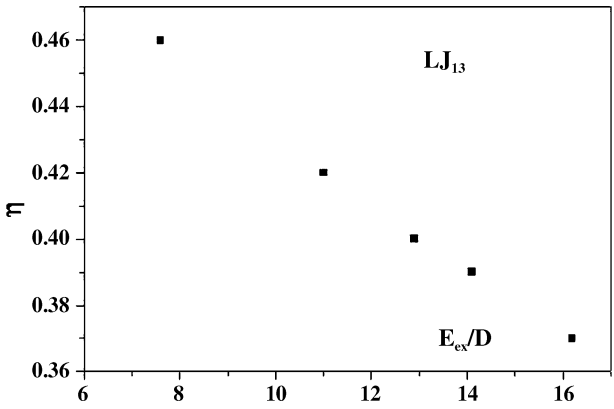

Fig. 7.9. The dependence on the excitation energy of the fraction of internal energy that is kinetic, η, for an isolated 13-atom Lennard-Jones cluster. This value is identical for the solid and liquid cluster states and is obtained in [80, 249] on the basis of the results [50].

From the above data, we find also the excitation energy of the cluster's liquid state,

$$\Delta E = \frac{K_{\rm sol} - K_{\rm liq}}{\eta(E_{\rm ex})} = E_{\rm ex}\left(1 - \frac{K_{\rm liq}}{K_{\rm sol}}\right) = (2.40 \pm 0.05)D\ . \tag{7.23}$$

In analyzing the data of computer simulation [50] for bimodal kinetic energy distribution of cluster atoms, we are based on thermodynamic equilibrium in each aggregate state. This two-state approach for a cluster as a microcanonical atomic ensemble allows us to introduce separately the temperature and other thermodynamic parameters for the solid and liquid states separately. Hence, formula (7.6) can be represented in the form

$$\ln p = \ln w_{\rm liq} - \ln w_{\rm sol} = \Delta F_{\rm sol} - \Delta F_{\rm liq} = S_{\rm liq}(T_{\rm liq}) - \frac{\Delta E}{T_{\rm liq}} - S_{\rm sol}(T_{\rm sol})\ , \tag{7.24}$$

where $\Delta F_{\rm liq}$, $\Delta F_{\rm sol}$ are the change of the free energies for the liquid and solid states respectively at a given cluster excitation, $T_{\rm liq}, T_{\rm sol}$ are the liquid and solid temperatures, $S_{\rm liq}(T_{\rm liq}), S_{\rm sol}(T_{\rm sol})$ are the entropies of the liquid and solid states at indicated temperatures. Basing on the results of computer simulation, we take the fusion energy ΔE to be independent on the excitation energy. Assuming also the cluster heat capacity to be independent of excitation far from the phase transition and to be given by formula (7.5), we obtain the value

$$\Delta T_{\rm m} = T^m_{\rm sol} - T^m_{\rm liq} = \frac{2\eta\Delta E}{33} \approx 0.06D \tag{7.25}$$

to be almost independent of excitation in a range of the phase transition. Here $T^m_{\rm sol} = E_{\rm m}/(C_{\rm o}\eta_{\rm m}) \approx 0.33D$, $T^m_{\rm liq} = T^m_{\rm sol} - \Delta T_{\rm m} = \approx 0.27D$ are the vibration temperatures for the solid and liquid states respectively at the melting point, and $E_{\rm m} = (13.9 \pm 0.2)D$ is the excitation energy for the solid state at the melting point, $\eta_{\rm m} = 0.39$ at the melting point. Next, the melting point $T_{\rm m}$ is

$$T_{\rm m} = \frac{T^m_{\rm sol} - T^m_{\rm liq}}{2} = (0.30 \pm 0.01)D\ . \tag{7.26}$$

We now determine the entropy of the phase transition for the LJ_{13} cluster on the basis of the above assumptions and formula 7.7. For simplicity, we restrict by the linear temperature dependencies for entropies

$$S_{\rm liq}(T_{\rm liq}) = \Delta S_{\rm o} + aT_{\rm liq}\ , \quad S_{\rm sol}(T_{\rm sol}) = bT_{\rm sol}\ , \tag{7.27}$$

where $\Delta S_{\rm o} = S_{\rm liq}(0) - S_{\rm sol}(0) = \ln 180 = 5.2$ is the entropy of configurationally excited state of the LJ_{13} cluster with one vacancy that corresponds to zero temperature. Equalizing expressions (7.7) and (7.24) and their derivatives, we have the following relations

$$\frac{\Delta E}{T^m_{\rm liq}} = \Delta S_{\rm m} - \frac{\Delta T_{\rm m}}{2}(a+b)\ , \quad \frac{1}{\delta E}\frac{{\rm d}E}{{\rm d}T} = \frac{\Delta E}{(T^m_{\rm liq})^2} + (a-b)\ , \tag{7.28}$$

where $\Delta S_{\rm m} = S_{\rm liq}(T_{\rm m}) - S_{\rm sol}(T_{\rm m}) + \Delta S_{\rm o} + (a-b)T_{\rm m}$ is the entropy change for the solid–liquid transition at the melting point.

In treatment the data of computer simulation [50], we find an error that does not allow us to separate variations of the entropies for the solid and liquid aggregate states and to find the difference due to different solid and liquid state temperatures. Nevertheless, we obtain for the entropy difference with a restricted accuracy

$$\Delta S(T) = S_{\rm liq}(T) - S_{\rm sol}(T) = 5.2 + (14 \pm 3)T \; . \tag{7.29}$$

In particular, this gives for the entropy jump at the phase transition

$$\Delta S_{\rm m} = 9.0 \pm 0.6 \; . \tag{7.30}$$

Comparing this with the entropy jump $\Delta S_{\rm o}$ of the cluster at zero temperature that is defined as $S_{\rm o} = \ln g$, where g is the ratio of statistical weights for excited and ground configurational states, we find

$$\frac{\Delta S_{\rm o}}{\Delta S_{\rm m}} = 0.58 \pm 0.04 \; . \tag{7.31}$$

Thus, the different character of atomic motion in the solid compact aggregate state and the liquid aggregate state with its sparser distribution of atoms increases the entropy jump.

One can introduce also the configurational cluster temperature $T_{\rm con}$ that follows from equilibrium between the solid and liquid cluster aggregate states and satisfies the formula

$$\frac{w_{\rm liq}}{w_{\rm sol}} = \exp\left(-\frac{\Delta F}{T_{\rm con}}\right) = \exp\left(-\frac{\Delta E}{T_{\rm con}} + \Delta S\right) \; . \tag{7.32}$$

Here $w_{\rm sol}$ and $w_{\rm liq}$ are the probabilities for the cluster to be found in the solid or liquid states respectively, and ΔF is the free energy jump at melting. In particular, at the melting point the configuration temperature is equal to

$$T_{\rm con}^{m} = \frac{\Delta E}{\Delta S_{\rm m}} = (0.27 \pm 0.03)D \; . \tag{7.33}$$

Thus, in an isolated cluster, coexisting solid and liquid aggregate states are characterized by three different temperatures of atom vibrations, $T_{\rm sol}$, $T_{\rm liq}$, $T_{\rm con}$. These temperatures obtained from treatment of the data [50] for the Lennard-Jones cluster of 13 atoms are given in Fig. 7.5.

7.5 The Cluster as a Canonical Ensemble of Bound Atoms

Here, we analyze the behavior of the heat capacity of this system near the melting point when the coexistence of phases is important. In the limit of an

infinite number of atoms, the phase transition is discontinuous and coexistence of phases is found only along the traditional coexistence curve of pressure and volume for a bulk system.

As we saw previously, only the configurational part of the energy contributes significantly to the change associated with passage between solid and liquid. Thus, as in the microcanonical case, we assume that the vibrational temperature and energy do not change in the phase change.

Let us introduce the total energies of atoms $E'_{\rm sol}(T)$ and $E'_{\rm liq}(T)$ for the solid and liquid aggregate states of a cluster. Considering a large cluster for which surface effects are negligible, we assume thermodynamic equilibrium for the motion of cluster atoms, characterized by a cluster temperature T. In particular, for estimations we use the limiting case in which the cluster's thermal energy significantly exceeds the Debye energy, that relevant to the Dulong-Petit law. Then $E'_{\rm sol}(T) = E'_{\rm liq}(T) = 3nT$, where n is a number of cluster atoms. Taking into account the dynamic equilibrium between aggregate states, so that the cluster is found in the solid state during some time intervals and in the liquid state at other times, one can use an appropriately time-weighted average to compute the cluster's mean internal energy. Then the internal energy of the cluster is equal to

$$E(T) = E'_{\rm sol}(T) w_{\rm sol} + \left[E'_{\rm liq}(T) + \Delta E\right] w_{\rm liq} = E'_{\rm sol} + \Delta E \frac{p}{1+p} \,, \qquad (7.34)$$

where we take $E'_{\rm sol} = E'_{\rm liq}$, i. e. the energy of atomic motion is identical for the solid and liquid states.

Let us find the heat capacity of the cluster:

$$\begin{aligned} C(T) &= \frac{{\rm d}E}{{\rm d}T} = C_{\rm o}(T) + \frac{\Delta E}{(1+p)^2} \frac{{\rm d}p}{{\rm d}T} \\ &= C_{\rm o}(T) + \frac{p}{(1+p)^2} \left(\Delta S_{\rm m}^2 + \Delta S_{\rm m} \frac{{\rm d}\Delta S}{{\rm d}T} \right) \,. \end{aligned} \qquad (7.35)$$

Here $\Delta S_{\rm m}$ is the entropy jump at the melting point, and the heat capacity

$$C_{\rm o}(T) = \frac{{\rm d}E'_{\rm sol}}{{\rm d}T} = \frac{{\rm d}E'_{\rm liq}}{{\rm d}T} = \frac{{\rm d}\left(K_{\rm sol}/\eta_{\rm sol}\right)}{{\rm d}T} = \frac{{\rm d}\left(K_{\rm liq}/\eta_{\rm liq}\right)}{{\rm d}T} \,, \qquad (7.36)$$

is determined by atomic oscillations and is characterized by a smooth temperature dependence, while the temperature dependence of the second term of formula (7.35) due to configurational excitation of the cluster is strong. We used above formula (6.32) for the probability of cluster location in the liquid cluster state. The heat capacity has a maximum at the temperature of equal free energies of the phases, which, for a bulk system, is the melting point $T_{\rm m}$. Near this maximum we have, under the assumption that the entropy difference $\Delta S_{\rm m} = \Delta E/T_{\rm m}$ does not depend on temperature,

$$C = C_{\rm o} + (C_{\max} - C_{\rm o}) \exp\left[-\alpha \left(T - T_{\rm m}\right)^2\right] \,, \qquad (7.37)$$

where

$$C_{\max} = \frac{\Delta E^2}{4T_{\rm m}^2} = \left(\frac{\Delta S_{\rm m}}{2}\right)^2 , \quad \alpha = \frac{\Delta E^2}{4T_{\rm m}^4} = \left(\frac{\Delta S_{\rm m}}{2T_{\rm m}}\right)^2 . \tag{7.38}$$

If we assume a linear temperature dependence for the entropy difference of the liquid and solid state, so that

$$\frac{{\rm d}\Delta S}{{\rm d}T} = \frac{\Delta S_{\rm m} - \Delta S_{\rm o}}{T_{\rm m}} , \tag{7.39}$$

we obtain from formula (7.37)

$$\begin{aligned} C(T) &= C_{\rm o}(T) + \Delta S_{\rm m}\,(2\Delta S_{\rm m} - \Delta S_{\rm o})\,\frac{p}{(1+p)^2} , \\ C_{\max} &= \frac{\Delta S_{\rm m}}{4}(2\Delta S_{\rm m} - \Delta S_{\rm o}) , \end{aligned} \tag{7.40}$$

where $\Delta S_{\rm m}, \Delta S_{\rm o}$ are the entropy difference at the melting point and zero temperature correspondingly, and $\Delta S_{\rm m} > \Delta S_{\rm o}$. These relations are valid under the condition that $\Delta E \gg T_{\rm m}$, or $\Delta S_{\rm m} \gg 1$. The resonance in the heat capacity refers to a narrow range of temperatures $\Delta T \sim \alpha^{-1/2} \sim T_{\rm m}/\Delta S_{\rm m} \ll T_{\rm m}$. Since the value $C_{\rm o}$ is proportional to n, the number of cluster atoms, and the fusion energy ΔE is proportional to n also, the influence of the phase transition on the heat capacity grows roughly as $\sim n$. For a bulk system of bound atoms this contribution at its maximum tends to infinity. Indeed, the ratio of the second term of formula (7.40) to the first one is $\sim n$, and the resonance width is $\sim 1/n$. Hence, the temperature dependence of the heat capacity of a large cluster allows us to determine its melting point with a high accuracy. As a demonstration of the resonance structure of the cluster heat capacity, Fig. 7.10 contains the temperature dependence for the heat capacity of sodium clusters near the melting point [244].

Because of the different character of cluster interaction with an environment depending on whether the conditions are microcanonical or canonical, the cluster parameters are different for the two cases. We will demonstrate this with the example of the Lennard-Jones cluster of 13 atoms and exhibit

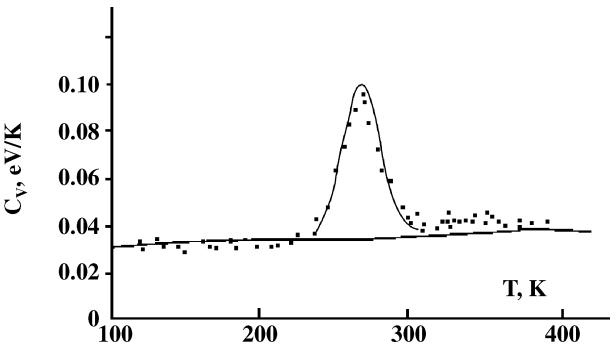

Fig. 7.10. The heat capacity of sodium clusters of 139 atoms as a function of temperature [244]

the role of the anharmonicity of atomic oscillations on the degree of the configurational excitation. Indeed, because the anharmonicity is greater for the liquid than for the solid cluster, the density of vibrational states increases faster with energy than does that of the solid, so that the average amplitude of oscillations for the isothermal liquid cluster is higher than that for the solid. If the melting temperatures are approximately equal for the isolated and isothermal clusters, i. e. for microcanonical or canonical ensembles, we find a special excess change of the cluster's potential energy in the isothermal case that does not appear in the constant-energy case. Taking the melting point $T_{\rm m} = 0.29D$ for both cases, and the corresponding kinetic energies of all the cluster atoms at this temperature to be $K_{\rm sol}(T_{\rm m}) = K_{\rm liq}(T_{\rm m}) \approx 2.9D$, we find the excess excitation energy $\Delta E'$ as a change of the average potential energy given by

$$\begin{aligned} \Delta E' &= \Delta E + \frac{K_{\rm liq}(T_{\rm m})}{\eta_{\rm liq}(T_{\rm m})} - \frac{K_{\rm sol}(T_{\rm m})}{\eta_{\rm sol}(T_{\rm m})} \\ &= \Delta E + K_{\rm sol}(T_{\rm m}) \left[\frac{1}{\eta(15.3D)} - \frac{1}{\eta(11.7D)} \right] = 3.0D \ , \end{aligned} \tag{7.41}$$

where $\Delta E = 2.4D$ is the energy difference for aggregate states of an isolated cluster at the melting point. An increase of the fusion energy of the isothermal 13-atom cluster in comparison with that of an isolated cluster results in an increase of the capacity of the liquid cluster in the isothermal cluster. Here, we are assuming that the anharmonicity parameter η is identical for both aggregate states of an isolated cluster at each excitation energy, and its dependence on the excitation energy is given in Fig. 7.8. Next, the various relevant temperatures of the isolated 13-atom Lennard-Jones cluster at the melting point, according to the data of Figs. 7.8 and 7.9, when $w_{\rm sol} = w_{\rm liq}$ and $E_{\rm ex} = 13.9D$, are approximately $T^m_{\rm sol} = 0.33D$ and, $T^m_{\rm liq} = 0.27D$, and the configuration temperature is $T_{\rm con} = 0.315D$. Correspondingly, the entropy jump is approximately $\Delta S = 9.0$ for the isolated Lennard-Jones cluster consisting of 13 atoms. Assuming this entropy corresponds also to the isothermal cluster, we obtain for the melting point of the isothermal cluster $T_{\rm m} = \Delta E/\Delta S \approx 0.27D$.

Thus the anharmonicity of the solid aggregate state under isothermal conditions is higher than that for an isolated cluster, whereas for the liquid state we have a different relation between these values. As a result, the isothermal phase transition requires a greater change of potential energy than that at constant energy, due to interactions between atoms for the Lennard-Jones 13-atom cluster. Due to anharmonicity, the energy change for an isothermal cluster exceeds that of the isolated cluster by approximately 20%.

7.6 Configurational Excitation of the Icosahedral Cluster of 55 Atoms

We now consider one more example of configurational excitation, that of the Lennard-Jones cluster consisting of 55 atoms. In contrast to configurational

excitation of a cluster of 13 atoms, for which the liquid state corresponds to excitation of one void, many voids partake in excitation of the liquid state for larger clusters. Therefore the aggregate state of such a system may be a mixture of excitation of several voids. We base our treatment of configurational excitation on the results of computer simulations and assume existence of the two aggregate states [48, 80, 235]. We use the dynamic coexistence of phases in clusters [50, 257–259] within a temperature range, i. e. part of the time, the cluster is in one aggregate state, and in the remainder, in the other state. (Strictly, clusters may exhibit more than two aggregate states in thermodynamic equilibrium; we consider such cases below.) In addition, while the cluster is residing in either aggregate state, vibrational equilibrium is established [43], so that the vibrational temperature for each aggregate state coincides with the thermostat temperature, if the cluster is in a canonical ensemble [6]. In this case the probability w_{liq} that the cluster is found in the liquid state is given by the formula (6.32) [48, 80, 235].

As in the previous case of a cluster of 13 atoms, the cluster of 55 atoms has the completed icosahedral structure with filled atomic shells, and the lowest configurational excitation consists of promotion of atoms out of the 42-atom external shell surface. But in contrast to the cluster of 13 atoms, several atoms may move from the external shell in typical configurational excitations. A typical configuration excitation may consist of any of several several elementary excitations: promotion of a vertex atom, an edge atom or a face atom. Figure 7.11 exhibits the character of configurational excitation if one surface atom is transferred to the cluster surface, and a hole is formed in the outer atomic shell. Transformation of this excitation with participation of many cluster atoms leads to formation of different relatively stable configurations, and the character of variation of the excitation cluster

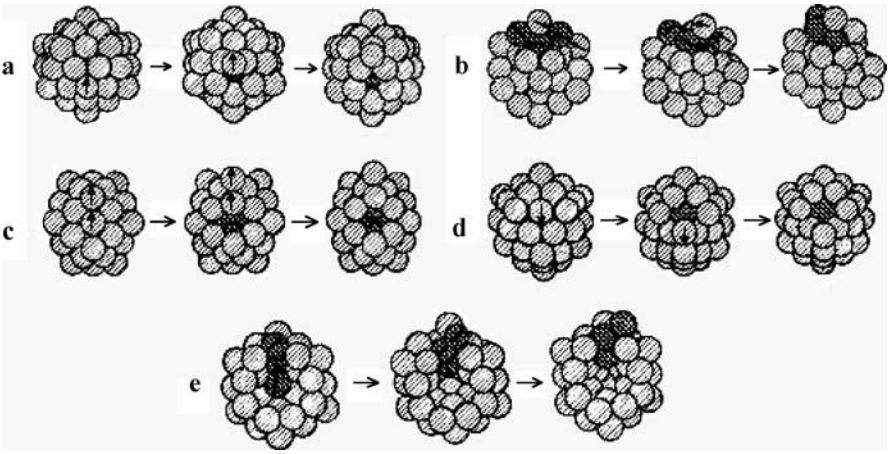

Fig. 7.11. Stages of simple configurational excitations for the 55-atom Lennard-Jones argon cluster [260]

energy [260] is given in Fig. 7.12. In the course of these transitions, the cluster passes through the minima of the PES that correspond to stable atomic configurations and through saddle points which separate these PES minima. Accounting for the oscillations of atoms in this picture is somewhat more complicated than for the 13-atom cluster. Figure 7.13 gives the evolution of the excitation energy E_{ex} of this cluster in time under isothermal conditions [252, 253] when this cluster is at constant temperature. If we ignore fluctuations of thermal atomic motion, one can distinguish three configurational states of this cluster. The caloric curve for these states [252, 253] is given in Fig. 7.14. There are three configurational states in this case, the solid state, the state with liquid outer shell and solid internal shell, and liquid state. As follows from Fig. 7.14, the latter two states are characterized by similar energies, and for simplification we will consider them as one configuration excitation in calculations of their parameters from the void standpoint.

To find the parameters of configurational excitation for the liquid aggregate state of the 55-atom Lennard-Jones cluster, we use numerical calculations for this cluster as a canonical ensemble of bound atoms. In particular, Fig. 7.15 shows the variation of the cluster energy and heat capacity for this system in the vicinity of the melting point [261–265].

From the aggregate of the data from computer simulations of this cluster [253, 261, 263–265], we obtain the following parameters of the phase transition between the solid and liquid cluster aggregate states within the following ranges: $\Delta E = 15 \pm 1$, $T_m/D = 0.31 \pm 0.01$, and $C_{res}^{max} = 650 \pm 50$. These values are relevant for a range near the melting point, and from this it follows that

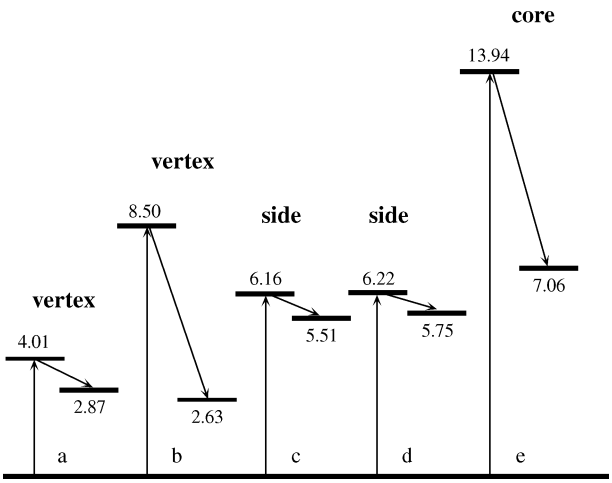

Fig. 7.12. The character of energy variation for configurational excitations for the 55-atom Lennard-Jones argon cluster [260]. The energies are given in units of the bond energy D. The initial positions of the moving atoms are indicated, as well as the character of excitation in accordance with Fig. 7.10

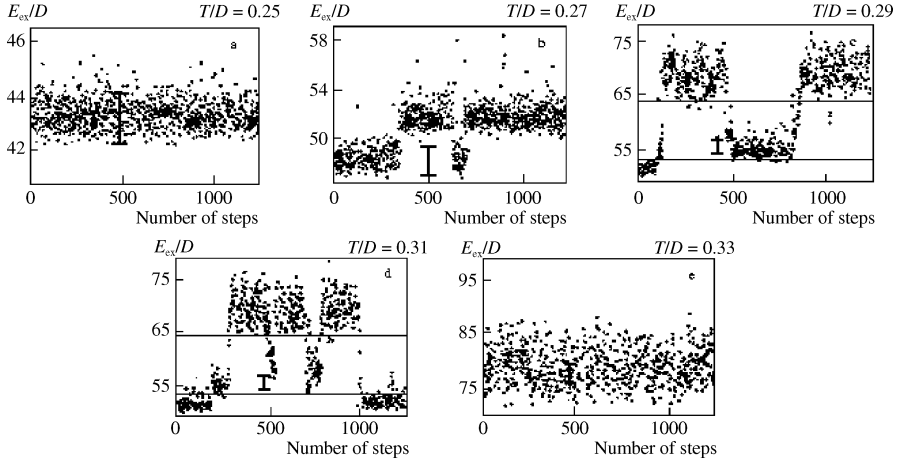

Fig. 7.13. The total binding energy distribution for the 55-atom Lennard-Jones (argon) cluster, under isothermal conditions [252, 253]. Averaging is taken over 1800 iteration steps. The displayed fluctuation of the binding energy has been obtained under the assumption that the motion of the cluster atoms is harmonic

the entropy at the melting point is

$$\Delta S_{\mathrm{m}} = \frac{\Delta E}{T_{\mathrm{m}}} = 48 \pm 5 \; . \tag{7.42}$$

From Eq. (7.40), we have for the entropy at zero temperature

$$\Delta S_{\mathrm{o}} = 2\Delta S_{\mathrm{m}} - \frac{4C_{\max}}{\Delta S_{\mathrm{m}}} \tag{7.43}$$

and from this formula and the above values we obtain the cluster entropy at zero temperature

$$\Delta S_{\mathrm{o}} = 36 \pm 15 \; . \tag{7.44}$$

A large uncertainty here makes this result relatively uninformative. We below find this value from another, more precise standpoint.

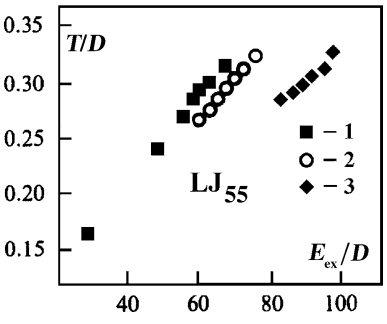

Fig. 7.14. The caloric curve of the 55-atom Lennard-Jones (argon) cluster [252, 253]. *1* – solid cluster, *2* – solid internal shell and liquid outer shell, *3* – liquid cluster

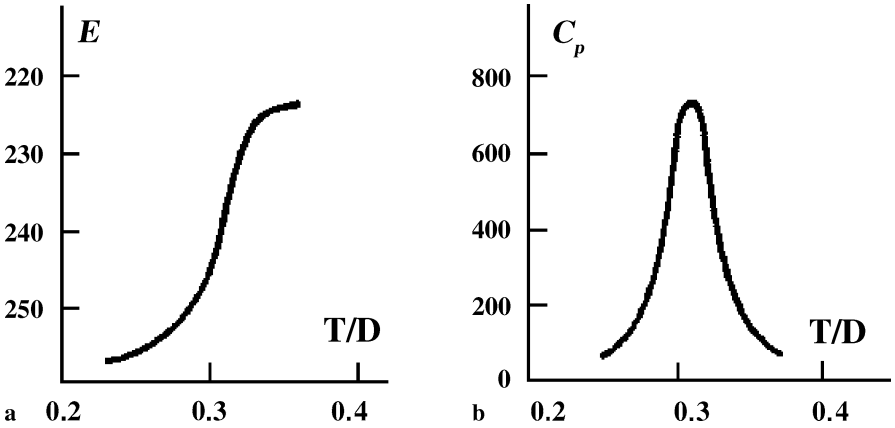

Fig. 7.15. Isothermal parameters of the 55-atom Lennard-Jones cluster near the melting point as a function of temperature [262, 263]: **a** the total binding energy of cluster atoms (*the caloric curve*); **b** the cluster heat capacity at zero external pressure

We now consider configurational excitation as a result of void formation – from perturbed vacancies on the external cluster shell. The energy of formation of one vacancy at zero temperature can be found by comparing the total binding energies of atoms ε_{55} and ε_{56} for the Lennard-Jones clusters of 55 and 56 atoms, and numerical calculations [139] give $\Delta\varepsilon = \varepsilon_{56} - \varepsilon_{55} = 2.64D$ at zero temperature. The direct calculations [260] for lower excitations of this cluster lead to a minimal excitation energy of this Lennard-Jones cluster of $2.63D$. The proximity of these values confirms the fact that an excited atom transferred onto the cluster surface can be treated as being well removed from the vacancy from which it came. Evidently, since the atom removed to the surface forms bonds with the atoms it contacts, the energy of promotion is less than the energy $\Delta\varepsilon$ of formation of the initial vacancy. From this it follows that the number of atoms which leave the external cluster shell or the number of forming voids for this cluster is

$$v \geq \frac{\Delta E}{\Delta\varepsilon} \approx 5 \, . \tag{7.45}$$

Note that atoms can transfer not only from the icosahedron's vertices, but also from the edges; here, we ignore the difference of the energy changes when an atom goes from a vertex or from an edge to the cluster surface. Transferring to the cluster surface, atoms become more mobile, than the surface cluster atoms. These atoms are called "floaters" [252, 253, 262, 263] and give the predominant contribution to the entropy. Therefore in determining the entropy of a configurationally excited state, along with formation of voids, we must account for the presence of floaters on the cluster surface.

Taking the number of voids in the liquid state of the Lennard-Jones cluster of 55 atoms to be $v = 5$–7, we determine the entropy jump at zero temperature ΔS_{o} as we treat the solid–liquid transition to be a consequence of transitions of atoms from the outer cluster shell onto its surface. Because of the icosahedral structure of this cluster, its outermost shell consists of 42 atoms, and there are 80 positions with 3-atom "hollows" on the surface for atoms promoted from the outer shell. A new vacancy on a cluster edge or surface has $l = 6$ neighboring atoms, and a vertex vacancy has only $l = 5$. Therefore if v atoms transfer onto the cluster surface, then $v \cdot l$ bonds are lost in the cluster surface for atoms transferred to any of 80 positions on the cluster surface, if we assume that v transferring atoms on the cluster surface do not border vacancies on the cluster shell. From this we found the entropy jump for this configurational excitation of the cluster at zero temperature which results from v atoms moving from the outermost shell. We have for this value

$$\Delta S_{\mathrm{o}} = \ln C_{\mathrm{m}}^{v} C_{42}^{v} \,, \tag{7.46}$$

where $m = 80 - v \cdot l$ is the number of positions on the cluster surface for transition of atoms from the outermost cluster shell. From this formula it follows for the entropy jump at zero temperature $\Delta S_{\mathrm{o}} = 28.5 \pm 0.3$ for $v = 5$, $\Delta S_{\mathrm{o}} = 31.6 \pm 0.4$ for $v = 6$, and $\Delta S_{\mathrm{o}} = 32.3 \pm 0.7$ for $v = 7$. Thus the entropy jump at zero temperature depends weakly from the number of transferred atoms, and the average value for the entropy jump at zero temperature is

$$\Delta S_{\mathrm{o}} = 31 \pm 2 \,. \tag{7.47}$$

One can see that this value is well within the range of formula (7.44). Because the accuracy in this case is higher than that in formula (7.44), we use formula (7.43) to determine ΔS_{m}. Then formula (7.43) gives

$$\Delta S_{\mathrm{m}} = \frac{\Delta S_{\mathrm{o}}}{4} + \sqrt{\frac{\Delta S_{\mathrm{o}}^2}{16} + 2C_{\mathrm{res}}^{\max}} \tag{7.48}$$

and on the basis of formula (7.47) and the calculated maximal heat capacity [261–265] $C_{\mathrm{res}}^{\max} = 650 \pm 50$ we obtain [133, 237]

$$\Delta S_{\mathrm{m}} = \frac{\Delta E}{T_{\mathrm{m}}} = 45 \pm 2 \,. \tag{7.49}$$

This result together with the range of its validity is consistent with formula (7.42), but we now have a result with greater precision and presumably with greater accuracy. Thus the analysis of computer simulations of these clusters by molecular dynamics allows us to determine some thermodynamical parameters of the phase transition within the framework of a simple scheme. Next, we will analyze these results together with the microscopic nature of the phase transitions.

Thus, we find parameters of the liquid state for the 55-atom Lennard-Jones cluster. This information will help us to analyze the properties of the liquid aggregate states of clusters.

7.7 Character of Configuration Transitions in Clusters

Considering a configurational transition of a cluster from the standpoint of transitions between nearest local minima of the PES, we sum up the peculiarities of this process that is accompanied by transition through a saddle point of PES, i. e. it has a barrier character. Figure 1.5 shows an atomic transition from a state of 6 bonds with nearest neighbors into a state of 3 bonds with nearest neighbors for a transferred atom. In the course of transition into a final state a transferred atom can have at most two nearest neighbors at the saddle point.

Let us reduce this transition to a general character of structural transitions. Figure 7.16 gives two types of structural transitions arising from one atom crossing a barrier between symmetric configurations. In these processes the moving atom passes from one group of atoms to another. The first type of these processes, DSD (diamond-square-diamond) [267], is typical for carbon-containing systems (for example [268, 269]). Another type of structural transition, EB process (edge-bridging) [270], leads to breaking some bonds in the course of the transition, and the atom rotates around an axis that conserves some bonds. The EB process is typical for systems with short-range interatomic interactions or for those for which a short-range interaction is the basis of the total interaction, in particular, for condensed inert gases [261, 271, 260]. Figure 7.16 shows only symmetric transitions when the initial and final states of the structure transitions are symmetrical. This type of structural transition is realized also if the initial and final states are characterized by a different number of bonds. In analyzing clusters and macroscopic systems with a basic short-range interaction, we will focus below only on EB structural transitions.

The barrier determines the rate of structural transitions between these states. We evaluate it [272] now for the Lennard-Jones cluster of 13 atoms,

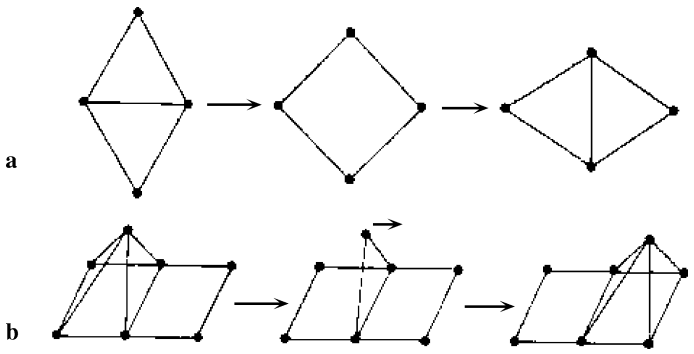

Fig. 7.16. The processes of structural transitions of an atom between symmetric atomic configurations. **a** DSD (diamond-square-diamond) process, **b** EB (edge-bridging) process

using the Frenkel model [93], according to which the transition takes place if the energy of the moving atom exceeds the barrier height. Assuming for simplicity that the barrier has an axial symmetry, we take it in the form

$$U(\rho) = U_{\rm o} + \frac{1}{2}\frac{{\rm d}^2U}{{\rm d}\rho^2}\rho^2 \ ,$$

where ρ is the distance from the point of minimum barrier in the saddle plane. From this we find for the transition rate

$$v = \frac{1}{\tau_{\rm o}}\frac{1}{4\pi R^2}\int\limits_0^\infty 2\pi\rho\,{\rm d}\rho\exp\left[-\frac{U(\rho)}{T}\right] = \frac{T}{2R^2\frac{{\rm d}^2U}{{\rm d}\rho^2}}\exp\left(-\frac{U_{\rm o}}{T}\right) \ . \qquad (7.50)$$

Here T is a current temperature, and R is the distance between an atom and the saddle point. Taking for an estimate $\dfrac{{\rm d}^2U}{{\rm d}\rho^2} \sim D/R^2$, we obtain from this for the 13-atom Lennard-Jones cluster, at the melting point $T_{\rm m} = 0.30D$,

$$\tau = \frac{1}{v} \sim 50\tau_{\rm o} \ . \qquad (7.51)$$

Thus the hierarchy of times is as we used above.

8

Phase Transitions in Macroscopic Systems of Atoms

8.1 Configurational Excitation of a Solid

Configurational excitation of a bulk crystal consists in formation of vacancies. At zero temperature and with only a small number of vacancies, (so they do not border with each other), atoms and vacancies form a crystal lattice. Such an atomic distribution is stable and is described by the lattice model. With greater excitation, when some vacancies become nearest neighbors, vacancies inside the crystal can lost their shape, and neighboring vacancies may join, but this process involves barrier crossings. In this way, the vacancy is transformed into a void, an empty space between atoms that varies its shape and volume in time due to atomic motion. In this manner, the order–disorder transition proceeds for the atomic distribution, so that, with enough voids, the atomic system transfers from the solid, lattice-based state to the liquid. We now consider this transition in a bulk atomic system.

Basing our approach on the lattice model for configurational excitation of a bulk ensemble of interacting atoms, we consider first configurational excitation for the solid state for which an elementary configurational excitation is a vacancy, and the number of vacancies is relatively small, so vacancies do not border in the crystal lattice. We assume thermal and configurational excitations to be separated, and thermal motion of atoms to be of relatively small amplitude, so that thermal motion of atoms does not influence significantly its configurational excitation. Therefore, in analyzing configurational excitation we will not take into account thermal motion of atoms.

Our guiding model is a solid, close-packed lattice of atoms with short-range interaction. Because each bond involves two atoms, and each internal atom of the crystal has 12 nearest neighbors, the binding energy of solid atoms per atom is $6D$, where D is the energy to break one bond. Formation of one vacancy corresponds to removal of one atom and is accompanied by breaking of 12 bonds, so that the energy of formation of one vacancy is

$$\varepsilon = 6D \,, \tag{8.1}$$

identical to the binding energy per crystal atom.

We now determine the solid parameters for the lattice model. The partition function of an excited crystal consisting of n atoms and v vacancies is

$$Z = \sum_v Z(v) = \sum_v C_{n+v}^v \exp\left(-\frac{v\varepsilon}{T}\right) , \tag{8.2}$$

where T is the temperature, and the partial partition function is

$$Z(v) = C_{n+v}^v \exp\left(-\frac{v\varepsilon}{T}\right) . \tag{8.3}$$

Since $n \gg 1, v \gg 1$, we obtain near the maximum of the partition function, assuming $v \ll n$,

$$Z(v) = \exp\left[v_{\mathrm{sol}} - \frac{(v - v_{\mathrm{sol}})^2}{2v_{\mathrm{sol}}}\right] , \tag{8.4}$$

where the maximum occurs at

$$v_{\mathrm{sol}} = n \exp\left(-\frac{\varepsilon}{T} - 1\right) . \tag{8.5}$$

The total partition function of the solid state is

$$Z_{\mathrm{sol}} = \int \mathrm{d}v \left(\frac{n}{v}\right)^v \exp\left(-\frac{v\varepsilon}{T}\right) = \int\limits_{v \sim v_{\mathrm{sol}}} Z(v)\,\mathrm{d}v = \sqrt{2\pi v_{\mathrm{sol}}}\exp(v_{\mathrm{sol}}) . \tag{8.6}$$

Correspondingly, the energy of configurational excitation is

$$E_{\mathrm{ex}} = \varepsilon v_{\mathrm{sol}} = n\varepsilon \exp\left(-\frac{\varepsilon}{T} - 1\right) \ll n\varepsilon . \tag{8.7}$$

Note that the difference

$$\ln Z_{\mathrm{sol}} - \ln Z(v_{\mathrm{sol}}) = \ln \sqrt{2\pi v_{\mathrm{sol}}}$$

is small in comparison to each term, in this case $v_{\mathrm{sol}} \gg 1$, allowing us to use the maximum value of the partial partition function instead of the total partition function of the solid state, within the accuracy of this estimation. We reiterate the assumption that neighboring vacancies do not border, i. e. the criterion $v \ll n$ is fulfilled.

From this analysis, it follows that the number of vacancies formed is relatively small at low temperatures, justifying the assumption that vacancies do not border. Existence of a maximum of the partition function (or minimum of the free energy) of this atomic system allows us to connect the aggregate state with elementary excitations of this system. We define the aggregate state as the group of excited states that dominate the region of the maximum of the partial partition function. We neglect excitations to other states whose probabilities are negligible. In this way the aggregate state is defined to be a specific group of configurationally excited states.

8.2 Modified Lattice Model for Configurational Excitation

Analyzing the scaling of condensed inert gases in Chap. 2, we established that properties of these systems are governed by a short-range interaction. Hence here we develop the lattice model in a form based on that short-range interaction to describe configurational excitation of a bulk system of bound inert gas atoms. Again, the ordered and disordered states for the lattice model correspond to solid and liquid aggregate states. We begin with a large solid cluster of bound atoms consisting of $n+v$ atoms and allow v atoms to escape to the outside, so that the cluster formed consists of n atoms and v vacancies. This cluster relaxes due to interatomic interactions, and this relaxation leads to a fast cluster shrinkage. A typical time of relaxation is of the order of atomic vibrational motion over a distance between nearest atoms, that is $\sim 10^{-12}$ s for real solids at room temperature. We now assume the cluster to be very large, allowing us to neglect surface effects, so the newly-formed voids are located inside the cluster.

Thus, we characterize the configurational excitation of the system by its number of voids and atoms. This is equivalent to introducing the total volume of the system. Although, in contrast to a vacancy, the shape and volume of an individual void, an elementary configurational excitation, varies in time, this approach is convenient for the analysis of statistics of excited states. We use the approach of a mean field, so that individual voids are independent. Each void is characterized by the energy of void formation ε and the statistical weight of a void g; these parameters depend on v and n. We generalize the lattice model by introducing the statistical weight of an individual void and treat the volume and energy of an individual void as different from that of a vacancy.

The partition function of this system has the form

$$Z(v) = C_{n+v}^{v} g^{v} \exp\left(-\frac{v\varepsilon}{T}\right) , \tag{8.8}$$

so the interaction of voids is taken into account by the dependence of the energy of void formation ε on the number of voids. Here C_{n+v}^{v} is the number of combinations for a given number of voids. We take the energy of formation of an individual void in the form

$$\varepsilon = \varepsilon_{\mathrm{o}} - U\left(\frac{v}{n}\right) , \tag{8.9}$$

where U is the effective interaction potential of voids, ε_{o} is the energy of formation of one vacancy in the crystal, i. e. when $v = 0$ ($\varepsilon_{\mathrm{o}} = 6D$ for a short-range interaction potential). Under these conditions, we have from the expression (6.8) for the partition function of a gas of voids in the limit $n \gg 1$, $v \gg 1$:

$$\ln Z(v) = v \cdot \left(1 + \ln\frac{ng}{v} - \frac{\varepsilon_{\mathrm{o}} - U}{T}\right) . \tag{8.10}$$

In the limit $v/n \to 0$ we have $g = 1$, $v = 0$ and obtain the results for the lattice model.

Applying these formulas to the liquid state of a bulk system of atoms with short-range interaction, we characterize a configurationally excited state of a bulk system of bound atoms by an excitation energy (or a number of voids) together with the temperature of atoms which is the characteristic of their kinetic energy. Because we assume these parameters are independent, this system is, in general, not in thermal equilibrium. The number of voids will vary in time as the system evolves toward equilibrium. A typical time to reach equilibrium depends on the system size because voids move to the system boundary or from it as a result of diffusion inside the system. Typical times of observation of this system are small compared to a time for establishment of this equilibrium. Next, in order to conserve the system of bound atoms during observational times, it is necessary to surround it with a gas of its atoms at the saturated vapor pressure for the chosen temperature of the system. Then the rates of processes of atom attachment and evaporation equalize, conserving the number of bound atoms of the system. In addition, we use the approach of a mean self-consistent field for voids. This allows us to consider configurational excitation as a gas of free voids, but parameters of an individual void depend on the relative number of voids.

Introducing the energy of formation of one void ε according to formula (8.9), we consider configurational excitation as formation of a gas of independent voids. The interaction potential of voids with one another is zero, as are their derivatives, when $v \sim 0$. An increase of a number of voids v leads to a decrease of the energy of void formation ε, i. e. $U \geq 0$ at any v. Next, formally $\varepsilon \to 0$ at large v. We use the simplest form of the function $U(v/n)$ which accounts for these properties and allows us to construct the liquid state of this system [46, 47]

$$U\left(\frac{v}{n}\right) = \varepsilon_{\mathrm{o}}\left[\exp\left(-\frac{\alpha n}{v}\right) - \exp\left(-k\frac{\alpha n}{v}\right)\right] , \tag{8.11}$$

where α, k are parameters of this quantity. Formula (8.11) is valid if v/n is not large. The void statistical weight is one at $v = 0$ and increases sharply as v grows. We take it in the form

$$g = 1 + a\frac{v}{n} , \quad a \gg 1 . \tag{8.12}$$

Modifying the lattice model in this way for a bulk system [166], one can apply this model to systems dominated by nearest-neighbor interactions. Thus this model is a bridge between the lattice model for configurational excitation and the saddle-crossing approach in which configurational excitation changes result from passages between nearest local minima of the PES. Generalizing the lattice model, we transfer from the vacancy concept to the void concept. The dependence of void parameters – the energy of its formation ε_{v} and the

void statistical weight $g_{\rm v}$ – on the void concentration and the atomic temperature allows us to include in consideration atomic thermal excitation and thermal motion. In contrast to a vacancy, a void occupies an indefinite space, shape and volume between nearest atoms, all of which can vary with time. Therefore we deal with average void parameters. We go from a dynamic description in terms of saddle-crossing to a statistical description, and pass from excitation of a specific configurations to describing a corresponding number of voids, as identical elementary excitations. Thus, within the framework of the void concept, any configurational excitation is a set of identical elementary excitations – voids.

8.3 Parameters of Voids for Liquid Inert Gases

We now find parameters of configurational excitation for liquid inert gases from the modified lattice model, the void model, and thermodynamic parameters of the liquid state of inert gases. In addition, we use the similarity or scaling law (Chapt. 2) that allows one to express various parameters of different inert gases through the parameters of the pair interaction potential of atoms. In this way, one can express various parameters of different rare gases through three parameters – m, the atom mass, $R_{\rm e}$, the equilibrium distance between atoms in the diatomic molecule, and D, the depth of the potential well for the pair interaction potential of atoms. Analyzing condensed rare gases in these terms, we found that this is a system in which interaction between nearest neighbors dominates. In this case the sublimation energy of the crystal is close to $6D$, because each internal atom has 12 nearest neighbors, and each bond refers to two atoms. In reality, this value is 6.4 ± 0.2 according to Table 2.5. Next, the reduced pressure near the triple point is $(1.9 \pm 0.2) \cdot 10^{-3}$, and we below ignore the pressure effects. Hence, one can characterize excitation of this system by the one parameter of configurational excitation, and we take the number of voids v as this parameter.

We will find the parameters of an individual void in the liquid state near the triple point on the basis of parameters of real rare gases. Additional information follows from there being one thermodynamically stable configurational state of this system, that is the liquid state in addition to the solid state. (This is of course an aggregation of a vast number of specific configurations.) Then the logarithm of partition function $\ln Z = -F/T$, where F is the free energy, as a function of the number of internal voids must have the form given in Fig. 8.1 and is characterized by two maxima. Thus, considering configurational excitation of a bulk system of n bound atoms as a result of formation of a gas of v identical voids, we represent formula (8.7) for the partition function of voids in the bulk limit $n \gg 1$, $v \gg 1$ in the form

$$\ln Z_v = n \ln \left(1 + \frac{v}{n}\right) + v \ln \left(1 + \frac{n}{v}\right) + v \ln g_{\rm v} - v \frac{\varepsilon_{\rm v}}{T} = v \left(\Delta S_{\rm v} - \frac{\varepsilon_{\rm v}}{T}\right) , \quad (8.13)$$

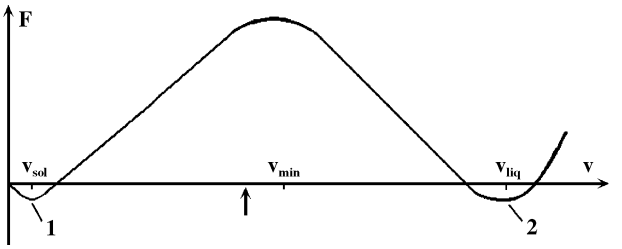

Fig. 8.1. Logarithm of the specific free energy for a bulk ensemble of bound atoms with a pair interaction as a function of the void concentration [46]

where the entropy variation due to void formation is

$$\Delta S_{\rm v} = \frac{1}{x}\ln(1+x) + \ln\left(1+\frac{1}{x}\right) + \ln g_{\rm v}\ , \quad x = v/n\ . \tag{8.14}$$

It is convenient to simplify this expression by [273]

$$\Delta S_{\rm v} = 1 + \ln\frac{g_{\rm v}}{x}\ , \tag{8.15}$$

this change leads to an error below 7% if $x \le 1/3$, which includes all the range between solid and liquid states. Then we have for the specific logarithm of the partition function

$$\Phi(x) \equiv \frac{1}{n}\ln Z_{\rm v} = x\left(1 + \ln\frac{g_{\rm v}}{x} - \frac{\varepsilon_{\rm v}}{T}\right)\ . \tag{8.16}$$

This simplification allows us to use our assumptions validly.

From this we get for the solid (crystal) state ($v \ll n, g_{\rm v} = 1, \varepsilon_{\rm v} = \varepsilon_{\rm sol}$)

$$\ln Z_{\rm v} = v\left(1 + \ln\frac{n}{v} - \frac{\varepsilon_{\rm sol}}{T}\right)\ ,$$

and the minimum condition gives the number of voids (vacancies) for the solid state in accordance with formula (8.4)

$$\frac{v_{\rm sol}}{n} = \exp\left(-\frac{\varepsilon_{\rm sol}}{T}\right)\ .$$

Applying these formulas to the liquid state of rare gases, we use the enthalpy of excitation $\Delta H_{\rm fus}$ for the liquid state

$$v\varepsilon_{\rm v} = n\Delta H_{\rm fus}\ . \tag{8.17}$$

We now represent the equations for the above dependence of $\ln Z(v)$, as it appears in Fig. 6.3 from the data of Fig. 7.1. The position of the minimum of the function $\ln Z(v)$ is given by the equation $\mathrm{d}\ln Z(v)/\mathrm{d}v = 0$ or

$$\frac{\mathrm{d}}{\mathrm{d}v}(vU)(v_{\rm min}) - \varepsilon_{\rm o} + T\ln\frac{ng(v_{\rm min})}{v_{\rm min}} + T\frac{\mathrm{d}\ln g(v_{\rm min})}{\mathrm{d}\ln v} = 0\ , \tag{8.18}$$

where we use equation (8.13) for $\ln Z(v)$ with expression (8.15) for $\Delta S_{\rm v}$. The same equation for the maximum of this function for the liquid state is

$$\frac{\mathrm{d}}{\mathrm{d}v}(vU)(v_{\rm liq}) - \varepsilon_{\rm o} + T\ln\frac{ng(v_{\rm liq})}{v_{\rm liq}} + T\frac{\mathrm{d}\ln g(v_{\rm liq})}{\mathrm{d}\ln v} = 0\,. \tag{8.19}$$

One more relation determines the melting point $T_{\rm m}$ of the bulk system under consideration. This temperature corresponds to the equality of the free energies for the solid and liquid states. Since we assume the pressure to be zero, this gives $Z_{\rm sol}(T_{\rm m}) = Z_{\rm liq}(T_{\rm m})$, and because of the scaling of values, we have $\ln Z_{\rm sol}(T_{\rm m}) = v_{\rm sol}(T_{\rm m}) = 0$. Thus, this equation takes the form

$$\ln Z(v_{\rm liq}) = 1 + \ln\frac{ng(v_{\rm liq})}{v_{\rm liq}} - \frac{\Delta H_{\rm fus}}{T_{\rm m}}\frac{n}{v_{\rm liq}} = 0\,, \tag{8.20}$$

where $\Delta H_{\rm fus}$ is the enthalpy of the phase transition, based on the values of the binding energy per individual void.

At the melting point, according to equations (8.19) and (8.20), we have

$$\Phi(x_{\rm liq}) = \Phi'(x_{\rm liq}) = 0\,, \tag{8.21}$$

where $\Phi(x)$ is defined by formula (8.16). Using the dependence (8.12) for the void statistical weight, we obtain from (8.21) at the melting point

$$\frac{\mathrm{d}U(x_{\rm liq})}{\mathrm{d}x} = 0\,, \tag{8.22}$$

Table 8.1. Reduced parameters of voids for bulk liquid inert gases [47–49, 273, 274]

	Ne	Ar	Kr	Xe	Average
$T_{\rm m}/D$	0.581	0.587	0.578	0.570	0.579 ± 0.007
$\varepsilon_{\rm o}/D$	6.1	6.5	6.7	6.7	6.5 ± 0.3
$\Delta H_{\rm fus}/D$	0.955	0.990	0.980	0.977	0.976 ± 0.017
$g_{\min}$	1.9	2.0	2.0	2.0	2.0
$g_{\max}$	1900	3700	4300	4100	3500 ± 1000
$n/v_{\rm liq}$	3.12	3.13	3.14	3.13	3.13 ± 0.01
$\varepsilon(v_{\rm liq})/D$	3.00	3.09	3.05	3.05	3.05 ± 0.04
$\Delta S(v_{\rm liq})/v_{\rm liq}$	5.16	5.26	5.28	5.35	5.26 ± 0.08
$V_{\rm void}/V_{\rm sol}$	0.49	0.46	0.50	0.47	0.48 ± 0.02
$g(v_{\rm liq})$	55	62	63	68	62 ± 5
a	171	189	193	207	190 ± 15
$g(v_{\min})$	15	17	17	18	17 ± 1
$U_{\rm liq}/D$	3.1(3.2)	3.4(3.4)	3.6(3.4)	3.6(3.4)	3.4 ± 0.2
$U_{\rm liq}/\varepsilon_{\rm o}$	0.51(0.52)	0.52(0.52)	0.54(0.52)	0.54(0.52)	0.52 ± 0.01
$\Delta S(v_{\min})/v_{\min}$	6.19	6.32	6.32	6.38	6.3 ± 0.1
$1 - T_{\rm m}\Delta S(v_{\min})/\varepsilon_{\rm o}v_{\min}$	0.41(0.42)	0.43(0.43)	0.44(0.46)	0.44(0.46)	0.44 ± 0.02
α	0.165 (0.162)	0.159 (0.159)	0.151 (0.157)	0.151 (0.157)	0.158 ± 0.005
$\alpha n/v_{\rm liq}$	0.51	0.50	0.48	0.48	0.49 ± 0.02
k	3.26	3.38	3.56	3.58	3.44 ± 0.15

or

$$\frac{\alpha}{x_{\rm liq}} = \frac{\ln k}{k-1} \ , \tag{8.23}$$

and we assume $g(v_{\rm liq}) \gg 1$. The function $U(v/n)$ is monotonic for obvious physical reasons, but (8.22) shows no liquid maximum for the monotonic partition function and therefore the function $U(x)$ has a complex form (8.11) valid when $v < v_{\rm liq}$. We establish one more equation assuming that the minimum of the function $\ln Z_{\rm v}$ of Fig. 6.1 corresponds to the void concentration when a test void has one void as a nearest neighbor. This gives $x_{\rm min} = 1/12$. Neglecting here the second term in the expression (8.11) for $U(x)$, and assuming $g(x_{\rm min}) \gg 1$, or $\alpha \gg 12$, we obtain from the second equation (8.21) $\Phi'(x_{\rm min}) = 0$

$$(1 + 12\alpha) \exp(-12\alpha) = 1 - \frac{(1 + \ln a) T_{\rm m}}{\varepsilon_{\rm o}} \ .$$

We give the values of some void parameters in Table 8.1, where $\varepsilon_{\rm v} = \varepsilon_{\rm sol} - U$ is the energy which is required for formation of one void in the liquid state from the initially void-free solid state. We take the energy of void formation on the basis of formula (8.9); the effective interaction potential of voids $U(v/n)$ and the void statistical weight $g(v)$ are given by formulas (8.11) and (8.12) correspondingly. Table 8.1 contains the values a in formula (8.12). In addition, we give in Table 8.1 the volume per void $V_{\rm void}$ for the liquid state that follows from the relation

$$V_{\rm void} = \frac{n}{v_{\rm liq}} \left(V_{\rm sol} - V_{\rm liq} \right) \ , \tag{8.24}$$

where $V_{\rm sol}$ and $V_{\rm liq}$ are the volumes per atom for the solid and liquid states (see Table 2.6), respectively.

As follows from the Table 8.1 data, the relative number of voids for the system of bound atoms with short-range interaction is $v_{\rm liq} = (0.320 \pm 0.001)n$, and the ratio of the number of voids for the liquid state and at the minimum of the partition function is $v_{\rm liq}/v_{\rm min} = 3.85 \pm 0.02$. The energy of formation of one void for the liquid state is approximately one half of that for the solid state. One can now analyze the character of relaxation of the excited state of the regular structure to the liquid state by transformation of vacancies into voids. In the first stage of the excitation process, when the cluster of n atoms develops its v vacancies, the average number γ of vacancies neighboring a given one is

$$\gamma = \frac{12v}{n+v} = 2.9 \ . \tag{8.25}$$

In addition, during relaxation of the initial excited state, when the system becomes liquid, the density of atoms varies from $\rho_{\rm ex}$ up to $\rho_{\rm liq}$, increasing about 14%. The specific energy released from this relaxation is about $0.48D$ per atom, approximately one half of the fusion energy.

8.4 Voids in a Macroscopic System of Bound Atoms

We consider a void as an elementary configuration excitation. For a cluster with completed atomic shells a void is a perturbed vacancy (see Fig. 1.5b), though the energy of void formation can differ significantly from that of vacancy formation. In the case of internal voids of configurationally excited ensembles, the operation of vacancy transformation into voids is more arbitrary, as one can see by considering the liquid aggregate state of inert gases. Indeed, because the shape and volume of an individual void vary in time, we use only average void parameters. Moreover, it is difficult to draw boundaries between neighboring voids. Therefore, although for convenience we take a void as a relaxed vacancy, such an introduction of a void has elements of arbitrariness.

Let us consider this problem from another standpoint. Any configurationally excited state of a bulk atomic system contains many elementary configurational excitations – voids. Let us ascertain changes in void parameters due to an increase or decrease an individual void volume. In this case the specific energy and specific volume of voids are fixed, so that the energy and entropy per void volume will be proportional to the void volume at any given specific void volume if we vary the void size. Thus, all thermodynamic parameters of the system of atoms and voids are proportional to the specific energy of configurational excitation, so that renormalization of voids does not lead to variation of specific void parameters in the first approximation. Therefore for a small parameter v/n or $\Delta H_{\text{fus}}/\varepsilon_{\text{o}}$ (ΔH_{fus} is the fusion enthalpy and ε_{o} is the binding energy per atom for the ground configuration state) the specific parameters of voids are constant.

Nevertheless, since the second approach for a small parameter v/n contains logarithmic terms, we must determine which method to choose the average void volume is correct. We can use the same logic we applied to clusters: the void forms when an arbitrary interior atom moves to the surface of the system, and then relaxes to equilibrium. This holds true for a crystal lattice when vacancies form inside it, and we assume that the same general process occurs in relaxation. One can see that this assumption is not precisely accurate because of the importance of surface effects in the cluster, but it is correct in a rough, general sense. Thus, we use a simple method of void definition, and our position is correct in principle. However we must recognize that the results will contain an error, i. e. the accuracy of final results is restricted.

8.5 Criterion of Existence of the Liquid State

We above postulate existence of the liquid aggregate state for a bulk ensemble of bound atoms. But it may be not correct in principle. For example, one cannot introduce aggregate states in an atom, i. e. a system consisting of a Coulomb center and many electrons located on electron shells. In the cluster

case one can analyze the conditions in which there is an excited thermodynamically stable configuration state. In this analysis we take into account that the solution of equation (8.20) exists whenever

$$g(v_{\rm liq}) > g_{\rm min} = \exp\left(\frac{\Delta H_{\rm fus}}{T_{\rm m}} - 1\right) . \tag{8.26}$$

Next, from this equation and the definition of the fusion energy $\Delta H_{\rm fus} = \varepsilon(v_{\rm liq})x_{\rm liq}$, it follows that

$$g(v_{\rm liq}) = \frac{\Delta H_{\rm fus}}{\varepsilon_{\rm liq}} \exp\left(\frac{\varepsilon_{\rm liq}}{T_{\rm m}} - 1\right) ,$$

where $\varepsilon_{\rm liq} = \varepsilon(v_{\rm liq})$ is the energy of void formation for the liquid state at the melting point. Because $g(v)$ is a monotonic function of $\varepsilon_{\rm liq}$, and $\varepsilon_{\rm liq} < \varepsilon_{\rm o}$, we obtain the condition

$$g(v_{\rm liq}) < g_{\rm max} = \frac{\Delta H_{\rm fus}}{\varepsilon_{\rm o}} \exp\left(\frac{\varepsilon_{\rm o}}{T_{\rm m}} - 1\right) . \tag{8.27}$$

Table 8.1 contains the values of $g_{\rm min}$ and $g_{\rm max}$. Thus the liquid state exists as a stable form only if the void statistical weight lies within a certain range. In particular, if the statistical weight of a void is equal to the statistical weight of a vacancy in the crystal lattice $g = 1$, the system has no stable liquid state. Because the void statistical weight is one at zero temperature and increases with an increase of the vibrational temperature, atomic thermal motion plays a significant role for existence of the liquid state; this is one reason the liquid aggregate state is not realized at low temperatures. In contrast, as we saw in Chap. 7, clusters with completed shells have stable liquid states because of the high statistical weights of their lowest configurationally excited states. The data of Table 8.1 allows us to determine various parameters of condensed rare gases. In particular, Fig. 8.2 contains the specific free energy of bulk inert gases as a function of the reduced excess volume which is proportional to the number of voids. This figure shows the existence of the freezing point below which the liquid state is not metastable. Figure 8.3 gives the caloric curves for the solid and liquid states of argon [266].

We now analyze the results from another standpoint. We represent the entropy of the solid–liquid phase transition as the sum of two parts

$$\Delta S = \Delta S_{\rm conf} + \Delta S_{\rm term} , \tag{8.28}$$

so that the first configurational term is associated with formation of internal voids, and the second term relates to thermal motion of atoms. The first term, according to formula (8.14), is equal to

$$\Delta S_{\rm conf} = n \ln\left(1 + \frac{v}{n}\right) + v \ln\left(1 + \frac{n}{v}\right) ,$$

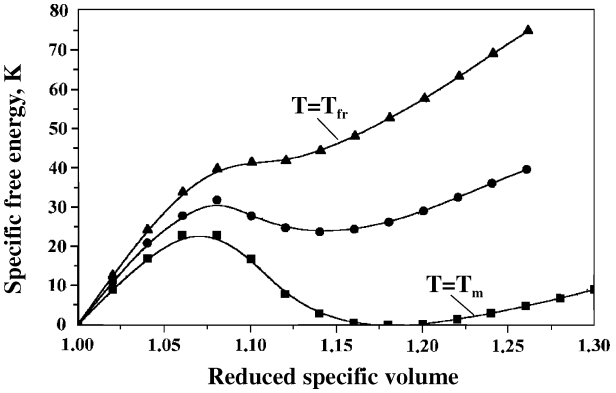

Fig. 8.2. The dependence of the specific free energy of bulk argon on the volume per atom [266]

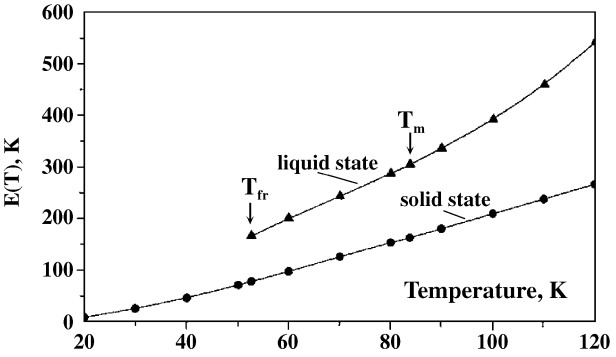

Fig. 8.3. The caloric curves of bulk argon [266]

and $\Delta S_{\rm conf}/n = 0.73$ for the above values of void parameters for liquid inert gases. We note that this value is only approximate because the definition of an elementary void is imprecise. Nevertheless, this value gives a correct guideline for the subsequent analysis.

Because the total entropy jump for the phase transition of rare gases is $\Delta S/n = 1.68$, we obtain for the part due to thermal motion of atoms

$$\Delta S_{\rm term} = 0.95 \, .$$

This term is due to atomic oscillations, and is 56% of the total entropy. As a result of the phase transition, the specific volume per atom increases, as well as the volume per atom. This leads to an entropy increase due to increasing amplitude of the atomic motion. If we think first of the atomic motion as harmonic, we recognize that this lowers the force constant and hence to a decrease of the Debye temperature of this system. Let us assume for simplicity that the melting point exceeds the Debye temperature $\theta_{\rm D}$, so that we use the limiting expression for the entropy of a bulk system of n bound atoms which, according to Table 2.5 is [4]

$$S_{\rm osc} = 3n \ln \frac{T}{\theta_{\rm D}} + 4n \, . \tag{8.29}$$

In this limit, taking $\Delta S_{\text{term}} = S_{\text{ocs}}$, we find an *increase* of about 40% in the Debye temperature as a result of the phase transition if we can assume that the Dulong-Petit law is valid here.

Thus, a simple scheme allows us to describe the character of the melting process for a bulk atomic system held by an interaction of such short range that only nearest-neighbor interaction needs to be considered. This scheme considers the melting as the configuration excitation of the atomic system, modelling excitations as formation of voids inside the system. Because the number of voids can be considered indefinite, we may vary the number of voids continuously, and in this way, connect parameters of the solid and liquid states of such a system. Condensed rare gases are real systems approaching these conditions and their thermodynamic parameters of the solid and liquid states at the triple point give the parameters for the microscopic description of the melting process and configuration excitation of the model system, and hence of a general level of understanding.

8.6 Freezing Points for Bulk Inert Gases

Condensed inert gases have two aggregate states, liquid and crystalline, and this holds true also for other bulk ensembles of bound atoms with dominant short-range pairwise interactions. In some temperature range one of these states is stable and other is metastable. Figure 8.1 demonstrates this fact for a bulk atomic ensemble, so that the free energy as a function of the volume per atom or the number of voids per atom has two maxima. Then relaxation of a configurationally excited state will transform this atomic ensemble into a stable or metastable state, depending on the initial specific number of voids for this state. The phase transition of course reduces the free energy of the particle ensemble. We will consider this process at temperatures below the melting point from the standpoint of configurational excitation.

Indeed, taking a void as an elementary configurational excitation, one can use minima of the free energy or maxima of the partition function as functions of the number of voids inside the system (Fig. 6.3), to define the aggregate states.

We ignore the pressure term in the free energy expression, as for condensed inert gases. At the melting point, the minimum values of the free energy (or maxima of the partition function) for the solid and liquid states coincide. But as the temperature decreases, the liquid minimum of the free energy curve rises with respect to the solid minimum and the curve itself becomes flatter. As a result, there is a critical temperature at which the liquid minimum disappears. This temperature is called the freezing limit and corresponds to the lowest point of the caloric curve for which the liquid state has any stability, as shown in Fig. 8.2 for argon [266]. Correspondingly, the freezing point is a critical point for the liquid state if we construct the caloric curve, as it is

given in Fig. 8.3 for argon [266]. Then the liquid state does not exist, even as a metastable state, at temperatures below the freezing limit.

Below the freezing limit, apart from the defects that occur in any solid at equilibrium at a temperature above 0 K, any configurationally excited state of an ensemble of bound atoms is unstable. This means that relaxation of such a state leads to a state with free energy near that of the global minimum. The number of voids is small in such a state and diffusion is slow, as in normal solids. The transition of a bulk system to this state occurs by departure of voids from the system, via their transport and evaporation. From the standpoint of the landscape of the potential energy surface, this process is a series of successive transitions between neighboring local minima of the surface. But any transition between local minima is an activation process, and the rate of such a transition decreases with decreasing temperature according to the Arrhenius law in which the rate of barrier crossing varies exponentially with the ratio of the energy to overcome the barrier to the temperature. Hence, configurationally excited states of such a cold, solid body are characterized by a long lifetime that grows with decreasing temperature. According to the usual definition [153, 275–277], a glassy state of a system of bound atoms is a thermodynamically unstable state that has an arbitrarily long lifetime if the kinetic temperature tends to zero. The rate of decay of this state is expressed by the Arrhenius exponential decay formula due to thermal barrier or barriers associated with this transition. (Strictly, for complex systems with multiple pathways between minima, the Arrhenius expression must be generalized [278].) Using the analogy with this definition, we will consider configurationally excited states of an ensemble of bound atoms at low temperatures as glassy-like or glassy states.

8.7 General Liquid Properties

In considering the void concept of macroscopic liquids and liquid clusters, we have considered only one aspect of liquid properties and liquid structures which result from configurational excitation of the solid state. The excitation to a liquid also changes the atomic correlation and causes other properties we associate with liquids [93–95, 100, 116, 279, 85, 280]. One of these properties is conservation of short-range order and loss of long-range order in the atomic distributions.

Considering liquid clusters from this standpoint, we recall that the cluster shell structure is approximately conserved in the liquid state, but atoms become more mobile and transfer partially onto the cluster surface. This is demonstrated in Fig. 8.4 where the atomic density is given for the Lennard-Jones cluster of 147 atoms [262, 263]. In its lowest-energy structure, this cluster has 3 completed icosahedral shells. As a result of configurational excitation to the degree of formation of the liquid state, several atoms transfer on the cluster surface. Figure 8.4 shows that the shell distribution of atoms is con-

served in this case, but these shells are spread. Hence, some short-range order is conserved in the liquid state here.

Note that in the analysis of clusters we deal mostly with surface melting whereas melting of a bulk atom ensemble was considered as formation of internal voids. At temperatures higher than that of the melting of the outer surface, the entire cluster becomes a liquid, with interior particles mixing almost as readily with the outer layers as the outer particles mix among themselves. A large cluster can have several aggregate states which are distinguished by the extent of inner-shell melting and mixing [252, 253, 262, 263]. For a large cluster or a bulk system, one can distinguish the surface and volume liquid states since the energies of their excitation are different. Moreover, melting of a macroscopic system starts from surface melting, according to experiment [256], and surface and volume melting may be separated experimentally [254, 255]. But surface melting of bulk systems includes only surface atoms, i. e. a small fraction of the atoms, and therefore it is not so important as the volume melting.

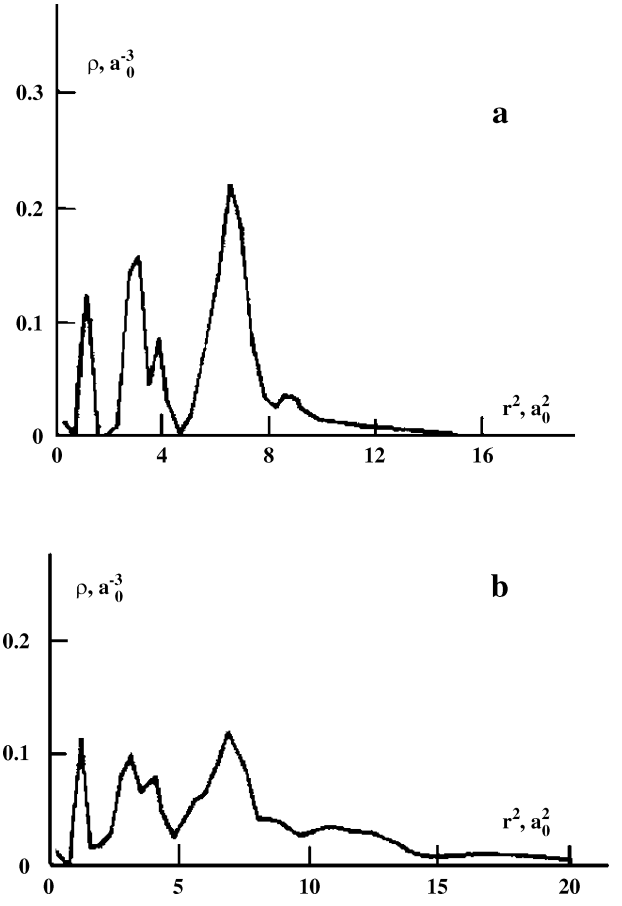

Fig. 8.4. The atomic density of the Lennard-Jones cluster of 147 atoms as a function of the squared distance from the cluster center [262, 263]: **a** solid state, **b** liquid state

9

Melting of Clusters and Bulk Atomic Ensembles

9.1 Entanglement of Thermal and Configurational Excitations in Clusters

We previously considered a sufficiently configurationally excited state of a 13-atom cluster as a liquid state. In principle, the liquid state is one in which atoms move inside the cluster relatively freely, while in the solid (or crystalline) state, atoms occupy certain positions in the cluster and seldom change those positions. Therefore configurationally excited and liquid states do not obviously correspond to equivalent concepts; one is dynamic, and the other, structural. Hence it is necessary to prove that they are equivalent, at least for certain situations. Although we will do this for clusters of 13 and 55 atoms, this is not a universal property.

For small systems, one of the striking properties for its difference from bulk matter is the way many clusters show dynamical coexistence of solid and liquid forms over a range of temperatures (or energies) and pressures. It is clearly observable, for example, in clusters of 7, 9, 13 and 19 atoms, among many others. However this is not a universal phenomenon. Some clusters, e. g. of 8, 14 or 17 atoms, pass from cold solid to warm liquid with no sharply discernable solid or liquid forms in the broad transition range between the limits where the nature of the phases is unambiguous [281].

Considerable attention has been paid to clusters that do exhibit well-defined coexisting phases in the temperature or energy range in which one can find a bimodal distribution of temperatures (for a constant-energy system) or of energies (for an isothermal system). By contrast, those that do not exhibit coexisting phases in dynamic equilibrium must be able to pass between liquid-like and solid-like forms with such ease, when both forms might be present, that they never reside long enough in either form to develop the characteristics we associate with the corresponding bulk phases. It is also possible that some clusters may pass directly from a solid form to vapor, with no stable liquid form between, analogous to the well-known sublimation of carbon dioxide ("dry ice") at ordinary atmospheric pressures. No examples of

this behavior have yet been demonstrated, but, being physically allowed, such examples will probably be found in due time.

A general condition for existence of a stable liquid aggregate state is that the statistical weight g or entropy $S = \ln g$ of this state, relative to that of the solid state, is large enough. According to the Boltzmann formula (6.32) the ratio of populations $w_{\rm liq}$ and $w_{\rm sol}$ for these states is

$$\frac{w_{\rm liq}}{w_{\rm sol}} = g \exp(-\Delta E/T) = \exp(-\Delta G/T) \ ,$$

where ΔE is the excitation energy of the liquid state, ΔG is the difference in (Gibbs) free energies of the two phases (for constant-pressure systems), $g = \exp(\Delta S)$, ΔS is the entropy difference of the two phases, and T is the temperature. Therefore the condition $w_{\rm liq} \gg w_{\rm sol}$ at high temperatures requires a sufficient entropic contribution $g \gg 1$ to the equilibrium ratio for the thermodynamical stability of the liquid state. We consider clusters with completed shells, for which this condition is fulfilled. (It is of course also fulfilled for some but not all other sizes of clusters.) The entanglement between configurational and vibrational degrees of freedom for clusters, arising from large-amplitude motions in void-rich systems, increases the relative statistical weight or entropy of the liquid state and therefore enhances the entropic term for the liquid.

Table 9.1 gives the parameters of configurational excitation of the 13-atom and 55-atom Lennard-Jones clusters and also these parameters for bulk inert gases. The quantity $\Delta S_{\rm o}$ is the entropy variation for this configurational excitation at zero temperature, and $\Delta S_{\rm m}$ is the same quantity at the melting point. (We define the melting point as the temperature at which the probability for a cluster in the solid and liquid states are equal). The value of the parameter $\Delta S_{\rm o}$ follows from the void concept, so that the relative statistical weight $g_{\rm o} = \exp \Delta S_{\rm o}$ is the ratio of the number of atomic configurations for configurationally excited and ground states at zero temperature, and the value $\Delta S_{\rm m}$ is the corresponding quantity at the melting point; the values follow from computer simulations or measured values for bulk inert gases.

The important conclusion from the data of Table 9.1 is the temperature dependence of the entropy change for configurational excitation. This means

Table 9.1. The entropy changes from melting of atomic clusters and macroscopic inert gases at zero temperature and the melting point. Results relate to low pressures; n is the number of atoms for each atomic ensemble [237]

	LJ_{13}	LJ_{55}	bulk in gas
$T_{\rm m}$	0.30 ± 0.01	0.31 ± 0.01	0.58
$\Delta S_{\rm o}/n$	0.4	0.56 ± 0.04	0.73
$\Delta S_{\rm m}/n$	0.69 ± 0.04	0.82 ± 0.04	1.68 ± 0.03
$\Delta S_{\rm o}/\Delta S_{\rm m}$, %	58 ± 4	70 ± 10	43 ± 1

that although the vibrational and configurational degrees of freedom are separated, thermal motion of atoms influences thermodynamic parameters of the configurationally excited state, i. e. thermal and configuration excitations are entangled. One can explain this effect insofar as atomic thermal motion of the compact ground configurational state differs significantly from that of an excited configuration state with a more rarefied distribution of atoms. This difference is a consequence of both the different anharmonicities for these configurational states and the different ranges of amplitudes of motion for the two forms. These both are reflected through different parameter values of these states. Hence if we assume the energy of this configurational excitation is independent of the temperature, just the increasing entropy of an excited state with temperature assures that its population increases also. Correspondingly, the phase transition between these states, melting, proceeds at lower temperatures than it would without this effect.

Together with the entropy change of the phase transition, Table 9.1 also provides energy parameters of this transition. Here n is a total number atoms in a cluster or a bulk system, D is the depth of the potential well for the pair interaction potential of atoms, T_{m} is the melting point and ΔE is the phase transition energy for an isolated atomic ensemble at the melting point, so that $\Delta E/n$ is the specific fusion energy, and T_{sol} and T_{liq} are the effective (kinetic-energy-based) temperatures of the solid and liquid states for an isolated cluster at the melting point. In determining the difference $T_{\mathrm{sol}} - T_{\mathrm{liq}}$, we assume the heat capacity for each aggregate state to be given by the Dulong-Petit law.

9.2 Parameters of Melting

Melting as a phase transition is a collective phenomenon with participation of many atoms, and hence the solid and liquid states differ by the nature of large-scale cooperative behavior of atoms in these aggregate states. In practice, it is convenient to use the Lindemann criterion [282] as a diagnostic for this phase transition. According to this rule, the phase transition occurs at the temperature at which the relative amplitude of atomic oscillations reaches a characteristic value; specifically, melting is said to occur when the ratio of the root-mean-square amplitude of atomic oscillations to the equilibrium distance between nearest neighbors is 0.10–0.15. Typically, in the range of this temperature, the ratio of distances increases sharply.

Of course, the Lindemann criterion [282] is the simplest criterion to characterize the solid or liquid aggregate state. With the development of numerical methods to simulate cluster dynamics, more precise criteria for the phase transition were introduced, which are based on pair correlations of positions of the cluster atoms. In particular, this correlation function can use the Etters–Kaelberer parameter [283–285] or the Berry parameter [247, 300]. These parameters are proportional to the fluctuations of the interatomic distances. These fluctuations give a somewhat more precise insight into how the

the solid and liquid states differ, and how the transition between them occurs over the range of their coexistence.

Here are explicit expressions for these correlation parameters. The first is the root mean square of the bond length fluctuation that is introduced as

$$\delta = \frac{2}{n(n-1)} \sum_{i<j} \left[\frac{\langle r_{ij}^2 \rangle - \langle r_{ij} \rangle^2}{\langle r_{ij}^2 \rangle} \right]^2 , \tag{9.1}$$

where r_{ij} is a distance between atoms i and j and n is the number of atoms. For the solid state, in which atoms are fixed in lattice sites, this parameter is typically smaller than 0.1, less than that for the liquid state with its mobile atoms. Figure 9.1 demonstrates this for the 13-atom Lennard-Jones cluster with the argon pair interaction parameters. One can see that the parameter δ has a jump at the melting point of this cluster. This jump may be used as the definition of the melting point, although the "jump" clearly takes place over a finite temperature interval.

Another parameter based on the correlation in positions of atoms characterizes the variation of positions of individual atoms in time as the mean square displacement of atoms from equilibrium, the traditional Lindemann parameter,

$$\langle r^2(t) = \frac{1}{nk} \sum_{i=1}^{n} \sum_{p=1}^{k} [\mathbf{r}_i(t_\mathrm{p} + t) - \mathbf{r}_i(t_\mathrm{p})] . \tag{9.2}$$

Here i is an atom number, $r_i(t)$ is its coordinate at time t, n is the total number of atoms, t_p is an initial time, k is the number of initial times over which an average is made. Figure 9.2 gives an example of the time dependence of this parameter. In a certain range of time atoms of the liquid state are mobile and hence the mean square of atomic displacement satisfies the diffusion law $r^2(t) \sim t$ until this displacement is small compared to the size of the atomic

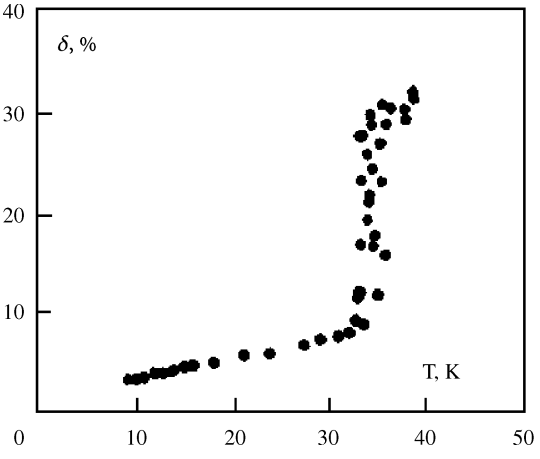

Fig. 9.1. The squared length of fluctuations of the bond length defined by formula (9.1) averaged over a long period for the 13-atom Lennard-Jones argon cluster [50]

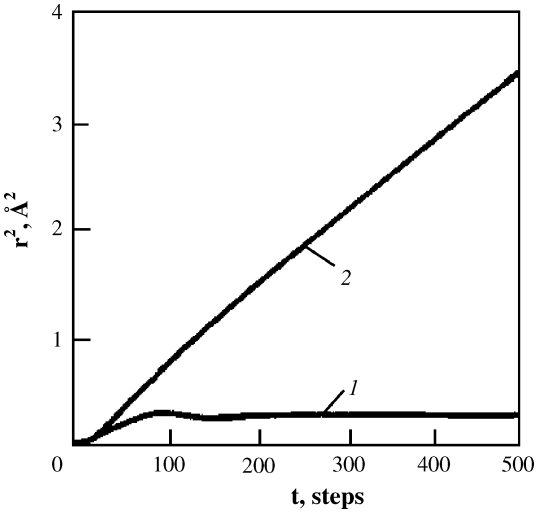

Fig. 9.2. The mean square of atomic displacement for the isolated 13-atom Lennard-Jones cluster. The excitation energy is $7.59D$ (*1*) for the solid state and $16.23D$ (*2*) for the liquid state [50]

ensemble itself. On this time scale, atoms in the solid state are fixed, and hence the mean square atomic displacement characterizes an amplitude typical of oscillation of individual atoms in the crystal.

Thus, one can associate the nature of melting with the different characters of atomic behavior in the solid and liquid states. An elegant way to use this fact with clusters is given in Fig. 9.3. Solid clusters are characterized by the magic numbers of atoms with heightened stability. Therefore if clusters are formed in a gas and the conditions of cluster formation permit existence of clusters of different sizes in the gas, the size distribution function of clusters will have extrema at magic numbers. Then the size distribution of solid clusters in the gas will have an aperiodic, non-monotonic structure. For the liquid state, this structure of the size distribution function disappears. As a demonstration of this, Fig. 9.3 gives mass spectra of ionized sodium clusters produced by near-threshold photoionization of clusters in a buffer gas at a fixed temperature [129, 130].

As clusters of a certain size melt, the maxima in the mass spectra near or at corresponding magic numbers disappear. This allows one to determine the melting point or range of coexistence of solid and liquid for clusters of a given size as given in Fig. 9.4. The cluster melting point is compared with the melting point T_{m} of bulk sodium. Evidently, clusters generally melt at a temperature lower than that of a bulk system because of the lower average binding energy of atoms in clusters. Note that each maximum in the mass spectra of Fig. 9.3 corresponds to an appropriate atomic shell. Variation of the number of atomic shells from 6 up 14, i. e. the number of cluster atoms from 923 up to 10,179, leads to the variation of the cluster melting point from $288 \pm 4\,\mathrm{K}$ up to $303 \pm 3\,\mathrm{K}$.

In analyzing the melting points of clusters of different sizes, we note also that clusters with completed shells have a heightened stability, characterized

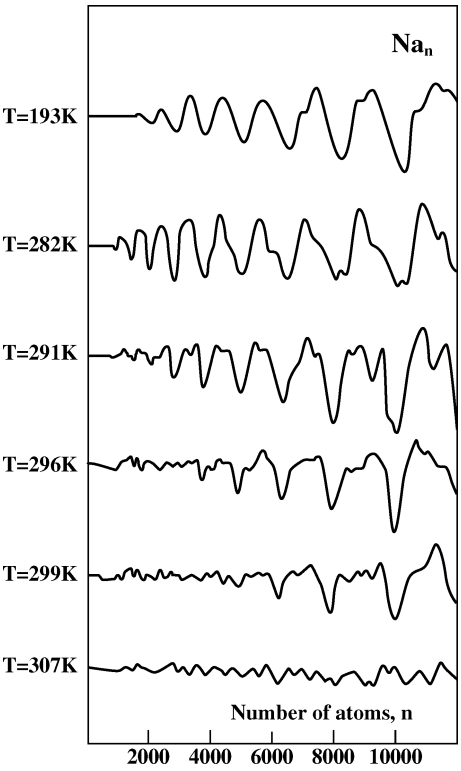

Fig. 9.3. Mass spectrum of photoionization of sodium clusters consisting of 10^3–10^4 atoms [129, 130]

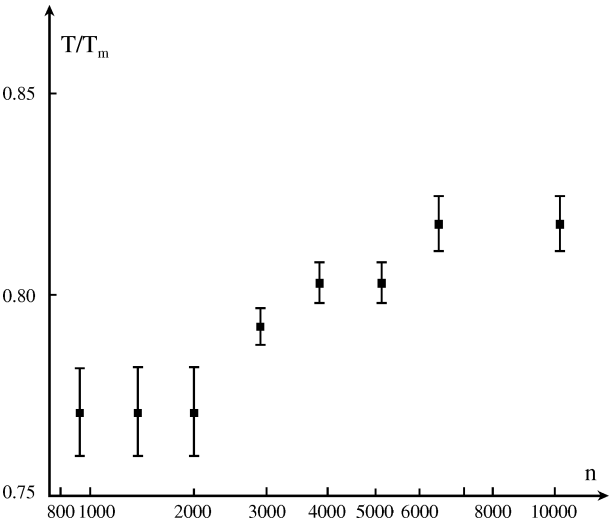

Fig. 9.4. The melting points for sodium clusters consisting of 10^3–10^4 atoms [129, 130]

by their higher melting points. Figure 9.5 gives the size dependence of the melting points of Lennard-Jones clusters [287]; the maxima correspond to magic numbers of cluster atoms. In addition to Fig. 9.4, Fig. 9.6 shows the dependence of the melting points of sodium clusters on their size in the region of small sizes, comparable to those of Fig. 9.4.

Because the solid cluster state is usually characterized by a specific lowest-energy structure and the liquid state is structureless, a cluster's melting corresponds to its becoming amorphous. As an example, Fig. 9.7 gives examples of melting of copper clusters with completed shells [125] when sufficient heating leads to the loss of the initial structures.

Small particles, whose surfaces have significant positive curvature, have higher vapor pressures and lower melting points than their bulk counterparts. William Thomson, Lord Kelvin, demonstrated this in 1871 [288]. Most clusters clearly obey this behavior; clusters of tens or hundreds of atoms melt at temperatures well below the bulk melting points. Many simulations and a growing number of experiments have demonstrated this. However there are at least two known and very dramatic exceptions. Clusters of tens of tin atoms and of gallium atoms exhibit, in unambiguous experiments of Jarrold and coworkers, melting points significantly *above* the bulk melting points of

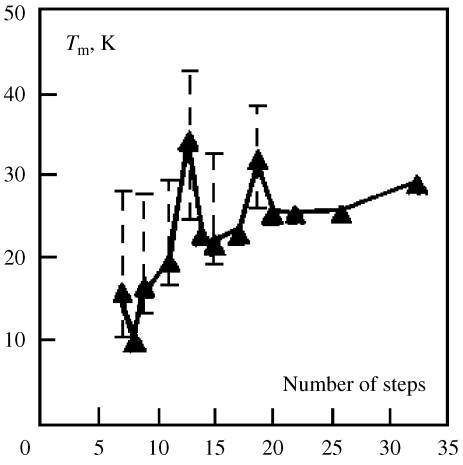

Fig. 9.5. The melting points for Lennard-Jones clusters of different sizes [287]. *Triangles* are the melting points obtained from the squared length of fluctuations of the bond length (formula (9.1)) averaged over a long period. *Dotted lines* mark the limits of coexistence of the solid and liquid phases

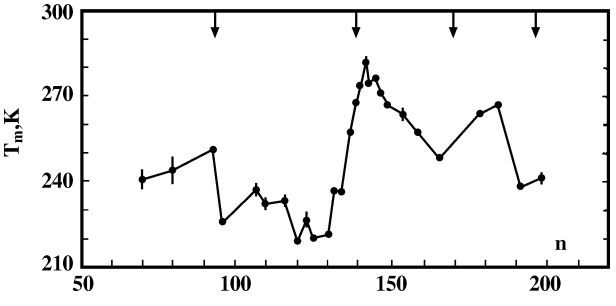

Fig. 9.6. Melting points for sodium clusters [244, 245]. Magic numbers of sodium clusters for the jellium cluster model are marked by *arrows*

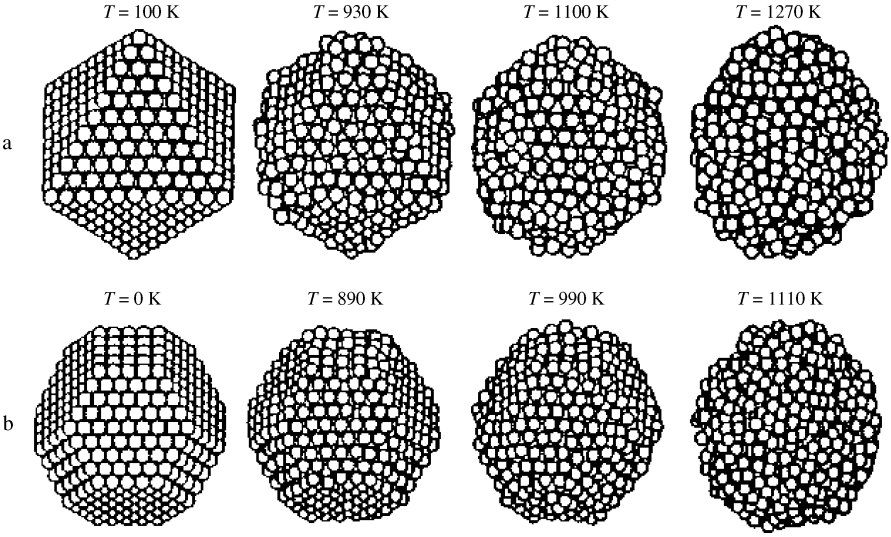

Fig. 9.7. The character of change of the copper cluster structure upon heating [125]. The initial structure is **a** octahedron consisting of 891 atoms, **b** truncated octahedron consisting of 1289 atoms

these elements [289, 290]. The interpretation of this surprising phenomenon is that the bonding and structures of these remarkable clusters is simply different from that of the bulk; the clusters are much more covalent and less metallic than the macroscopic aggregates [291–294].

9.3 Contradiction Between the Melting Criterion and Its Nature

We defined the difference between solid and liquid aggregate states on the basis of their different spatial distributions of atoms. That change in capacity of the atoms to move is responsible for establishing the fluidity that is perhaps the most universal character of any liquid. In contrast, we have described this phase transition in terms of thermal excitations related to thermal motion of atoms. This leads to a paradox or apparent contradiction between the nature of the "cause" of the phase transition and the parameters typically used to characterize this phenomenon. Still, we can recognize that in the melting process, the structural changes that produce vacancies and then voids begin before the motions associated with fluidity set in. Briefly, the essence of the melting, i. e. the onset of fluidity in a dense medium, consists in configurational excitation and introduction of voids in the system, the parameters for its description, such as the Lindemann criterion, are based on the atomic thermal motion. The former is the cause; the latter is the effect. In that sense,

the structural, configurational changes are the cause and the large-amplitude motions and fluidity are the effects.

The void concept for configurational excitation, interpreted given quantification with the help of computer simulations and thermodynamic parameters of condensed inert gases, shows that the origin of this apparent paradox lies with the changes of thermal vibrations of atoms in the melting process and their consequent striking contribution to the entropy jump at the melting transition. Indeed, the lower density of atoms in the liquid state allows the thermal motion that makes the crucial contribution to the entropy that enables the phase transition. The entropy jumps ΔS_{o} and ΔS_{m} at zero temperature and at the melting point are quite different, as follows from the data of Table 9.1. This allows us to characterize the phase transition also by the value of the difference $\Delta S_{\mathrm{m}} - \Delta S_{\mathrm{o}}$, determined by the atomic thermal motion. Thus, although the ideas inherent in the Lindemann criterion and other melting criteria are not rooted in the cause of the transition, these criteria reflect correctly the consequences of this phenomenon.

9.4 Definition of the Cluster Aggregate State

In this section, we emphasize the differences between the descriptions of small systems, notably clusters, and their bulk counterparts. Yet we also show how we can bridge between the small and the large, and gain new insights into the properties of large systems by seeing how they emerge as systems are made larger and larger.

One can see the difference between the definition of the cluster liquid aggregate state we use here and that in classical thermodynamics, in which the phase or aggregate state of bulk corresponds to a uniform, long-time average distribution of atoms in some bounded spatial region. This means that the phase or aggregate state in classical thermodynamics includes many elementary configurational excitations while in the case of a 13-atom cluster this state can result from one elementary configuration excitation. There is a middle ground, too, for dealing with small systems such as clusters. We may consider the aggregate state of the excited cluster as the collection of states with a given number of configurational excitations, or as the set of all states of specific configurational excitations that lie within a specified energy band, or even the set of specific configurational excitations that are accessible within a chosen time interval, typically associated with the method of measurement one uses. One should be pragmatic and use whichever of these best enables us to interpret and understand the physical process we are studying. Of course, it is often necessary to apply additional criteria for two-body correlations that are different for the solid and liquid states (for example [50, 246, 247]). Moreover, in order to study metals, semiconductors and strongly bound insulating materials, we must be prepared to go beyond two-body, nearest-neighbor interactions to get even the most basic understanding.

This analysis makes clear that the cluster aggregate states have special peculiarities differentiating them from bulk systems. One of the most important of these is dynamical coexistence of phases [40, 50, 246–248]. This coexistence is partly a consequence of the time scales for phenomena at the nanoscale. In contrast to the time scales for bulk matter, those of clusters and nanoscale materials allow us to make observations that can be slow enough to obtain time averages over different phases or, if the observation times are somewhat shorter, say tens of nanoseconds or less, to distinguish clusters in specific, recognizable phases. Many, but not all, kinds of clusters, in some range of parameters near the melting point, exhibit a dynamic equilibrium like that of chemical isomers; each cluster is found part of the time in the solid state, and the rest of the time, in the liquid state – in cases in which there are two distinguishable aggregate states. This situation means that for clusters, the distinction between "phase" and "component" is lost, and the Gibbs phase rule loses its applicability.

Thus, in dealing with clusters, we must be cautious in how we use classical thermodynamics, and in particular, we must be especially aware of hidden assumptions that are entirely valid at the bulk scale but not at the nanoscale. To understand the phase behavior of clusters and relate that to the phase transitions of bulk matter we must change slightly the definition of aggregate states from the classical thermodynamic definition of states of bulk systems. Within the framework of this description, we consider the cluster aggregate state as a group of configurationally excited cluster states with comparable excitation energies.

We now formulate the steps we need to transfer the description of configurational excitation of clusters to the phase transitions in classical thermodynamics. In considering clusters with pairwise atomic interactions, we start from the potential energy surface (PES) in a many-dimensional space of atomic coordinates, in which cluster evolution is described as motion on this PES. A special characteristic of such a PES is the immensely large number of local minima. In the course of its evolution, a cluster dwells for some time interval near each PES minimum it visits, so that it has many oscillations in the phase space near each minimum until it passes on to a neighboring minimum. In this manner we have separated thermal motion of atomic oscillations from configurational excitation identified with each PES minimum. In the next step of the analysis, in order to simplify the problem, we introduced an elementary configurational excitation, a void, and here we assume all single configurational excitations to be equivalent. One can see that this assumption is valid more or less, if the voids are few enough, the cluster is large enough and we consider a void as a result of relaxation of an initially formed vacancy.

Then, basing our next step on the shell cluster model, we introduce groups of individual vacancies or groups of voids. Again, all states with the same number of voids fall into a class whose members we consider indistinguishable. Of course, interaction between voids (or interaction between atoms for a configurationally excited ensemble) violates this picture, and hence the isolated-void

description of configurational excitation is an oversimplified model. In transition to bulk systems, if we restrict our discussion to internal voids, these voids all correspond to the same kind of configuration excitation, i. e. we deal with identical voids. In the next step of the transition to classical bulk thermodynamics, we form the liquid aggregate state of a bulk ensemble of bound atoms by excitation of a sufficient number of voids in the solid aggregate state. This state includes enough elementary configurational excitations, voids, to permit diffusive motion of the atoms, and therefore it is sufficient for the classical definition of the liquid phase that we can describe it as a uniform distribution of atoms. In addition, we take as the liquid state the thermodynamically most favorable state that contains the optimal number of voids. This means the state with the lowest free energy with respect to the number of voids or the maximum of the partition function, as follows from Fig. 8.1. In this way, moving from the mechanical description of a bulk ensemble of bound atoms, one can transfer to its thermodynamic description at the nanoscale by incorporating some additional assumptions and avoiding some that may be tacit in the classical framework.

Thus, to go to classical thermodynamics, one can see that additional assumptions are required for this transition. Simultaneously it leads to simplifications and gives a universal description of the phase transition within the framework of classical thermodynamics on the basis of some thermodynamic parameters. Returning back to a cluster, one can see that thermodynamic parameters can be used even when classical macroscopic thermodynamics is not applicable for clusters in principle. Indeed, using the entropy S, the internal cluster energy E, the cluster free energy F and other thermodynamic parameters is useful for configurationally excited clusters although it requires additional analysis of the validity of some thermodynamic relations. Following this path to classical thermodynamics, we use the two-state approach for cluster aggregate states; it is useful also for describing clusters.

9.5 Voids as Gateways to Fluidity

Up to this point, we have avoided the question of how fluidity arises from the presence of some sufficient concentration of voids. While we cannot give a precise, mechanistic elucidation of this question, we can lay out the essential physical properties that underlie that link. The most essential point is that the density of voids must be high enough that the barriers between local minima are low, and, more specifically, must be low between many neighboring minima so that the atoms can move to new positions, new spatial configurations, on time scales of tens of typical vibrational periods. Only in this way can changes of boundary conditions, such as changes of the shape of a containing vessel or release of a droplet, make possible the changes of shape of the fluid on a time scale we associate with liquids, however inviscid or viscous.

Let us follow this connection. When the number of voids v is very small compared with the number of atoms n, so that neighboring voids do not border, the elementary configurational excitations are equally well described as vacancies or as voids, and the volume per atom is very nearly equal to the volume per void. Correspondingly, all permutations of atoms and voids, when they form a crystal lattice, lead to stable configurations of atoms with the same energy of configurational excitation. Then the energy of configurational excitation, as well as variation of the total volume of the system relative to that of the ground state, is proportional to the number of vacancies v. The same relates to the entropy variation associated with configurational excitation of the atomic system.

Relaxation of this atomic system when the number of voids is not small leads to some shrinkage that moves the atomic system to a stable configuration. There is likely to be some short-range order in the atomic distribution because each final state yields a stable configuration. However in these circumstances, we can think of the voids, rather than the atoms, as being the species with high mobility. Passage from one configuration to another, and to another and another, in the course of fluid motion, is thus construed as the motion of many voids. Near the onset of melting, we may consider the voids to be independent; this assumption was used previously, in the determination of void parameters for a liquid aggregate state of inert gases. However a more refined treatment will require including interactions among voids, and analysis of how the effective barriers separating different configurations drop in energy with increasing void concentration and temperature. It will be necessary to infer the amount of configurational change necessary for a system to be able to flow enough to conform to the shape of its container, for example, in order to extend this analysis to describe all the properties we associate with fluids. A useful approach to this may well be to focus on the critical state, at which the distinction between liquid and vapor disappears. Nevertheless, in description of a fluid state with a certain number of voids we compare it with the solid state starting from an excited solid state with a certain number of vacancies. This approach leads to unambiguity of our consideration.

Note one more aspect of our consideration. The basic property of an atomic system with a pairwise interaction is separation of its ground electron state from the first electronically excited state by a wide energy gap, and therefore we deal with the ground electronic state only. The total electronic energy and the electron–nuclear and nuclear–nuclear potential energy contributions to the total energy of the ground state defined the effective potential energy surface in the space of atomic coordinates. This is, of course, the Born–Oppenheimer approximation. Consequently evolution of this macroscopic system of atoms may be represented as a motion along the potential energy surface in a many-dimensional space of atomic coordinates. A characteristic property of virtually any potential energy surface for a many-particle system is its large number of local minima in this space [38]. The system of atoms spends almost all its time in regions near the local minima of the potential energy surface; only

a small part of the time is consumed in transitions between neighboring local minima. Local minima of the potential energy surface characterize stable atomic configurations; we associate these stable configurations with configurational excitations from the ground configurational state. Each configuration of atoms has a specific number of voids.

9.6 Liquid-Gas Interface

In considering the behavior of a system of interacting classical particles (atoms), we discuss the internal cluster structure in which each atom is surrounded by and bonded to several other atoms. We now turn our attention to the surface of a large liquid cluster in equilibrium with its surrounding gas. Thus the equilibrium is achieved by equal rates of the processes of atomic attachment to the cluster surface and evaporation of bound atoms from that surface. Hence we find a cluster surface that, within the framework of classical thermodynamics [295], constitutes a fine layer of atoms which partake in the above processes. A thermodynamic analysis of the liquid-gas interface gives the general properties of this interface (for example [296]). However, in order to investigate the microscopic structure of the interfacial layer, we must study the behavior of surface atoms beyond thermodynamics.

To carry this out, we must distinguish atoms near the interface that belong to the liquid from those in the gas. According to Stillinger's definition [297], an atom belongs to the liquid cluster or droplet if its distance from any cluster atom is less than the distance between nearest neighbors r_b of the cluster. But this definition makes the number of cluster atoms dependent on this distance as $n(r_\mathrm{b})$. According to molecular dynamic simulations [298], this function has a minimum, and therefore one can define unambiguously the distance between nearest neighbors and the number of cluster atoms according to the definition $\mathrm{d}n/\mathrm{d}r_\mathrm{b} = 0$.

This definition allows one separate atoms near the liquid-gas interface which are pertinent for the cluster surface. This in turn allows one to analyze the behavior of the liquid-gas interface by methods of molecular dynamics [298–302]. In particular, computer simulation for Lennard-Jones clusters consisting of 10^3–10^5 atoms [300, 302] lead to the following surface structure. All the cluster atoms may be separated into three types which are characterized by different numbers of bonds. The internal atoms form a dense core, the surface atoms have several bonds with surrounding atoms, and atoms of the third group have only one or two bonds and form virtual chains. If we restrict ourselves first to the first two groups of atoms, the distribution over the number of bonds has a bimodal character, i. e. internal and surface atoms may be separated unambiguously. Moreover, surface atoms form a strongly curved monolayer on the core.

Within this model of the liquid-gas interface for clusters, chain-like structures of weakly bonded atoms are responsible for fluctuations at the inter-

face. These transient chains are formed and destroyed rapidly; lifetimes of the chains, in which atoms pass between surface and gas are very brief compared to those of atoms lying in the surface layer. The atoms in these transient chains are responsible for cluster evaporation. Hence the transitions of atoms between surface chains is important for the vapor-liquid equilibrium.

In addition, note that a strongly curved cluster surface changes its shape as surface atoms attach, leave or move about. If the cluster surface has elastic properties, thermal fluctuations of that surface result in generation of capillary waves [303]. But the analysis of the fluctuation spectra for the Lennard-Jones cluster [302] shows that surface fluctuations are realized over distances small compared to the lengths of capillarywaves, i. e. the elasticity of the cluster surface is not the result of motion of individual atoms. Thus, the liquid-gas interface is a specific physical object, collective in nature, whose properties differ from those we would infer just from atomic motions.

Part III

Dynamics of Configurational Excitations in Ensembles of Classical Particles

10

Coexistence of Cluster Phases

10.1 Hierarchy of Equilibrium Times in Clusters

In contrast to bulk systems of interacting atoms, solid and liquid phases of clusters may coexist throughout the range of local stability for both phases. In fact, as mentioned previously, more than two phases of clusters may coexist in thermodynamic equilibrium, in observable quantities, over a range of conditions. This creates an apparent paradox when this phenomenon is compared with the way bulk phases behave, following the Gibbs Phase Rule linking the number of degrees of freedom f, the number of components c, and the number of phases p that are in equilibrium together: $f = c - p + 2$, perhaps the simplest equation in all of thermodynamics and one of the most easily understood – up to a point. Each component adds a degree of freedom insofar as the relative amount of that component can be varied. Each phase required to be present must satisfy its own equation of state, which adds a constraint for each phase. The only subtlety that we can only derive from observation is the number 2! The apparent paradox is in reality simply a reflection of the difference between a system of a small number of particles and a system of very many particles. We shall see this in detail in this chapter.

Let us consider the character of equilibrium in clusters under conditions that allow two or more phases to coexist. This equilibrium, in contrast to phase equilibrium in bulk systems, is dynamic, as we have already seen. Individual clusters pass back and forth between (or among) the coexisting phases, roughly randomly. Because we believe these systems are ergodic, the relative amounts of each phase present in a large ensemble of clusters is the same as the relative amounts of time each cluster spends in its different phases.

Now we focus on clusters that exhibit well-characterized, distinct phases when they are in conditions allowing coexisting phases; we will not examine the much-less-studied and rather rare examples in which passage between different phase-like forms is almost as fast as vibrational equilibration. Starting

from this viewpoint, we introduce a typical time $\tau_{\rm ag}$ that a cluster resides in one phase, either the solid or liquid state if we consider only two phases. We hence assume that this criterion is valid:

$$\tau_{\rm eq} \ll \tau_{\rm ag} \ , \tag{10.1}$$

where $\tau_{\rm eq}$ is a typical time required for thermal equilibration of the vibrations of a given phase. This criterion allows us to introduce the cluster temperature because during cluster's dwell time in one phase, thermal equilibrium is established. The criterion (10.1) determines the character of dynamic coexistence of cluster phases [40, 247, 248].

There are two possibilities with respect to cluster interaction with an environment, depending on the ratio of $\tau_{\rm ag}$ and a typical time of exchange of energy $\tau_{\rm th}$ between the cluster and its thermostat (see Fig. 7.8). The cluster, were it isolated, would be a microcanonical ensemble of bound atoms if (Fig. 7.8a)

$$\tau_{\rm ag} \ll \tau_{\rm th} \ , \tag{10.2}$$

i. e. the cluster would be an isolated particle. Another case corresponds to the converse criterion

$$\tau_{\rm ag} \gg \tau_{\rm th} \ , \tag{10.3}$$

when the cluster exchanges energy very efficiently and rapidly with a thermostat; in this case, the cluster is a canonical ensemble of bound atoms (see Fig. 7.7b). One can take as a thermostat a gas of atoms colliding with the cluster and metallic walls that are maintained at a fixed temperature. Then we have

$$\tau_{\rm th} \sim (N v \sigma)^{-1} \ , \tag{10.4}$$

where N is the number density of "heat bath" atoms surrounding the cluster, v is a typical atomic velocity, σ is the cross section for atom-cluster collisions, which is comparable with the cluster's geometric cross section for large clusters.

We now examine the behavior of clusters under conditions that allow coexistence of two or more phases. First, we begin by recognizing that a cluster, whether at constant energy or constant temperature, explores the accessible region of its phase space and configuration space. We do make the assumption that the system is ergodic, i. e. that it does fully explore that accessible region. More strictly, we assume that the trajectory takes the system arbitrarily near every accessible point in that space, i. e. that the system is quasi-ergodic. However that full exploration takes time, and one of the most interesting and important characteristics of a system of this kind is the time scale for the system to reside in the region of one of its *free energy* minima; that is, how long does the system remain in a single, well-defined phase [304]. We cannot consider the system to exhibit true thermodynamic equilibrium when we examine it just during one of those dwell periods in a single phase-like region, of course. However we can describe it as

a thermodynamic system in equilibrium if we use the appropriate, dwell-time-weighted averaging over the thermodynamic parameters for each aggregate state. Second, we note that the range of phase coexistence where the probabilities of each aggregate state are comparable, is the narrower, the larger is the cluster. Third, in the range of cluster coexistence, in some senses the distinction between the phase transitions of the first and second orders is lost. Thus, phase coexistence leads to unusual, perhaps surprising differences in behavior from the familiar phase transition properties of bulk matter.

10.2 Character of Phase Coexistence in Clusters: Surface Melting

This subject is especially interesting because of the insights it provides regarding the relationship of thermodynamics and time scales. We ordinarily think of thermodynamics as a means of describing systems in or very near equilibrium *in the sense of having values of its thermodynamic variables that do not change with time*. A typical way of presenting this concept is to assume tacitly that the time interval to which that condition of constancy is valid is either infinite or so much longer than any human experience that it could be treated as infinite. Here, however, we have a dynamical system in which we recognize that some properties may show bimodal or multimodal distributions if they are determined on a sufficiently short time scale, but show stable average values of those properties if they are determined over a time scale long enough to give average values that fluctuate no more that other thermodynamic quantities. The insight comes when we realize that, within those time intervals in which the multimodal properties take on single, unchanging values, here characteristic of a single phase, many degrees of freedom come to equilibrium so that the system can be treated as being in a well-defined thermodynamic state corresponding to that particular phase. What we find depends on how we look!

Because the total energy of an isolated atomic ensemble is conserved in time, the *kinetic* energy of the system (and, correspondingly, the potential energy) changes in time. In particular, these changes occur in rapid transitions of magnitudes well outside normal fluctuations when they occur as a result of transition between configurational, phase-like states. This is demonstrated in Fig. 7.13 for Lennard-Jones clusters of 55 atoms. Likewise under isothermal conditions, the excitation energy changes in time, carrying the system between solid and liquid forms when these two can coexist. This is shown in Fig. 10.1 for Lennard-Jones clusters of 147 atoms. We can think of this in a very straightforward way, especially when there are only two aggregate states involved, solid and liquid. The solid form is in a region of the potential energy surface that must be deep and narrow, confining and with low potential energy. The liquid region is much more like a rolling plain, with many readily

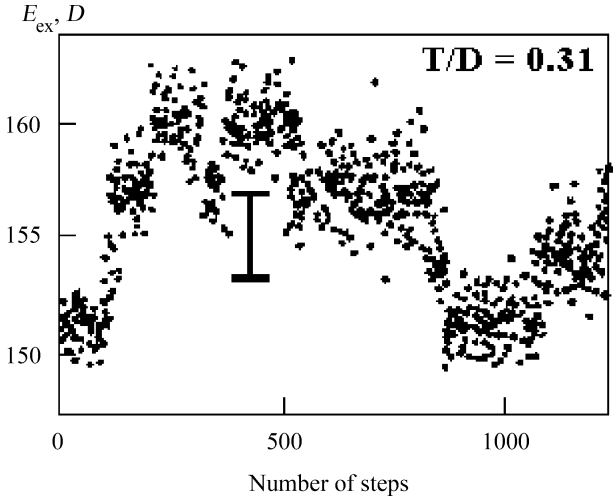

Fig. 10.1. The total binding energy distribution for the Lennard-Jones argon cluster of 147 atoms under isothermal conditions [253]. Averaging is made over 1800 iteration steps. The displayed fluctuation of the binding energy has been obtained under the assumption that the motion of cluster atoms is harmonic

accessible local minima separated by low barriers – but all at a relatively high potential energy. Since the total energy is constant here, low potential energy means high kinetic energy, so the solid has a high effective temperature. Likewise, the high potential energy of the liquid means that its kinetic energy is low and hence so is the temperature. Thus we have a dynamic equilibrium in this constant-energy system between a hot solid and a cold liquid!

Clusters of Figs. 7.13 and 10.1 have completed shells and hence are characterized by maximum energies of configurational excitation. Nevertheless, due to fluctuations, the dependencies of Figs. 7.13 and 10.1 allow us to distinguish only configurational states with relative large differences of configurational energies. For this reason we restrict our use of the two-state approximation for the phase transition by combining configurational states with similar energies into one single, comprehensive state. Thus many configurations that could be assumed by a liquid, all with similar energies and with relatively ready passage among them, are classified together as a single aggregate state. For a bulk atomic system, this classification corresponds to two aggregate states, the solid and liquid, in which internal atoms play a key role in forming the set of configurations that constitute the liquid state.

It is also possible in some systems to distinguish something we can call a liquid state that involves only the surface atoms. We shall discuss this later. But for a bulk system, with a very small fraction of its atoms on its surface, the surface-melted state seems to play a relatively unimportant role-except, perhaps, in contexts of chemical reactions and other interactions with objects in the environment of the system.

Thus, we find a two-temperature regime of coexistence of such a cluster. Coexistence of phases in this situation involves the cluster spending a part of its time in one aggregate state, and the remainder, in the other. Thermodynamic equilibrium of the vibrational degrees of freedom is established in each aggregate state during a time brief compared to the residence time in this state. If we were to observe the system for times long compared with times of residence in each aggregate state, we would reduce what we mean by "the cluster's state" to that at thermodynamic equilibrium with an average temperature (Fig. 10.2) and with properties that would be the averages over the behavior in the two aggregate states. Shortly, we shall find an appropriate mean temperature for this cluster and ascertain the validity of the long-time average thermodynamic description of this cluster.

The clusters of Figs. 7.13 and 10.1 have completed shells and hence exhibit maximum energies of configurational excitation. Nevertheless, due to fluctuations, the dependencies of Figs. 7.13 and 10.1 allow us to observe and distinguish configurational states whose configurational energies differ fairly significantly. In these two cases, we see only two aggregate states in dynamic equilibrium. When the energies and entropies for configurational excitation of the outermost shell and of the inner shells differ sufficiently, it is possible to see coexistence of the solid, the liquid and the intermediate, surface-melted state all in dynamic equilibrium together. Such a phenomenon appears in Lennard-Jones clusters of about 50 atoms or more. It is clearly apparent in the trimodal distribution of kinetic energies of Fig. 7.13d.

Such surface melting was first recognized by Nauchitel and Pertsin [305]. However it was only through animations that one could truly see the nature of this "surface melting" [262, 263]. To carry out any analysis of this sort, of course one must distinguish between the surface atoms and those

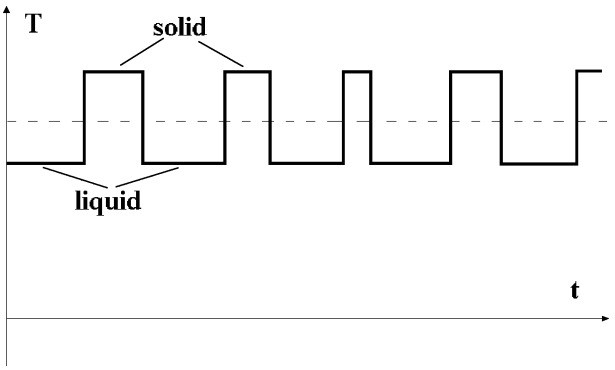

Fig. 10.2. A schematic representation of the change of the atomic temperature in the course of cluster evolution as a result of a transition between two aggregate states given by *solid line*. The mean behavior is modelled by the *dotted line* that corresponds to a long-time average thermodynamic state with an appropriate temperature

in the core. In the "surface melted" state, the core atoms retain all the characteristics of the solid form: order, very slow diffusion, small amplitudes of oscillation and essentially permanent, well-defined structure. The surface atoms show, in traditional diagnostics, just what one would expect for a liquid: rapid diffusion, large-amplitude motion and, as revealed in snapshot images, disorder. However, when one watches animations of a cluster of 50 or 100 atoms, one can discern immediately what those diagnostics really say about the surface melted state; the animations are simply more revealing than still photographs or numerical diagnostics. In fact, most of the atoms in the surface layer undergo very large-amplitude, very anharmonic oscillations, especially away from the surface and back. But these motions of the atoms are, as the eye detects in the animation, very highly coordinated oscillations of the surface of a polyhedron! However not all the atoms that were initially in the surface prior to its "melting" remain in the surface, though. Roughly one atom in about 30, on average, leaves the surface and moves rather freely around the exterior of the cluster, yet remains bound to it. These are what we previously called "floaters". It is the floaters that are responsible for the rapid diffusion, but it is the large-amplitude, anharmonic motion that gives the outer surface the appearance of disorder. The floaters exchange with surface atoms every few thousand vibrational periods, so that all the surface atoms eventually get to be floaters. It is this exchange that yields the permutations of all the surface atoms, eventually making them all equivalent. Hence what we call "surface melting" is in many ways like what we mean by "melting", but it is not really quite the same phenomenon at all.

Let us put this kind of phase coexistence into another relevant context, and shift our viewpoint a bit. The coexisting phase-like forms of a cluster, within the range of their observable coexistence, is precisely analogous to the dynamic equilibrium between chemical isomers, such as the equilibrium of left-and right-handed forms of the doubly-substituted, pyramidal ammonia molecule, NHDT, which undergoes rapid inversion, interconverting the two isomers at a very rapid rate. Another example is ionization equilibrium (6.6). In that case, the probabilities of the atomic species being atoms or ions and electrons are comparable within some range of temperatures. The partially-ionized gas contains a certain number n_{A} of A atoms and n_+ of A^+ ions, whose ratio is determined by the difference between the free energies $\Delta F(T) = F_{\mathrm{A}}(T) - F_{\mathrm{A}^+}(T)$ of the two forms. Explicitly, this ratio is the equilibrium constant, the temperature-dependent exponential of that free energy difference: $K(T) = n_{\mathrm{A}}/n_+ = \exp(-\Delta F/T)$. Precisely the same expression describes the ratio of two phase-like forms coexisting, with the numbers of species in each phase replacing the numbers of atoms and ions in this expression:

$$K_{\frac{\mathrm{liq}}{\mathrm{sol}}}(T) = \exp\left(-\frac{\Delta F}{T}\right) = \exp\left(-\frac{F_{\mathrm{liq}} - F_{\mathrm{sol}}}{T}\right) . \tag{10.5}$$

This expression and its origin are discussed in the following section.

10.3 Two-Temperature Regime for Cluster Equilibrium

We now consider the two-temperature regime of cluster equilibrium near the melting point if criteria (10.1) and (10.2) hold true. This hierarchy of cluster times leads to a specific kind of cluster behavior. Indeed, during $\tau_{\rm eq}$, thermal equilibrium is established for the atomic vibrational motion so those degrees of freedom can be characterized by a temperature. Thermodynamic equilibrium is established for each aggregate state occurring in this dynamic equilibrium, but, under conditions of constant energy, the temperatures are different for these aggregate states. Therefore we introduce the temperatures of atoms for the solid $T_{\rm sol}$ and liquid $T_{\rm liq}$ aggregate states separately. In particular, in the classical limit, when atoms interact as classical particles, we have for the cluster energy

$$E = \frac{(3n-6)}{\eta} T_{\rm sol} = \Delta E_{\rm f} + \frac{(3n-6)}{\eta} T_{\rm liq} \; , \tag{10.6}$$

where η is an energy parameter that relates the units of average kinetic energy to those of temperature. As usual, n is the number of cluster atoms, $\Delta E_{\rm f}$ is the fusion energy, and we have used the kinetic temperature definition

$$K_{\rm sol} = \frac{(3n-6)}{2} T_{\rm sol} \; , \quad K_{\rm liq} = \frac{(3n-6)}{2} T_{\rm liq} \; , \quad \Delta T = T_{\rm sol} - T_{\rm liq} = \frac{\eta \Delta E_{\rm f}}{3n-6} \; , \tag{10.7}$$

where $K_{\rm sol}$ and $K_{\rm liq}$ are the total kinetic energies of atoms for the solid and liquid aggregate states correspondingly, and $\Delta T = 0.06D$, the average for an isolated 13-atom Lennard-Jones cluster according to formula (7.26). Figure 7.5 represents the temperatures of the solid $T_{\rm sol}$ and liquid $T_{\rm liq}$ aggregate states of this cluster, chosen as an example and constructed on the basis of data of Fig. 7.1. Besides these temperatures, one can also introduce a general cluster temperature T for times of cluster observation very long compared with a typical dwell time in each of the aggregate states; during such times the cluster can change its aggregate state many times. We will next consider this common cluster temperature.

Since a cluster near the melting point spends a certain part of time in the solid aggregate state, and the rest of the time is in the liquid aggregate state (we assume only two phases here), we consider cluster properties on the basis of the two-state approximation for its aggregate states, as discussed in Chap. 6. In this approach we have for the total partition function of a cluster

$$Z = Z_{\rm sol} + Z_{\rm liq} \; , \tag{10.8}$$

where $Z_{\rm sol}$ and $Z_{\rm liq}$, the partition functions for the solid and liquid cluster states respectively, are given by

$$p(T) = \frac{Z_{\rm liq}}{Z_{\rm sol}} \; . \tag{10.9}$$

The probabilities $w_{\rm sol}, w_{\rm liq}$ that the cluster be found in the solid and liquid states respectively are equal according to formulas (6.32)

$$w_{\rm sol} = \frac{1}{1+p} \ , \quad w_{\rm liq} = \frac{p}{1+p} \ . \tag{10.10}$$

Along with the vibrational temperatures for the solid $T_{\rm sol}$ and liquid $T_{\rm liq}$ aggregate states of an isolated cluster, the temperature $T_{\rm con}$ of configurational excitation follows from the relation (6.30)

$$p = \exp\left(-\frac{\Delta E}{T_{\rm con}} + \Delta S\right) \ . \tag{10.11}$$

We now evaluate the configurational temperature $T_{\rm con}$ in the two-temperature approach, taking into account that the rate or probability of transition from the solid to liquid is determined by the solid temperature and the transition from the liquid solid aggregate state is determined by the liquid temperature. Correspondingly, at equilibrium between these aggregate states, the entire system satisfies the balance equation

$$w_{\rm sol}\nu_{\rm sol}(T_{\rm sol}) = w_{\rm liq}\nu_{\rm liq}(T_{\rm liq}) \ , \tag{10.12}$$

where $\nu_{\rm sol}$ is the rate of solid-to-liquid transition, and $\nu_{\rm liq}$ is the rate of liquid-to-solid transition. These rates are connected by the principle of detailed balance [48, 61, 80, 306–308]

$$\frac{\nu_{\rm sol}(T)}{\nu_{\rm liq}(T)} = g\exp\left(-\frac{\Delta E}{T}\right) \ , \tag{10.13}$$

where g is the ratio of statistical weights of the liquid and solid aggregate states, which is directly related to $S = \ln g$, the transition entropy, and ΔE is the energy of configurational excitation for this transition.

We assume that the basic temperature dependence of the rates is due to the activation character of these transitions, so that

$$\nu_{\rm sol}(T) \sim \exp\left(-\frac{\Delta E}{T} - \frac{E_{\rm b}}{T}\right) \ , \quad \nu_{\rm liq}(T) \sim \exp\left(-\frac{E_{\rm b}}{T}\right) \ , \tag{10.14}$$

where T is the atomic vibrational temperature for the initial aggregate state, ΔE is the energy of configurational excitation, and $E_{\rm b}$ is the energy of the barrier that separates local minima of the potential energy surface. From this we have

$$p = \frac{w_{\rm liq}}{w_{\rm sol}} \equiv \exp\left(\Delta S - \frac{\Delta E}{T_{\rm con}}\right) = \exp\left[\Delta S - \frac{\Delta E}{T_{\rm sol}} - E_{\rm b}\left(\frac{1}{T_{\rm sol}} - \frac{1}{T_{\rm liq}}\right)\right] \ , \tag{10.15}$$

this is the definition of the configuration temperature. This relation allows us to express the temperature through the temperatures of the aggregate states

$$T_{\rm con} = \frac{T_{\rm sol}}{1 + \frac{E_{\rm b}}{\Delta E}\frac{\Delta T}{T_{\rm liq}}} \ , \tag{10.16}$$

where $\Delta T = T_{\rm sol} - T_{\rm liq}$. In particular, for the isolated 13-atom Lennard-Jones cluster, LJ_{13}, we have from this, with ($E_{\rm b} = 0.56D$ and $\Delta E = 33\Delta T/2\eta$)

$$T_{\rm con} = \frac{T_{\rm sol}}{1 + \frac{0.034D\eta}{T_{\rm liq}}} \ . \tag{10.17}$$

Together with the vibrational temperatures inferred from computer simulations for LJ_{13} whose results are given in Fig. 7.1 [50], Fig. 7.5 contains the configurational temperature of this cluster obtained from formula (10.17). We also give the temperatures of this cluster at the melting point ($p = 1$): $T^m_{\rm sol} = 0.33D, T^m_{\rm liq} = 0.27D, T^m_{\rm con} = 0.315D$. The latter differs from that defined by formula (7.33). Since $E_{\rm b} \approx 0.6D < \Delta E$ for this cluster, the configurational temperature is closer to the solid temperature than to the liquid one.

10.4 Entropy of an Isolated Cluster in the Two-State Approach

The condition (10.1) for an isolated (and therefore constant-energy) cluster allows us to associate a different temperature with each of the phases when they are in the regime of coexistence. Here, we will compare thermodynamic parameters of this system with those of a thermodynamically equilibrated cluster with an average temperature. That is, we will relate the two separate temperatures of the individual phases to that of the long-time average, which is the temperature of the equilibrated system.

We have, thus far, used as the definition of temperature the mean kinetic energy per degree of freedom. Alternatively, one can define the cluster temperature from the thermodynamic relation [4]

$$\mathrm{d}E = T\,\mathrm{d}S \ , \tag{10.18}$$

where E, S are the cluster energy and entropy. While the two definitions are equivalent for a canonical ensemble, for any other ensemble, such as a microcanonical, they are not. This entropy-based definition may be used for each aggregate state separately, or for the long-time average over both aggregate states, if we assume the validity of the concept of an internal thermodynamic equilibrium among the internal degrees of freedom for this cluster. That average temperature is simply taken over both states, for times long enough to establish a stable ratio of the frequencies of the two forms. Here we use the latter option and evaluate the entropy S of a cluster in a long-term equilibrium. This can be done for the microcanonical, constant-energy system we have been discussing or, equally well, for a dynamic equilibrium in a canonical, constant-temperature system in contact with an environment.

There is one significant difference between these two applications, i. e. to a canonical or microcanonical system, that is often overlooked. In applying

(10.18) to determine a temperature, we of course use the standard constant-temperature entropy if we are dealing with a canonical ensemble. If, however, we are treating a constant-energy system, we must use the *microcanonical* entropy to infer a temperature from the energy via (10.18). This entropy measures the system's available volume of phase space on the fixed, chosen energy shell, in contrast to the canonical entropy which measures the accessible volume over a range of energies. While the relation (10.18) is fundamental and general for a canonical ensemble, it is, in effect, an arbitrary definition of an effective temperature for a microcanonical system. It is important to keep in mind that for any but a canonical ensemble, "temperature" is a concept that carries considerable arbitrariness of definition, and that, in contrast to the canonical situation, the values assigned to this property depend on which definition one chooses.

Basing this analysis on the general entropy formula [4], and setting the Boltzmann constant $k = 1$, we have

$$S = -\langle \ln w \rangle = -\sum_i w_i \ln w_i \ , \tag{10.19}$$

where i is a cluster state, and w_i is the probability that the cluster is found in this state ($\sum_i w_i = 1$). Let us introduce, along with $w_{\rm sol}$ and $w_{\rm liq}$ on the basis of formula (10.9), the probability X_j for the cluster to be in the j-th state, if it is first found in the solid aggregate state, and the probability Y_k for the cluster to be in k-th state, if it is initially in the liquid aggregate state. That is, we introduce a kind of conditional probability. According to this definition, we have

$$w_{\rm sol} + w_{\rm liq} = 1 \ , \sum_j X_j = \sum_k Y_k = 1 \ . \tag{10.20}$$

From this we obtain for the cluster entropy [309]

$$\begin{aligned} S &= -w_{\rm sol} \sum_j X_j \ln(w_{\rm sol} X_j) - w_{\rm liq} \sum_k Y_k \ln\left(w_{\rm liq} Y_k\right) \\ &= w_{\rm sol} S_{\rm sol} + w_{\rm liq} S_{\rm liq} + S_{\rm con} \ , \end{aligned} \tag{10.21}$$

where

$$S_{\rm sol} = \sum_j X_j \ln X_j \ , \quad S_{\rm liq} = \sum_k Y_k \ln Y_k \tag{10.22}$$

are the entropies of the corresponding aggregate states. We thus express the entropy of a cluster with two aggregate states through entropies of each aggregate state and the entropy of the cluster configurational state $S_{\rm con}$,

$$\begin{aligned} S_{\rm con} &= -\sum_i x_i \ln x_i = -w_{\rm sol} \ln w_{\rm sol} - w_{\rm liq} \ln w_{\rm liq} = \ln(1+p) - \frac{p}{1+p} \ln p \ , \\ \frac{{\rm d}S_{\rm con}}{{\rm d}p} &= -\frac{\ln p}{(1+p)^2} \ , \end{aligned} \tag{10.23}$$

where x_i is the probability for the cluster to be in a given aggregate state. This expression is valid under the assumption that the cluster is observed in long-term equilibrium, i. e. that during a time of observation, it can be located many times in each aggregate state. Thus, the expression (10.23) for the cluster entropy is a sum of terms corresponding to the solid and liquid aggregate states, and also of the term which accounts for configurational excitation.

One can divide the entropy variation in two parts $\mathrm{d}S = \mathrm{d}S_{\mathrm{th}} + \mathrm{d}S_{\mathrm{con}}$, so that the first part is connected with atomic vibrations, and the other, to the phase transition; we have

$$\begin{aligned} \mathrm{d}S_{\mathrm{th}} &= w_{\mathrm{sol}}\,\mathrm{d}S_{\mathrm{sol}} + w_{\mathrm{liq}}\,\mathrm{d}S_{\mathrm{liq}}\ ,\ \mathrm{d}S_{\mathrm{con}} = \mathrm{d}S_{\mathrm{ph}} + S_{\mathrm{sol}}\,\mathrm{d}w_{\mathrm{sol}} + S_{\mathrm{liq}}\,\mathrm{d}w_{\mathrm{liq}} \\ &= \ln\frac{w_{\mathrm{sol}}}{w_{\mathrm{liq}}}\,\mathrm{d}w_{\mathrm{liq}} + \Delta S\,\mathrm{d}w_{\mathrm{liq}}\ . \end{aligned} \tag{10.24}$$

We must retain the constraint that $w_{\mathrm{liq}} + w_{\mathrm{sol}} = 1$ or $\mathrm{d}w_{\mathrm{liq}} + \mathrm{d}w_{\mathrm{sol}} = 0$; $\Delta S = S_{\mathrm{liq}} - S_{\mathrm{sol}}$ is the entropy jump associated with the phase change. One can see that the variation $\mathrm{d}S_{\mathrm{con}}$ does not depend on thermal motion of atoms, while $\mathrm{d}S_{\mathrm{th}}$ is determined by this set of degrees of freedom. Thus the phase transition gives an additional contribution to the total cluster entropy and its variation.

10.5 Temperatures of an Isolated Cluster Near the Melting Point

We have seen how an isolated cluster is characterized by three different temperatures, $T_{\mathrm{sol}}, T_{\mathrm{liq}}$ and a long-time average temperature T_{con}.

An effective temperature that can be used in cluster thermodynamics depends on the temperature definition [309, 310], as we discussed in the previous section. Now when we express the thermodynamic cluster temperature through the temperatures T_{sol} and T_{liq} of aggregate states in different ways, the degree of coincidence these thermodynamical temperatures near the melting point reveals the accuracy of an approach treating the coexistence region as a single thermodynamic system.

First we use the connection between the kinetic energy of cluster atoms and their temperature. Then connecting the mean kinetic energy of cluster atoms averaged over a time long enough to reflect the kinetic energies of atoms in both aggregate states, we define the (long-term) cluster temperature as [309]

$$T = w_{\mathrm{sol}} T_{\mathrm{sol}} + w_{\mathrm{liq}} T_{\mathrm{liq}}\ . \tag{10.25}$$

This is the definition of temperature one would use in the context of traditional statistical physics, i. e. on the basis of a very long-time average. This remains a useful and valid approach, but the availability of many kinds of measurement fast enough to enable us to observe the individual aggregate states justifies the extension of the conceptual framework to describe each aggregate state by itself, to supplement our long-time average description.

Now turning to the two-temperature approach for a cluster, we assume the cluster heat capacity *in each phase* to be independent of the temperature in the range of phase coexistence, i. e. the caloric curves for the solid and liquid states are straight lines, as shown in Fig. 7.5 for the LJ_{13} cluster. At this point, we introduce two parameters of this curve that do not weight the temperatures for the fraction of time spent in each form,

$$\overline{T} = \frac{T_{\rm sol} + T_{\rm liq}}{2} \ , \quad \Delta T = T_{\rm sol} - T_{\rm liq} \ , \tag{10.26}$$

and for simplicity below we assume that

$$\Delta T \ll \overline{T} \ . \tag{10.27}$$

According to formula (10.21), the statistical temperature T is expressed through these parameters as

$$T = \overline{T} + \frac{\Delta T}{2} \frac{1-p}{1+p} \ . \tag{10.28}$$

Thus, formula (10.28) gives the kinetic cluster temperature that tends, far from the point of equal free energies, that we call the melting point here, to the solid state temperature $T_{\rm sol}$ at low temperatures and to $T_{\rm liq}$ at high temperatures. This cluster behavior is natural since a cluster is a thermodynamically equilibrated system of atoms in the sense we have discussed when the cluster is in a specific aggregate state long enough for its vibrations to come to a common equilibrium.

We now determine a general cluster temperature in another way. Let us use formula (10.18) as the thermodynamic definition of the cluster temperature T

$$\frac{1}{T} = \left[\frac{{\rm d}S}{{\rm d}E} \right]_V \ . \tag{10.29}$$

That is, here we use the entropy-energy definition, rather than the mean kinetic energy definition for the temperature of an atomic ensemble. Since this formula is valid – with the provisos we gave – also for each aggregate state, we have the relations

$$\frac{1}{T_{\rm sol}} = \frac{{\rm d}S_{\rm sol}}{{\rm d}E} \ , \quad \frac{1}{T_{\rm liq}} = \frac{{\rm d}S_{\rm liq}}{{\rm d}E}$$

for the cluster temperature of a given aggregate state. On the basis of these formulas and formula (10.23) for the entropy of a cluster with two aggregate states, we have for the cluster thermodynamic temperature [309]

$$\frac{1}{T} = \frac{w_{\rm sol}(T_{\rm sol})}{T_{\rm sol}} + \frac{w_{\rm liq}(T_{\rm liq})}{T_{\rm liq}} + \frac{{\rm d}S_{\rm con}}{{\rm d}E} = \frac{1}{(1+p)T_{\rm sol}} + \frac{p}{(1+p)T_{\rm liq}} - \frac{\ln p}{(1+p)^2} \frac{{\rm d}p}{{\rm d}E} \ , \tag{10.30}$$

where, according to formula (10.23), we have

$$\frac{\mathrm{d}S_{\mathrm{con}}}{\mathrm{d}E} = -\frac{\ln p}{(1+p)^2}\frac{\mathrm{d}p}{\mathrm{d}E} \,. \tag{10.31}$$

If we ignore the last term due to configurational excitation in formula (10.30) and use a small parameter (10.27), this formula coincides with the expression (10.28) for the kinetic temperature. Thus, in the limit (10.27) the kinetic (10.28) and entropic (10.30) cluster temperatures coincide. The last term of formula (10.30) is also zero at the melting point ($p = 1$), so, in the limit (10.27), the kinetic and entropic temperatures coincide strictly at the melting point.

One can estimate the contribution of the last term of formula (10.30) to the cluster temperature according its thermodynamic definition with formula (10.30) in the limit (10.27) in the form

$$\frac{1}{T} = \frac{1}{T_{\mathrm{th}}} + F(p) \,, \quad F(p) = \frac{\mathrm{d}S_{\mathrm{con}}}{\mathrm{d}E} = -\frac{\ln p}{(1+p)^2}\frac{\mathrm{d}p}{\mathrm{d}E} \,, \tag{10.32}$$

where T_{th} is given by formula (10.28). The function $F(p)$ has symmetry with respect to the change $p \to 1/p$. Using formula (7.7) for the LJ_{13} cluster, one can find the maximum value of $F(p)$; that is approximately 0.22. Since near the melting point for the Lennard-Jones cluster of 13 atoms we have $T_{\mathrm{lig}}/\delta E < 5$, so that the contribution of the last term in formula (10.30) is less than 10%. As the cluster size increases, the melting point typically increases weakly, whereas the parameter δE grows larger, so that the contribution of the last term is small for both small and large clusters. Therefore the kinetic (10.25) and thermodynamic (10.30) cluster temperatures, while strictly different, are frequently quite similar for clusters.

In parallel with formula (10.11) for the configurational temperature as defined by kinetic energy, we use the entropic definition of the configurational temperature

$$T_{\mathrm{con}} = \frac{\mathrm{d}E_{\mathrm{con}}}{\mathrm{d}S_{\mathrm{con}}} = \frac{\Delta E}{\Delta S + \ln \dfrac{w_{\mathrm{sol}}}{w_{\mathrm{liq}}}} \,, \tag{10.33}$$

where $\Delta E, \Delta S$ are the jumps of the cluster energy and entropy at the phase transition, and we use the expression $\mathrm{d}E_{\mathrm{con}} = \Delta E\, \mathrm{d}w_{\mathrm{liq}}$ for the change of the configurational energy, and formula (10.24) for the change of the configurational entropy $\mathrm{d}S_{\mathrm{con}}$. We are also using the approach of two aggregate states and assume the energy of configurational excitation ΔE to be independent of the cluster energy in the range of the phase transition. One can see that this entropic definition of the configurational temperature coincides with the kinetic definition (10.11) at the melting point, while far from the melting point these formulas give different values of the configurational temperatures. Since the entropy jump is large $\Delta S \gg 1$, the difference of these definitions is not important, close to the melting point.

Thus, an isolated cluster in equilibrium (10.1) is described by three temperatures, $T_{\mathrm{sol}}, T_{\mathrm{liq}}, T_{\mathrm{con}}$, and considering a cluster as a thermodynamic object,

we describe the cluster by a common temperature T. Figure 7.5 shows these temperatures for the LJ_{13} cluster, as based on the data of Fig. 7.1. The notion of treating an isolated cluster as a thermodynamic object near the phase transition can be dangerous, and can only be done with care and full realization of the issues of time scale and of what averages one uses. Nevertheless, our experience for the LJ_{13} cluster shows that although the kinetic and thermodynamic vibrational temperatures are given by different formulas (10.25) and (10.30), their values coincide within the limits of accuracy in a range near the melting point, although not necessarily throughout the coexistence region. In the same manner, the configurational temperatures given by formulas (10.24) and (10.33) according to kinetic and thermodynamic considerations are similar near the melting point. But the vibrational and configurational temperatures are different.

In general, the vibrational temperature of an isolated cluster and its configurational counterpart are characterized by different asymptotic behavior. Indeed, a general vibrational temperature tends to the solid $T_{\rm sol}$ and liquid $T_{\rm liq}$ temperatures respectively, far from the melting point when the cluster is found mostly in one aggregate state or the other. Since the rate of the phase transition is determined by the atomic temperature in the initial aggregate state, and energy is absorbed into potential energy at the solid–liquid transition, the configurational temperature is generally closer to the solid temperature than to the liquid one. Therefore, modelling an isolated cluster as a thermodynamic object, it is necessary to consider the cluster vibrational and configurational temperatures to be different.

10.6 Cluster Heat Capacity Near the Phase Transition

The heat capacity of an isolated cluster in the coexistence range differs in principle from the heat capacity of an isothermal cluster [311–314]. On the other hand, the heat capacity of this microcanonical ensemble of atoms is a meaningful thermodynamic parameter, but near the point corresponding to the bulk phase transition, where the two phases have equal free energies, concepts of classical bulk thermodynamics are inadequate and we must use this quantity with care. Hence this parameter has a restricted accuracy and its value depends on the method of its definition [309, 310]. The most startling property of this quantity is the possibility of its having a negative value in the coexistence region, near the melting point. We shall use different methods to determine thermodynamic cluster parameters and, in this way, to reduce an isolated cluster to a thermodynamic object and determine the accuracy, and even the meaning, of these results.

To carry this out, we assume the regime (10.1), (10.2), i. e. that a typical time $\tau_{\rm eq}$ for thermodynamic equilibration of the atomic thermal motion in each aggregate state is short compared with the dwell time $\tau_{\rm ag}$ of the cluster in each aggregate state. This allows us to introduce separate temperatures $T_{\rm sol}$

and T_{liq} for the solid and liquid aggregate states. Next, modelling a cluster by a thermodynamic system, we introduce a general vibrational temperature T for the cluster atoms and then can apply a thermodynamic description to the cluster. We now analyze the cluster heat capacity by describing a cluster near the phase transition as a thermodynamic object.

We define the cluster heat capacity as

$$C = \frac{\mathrm{d}E}{\mathrm{d}T} \,, \tag{10.34}$$

where $\mathrm{d}E$ refers to the total cluster energy that includes both vibrational motion of atoms and configurational excitation, whereas the cluster temperature T in (10.34) characterizes thermal motion of atoms only. To analyze the heat capacity of an isolated cluster, we assume establishment of equilibrium whenever the cluster's energy changes. Then each new addition to the cluster's energy in the coexistence range, around the melting point, goes in part to excite vibrational (i. e. thermal) motion, and in part to configurational excitation. This appears to lead to a positive heat capacity. But it is possible that, near the melting point, that most or all of a new portion of energy goes into configurational excitation, specifically to generate configurations of high potential energy. Such a case reveals itself as an S-bend in the cluster's caloric curve. This is precisely what corresponds to the negative heat capacity near the melting point [264, 312, 314–317]. In principle, both possibilities are possible – a heat capacity everywhere positive, or one that has a negative region. In experiments with isolated clusters, effectively clusters under conditions of constant energy, both kinds of behavior have appeared.

For an isolated cluster in a microcanonical ensemble, we may assume that the caloric curve far from the melting point can be approximated by straight lines. One can expect two forms of the caloric curves near the melting point, as shown in Fig. 10.3. In case 1, the cluster heat capacity is positive at every temperature; in case 2, it is negative near T_{m}; both cases may and have been be realized. Based on their experimental study of positively-charged sodium clusters of hundreds atoms, Haberland and coworkers [318, 319] infer that the negative cluster heat capacity near T_{m} is more representative, at least for that class of system, clusters of alkali atoms carrying a single positive charge. Initially, the accuracy of the experimental data [244, 245, 320, 321] left some possibility to question that inference, but more recent, independent measurements have confirmed the case for some microcanonical negative heat capacities, making the general concept much more plausible [322, 323]. All these experiments, in effect, base the evaluation of temperature on the kinetic energy of the particles of the clusters. It is easy to understand how this definition allows for negative heat capacities.

Let us consider this problem under assumption that the caloric curves for the solid and liquid states are parallel straight lines, as shown in Fig. 10.3, i. e.

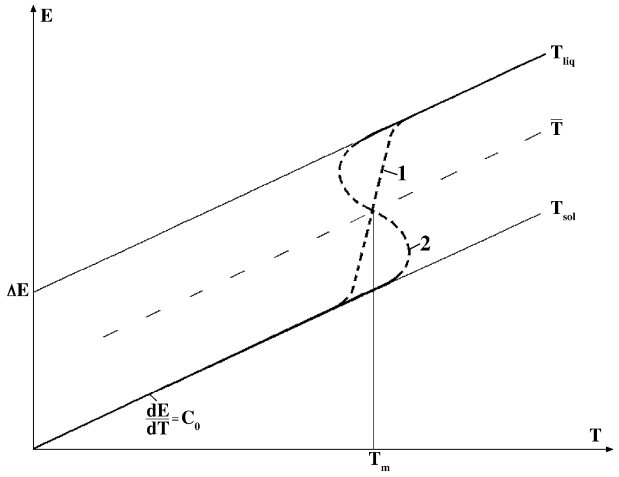

Fig. 10.3. Caloric curves of an isolated cluster with two aggregate states in the one-temperature approach [309]. *1* – the case of a positive heat capacity; *2* – the case of a negative heat capacity near the melting point

the transition energy ΔE is independent of the excitation energy or effective temperature. On the basis of the kinetic temperature (10.25) we have

$$T = w_{\rm sol} T_{\rm sol} + w_{\rm liq} T_{\rm liq} = T_{\rm sol} - \Delta T w_{\rm liq} \,, \tag{10.35}$$

and we assume the temperature difference $\Delta T = T_{\rm sol} - T_{\rm liq}$ does not depend on the kinetic temperature under the above assumption. This gives for the temperature variation

$$\mathrm{d}T = \mathrm{d}T_{\rm sol} + \Delta T \, \mathrm{d}w_{\rm liq} \,. \tag{10.36}$$

Since vibrational and configurational degrees of freedom are separated, the total energy of a particle ensemble E is a sum of thermal $E_{\rm th}$ and configurational $E_{\rm con}$ energies ($E = E_{\rm th} + E_{\rm con}$). The variation of the thermal energy $\mathrm{d}E_{\rm th} = C_{\rm o} \, \mathrm{d}T_{\rm sol} = C_{\rm o} \, \mathrm{d}T_{\rm liq}$ is responsible for a shift along the solid or liquid caloric curve of Fig. 10.3. The variation of the configurational energy $\mathrm{d}E_{\rm con} = \Delta E \, \mathrm{d}w_{\rm liq}$ is responsible for displacement between two caloric curves. Then we have for the total energy change $\mathrm{d}E$ of an isolated cluster

$$\mathrm{d}E = \mathrm{d}E_{\rm th} + \mathrm{d}E_{\rm con} = \mathrm{d}E_{\rm th} = C_{\rm o} \, \mathrm{d}T_{\rm sol} + \Delta E \, \mathrm{d}w_{\rm liq} \,. \tag{10.37}$$

Formulas (7.4) and (7.20) give the cluster's heat capacity far from the melting point

$$C_{\rm o} = \frac{\mathrm{d}E}{\mathrm{d}T} = \frac{3n-6}{2\eta} \,. \tag{10.38}$$

Next, using the expression (6.32) for the probability $w_{\rm liq}$ of the liquid state and the definition (10.11) of the configurational temperature, we represent formula (10.37) in the form

$$\mathrm{d}E = C_{\rm o} \, \mathrm{d}T_{\rm sol} + \frac{p}{(1+p)^2} \frac{\Delta E^2 \, \mathrm{d}T_{\rm con}}{T_{\rm con}^2} \,. \tag{10.39}$$

On the basis of (10.16), we have

$$\frac{\mathrm{d}T_{\mathrm{con}}}{T_{\mathrm{con}}} = \frac{\mathrm{d}T_{\mathrm{sol}}}{T_{\mathrm{sol}}}\left(1 - \frac{E_{\mathrm{b}}}{C_{\mathrm{o}}T_{\mathrm{liq}}}\right) . \tag{10.40}$$

The second term in parentheses is small. In particular, for the Lennard-Jones cluster consisting of 13 atoms this term is 1/20. Neglecting this term, we obtain

$$\frac{\mathrm{d}T_{\mathrm{con}}}{T_{\mathrm{con}}} = \frac{\mathrm{d}T_{\mathrm{sol}}}{T_{\mathrm{sol}}} . \tag{10.41}$$

Substituting this in formula (10.39) and taking $T_{\mathrm{sol}} = T_{\mathrm{con}}$, we obtain

$$\mathrm{d}E = C_{\mathrm{o}}\,\mathrm{d}T_{\mathrm{sol}}\left[1 + \frac{p}{(1+p)^2}\frac{C_{\mathrm{o}}\Delta T^2}{T_{\mathrm{con}}T_{\mathrm{sol}}}\right] . \tag{10.42}$$

This formula allows us to determine the cluster heat capacity as that of a canonical ensemble of atoms, as if this cluster were in a thermostat. Indeed, according to formulas (10.11) and (10.15) we have approximately $T_{\mathrm{sol}} \approx T_{\mathrm{con}}$, and if we introduce a general temperature $T \approx T_{\mathrm{sol}} \approx T_{\mathrm{con}}$, so that $\mathrm{d}T = \mathrm{d}T_{\mathrm{sol}}$, we obtain for the heat capacity

$$C = \frac{\mathrm{d}E}{\mathrm{d}T_{\mathrm{sol}}} = C_{\mathrm{o}} + \frac{p}{(1+p)^2}\frac{\Delta E^2}{T_{\mathrm{sol}}^2} \tag{10.43}$$

in accordance with formulas (7.37) and (7.38), appropriate when the parameters $\Delta E, \Delta S$ are independent of the temperature, and $\Delta T \ll T_{\mathrm{sol}}$.

In the case of an isolated cluster we use formula (10.25) for a general vibrational cluster temperature, giving

$$\begin{aligned} \mathrm{d}T &= \mathrm{d}T_{\mathrm{sol}} - \Delta T\,\mathrm{d}w_{\mathrm{liq}} = \mathrm{d}T_{\mathrm{sol}} - \frac{p}{(1+p)^2}\frac{\Delta E^2\,\mathrm{d}T_{\mathrm{con}}}{T_{\mathrm{con}}^2} \\ &= \mathrm{d}T_{\mathrm{sol}}\left[1 - \frac{p}{(1+p)^2}\frac{C_{\mathrm{o}}\Delta T^2}{T_{\mathrm{con}}T_{\mathrm{sol}}}\right] , \end{aligned} \tag{10.44}$$

and from formulas (10.42), (10.44) we have the heat capacity of an isolated cluster

$$C = C_{\mathrm{o}}\frac{1-X}{1+X} , \quad X = \Delta T\frac{\mathrm{d}w_{\mathrm{liq}}}{\mathrm{d}w_{\mathrm{sol}}} = \frac{p}{(1+p)^2}\frac{C_{\mathrm{o}}\Delta T^2}{T_{\mathrm{con}}T_{\mathrm{sol}}} . \tag{10.45}$$

From this we find the criterion for a negative heat capacity. Since the optimal conditions for a negative heat capacity correspond to those in the vicinity of the melting point ($p = 1$), we obtain the criterion of the negative heat capacity, taking for simplicity $T_{\mathrm{con}} = T_{\mathrm{sol}}$:

$$\frac{\Delta T}{T_{\mathrm{sol}}} > \sqrt{\frac{2}{C_{\mathrm{o}}}} . \tag{10.46}$$

Since $C_o \sim n$, where n is a number of cluster atoms, one can expect that the heat capacities of large clusters in the coexistence region will be negative. We add to this criterion that simulation of an isolated cluster is fairly reliable, and it is the better, the smaller is the parameter $\Delta T/T_{sol}$, so that the negative heat capacity is particularly likely in large clusters. According to formula (10.45) far from the melting point $C = C_o$, and for a large cluster

$$n \gg \left(\frac{T_{sol}}{\Delta T}\right)^2 \tag{10.47}$$

the maximum negative heat capacity is $C = -C_o$ at the melting point $p = 1$, as given in Fig. 10.4.

Figure 10.4 shows the heat capacity of an isolated cluster as a function of the excitation energy, specifically for a large cluster for which the criterion (10.2) holds true. The negative heat capacity of the cluster is realized in a restricted range of excitation energies near the melting point that corresponds to the excitation energy E_m. The boundaries of this range are denoted by E_1 and E_2, which satisfy to the relation $C(E_1) = C(E_2) = \infty$, so that

$$p(E_1) = \frac{1}{p(E_2)} = \frac{T_m^2}{C_o \Delta T^2} \ . \tag{10.48}$$

The width of the region of negative heat capacity is

$$\delta E = E_1 - E_2 \ . \tag{10.49}$$

Table 10.1 contains the reduced values of $\delta T = \delta E/C_o$ for some cluster systems and bulk inert gases. We take the heat capacity far from the phase transition on the basis of the Dulong-Petit formula $C_o = 3n - 6$ that describes a bound system of classical atoms whose motions are a sum of harmonic oscillations, $\Delta T = T_{sol} - T_{liq} = \Delta E/C_o$. One can add to this that contribution

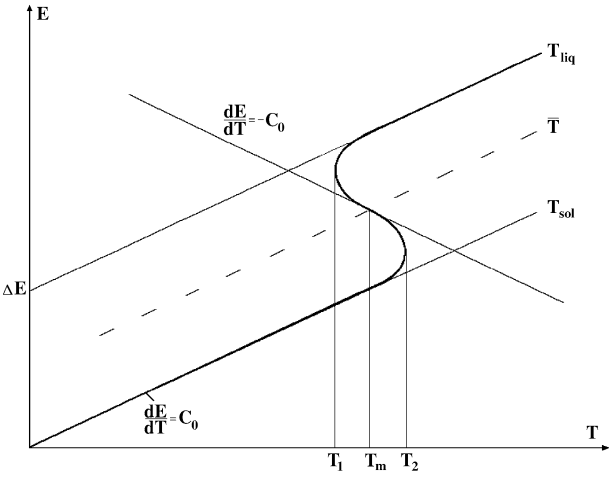

Fig. 10.4. Caloric curves of an isolated cluster with two aggregate states in the one-temperature approach [309]

due to an uncertainty of the mean vibrational and configurational temperatures, since the accuracy of these figures is limited. One can definitely state that an isolated cluster is characterized by a range of excitation energies (or effective temperatures), in which the cluster heat capacity is negative, only if the following criterion is satisfied, i. e. this is a *necessary* condition:

$$\ln\left(C_{\mathrm{o}}\frac{\Delta T^2}{T_{\mathrm{m}}^2}\right) \gg 1\,. \tag{10.50}$$

Table 10.1 contains this parameter; the data show that an isolated Lennard-Jones cluster consisting of 13 atoms cannot have a negative heat capacity, while other systems of Table 10.1 definitely have ranges where their heat capacities are negative.

A qualitative way to think of this phenomenon is this. If the potential energy of the liquid form is high and that of the solid is low, then, under conditions of constant energy, the solid is hot and the liquid, relatively cold, if their temperatures are based on mean kinetic energies. If the density of states in the liquid region increases with energy much more rapidly than that in the solid region, then an increase in energy must shift population from the (warm) solid to the (cold) liquid, making the overall average temperature drop as the total energy increases. Hence the system can exhibit a negative heat capacity under these conditions.

This view of the problem of heat capacities of clusters puts it outside the traditional thermodynamic context for two reasons. First, we introduce a time scale for observation that allows us to distinguish the two coexisting phases. This, however, is in much the same spirit as the widely-used approach of "local thermal equilibrium", in which one can use thermodynamics for regions local in space or time, even though the entire system is out of equilibrium. (Typically, one uses this approach for steady-state flows.) In particular, for the time hierarchy of (10.2) and (10.4), we describe a cluster with two aggregate states as having two different vibrational temperatures. Second, the vibrational temperature does not coincide with the configurational one. This is another kind of separation, again associated with time scale separability, in which two sets of degrees of freedom interact so weakly that it becomes possible to determine their population distributions separately and hence to assign

Table 10.1. Parameters characterizing a range of negative heat capacity of isolated clusters [133] ($^*n$ is the number of atoms)

	LJ_{13}	LJ_{55}	bulk inert gases *	Na_{139}
C_{o}	42	160	$3n$	410
$\Delta T/T_{\mathrm{m}}$	0.18	0.32	0.56	0.21
$\delta T/T_{\mathrm{m}}$	0.08	0.11	$\frac{1.2}{n}\ln n$	0.07
$\ln\left[C_{\mathrm{o}}\Delta T^2/T_{\mathrm{m}}^2\right]$	0.3	2.8	$\ln n$	2.9

each of them its own temperature, provided those distributions correspond to a temperature at all. In reality, the vibrational temperature is assured, in this context, to be associated with a thermal distribution. The distribution of population among configurational states may not actually correspond as closely to a thermal distribution. However we assume here that in the cases we consider, that distribution is close enough to thermal to allow us to assign an effective configurational temperature. Hence it is not appropriate to describe a microcanonical ensemble with two phases in dynamic equilibrium in terms one would use for a system in thermodynamic equilibrium, with a single temperature. The negative heat capacity exhibited in some such systems is a reflection of changes of population distributions, but not of thermodynamic conditions [133, 309].

11

Glassy States of an Ensemble of Bound Atoms

11.1 Glassy State from the Void Standpoint

By "freezing point", sometimes called the "freezing limit", we mean the temperature below which the liquid aggregate state has no thermodynamic stability. This means that at temperatures below the freezing point, the liquid minimum of the free energy, whether Gibbs or Helmholtz, disappears, and whether it is described as a function of the specific volume per atom (Fig. 8.2) or of the void concentration. Therefore relaxation of any atomic distribution below the freezing point leads to formation of the solid aggregate state because this corresponds to the only minimum of the Gibbs free energy. Hence, in the course of relaxation from a highly disordered state, voids must move outside this atomic system. But because void transport occurs either by tunneling or by passage over barriers for which the rate of void displacement is determined by the Arrenius law, the relaxation rate decreases strongly with a temperature decrease. Therefore, voids may be frozen inside the atom system, to produce a disordered metastable state. As a result, we obtain a non-equilibrium system whose relaxation time to the thermodynamically stable state is so long that the metastable state is easy to observe and to study. The lower is the temperature, the longer is the lifetime of the disordered metastable state. For many substances, this state can be perceived and treated as a stable state. This non-stable but long-lived state of an atomic system is a glassy state and will be the next object for our consideration.

Hence, in addition to the melting curve that separates the solid and liquid aggregate states, one can construct the boundary curve that is the limit of liquid metastability at temperatures below the triple point T_{fr}. For atomic systems with short-range interaction, such as condensed inert gases, this boundary corresponds to the freezing point, i. e. on the p–T diagram this corresponds to the line $T = T_{\mathrm{fr}}$ at low to moderate pressures. Beyond this boundary, a supercooled liquid cannot exist as a metastable state despite the long lifetime of this state at low temperatures. In order to categorize this state with the liquid, these states are called by the same term-fluid.

Evidently, an overheated or superheated solid state may also exist, in a restricted temperature range. Indeed, according to [236, 324], a solid above the melting point exhibits an instability due to correlation and coupling of phonons of different frequencies resulting from an increase in the amplitude and anharmonicity of atomic vibrations with increasing temperature. This reduces the energy of vacancy formation and softens the solid. Evidently, this phenomenon of an instability of a superheated solid at temperatures above the melting point restricts the regime of the thermodynamically stable solid aggregate state.

11.2 Diffusion of Voids in a Bulk Ensemble of Atoms

As previously, we envision the formation of the liquid aggregate state as the formation of internal voids, enough to allow the ready mobility and easy change of atomic configuration that we associate with the liquid, in its ability to flow. This allows us to represent the solid–liquid phase transition and its inverse, the freezing transition, as a result of diffusion of voids from the boundaries of an atomic system or to its boundaries. Diffusion of voids consists of elementary acts of void jumps inside the atomic system between neighboring void positions; an elementary void jump is a transition between neighboring local minima of the potential energy surface. Residence of a void in a given local minimum in a glassy system is of course much longer than in a liquid, but voids in a glassy system can diffuse into neighboring local minima of the potential energy surface.

Figure 11.1 [308] shows a change of atomic distribution resulting from one void jump. For a regular solid (Fig. 11.1a), this transition has a simple character because a void corresponds to a perturbed vacancy, a hole in the crystal lattice. In that case, transition of a vacancy between two neighboring sites does not change the distribution of surrounding atoms. But in the case of the liquid state, such a transition is a cooperative process; a change of the position of one atom shifts positions of surrounding atoms. Typically a potential barrier separates possible atomic configurations from one another. Thus, considering the configuration excitations as due to formation of internal voids and describing configurational transitions between neighboring local minima as transport of voids, we go to a general void concept that joins the character of formation of configurational excitations with the dynamics of these excitations as a result of formation and transport of voids.

One can connect the diffusion coefficients of voids and atoms in an atomic system. Indeed, a displacement of an individual atom results from its passage from the region around one minimum to a neighboring well, a displacement of the order of the interatomic distance. The activation energy of this process is the potential barrier that separates neighboring local minima. Correspondingly, the void diffusion coefficient is given by the

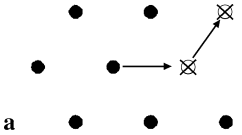

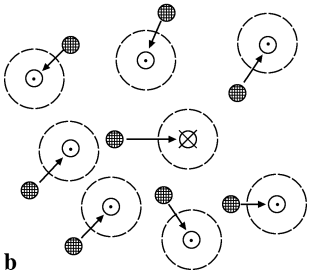

Fig. 11.1. The mechanisms of vacancy displacement in a condensed system of atoms: **a** transition of an individual atom; **b** as a result of collective motion of atoms [308]

formula [308]

$$D_{\mathrm{v}} = d_{\mathrm{o}} \exp\left(-\frac{E_{\mathrm{a}}}{T}\right) , \tag{11.1}$$

where E_{a} is the activation energy of this process. Note that a void displacement leads to simultaneous displacement of atoms, and therefore the diffusion coefficient of voids in the aggregate states is expressed through the self-diffusion coefficient of atoms D_{a} for these aggregate states. This connection has the form

$$|D_{\mathrm{v}} c| = |D_{\mathrm{a}}| . \tag{11.2}$$

It is clear that a displacement of a void is simultaneously the same displacement of an atom in the opposite direction.

Table 11.1 gives the parameters of formula (11.1) for the diffusion coefficient of voids obtained from measured self-diffusion coefficients in solids [325] and liquid inert gases [326–328]. Comparison between the activation energies of the diffusion process of voids and energies of formation of vacan-

Table 11.1. The parameters of diffusion of voids for solid and liquid inert gases [133]

	E_{sol}/D	$E_{\mathrm{sol}}/\varepsilon_{\mathrm{o}}$	d_{sol}, $10^{-4}\,\mathrm{cm}^2/\mathrm{s}$	E_{liq}/D	$E_{\mathrm{liq}}/\varepsilon_{\mathrm{liq}}$	d_{liq}, $10^{-3}\,\mathrm{cm}^2/\mathrm{s}$	$l^2\left\|(\mathrm{d}T/\mathrm{d}t)_{\mathrm{lim}}\right\|$, $10^{-4}\,\mathrm{K}\cdot\mathrm{cm}^2/\mathrm{s}$
Ne	5.3 ± 0.5	0.9 ± 0.1	3	2.7	0.9	2.6	1.4
Ar	6.8 ± 0.7	1.0 ± 0.1	3	2.5	0.8	3.6	11
Kr	5.8 ± 0.5	0.9 ± 0.1	2	2.1	0.7	1.5	16
Xe	6.6 ± 0.4	1.0 ± 0.1	1	2.2	0.7	2.2	22

cies and voids is given also in Table 11.1 for the solid and liquid aggregate states of inert gases and shows the correspondence of these values. Thus, the activation energy of the void diffusion process can be expressed through the energy of vacancy or void formation, whose values are given in Table 11.1.

11.3 Cell Model for Vacancy Diffusion Coefficient

We now estimate the diffusion coefficient of particles or vacancies in a dense ensemble of disks-particles within the framework of the two-dimensional cell model [240, 239, 241]. Transition of particles between cells is shown in Fig. 11.2; each of these is equivalent to a transition of a vacancy in the reverse directions. Hence the diffusion coefficients of particles $D_{\rm p}$ and vacancies $D_{\rm v}$ are connected by a simple relationship

$$D_{\rm p} = c \cdot D_{\rm v} \,, \tag{11.3}$$

because they result from the same process.

We first estimate a typical time for a particle to make a transition to a neighboring cell (see Fig. 11.3). For simplicity, we place a transferring particle-disk in the center of its cell. The transitions are possible along the direction of or very close to the arrow of Fig. 11.3 if a transferring disk does not touch its intervening neighbors in the course of the transition. If a test particle is moving along the direction of the arrow and a neighboring particle occupies a favorable position in its cell e. g. touching the outer edge of the cell's circle, the gap between particles is

$$\Delta = (1 + \sqrt{3})r - 3a \,. \tag{11.4}$$

From this, on the basis of the condition $\Delta > 0$ we obtain the packing density of particle-disks when the diffusion coefficient for particles or vacancies is nonzero, and displacement of vacancies and particles is possible within the

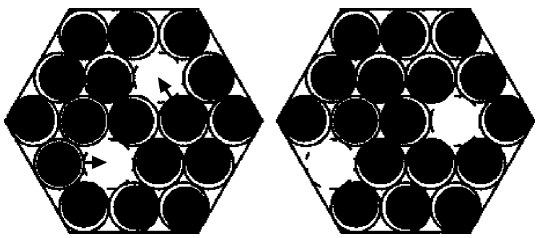

Fig. 11.2. Transition of particles-disks to neighboring positions within the framework of the cell model. The initial configuration of particles is on the *left* and the final configuration is given *right*; the *arrows* indicate the transferring particles [362]

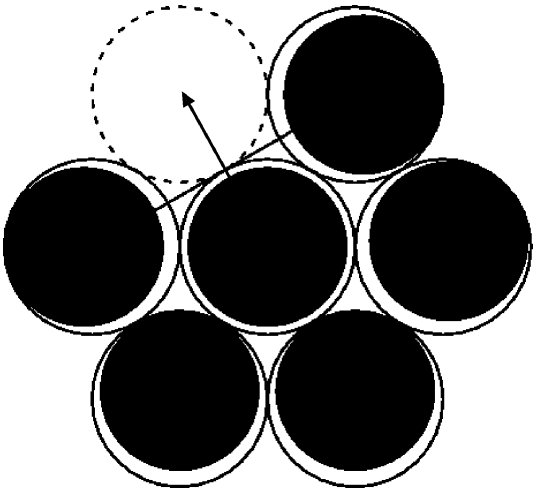

Fig. 11.3. Transition of a particle-disk to a neighboring cell through a line separated neighboring cells. The transition proceeds along an *arrow* or at small angles to it [362]

particle ensemble

$$\varphi < \varphi_{\rm hex} \cdot \left(\frac{1+\sqrt{3}}{3} \right)^2 = 0.75 \, . \tag{11.5}$$

The diffusion process for particles in this ensemble ceases at and above this value of packing parameter.

To estimate the vacancy diffusion coefficient, we assume that transferring particles collide elastically many times with their nearest neighbors as a result of its thermal motion until the angle between its velocity direction and the arrow of Fig. 11.3 falls below a critical angle θ, so that

$$\theta \sim \frac{\Delta}{r} \, . \tag{11.6}$$

Correspondingly, a typical transition time of a test particle to a free neighboring cell is

$$\tau \sim \frac{r-a}{v_{\rm t}} \theta \sim \frac{(r-a)\Delta}{v_{\rm T} r} \, . \tag{11.7}$$

We consider a range of the packing parameter values when $R \sim a$ and $r - a \ll a$. Note that $r - a \approx 0.1a$ at $\Delta = 0$.

From this we obtain an estimate for the vacancy diffusion coefficient in a dense ensemble of particle-disks

$$D_{\rm v} \sim \frac{r^2}{\tau} \sim \frac{a \Delta v_{\rm T}}{r-a} \, . \tag{11.8}$$

Thus the vacancy diffusion coefficient $D_{\rm v} \to 0$ if $\Delta \to 0$.

We again take into account that the disk model for an ensemble of repelling particles represents this ensemble as a dense gas of particles and therefore cannot describe some properties of this system. In particular, this model gives the

general character of particle diffusion within this system, but, apart from the distribution of velocities of the caged particles, does not reveal the temperature dependence for this quantity. We now refine the analysis and estimate this dependence within the framework of the cell model. The diffusion process has an activation character, and the temperature dependence for the diffusion coefficient has the Arrhenius form

$$D_{\rm v} \sim \exp\left(-\frac{E_{\rm a}}{T}\right) , \tag{11.9}$$

where $E_{\rm a}$ is the activation energy, and T is the temperature expressed in energy units.

Let us locate particles in the centers of their cells and determine the activation energy of the diffusion process at this particle configuration. This means that the activation energy is the difference of the interaction energy for a transferring particle located midway between the initial and final positions and the energy in the initial (or final) position. Accounting for interaction of the moving particle with nearest neighbors for initial and final positions we obtain, in this case

$$E_{\rm a} = 2U\left(\frac{r\sqrt{3}}{2}\right) + 4U\left(\frac{r\sqrt{7}}{2}\right) + 2U\left(\frac{3r}{2}\right) - 5U(r) - 2U(r\sqrt{3}0 - U(2r) . \tag{11.10}$$

In particular, approximating the pair interaction potential by the power-law form $U(r) \sim r^{-k}$ and taking $k = 8$, we obtain

$$E_{\rm a} = 0.36U_{\rm o} , \tag{11.11}$$

where $U_{\rm o} = 5U(r)$. Accounting for displacements of particles inside their cells would decrease the barrier energy. Then the diffusion coefficient for vacancies becomes

$$D_{\rm v} \sim \frac{r^2}{\tau} \sim \frac{a\Delta v_{\rm T}}{r-a} . \tag{11.12}$$

It follows from this formula, within the framework of the hard disk model, that the diffusion coefficient of vacancies becomes zero for values of the packing parameter (11.5) or greater, because a high particle density blocks a particle from transfering to a neighboring free cell. Repulsive interaction between particles can reinforce this effect at low temperatures, making diffusion of vacancies and particles cease at even lower densities.

11.4 Kinetics of Transitions Between Aggregate States

The rate voids diffuse determines the rate of transitions between aggregate states. For definiteness, let us consider an ensemble consisting of a plane film of atoms with a thickness l located on a plane substrate. We assume the

film to be macroscopic, i. e. $l \gg a$, where a is a typical distance between atoms. Suppose this film has two aggregate states, solid and liquid; one can control which is the favorable state through the substrate temperature that becomes the temperature of the film. If the temperature drops below the melting point, the film will change from the liquid state to the solid. Since the liquid aggregate state differs from the solid by presence of a significant density of voids inside the ensemble, the transition from the liquid state to the solid occurs by departure of internal voids to the outside of the film, a process realized through void diffusion. Therefore, a typical time of this transition between aggregate states is the relaxation time $\tau_{\rm rel}$ for this film and is given by

$$\tau_{\rm rel} \sim \frac{l^2}{D_{\rm v}} \sim \exp\left(\frac{E_{\rm a}}{T}\right) , \tag{11.13}$$

where $D_{\rm v}$ is the diffusion coefficient of voids, and the temperature dependence for the relaxation is based on formula (11.13).

It is important that the diffusion process has an activation character. This means that this process is slow, and its rate decreases sharply with decreasing temperature. Therefore, if the temperature is lowered fast enough, the liquid state can be frozen in; i. e. voids may remain trapped for arbitrarily long times inside the system when the temperature is well below the melting point. We now analyze the character of this process and find the conditions to form a frozen liquid state at low temperatures [329, 330].

Let us denote by $P_{\rm sol}(t), P_{\rm liq}(t)$ the probabilities that the system be in the solid and liquid states, respectively ($P_{\rm sol} + P_{\rm liq} = 1$) and consider the balance equations for evolution of this system as the temperature decreases. These balance equations have the form

$$\frac{{\rm d}P_{\rm sol}}{{\rm d}t} = -\nu_{\rm sl}P_{\rm sol} + \nu_{\rm ls}P_{\rm liq}, \frac{{\rm d}P_{\rm liq}}{{\rm d}t} = \nu_{\rm sl}P_{\rm sol} - \nu_{\rm ls}P_{\rm liq} , \tag{11.14}$$

where, $\nu_{\rm sl}$ is the rate of transition from the liquid to the solid state, $\nu_{\rm ls}$ is the rate of the reverse transition, and $\nu_{\rm sl} = 1/\tau_{\rm rel}$, where a typical relaxation time is given by formula (11.13). Evidently, the rates of transitions between aggregate states are connected by the principle of detailed balance [61, 80, 306–308]

$$\nu_{\rm sl} = \nu_{\rm ls} \cdot \exp\left(\Delta S - \frac{\Delta E}{T}\right) , \tag{11.15}$$

where ΔS and ΔE are the changes of the entropy and internal energy as a result of the phase transition at a given temperature T where both aggregate states are stable or metastable.

If the rate of temperature variation ${\rm d}T/{\rm d}t$ is small, the left-hand sides of equations (11.14) are relatively small, and the system is very close to equilibrium at any time according to balance equations (10.12), and

$$P_{\rm sol}(t) = w_{\rm sol}[T(t)] , \quad P_{\rm liq}(t) = w_{\rm liq}[T(t)] , \tag{11.16}$$

so the equilibrium probabilities $w_{\rm sol}(T)$, $w_{\rm liq}(T)$ are given by formulas (6.32). In the other limiting case, when a system is cooled rapidly, the probability of transition from the liquid state is small. Then from the set of equations (11.16) it follows that the probability is to conserve the disordered configuration and void concentration associated with the liquid state of the system at temperatures below the melting point $T_{\rm m}$

$$P_{\rm liq} = \exp\left(- \int\limits_{T}^{T_{\rm m}} \nu_{\rm ls}(T) \left(\frac{{\rm d}T}{{\rm d}t} \right)^{-1} {\rm d}T \right) . \tag{11.17}$$

Because of the activation character of transition between aggregate states, in accordance with formula (11.13), we have, for the rate of transition from the liquid state

$$\frac{1}{\tau_{\rm rel}(T_{\rm m})} = \nu_{\rm ls}(T) \sim \exp\left(-\frac{E_{\rm a}}{T} \right) ,$$

and according to formula (10.14) the activation energy of this process corresponds to the barrier energy $E_{\rm b}$. The integral (11.17) is valid if $P_{\rm sol} \ll 1$, and, assuming that the integral (11.17) converges near the melting point $T_{\rm m}$, we obtain this formula in the form

$$P_{\rm liq} = 1 - \frac{T_{\rm m}^2}{E_{\rm a} \frac{{\rm d}T}{{\rm d}t} \tau_{\rm rel}(T_{\rm m})} . \tag{11.18}$$

This formula applies when the system reaches a low temperature $T < T_{\rm m}$, when the transition process is complete. Thus, the transition to the ordered solid state is improbable, and formula (11.18) becomes the applicable one, if the cooling rate satisfies the condition

$$\left| \frac{{\rm d}T}{{\rm d}t} \right| \gg \left| \frac{{\rm d}T}{{\rm d}t} \right|_{\rm lim} = \frac{T_{\rm m}^2}{E_{\rm a} \tau_{\rm rel}(T_{\rm m})} . \tag{11.19}$$

Note that the rates of the direct and inverse processes are equal at the melting point $\nu_{\rm ls}(T_{\rm m}) = \nu_{\rm sl}(T_{\rm m})$. The criterion (11.19) characterizes the possibility of conserving voids inside the sample under conditions of fast cooling. Table 11.1 contains the limiting rates of temperature variation at which a overcooled liquid is formed for inert gases.

11.5 Formation of a Glassy State

Thus, one can obtain an undercooled or supercooled liquid at temperatures below the melting point by fast cooling of the liquid. A configuration of atoms so generated conserves internal voids, to produce an undercooled liquid, a metastable state of the atomic system. Subsequent cooling of this system

below the freezing temperature (see Figs. 8.2, 8.3) makes this state thermodynamically unstable. We call it the glassy state by analogy with properties of glasses. This is strictly an unstable state, but typically with a very long lifetime. For example, the triple point temperature of argon is about 84 K, the freezing temperature is approximately 52 K, and according to formula (11.13) and data of Table 11.1 the rate of relaxation in the course of transition from the triple point to the freezing temperature decreases approximately tenfold. Therefore, in spite of an instability, this glassy state lives very long.

While the glassy state that we discuss here is thermodynamically unstable and cannot correspond to a minimum of the free energy, its frozen configurations nevertheless occur at local minima on the multidimensional *potential energy* surface of the many-body system. It is the passage from one of these minima to another that corresponds to the movement of voids and the corresponding movement of particles. In looking at the system's behavior in terms of its energy, rather than its free energy, we avoid bringing in the entropic contribution to the stability or instability of the state, and focus only on the mechanical behavior of the constituent atoms.

There are two methods to prepare a glassy state of this atomic system whose real examples are inert gases. The first method, just discussed, is realized by fast cooling of the liquid. The second method is deposition of atoms on a surface at a very low temperature. If the deposition is slow and careful, with no heating of the forming sample, the deposited atoms cannot diffuse, and therefore remain where they attach to the surface, presumably in a random fashion, and hence form an amorphous structure that is an analog of a glassy state. This state is also characterized by a very long lifetime and can be converted into the crystal structure, the thermodynamically stable structure, by heating enough to allow diffusion. This method of deposition onto a very cold surface is used, for example, to prepare glassy ice.

Let us consider relaxation of a glassy state resulting from heating, but below the melting point. A glassy state prepared at low temperatures is preserved due to its very long lifetime, but heating can lead to its transition into the ordered solid state, in which atoms form a crystal lattice. This occurs at the glass temperature T_g, the temperature at which the rates of heating and transition into the solid state are equal. Hence according to the above formulas, we obtain the relation

$$\frac{\mathrm{d}T}{\mathrm{d}t} = \frac{T_\mathrm{g}^2}{E_\mathrm{a}\tau_\mathrm{rel}(T_\mathrm{g})} \,. \tag{11.20}$$

11.6 Saturated Vapor Pressure Over a Surface in a Glassy State

There are several methods to distinguish glassy states, i. e. to detect their difference from the thermodynamically stable solid state. Relaxation of a glassy

state leads a change of various parameters of the system, such as its density, heat release, thermal expansion coefficient, dielectric constant and other parameters which depend on the system's structure. Here, we once again use the system of atoms with pairwise interaction to illustrate one particular example, the change of the saturated vapor pressure over the plane surface of a system of bound atoms. Characterizing the degree of configurational excitation of this system of interacting atoms by the concentration of voids, we connect that concentration with the pressure of saturated vapor above the system. The Clausius-Clapeyron equation gives for the saturated vapor pressure above a plane surface

$$p(v,T) = p_{\rm v} \exp\left(-\frac{\varepsilon_{\rm v}}{T}\right) , \tag{11.21}$$

where $\varepsilon_{\rm v}$ is the binding energy of a surface atom, the sublimation energy per atom for a bulk system. This value corresponds to a specific density of voids v for a specific number n of atoms of this system. We assume that the saturated vapor pressures corresponding to any specific concentration of voids v/n are identical at the triple point. That is, the vapor pressure depends on the void concentration and not on the configutation. This gives for the pre-exponential coefficient

$$p_{\rm v} = p_{\rm o} \exp\left(\frac{\varepsilon_{\rm v} - \varepsilon_{\rm sol}}{T_{\rm tr}}\right) , \tag{11.22}$$

where $\varepsilon_{\rm sol}$ is the binding energy per atom for the solid state, $p_{\rm o}$ is the pre-exponential factor in formula (11.21) for the solid, and $T_{\rm tr}$ is the triple point temperature. It follows from this formula that the pre-exponential factor in formula (11.21) drops in magnitude as the relative number of voids increases. Of course, formula (11.22) is correct for the liquid state.

From this we have

$$\frac{p(v,T)}{p_{\rm sol}(T)} = \exp\left[(\varepsilon_{\rm sol} - \varepsilon_{\rm v})\left(\frac{1}{T} - \frac{1}{T_{\rm tr}}\right)\right] , \tag{11.23}$$

where $p_{\rm sol}(T)$ is the saturated vapor pressure over the solid surface at a given temperature. In particular, for the metastable liquid state at a temperature T below the triple point formula (11.23) gives

$$\frac{p_{\rm liq}(T)}{p_{\rm sol}(T)} = \exp\left[\Delta H_{\rm fus}\left(\frac{1}{T} - \frac{1}{T_{\rm tr}}\right)\right] , \tag{11.24}$$

where $\Delta H_{\rm fus}$ is the fusion enthalpy.

Let us consider the transition into the regular solid as a result of heating a glassy state, starting from a low temperature, at which this glassy state has a very long lifetime. If this transition starts at a temperature T_1, finishes at a temperature T_2, and the saturated vapor pressure does not vary significantly in this temperature range, we have from the equation $p(v,T_1) = p_{\rm sol}(T_2)$, and

formulas (11.21) and (11.22),

$$\varepsilon_{\rm v}\left(\frac{1}{T_1}-\frac{1}{T_{\rm tr}}\right)=\varepsilon_{\rm sol}\left(\frac{1}{T_2}-\frac{1}{T_{\rm tr}}\right)\ . \tag{11.25}$$

In particular, Fig. 11.4 contains the experimental dependence of the saturated vapor pressure of amorphous argon which was prepared by deposition of an argon stream on a copper substrate at a temperature of 10 K. (The triple point of bulk argon is $T_{\rm tr}=83.7\,{\rm K}$.) Amorphous argon is formed when deposited on such a surface at low rates, below $3\times10^{-9}\,{\rm cm/s}$. We consider this amorphous structure of argon as glassy, and, according to the data of Fig. 11.2, the transition into the ordered solid state starts at a temperature $T_{\rm g}=20\pm1\,{\rm K}$ and finishes at the temperature $T_2=24\pm1\,{\rm K}$. According to formula (9.15), this corresponds to the ratio between the binding energies of the glassy and solid states $\varepsilon_{\rm v}/\varepsilon_{\rm sol}=0.78\pm0.10$. The ratio of the binding energies of the liquid $\varepsilon_{\rm liq}$ and solid $\varepsilon_{\rm sol}$ states is $\varepsilon_{\rm liq}/\varepsilon_{\rm sol}=0.85\pm0.10$ for rare gases, and is 0.86 ± 0.02 for argon. One can see that the binding energy per atom of the glassy state $\varepsilon_{\rm v}$ that follows from this experiment, coincides with the binding energy per atom $\varepsilon_{\rm liq}$ for the liquid state, within the limits of the accuracy of these data. The liquid state does not exist in the transition temperature range as a metastable aggregate state. (The freezing limit below which the liquid state is not metastable is equal to 52 K for argon). Hence, we deal with the glassy state at such temperatures, even if the concentration of voids for this state coincides with that of the liquid state.

We now consider the heat-induced glassy transition under conditions of Fig. 11.4. In this case an amorphous state of argon is formed at a low temperature by deposition of an atomic flux on a cold target. This unstable amorphous or glassy-like state forms a structure determined by kinetics of the deposition process. However, as we saw, this state has a long lifetime at low temperatures. Increasing the temperature leads to the transition to the stable solid state, as shown in Fig. 11.4. Assuming that a deposited condensed rare gas forms a plane film of depth l on a target, and assuming the rate of the temperature variation ${\rm d}T/{\rm d}t$ to be constant in the transition temperature range, we obtain from formula (11.20), the temperature of the glassy transition

$$T_{\rm g}=\frac{E_{\rm a}}{\ln\left(\frac{d_{\rm o}}{l^2}\frac{T_{\rm g}^2}{E_{\rm a}\frac{{\rm d}T}{{\rm d}t}}\right)}\ , \tag{11.26}$$

where $E_{\rm a}$ is the activation energy of this process.

Applying this formula to the experimental parameters of Fig. 11.4, we find the parameters of the decaying glassy state. Under conditions of Fig. 11.4, a typical film thickness is 10 μm, greater than the distance between nearest neighbors of bulk condensed argon by more than three orders of magnitude. Thus, this film can be considered as bulk condensed argon. A rate of heating ${\rm d}T/{\rm d}t\approx2\,{\rm K/min}$ leads to the glassy transition at $T_{\rm g}=20\pm1\,{\rm K}$. Then on

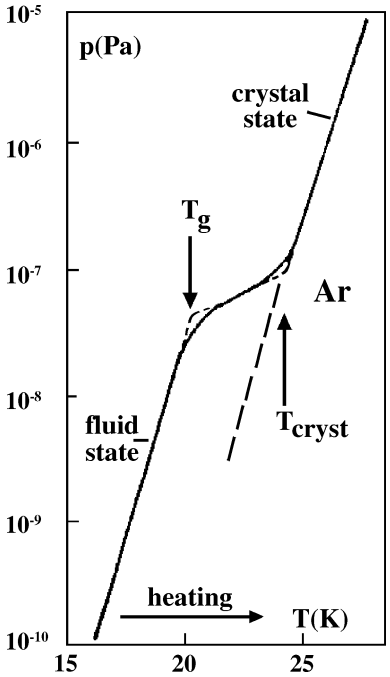

Fig. 11.4. The temperature dependence of the saturated vapor pressure above a heated amorphous argon formed by deposition of the argon flux on a copper substratum at the temperature 10 K [331, 153] referred to the glassy-like and crystalline argon states

the basis of formula (11.25) one can find the binding energy $\varepsilon_{\rm v}$ of an atom in the glassy state. Formula (11.26) gives the activation energy $E_{\rm a}$ of the process of void diffusion which depends sensitively on the void concentration. These parameters are given in Table 11.2.

Next we determine the parameters of the curve of Fig. 11.4, assuming that parameters of the glassy state have the same values as corresponding parameters of the liquid state, i. e. $E_{\rm a} = E_{\rm liq}$, and $\varepsilon(v)$ is the atomic binding energy for the liquid state. The theoretical values of $T_{\rm g}$ and T_{cryst} given in Table 11.2 as well as other theoretical values of this table are calculated under assumption that the glassy state is a frozen liquid state. This comparison demonstrates the identity of the amorphous state of argon obtained by deposition of atoms on a cold target and the glassy-like state that we have described as a frozen liquid state at low temperatures.

Table 11.2. Parameters of the glassy transition under conditions of Fig. 11.4

	$T_{\rm g}$, K	T_{cryst}, K	$E(v)$, K	$\varepsilon_{\rm a}$, K
Experiment [331]	20 ± 1	24 ± 1	730 ± 90	330 ± 20
Theory for liquid [329, 330]	21	23	790	350

11.7 Glassy State for an Ensemble of Repelling Particles

The thermodynamically stable state of a system of repelling classical particles depends on the packing parameter value (Fig. 5.2). Indeed, for values of this parameter above a critical size, $\varphi > \varphi_s = 0.545$, the solid (polycrystalline) aggregate state of this system is thermodynamically stable. In reality, the transition in this state persists to a larger value in metastable, random colloidal solutions, up to $\varphi_d = 0.644$. A typical time of this transition increases dramatically with increasing packing parameter. In particular, a typical time of crystallization of the colloidal solution with PMMA particles at room temperature and $\varphi = 0.619$ lasts almost 1 year under laboratory conditions and shortens up to approximately 4 days under conditions in a spacecraft. This reveals the role of gravitational forces in the crystal state; other effects may also be observed for the glass-solid transition; see, for example [332–334].

Let us suppose that the glassy state of a system of repelling atoms starts from the packing parameter of $\varphi_g = 0.57$–0.58 as follows from the analysis of colloid solutions [177, 176]. Nevertheless, the glassy state is also a form exhibited by hard-sphere systems [335–337] and is identified with the metastable state of the phase diagram of Fig. 5.2 that is generated at low temperatures. This state corresponds to a random spatial distribution, as shown in computer simulation for an ensemble of hard spheres [161], from the analysis of the correlation function Q_6 [338]. The latter is zero for a truly amorphous structure and is not zero if the particle ensemble is composed of individual crystallites. According to these computer simulations [161, 162], this correlation function is zero for the metastable state of the phase diagram of Fig. 5.2.

Let us analyze the glassy state of an ensemble of repelling atoms from a general standpoint, so that at low temperatures and high particle density voids are locked inside the system. Figure 11.5 shows a mean size of voids [162, 339] for the hard-sphere system depending on the packing parameter value; Fig. 11.6 shows the mean distance between nearest-neighbor particles. One can see that when a gap between nearest neighbors becomes small, transitions of voids between neighboring positions takes an activation character, and hence, at low temperatures, the voids are locked between particles. Figure 11.7 also gives the coordination number, the number of nearest neighbors of a test particle at a distance less than a chosen characteristic value. This amorphous character of the particle system is described by an ensemble of plasticine spheres [157, 159].

We note one more peculiarity of the glassy state for the ensemble of repelling particles. We consider the glassy-to-solid transition as a result of voids travelling out of the system, by diffusion. Because the relaxation process is very slow compared to typical oscillation times, under real conditions various other weak interactions and processes can influence the time of this transition. In particular, cooperative phenomena are of importance for relaxation processes in colloidal solutions [179]. As a demonstration of this, Fig. 11.8

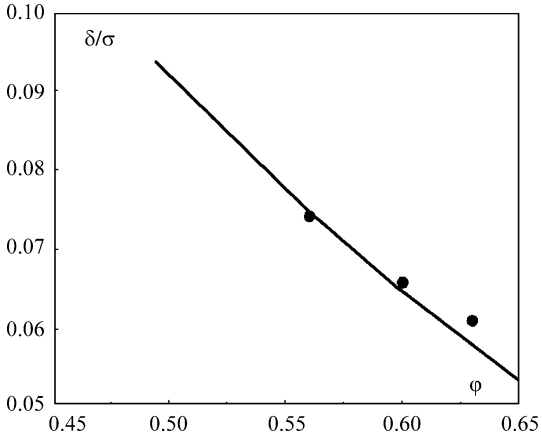

Fig. 11.5. The relative mean size of pores between hard-sphere particles as a function of the packing parameter; (δ is the pore radius, σ is the particle diameter). The *solid curve* corresponds to evaluation [339] and *closed circles* are results of computer simulation [162]

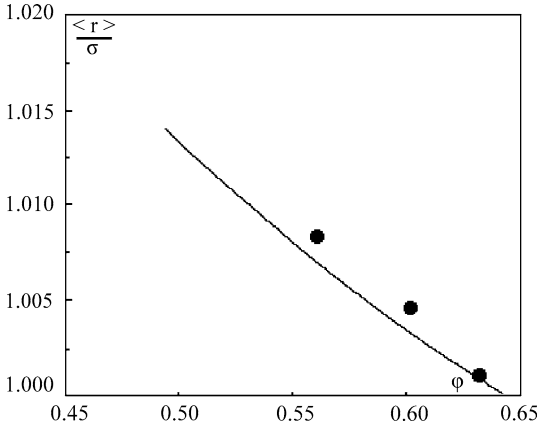

Fig. 11.6. The average distance between nearest neighbors for a system of hard-sphere particles of a diameter σ. The *solid curve* corresponds to evaluation [339] and *closed circles* are results of computer simulation [162]

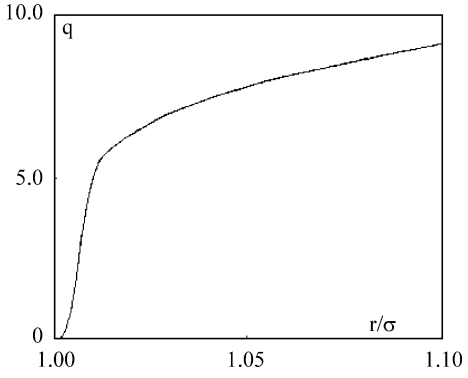

Fig. 11.7. The average number of nearest neighbors whose centers are located in a sphere of an indicated specific radius if this sphere is drawn around a test atom. The *solid curve* corresponds to evaluation [339] and *closed circles* are results of computer simulation [162]

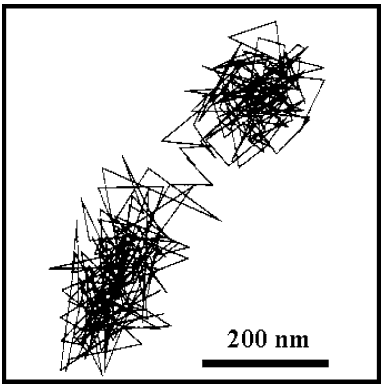

Fig. 11.8. A typical projection for the trajectory of a colloid particle in a colloid solution. The average particle radius is 1.18μ, the packing parameter for colloid particles is $\varphi = 0.56$, and the total observation time is 100 min [179]

represents the trajectory of an individual particle in a colloid. One can see that along with small particle displacements resulting from the random Brownian particle motion, displacements over relatively large distances were also observed in this experiment. The authors attribute them to cooperative phenomena.

Thus, glassy states of colloidal solutions [172, 332, 335, 336] and of ensembles of hard-sphere particles exist at low temperatures and the packing parameter values between $\varphi_{\mathrm{g}} = 0.58$ and $\varphi_{\mathrm{d}} = 0.64$ can be realized due to the activation required to allow void travelling. This possibility also implies something about a specific structure of the system of hard spheres.

11.8 More Peculiarities of Glassy States for Simple Atomic Systems

One peculiarity associated with void concentrations in glasses is best considered from the viewpoint of the different densities of structures for the initial and final states in the glass-to-crystal transition, as voids transport to the system's boundary. Turning now to such simple bulk systems of bound atoms as condensed inert gases, we find that in their disordered, metastable forms there is of course no restructuring of any chemical bonds, but transport of voids not only requires activation, but has another inhibiting factor. The very long lifetimes of glassy states of macroscopic atomic systems is determined not only by the activation required for their relaxation and decay, but also by the large size of a sample compared to a typical atomic size. A void must make many jumps between neighboring positions in order to reach the boundaries and leave the sample. Obviously this latter property plays no role in small clusters. First, a cluster has a restricted number of shells, and a void's pathway to the boundary cannot be long. Second, the simplest configurational excitation of a cluster corresponds to void formation in a surface shell, so that void departure can proceed in one stage. Still, due to the large statistical

weight of a surface void, its displacement along the cluster surface resembles motion by diffusion, as demonstrated in Fig. 11.9. This surface diffusion increases the lifetime of a glassy cluster state [329, 330]. Furthermore in a small system such as a cluster, a large fraction of the possible locations for a void are in or near the outermost layer, so that random diffusion is likely to bring the void to a location where it can leave the system.

One more consideration helps in preparing clusters in glassy states. If we deposit a cluster in a helium atmosphere, as shown in Fig. 7.8b, one can vary the cluster temperature very rapidly. Indeed, a cluster has an interactive surface, so collisions of a cluster with helium atoms which collide also with metallic walls of a thermostat allow one to make rapid changes of cluster temperatures. The rate of the temperature change for a cluster exceeds by several orders of magnitudes that of macroscopic samples. This enhances the ease of formation and observation of the cluster glassy states. This method can be extended by co-depositing many kinds of clusters together with an inert gas onto a surface where the clusters become embedded in an inert matrix.

Just as the small sizes of clusters allowed solid and liquid forms to coexist in thermodynamic equilibrium over a range of temperatures and pressures, exactly the same reasoning tells us that the glassy and regular solid forms of a cluster can coexist in thermodynamic equilibrium *in observable amounts* over a range of conditions. However there is one very important difference between this case and that of the solid and liquid coexistence. In that case, the equilibrium was dynamic, with the system changing phase on a time scale of order of nanoseconds. In the present example of equilibrium of the glassy and ordered solid states, there may well be no interconversion on any observable time scale. Hence, even if both forms are present under conditions that allow them both as thermodynamically stable forms, there is no reason to expect that the ratio of the amounts of the two forms would be that at thermodynamic equilibrium for those specific conditions.

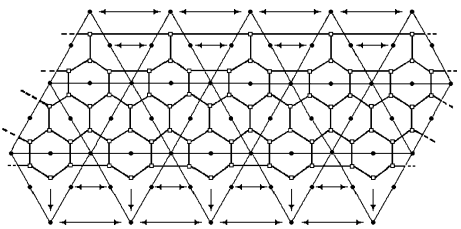

Fig. 11.9. The developed view of the surface of the 55-atom icosahedral cluster with its completed layers. Solid circles are the surface cluster atoms, and the open squares are positions of atoms located on the cluster surface; transitions of these atoms on the cluster surface are shown by solid lines, while boundaries of the surface cluster triangles are denoted by fine solid lines. Arrows show transitions of the last-moving atom into the ground state, and double arrows describe the same atom in the three-dimensional structure; dotted lines indicate transition pathways for the three-dimensional cluster. [329]

One can see an analogy of a glassy state for a macroscopic system of bound atoms and general properties of nonequilibrium systems. We have long considered two kinds of degrees of freedom for the system of bound atoms, those associated with thermal vibrational motion configuration excitation. If transitions between configurationally excited states proceed sufficiently slowly in comparison with typical times of thermal equilibration of vibrations, the vibrational and configurational degrees of freedom decouple, and the degree of configurational excitation of the system does not depend on its temperature. The glassy state is precisely an example of this kind.

This approach is complementary to a more traditional free-volume model, in which detailed attention is directed toward the change in available free volume as a system goes between liquid and glass [340–342]. Here our emphasis is on the change of the kinetics with temperature, specifically on the way reducing temperature inhibits passage over saddles when the free volume remains relatively unchanged. In this sense, this treatment differs in emphasis but is not inconsistent with a model that emphasizes relatively small but perhaps important changes in the volumes of vacancies at the glass transition. It is those local volume changes that correspond to our discussion in connection with Fig. 11.3.

Focusing on simple bulk systems of bound atoms such as condensed inert gases, we find no need to invoke restructuring of chemical bonds in such systems, as apparently takes place in real glasses [153]. Rather, transport of voids proceeds by analogy with conventional glasses, requiring activation [40, 42]. In the case of clusters, cold systems exhibiting a finite number of locally-stable configurationally-excited states formed by transition of atoms from completed cluster shells to the surface conform to the model of a glassy state. This corresponds to formation of surface voids, and annihilation of voids results in transition of atoms from the cluster surface to its outermost, incomplete shell. From the other standpoint, these atomic transitions result from transitions between local minima of the potential energy surface of this cluster which are separated by barriers [40, 42], and these transitions have the activation character. Thus, known excited structures of simple systems of bound atoms conform to the definition of the glassy state. Recognizing that glassy-like states of simple systems are produced by formation of voids, one can analyze these states in considerable detail.

12

Transport of Voids in Nucleation Processes

12.1 Peculiarities of Nucleation Processes

Let us consider an infinite system of identical atomic particles which can form both the solid and the liquid aggregate states, each with its own local minimum of free energy. In particular, in the case of particles with short-range interaction, the partition function or the free energy has extrema as shown in Figs. 8.1 and 8.2. For systems with such interaction, the triple point appears at a relatively low pressure. Hence if we include in our consideration the pressure dependence of thermodynamic parameters, the Gibbs function G is the appropriate state function, rather than the Helmholtz free energy F. In the limit in which the parameters of the system are independent of the pressure, these thermodynamic potentials coincide, $F = G$. Hence, in considering the phase state of this system,we will characterize it by the Gibbs function G or the Gibbs function per particle, μ, the chemical potential. Then of the two states we consider, so long as the chemical potentials are unequal, the truly stable state is that with the lower value, either $\mu_{\rm sol}(T)$ or $\mu_{\rm liq}(T)$; the other aggregate state is metastable. Correspondingly, the melting point $T_{\rm m}$, as we have used this term, satisfies to the relation

$$\mu_{\rm sol}(T_{\rm m}) = \mu_{\rm liq}(T_{\rm m}) \; . \tag{12.1}$$

This is precisely the general condition of coexistence of two bulk phases.

Let us imagine we now vary the temperature or some other parameter that leads to a change of the thermodynamically stable state. For example, we may decrease the temperature below the melting point, so that the stable state changes from the liquid to the solid. Our task now is to understand the nature of this process, for which we shall draw largely on classical thermodynamics. Evidently, this transition starts from formation of small regions of the solid phase that then grow in time. For simplicity, we suppose these regions to be spherical.

We make the plausible assumption that the probability to form a nucleus of a new phase is proportional to $\exp[-G(r,T)/T]$, where G is the Gibbs free

energy function for the nucleus of the new phase, a ball of a radius r. The Gibbs function of this nucleus is

$$G = \Delta\mu n + \Delta\sigma \cdot 4\pi r^2 \,, \tag{12.2}$$

where $\Delta\mu = \mu_{\rm sol}(T) - \mu_{\rm liq}(T)$ is the difference of chemical potentials of the two phases, $n \sim R^3$ is the number of particles in the nucleus, and $\Delta\sigma$ is the difference of surface tensions on the nucleus surface (see Fig. 12.1). We suppose that the parameters of the nucleus depend continuously on its radius or number of particles. This is appropriate for all but very small clusters, for which details of the geometric structure have a strong influence on the cluster's properties. From this expression, it follows that although an infinitely large new phase is formally the thermodynamically stable limit, a new phase must evolve under constraints of surface interactions. Next, we see from its form that the Gibbs function has a maximum as a function of its radius. The value of that radius at the maximum of G is called the critical radius $r_{\rm c}$, where $({\rm d}G/{\rm d}r(r_{\rm c}) = 0$. For the phase transition to proceed beyond that $r_{\rm c}$, the system must overcome a barrier at that critical nuclear size. Consequently the concept of the critical nuclear radius is integral to interpreting the growth of a new phase [93, 345, 344, 346] and the process of the growth of such a nucleus is considered as a nucleation phenomenon [153, 347].

Recall that, within the void concept, the liquid aggregate state differs from the solid by the presence of a significant density of voids. Hence the growth of a solid nucleus within the framework of this model results from transport of voids from a solid nucleus to its environment. This process has an analogy with Ostwald ripening [348] in which nuclei are found in equilibrium with the particles – their constituents, and growth of a new phase occurs by attachment of free particles to large nuclei and, simultaneously, evaporation of small nuclei. This process is important for growth of thin films on a surface [349–355]. It is also analogous to growth of grains of a component in a solid solution [356–358]; in the course of the grain growth, an automodel size distribution of grains is established [352, 359].

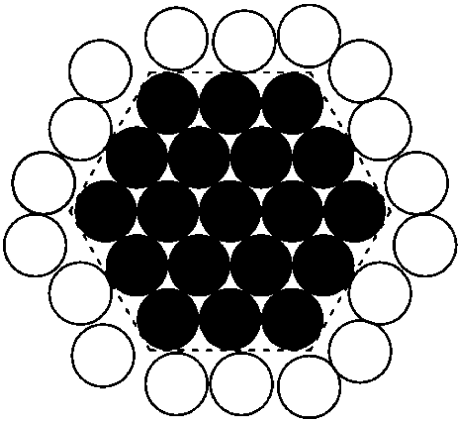

Fig. 12.1. The distribution of particles when a solid nucleus is formed in a liquid with a random distribution of particles in two-dimensional space. This demonstrates the increase of surface energy of a growing nucleus on its boundary

All these processes have a parallel in our representation of the growth of a new phase insofar as they are determined by diffusion of constituents in a dense system. Moreover, during growth of grains in solid solutions, diffusion of nucleating atoms in the solid restricts the rate of the nucleation process. Therefore, in considering the phase transition between the solid and liquid aggregate states of an atomic system as a result of transport of voids, we take into account the experience of the above study. For clarity and simplicity, we now consider the case in which the size of a growing nucleus is much above the critical size.

12.2 Transport of Voids in a Nonuniform Bulk Atomic System

Until now, our model of the glassy state has been based on the assumption that the distribution of atoms is, on average, uniform in space, so that the transition from the glassy state to the ordered solid reduces the effective symmetry from continuous to the periodic symmetry of a lattice and, in so doing, causes all the voids to leave the system. We now consider a non-uniform atomic distribution with a gradient of the void density in a bulk atomic system. Transport of voids tends to bring the system to a stable state with an uniform distribution of atoms and voids. This process can happen during a nucleation process as a new phase grows in a bulk old phase. With this in mind, we first consider transport of voids in a non-uniform bulk atomic system. For definiteness, we treat the case in which the new phase is solid and stable, while the old phase is liquid and metastable.

This problem deals with transport of voids with only a weak non-uniformity and in an external field. Then the void flux is given by

$$j = -D_{\mathrm{v}} N_{\mathrm{a}} \frac{\mathrm{d}c}{\mathrm{d}x} + w N_{\mathrm{a}} c \,. \tag{12.3}$$

Here N_{a} is the number density of atoms, c is the volume fraction of voids (defined as the ratio of the number of voids to the number of atoms in a volume large enough to make this ratio independent of volume), D_{v} is the diffusion coefficient of voids in this system, and w is the drift velocity of voids. We now consider the one-dimensional case; the first term of this formula corresponds to the diffusion flux, and the second characterizes the hydrodynamic flux. The inclusion of the hydrodynamic flux accounts for the effect of the force that results from variation of the void chemical potential. This force compels the ensemble of bound atoms to shrink or stretch depending on the position of the nearest minimum of the free energy, and this causes a displacement of voids until this minimum is reached.

In order to connect the drift velocity and the diffusion coefficient, we note that we cannot use thermodynamic relations for voids (since they are not conserved), although they are valid for atoms, and a void flux in an ensemble

of bound atoms causes an inverse flux for atoms. This leads to a simple relation between the atomic and void transport coefficients. Then from the Einstein relation between the mobility and diffusion coefficient of atoms, we obtain the ratio between transport coefficients of voids at equilibrium, $j = 0$ and $c \sim \exp(-\mu_{\rm v}/T)$, where T is the temperature, and $\mu_{\rm v}$ is the chemical potential of voids, i. e. the difference of the Gibbs free energies per particle for a system with a given number of voids and in the absence of the voids. From an analog of the Einstein relation between the mobility and diffusion coefficient of a void in a gas we obtain

$$w = \frac{D_{\rm v}}{T} F = \frac{D_{\rm v}}{T} \frac{{\rm d}\mu_{\rm v}}{{\rm d}x} \ , \tag{12.4}$$

where F is an effective force that acts on a void, and $\mu_{\rm v}(c)$ is the chemical potential for a void gas, i. e. the free energy of a configurationally excited atomic system per void.

Note that physically, there is only one real atomic chemical potential $\mu_{\rm a}$, the difference of the Gibbs free energies per atom. In introducing the void chemical potential $\mu_{\rm v}$, we must have this connection, really a definition, with the atomic chemical potential:

$$\mu_{\rm a} = c\mu_{\rm v} \ . \tag{12.5}$$

Defined this way, the atomic chemical potential is zero in the absence of voids, i. e. for the perfect solid. This sets the origin of the scale for these potentials, and their values are determined by the density of voids. Ignoring the pressure term in the expression for the Gibbs free energy and taking the chemical potential as the Gibbs free energy per atom relative to that of the solid, we have, for the atomic chemical potential of our system,

$$\mu_{\rm a}(c) = -\frac{T \ln Z}{n} = c \cdot [\varepsilon(c) - Ts(v)] = c \cdot [\varepsilon(c) - T \ln g(c)] \ . \tag{12.6}$$

Here Z is the partition function of the void gas, determined by formula (8.13) for a bulk atom system, $\varepsilon(c)$ is the energy of formation of one void at a given void concentration, $s(c)$ is the entropy of formation of one void, and $g(c)$ is the statistical weight of an individual void. Although we consider a gas of voids, i. e. we suppose the individual voids inside the cluster to be independent, the interaction of voids is taken into account by the dependence of the energy of their formation on the void concentration. At small void concentrations, when they are assumed to be essentially vacancies, we have also $g(c) = 1$. Figure 12.2 contains the dependence of the atomic chemical potential on the void concentration. This dependence is constructed on the basis of formula (12.6) with data from Table 8.1. The maximum value of the chemical potential between the solid and liquid minima, averaged over different inert gases, is $\mu(T_{\rm m}, c_{\rm max}) = 0.15 \pm 0.01$, and $\mu(T_{\rm m}, c_{\rm max})/T_{\rm m} = 0.26 \pm 0.02$, where $c_{\rm max} = 1/12$.

One can solve equation (12.3) $j = {\rm const}$ formally in the one-dimensional case. Let us take the boundary conditions such that for $x < 0$ the system is

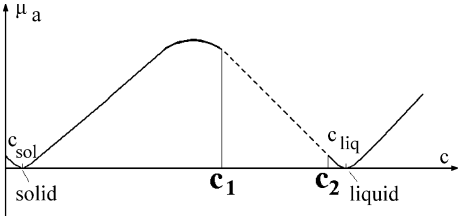

Fig. 12.2. The dependence of the atomic chemical potential $\mu_{\rm a}$ on the void concentration c for a system of bound atoms with a pair interaction between atoms and a void gas inside it. The void concentrations $c_{\rm sol} \approx 0$ and $c_{\rm liq}$ correspond to the solid and liquid aggregate states, the maximum of the chemical potential corresponds to the void concentration $c_{\max}$, and the range between c_1 and c_2 is not stable, i. e. small nonuniformities lead to an instability that separates the system in two phases

solid, and for $x > l$ it is liquid. In an intermediate region $0 < x < l$ the void concentration $c(x)$ varies from $c(0) = 0$ up to $c(l) = c_{\rm liq}$, where $c_{\rm liq}$ is the void concentration for the liquid aggregate state. Then the void flux j inside this system given by formula (12.3) can be represented in the form

$$j = -D_v N \exp\left(\frac{\mu_{\rm v}}{T}\right) \frac{\mathrm{d}}{\mathrm{d}x}\left[c \exp\left(-\frac{\mu_{\rm v}}{T}\right)\right] . \tag{12.7}$$

Because $j = \text{const}$ in a space between planes, this formula can be considered as an equation for $c(x)$. Assuming formally that the chemical potential of voids $\mu_{\rm v}$ depends on c, we obtain the void flux [343]

$$j = -D_v N \cdot \left(1 + \frac{c}{T}\frac{\mathrm{d}\mu_{\rm v}}{\mathrm{d}c}\right) \frac{\mathrm{d}c}{\mathrm{d}x} . \tag{12.8}$$

Solving this equation under the above boundary conditions, we obtain the void flux as

$$j = \frac{N}{l} \int\limits_0^{c_{\rm liq}} D_{\rm a}(c) \cdot \left(1 + \frac{1}{T}\frac{\mathrm{d}\mu_{\rm a}}{\mathrm{d}c}\right) \frac{\mathrm{d}c}{c} , \tag{12.9}$$

where we have reduced the problem to transport of atoms on the basis of formulas (12.4) and (12.5).

One can apply these relations to the problem of growth of a solid phase in a liquid by assuming the nucleus of the new phase to be a spherical cluster. Thus, we have a growing solid cluster of radius $r_{\rm o}$ in a bulk liquid at a temperature T below the melting point, whose growth results from void diffusion. Our task now is to evaluate the rate of this cluster's growth.

Going now from the initial one-dimensional problem to that of the growth of a spherical cluster, we find the total flux of voids J through a sphere of radius r due to diffusion

$$J = 4\pi r^2 j(r) = -4\pi r^2 D_{\rm v} N \frac{\mathrm{d}c}{\mathrm{d}r} , \tag{12.10}$$

a flux independent of r. Now we can reduce this problem to the previous one-dimensional case by a change of variable

$$x = \frac{1}{4\pi r} \, .$$

Then the variable x varies from $x = 0$ for the liquid state up to $x = 1/(4\pi r_{\rm o})$ for the solid state, where $r_{\rm o}$ is the current radius of the growing nucleus, and the void flux according to formula (12.10) is [343]

$$J = 4\pi r_{\rm o} N \int\limits_0^{c_{\rm liq}} D_{\rm a}(c) \cdot \left(1 + \frac{1}{T} \frac{{\rm d}\mu_{\rm a}}{{\rm d}c} \right) \frac{{\rm d}c}{c} \, . \tag{12.11}$$

Thus we formally express the void flux that determines the rate of growth of a new phase inside the old one in terms of thermodynamic and kinetic parameters of the matter where voids are located.

It follows from formula (12.8) that the void concentrations can not be realized if [238, 343]

$$1 + \frac{c}{T} \frac{{\rm d}\mu_{\rm v}}{{\rm d}c} < 0 \, . \tag{12.12}$$

Indeed, at these concentrations, transport of voids would be directed opposite to a void gradient, enhancing growth of the concentration gradient. The critical void concentrations satisfy the relation

$$\left(\frac{{\rm d}\mu_{\rm a}}{{\rm d}c} \right)_{c_{\rm cr}} = -T \, ; \tag{12.13}$$

the values of the critical void concentrations for inert gases are given in Table 12.1. Since continuous variation of void concentration is impossible, a dividing surface forms, to separate the solid and liquid phases as the nucleus grows.

12.3 Growth of a Solid Cluster Inside a Liquid as Transport of Voids

Thus, we reduce the problem of the growth of a solid nucleus in a liquid at a temperature below the melting point to transport of voids away from the growing solid nucleus. A solid nucleus is separated from its surrounding liquid by a dividing surface, as shown in Fig. 12.3. The difference of the atomic chemical potential between these two phases creates a force that drives the atoms with the higher chemical potential to move towards the dividing sphere. Correspondingly, voids move out of this surface. As a result, the spherical dividing surface moves and the solid nucleus grows. Thus, the growth of this new phase does not result in formation of a smooth void gradient over a wide

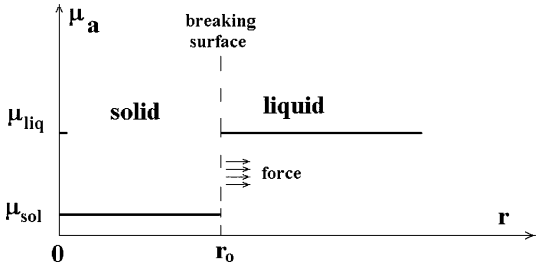

Fig. 12.3. Spatial distribution of the atomic chemical potential. A breaking surface separates the nucleus of the solid phase and a surrounding liquid, and a force acts on atoms of the liquid phase and correspondingly on voids. This force compels atoms to move towards the breaking surface and voids from it, leading to growth of the spherical solid nucleus

space. Rather, a density jump develops at the dividing surface, while the densities of atoms and voids are essentially constant in the solid and liquid regions. Nucleus growth results from an effective force that acts on atoms and voids of a liquid due to a jump of the chemical potential on the breaking surface.

Because of the spherical symmetry of the problem, the force $F(r)$ on atoms or voids of the liquid depends on the distance r from the nucleus center. In addition, this force satisfies the relation

$$\Delta\mu = \mu_{\mathrm{liq}} - \mu_{\mathrm{sol}} = \int\limits_{r_{\mathrm{o}}} F(r)\,\mathrm{d}r \ . \tag{12.14}$$

The values μ_{liq} and μ_{sol} relate to the surface of the growing nucleus, i. e. they take into account surface effects. The requirement that the void or atom flux, integrated over a sphere of a radius r, does not depend on r gives $F(r) \sim r^{-2}$, that leads to the relation for the force $F(r)$ that acts on voids located on a distance r from the nucleus of a radius r_{o}

$$F(r) = \Delta\mu \frac{r_{\mathrm{o}}}{r^2} \ ,$$

and $\Delta\mu$ is the difference of the chemical potentials for the solid and liquid state at the interface. From this, on the basis of formula (12.4), we have for the drift velocity of voids w at a distance r from the nucleus

$$w(r) = \frac{D_{\mathrm{v}}}{T} \Delta\mu \frac{r_{\mathrm{o}}}{r^2} \ , \tag{12.15}$$

and the total flux of voids J through a sphere of radius r due to void drift is equal to

$$J = 4\pi r^2 N_{\mathrm{a}} c w(r) = 4\pi N_{\mathrm{a}} D_{\mathrm{a}} \frac{\Delta\mu}{T} \ . \tag{12.16}$$

Of course, at thermodynamic equilibrium, when $\Delta\mu = 0$, net fluxes of atoms and voids are zero.

On the other hand, one can connect the total void flow from the nucleus J with variation of the radius of the growing nucleus

$$J = 4\pi r_{\rm o}^2 N_{\rm a} c \frac{{\rm d}r_{\rm o}}{{\rm d}t} \ ,$$

so the rate of radius growth in time is

$$\frac{{\rm d}r_{\rm o}}{{\rm d}t} = \frac{D_{\rm liq}}{r_{\rm o}} \frac{(\mu_{\rm liq} - \mu_{\rm sol})}{T} \ . \tag{12.17}$$

Here $r_{\rm o}$ is a current nuclear radius, and $D_{\rm liq}$ is the diffusion coefficient of voids for the liquid state. Thus, in accordance with a general principle of thermodynamics, equality of the atomic chemical potentials is fulfilled at equilibrium conditions on the dividing surface that separates the two phases. In the case considered here, which is not one of equilibrium, the growth of a new phase, this equality is violated, and the difference of the chemical potentials from two sides of the breaking surface creates a force which causes motion of voids and displacement of the breaking surface.

Let us evaluate the rate of growth of the solid nucleus if the temperature T is close to the melting point $T_{\rm m}$. Then we have $\mu_{\rm liq} - \mu_{\rm sol} = (T_{\rm m} - T)s$, where s is the transition entropy per atom, and formula (12.17) gives the time dependence of the change of area of the nucleus [238, 343]

$$\begin{aligned} &\frac{{\rm d}r_{\rm o}^2}{{\rm d}t} = \delta_{\rm sol} \frac{(T_{\rm m} - T)}{T} \exp\left[-\alpha_{\rm sol} \frac{(T_{\rm m} - T)}{D}\right] \ , \\ &\delta_{\rm sol} = \frac{1}{2} D_{\rm liq}(T_{\rm m}) s \ , \quad \alpha_{\rm sol} = \frac{E_{\rm liq} D}{T_{\rm m}^2} \ , \end{aligned} \tag{12.18}$$

and D is the binding energy of two inert gas atoms (see Fig. 1.1). Table 12.1 contains the values of parameters $\delta_{\rm liq}$ and $\alpha_{\rm liq}$ for inert gases.

Thus growth of a solid nucleus inside a liquid results from an effective force induced by a difference between the chemical potentials for the solid and liquid aggregate states. This effective force acts on each void independently

Table 12.1. The parameters of growth of a solid nucleus in liquid inert gases and a liquid nucleus in solid inert gases [238, 343]

	$c_{\rm liq}$	c_1	$\delta_{\rm sol}$, 10^{-5} cm^2/s	$\alpha_{\rm sol}$	$\delta_{\rm liq}$, 10^{-8} cm^2/s	$\alpha_{\rm liq}$
Ne	0.31	0.25	8.2	8.0	$10 \cdot 10^{\pm 0.4}$	16 ± 2
Ar	0.32	0.25	17	7.2	$1 \cdot 10^{\pm 0.5}$	20 ± 2
Kr	0.32	0.26	14	6.3	$3 \cdot 10^{\pm 0.4}$	17 ± 2
Xe	0.31	0.25	17	6.8	$0.4 \cdot 10^{\pm 0.3}$	20 ± 1

and compels it to move from the dividing surface. The rate of growth of the solid nucleus is determined by the friction experienced by the moving voids, with the frictional force expressed through the diffusion coefficient of the voids. This also allows us to analyze the growth of the liquid nucleus in a solid that proceeds by the same scenario as growth of the solid nucleus in a liquid. The rate of increase of the radius of the liquid nucleus inside a solid, by analogy with formula (12.18), is given by [238, 343]

$$\begin{aligned} \frac{\mathrm{d}r_{\mathrm{o}}^2}{\mathrm{d}t} &= \delta_{\mathrm{liq}} \frac{(T_{\mathrm{m}} - T)}{T} \exp\left[-\alpha_{\mathrm{liq}} \frac{(T_{\mathrm{m}} - T)}{D}\right] , \\ \delta_{\mathrm{liq}} &= \frac{1}{2} D_{\mathrm{sol}}(T_{\mathrm{m}}) s , \quad \alpha_{\mathrm{liq}} = \frac{E_{\mathrm{sol}} D}{T_{\mathrm{m}}^2} . \end{aligned} \tag{12.19}$$

For condensed inert gases the parameters of this formula are given in Table 12.1. They are found by the same method as in the previous case. One can see readily that the growth rate for the liquid nucleus is lower than that for the solid because the void diffusion coefficient in solids is lower than that in liquids.

We have been guided by the model of an ensemble of classical particles with short-range interaction, such as condensed inert gases, near their triple point. Then one can neglect the pressure term in the expression for the Gibbs free energy in Table 12.1. Nevertheless, since we have operated in terms of the chemical potentials, and final expressions for the rate of growth of the nucleus (12.18), (12.19) do not contain the void parameters, these expressions may be used for a wider range of conditions. Thus, although we explicitly consider the growth rates for a specific model, considering it as transport of voids in the liquid phase, the rate of growth of the nucleus in formulas (12.18), (12.19) is explicitly in terms of the chemical potentials. Therefore this expression can be used under more general conditions of this process.

12.4 Wave Mechanism of the Phase Transition

Above and below the melting point, only one of the two states, solid or liquid, is stable, whereas the other is metastable. The transition from the metastable state to the stable proceeds through growth of nuclei of a new phase [4, 153, 344, 93, 345], as we just considered. In addition to this mechanism, the transition to a new phase is also possible in the form of a moving wave that propagates the new phase into the old one. This kind of phase transition was observed in a dusty plasma [214]. Here, we examine the conditions under which this form of the phase transition is possible.

In contrast to the nucleation mechanism of growth of a new phase, in this case, due to the large interface dimension, heat processes are important because the phases have very different internal energies, so that there is a large change from the latent heat of the transition, either absorbed or released, in

the transition. We assume that the interface region is narrow and the phase transition to be fast. As a result, adiabatic conditions are fulfilled at the interface. To work with a specific example, in this analysis we examine an overcooled liquid on one side of the breaking or dividing surface and the solid state as a final phase state on the other side. Let T_1 be the temperature of an initial liquid state, that is connected with the temperature T_2 of the final solid state on the breaking boundary by the relation

$$\Delta T = T_2 - T_1 = \frac{\Delta E}{C_\mathrm{o}} \leq T_\mathrm{m} - T_1 \ , \tag{12.20}$$

where ΔE is the transition energy per particle, C_o is the heat capacity per particle, including the contribution of the heat of the transition. Figure 12.4 shows this transition in terms of the caloric curves. Evidently, this phase transition is thermodynamically favorable, if

$$T_2 \leq T_\mathrm{m} \ , \tag{12.21}$$

and

$$\mu_\mathrm{liq}(T_1) \geq \mu_\mathrm{sol}(T_2) \ . \tag{12.22}$$

Here $\mu_\mathrm{liq}(T), \mu_\mathrm{sol}(T)$ are the chemical potentials for the liquid and solid states correspondingly at the temperature T. For simplicity we take the entropy of each phase to be independent of the temperature in the range of the phase transition. Defining the chemical potential with accuracy up to an additive constant, we have

$$\mu_\mathrm{liq}(T) = s_\mathrm{liq}(T - T_\mathrm{m}), \mu_\mathrm{sol}(T) = s_\mathrm{sol}(T - T_\mathrm{m}) \ , \tag{12.23}$$

where T_m is the melting point. From this we obtain the condition for the wave form of the phase transition.

The requirement for the adiabatic character of an interface in the wave mechanism of the phase transition is simply that the final temperature after a fast liquid-solid phase transition must be below the melting point. If this

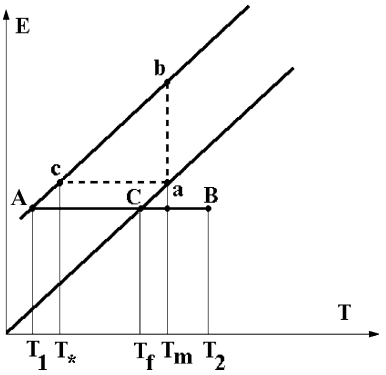

Fig. 12.4. The caloric curves for the liquid (the *upper line*) and solid (the *lower line*) aggregate states. T_m is the melting point; under adiabatical conditions at the wave front, the phase transition proceeds along a *horizontal line* (for example, along a line AB) below the line ab. Hence the temperature of an undercooled liquid at the liquid–solid phase transition is below T_*

condition is not fulfilled, only partial freezing takes place, yielding a final state that is a mixture of liquid and solid regions. Then we have a non-uniform system, so this case is similar to growth of individual nuclei of a new phase within an old one.

One can demonstrate that the ensemble of bound atoms with short-range interaction, such as condensed inert gases near the triple point, cannot satisfy the condition (12.21). Indeed, the melting point $T_{\rm m}$ for these systems in units D, the energy to break one bond, is approximately $0.58D$ [32], while the freezing point, i. e. the temperature below which the liquid state of this system is thermodynamically unstable (the glassy state) is about $0.36D$ [329, 330]. The energy change as a result of the liquid–solid phase transition is $0.98D$ [32] on average for inert gases. So, if we take the maximum heat capacity per atom $C_{\rm o} = 3$, and assume the temperature under consideration significantly exceeds the Debye temperature and adiabatic behavior, formula (12.20) implies a temperature change $\Delta T < 0.33D$, which does not allow the transition from the metastable liquid to the stable solid to bring the final solid temperature below the melting point.

We analyze the validity of this condition for inert gases over a wide range of pressures by using the free energies for the solid and liquid states according to [360] and their parameters according to [76, 361]. Consider the possibility of a wave-like transition from solid to liquid. Figure 12.5 gives the temperature change due to the phase transition for argon as a function of pressure. We see that condition (12.20) is not fulfilled at low pressures. Indeed, the melting point of argon is $T_{\rm m} = 83.4$ and it can exist in a metastable liquid state above the freezing limit, the lower minimum of the spinodal below which the metastable state does not exist, approximately 54 K. Below this temperature it can exist in an unstable glassy state [329, 330], as the previous chapter described. According to Fig. 12.5, for a melting wave form of phase transition, the final state temperature must be above the melting point, and the initial temperature must be below the freezing point. At high pressures, the temperature change becomes small, and the criterion (12.20) may hold.

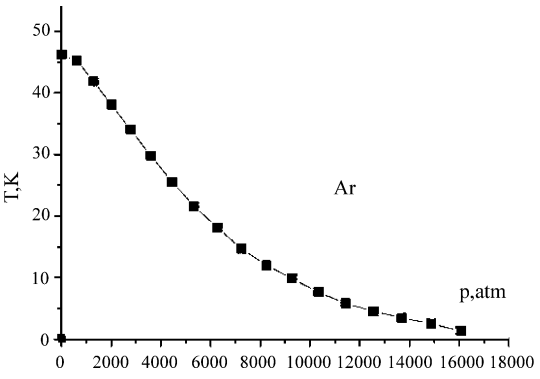

Fig. 12.5. The pressure dependence of the temperature change as a result of the liquid–solid phase transition in argon under adiabatic conditions

On the contrary, the criterion (12.20) is fulfilled for a system of repelling particles, for which we have

$$\Delta T = \frac{T\Delta S - p\Delta V}{C_{\rm o}} \ . \tag{12.24}$$

Here ΔS and ΔV are the jumps of the specific entropy and volume as a result of the phase transition, and in contrast to an ensemble of bound atoms with a short-range interaction near the triple point, the second term of the numerator may be comparable to the first term for a system of repelling particles. In particular, for the system of hard spheres, these two terms are equal, and in this case, as well as for other systems of repelling particles, the temperature change at the phase transition may be small enough to satisfy to the criterion (12.20).

Let us analyze the properties of the interface between two phases which differ by presence or absence of voids. Strictly, due to thermodynamics, the interface is a narrow boundary between regions of the stable and metastable phases. The growth of a stable phase results from motion of this breaking boundary from the stable into the metastable phase. At the microscopic level, we focus on condensed inert gases as the simplest system of atoms with a short-range atomic interaction. The void flux to the breaking surface is given by formulas (12.3), (12.4)

$$j_{\rm v} = -D_{\rm v}\frac{{\rm d}N_{\rm v}}{{\rm d}x} + w_{\rm v}N_{\rm v} = -D_{\rm a}N_{\rm a}\frac{{\rm d}c}{c\,{\rm d}x}\left(1 + \frac{1}{T}\frac{{\rm d}\mu_{\rm a}}{{\rm d}c}\right) \ , \tag{12.25}$$

where we assume that the number density of atoms $N_{\rm a}$ varies in the interface region only due to presence of voids. Formula (12.25) and the dependence of the atomic chemical potential on the void concentration (Fig. 12.2) exhibit an instability [238, 343] according to formula (12.12).

Let us examine the process of void transport. Assuming that the force from the breaking plane ${\rm d}\mu/\,{\rm d}x$ acts over a distance Δx, we obtain for the drift velocity of voids

$$w_{\rm v} = \frac{D_{\rm v}}{T}\frac{\Delta\mu}{\Delta x} = \frac{D_{\rm a}}{cT}\frac{\Delta\mu}{\Delta x} \ , \tag{12.26}$$

that leads to the void flux $j_{\rm v} = N_{\rm v}w_{\rm v}$. This implies that a typical time τ of propagation of the breaking plane over a distance Δx with a number $N_{\rm v}\Delta x$ of voids per unit area is

$$\tau = \frac{cT\Delta x^2}{D_{\rm a}\Delta\mu} \ . \tag{12.27}$$

From this it follows that propagation of the breaking plane corresponds to a diffusion process with an effective diffusion coefficient

$$D_{\rm ef} = \frac{\Delta x^2}{\tau} = D_{\rm a}c\frac{\Delta\mu}{T} \ . \tag{12.28}$$

Introducing a typical width Δx of the interface between solid and liquid regions, we consider some aspects of the phase transition and the character of its

propagation. First, the solid–liquid phase transition in the form of a wave leads to tensions because of the different densities of the solid and liquid aggregate states. This tension is removed due to the acoustic wave that a may be either a compression wave or a rarefication wave. We can suppose that the width of a transition region corresponds roughly to the wavelength for an acoustic wave. Hence, the velocity $v_{\rm ph}$ of the phase transition wave is connected with the width of a transient region Δx

$$v_{\rm ph} \sim \frac{\Delta x}{\tau} \sim \frac{D_{\rm ef}}{\Delta x} \,. \tag{12.29}$$

Since the wavelength of a propagating acoustic wave is of the order of the width of a transient region Δx, one can reduce this relation to the form

$$v_{\rm ph} \sim \frac{D_{\rm ef}\omega}{c_{\rm s}} \,, \tag{12.30}$$

where ω is a typical frequency of the acoustic wave, and $c_{\rm s}$ is the sound speed. It is possible that the parameters of propagating waves may depend on the geometry of the atomic system.

Another transport process from the interface is heat transport. As a result of the phase transition, the temperature varies significantly according to formula (12.20). Heat transport due thermal conductivity is diffusive in character also. A typical time $\tau_{\rm h}$ of this process is

$$\tau_{\rm h} \sim \frac{\Delta x^2}{\chi} \sim \Delta x^2 \frac{c_{\rm p} N_{\rm a}}{\kappa} \,, \tag{12.31}$$

where $\chi = \kappa/(c_{\rm p} N_{\rm a})$ is the thermal diffusivity coefficient, so that $c_{\rm p}$ is the heat capacity per atom for the solid, and $N_{\rm a}$ is the number density of the solid. We have $\chi \gg D_{\rm ef}$ since diffusion of voids requires activation, in contrast to heat transport. Hence, heat from the phase transition can be transported by thermal diffusion through distances longer than the width of the transient region, and then it can be transported outside the atomic system by real acoustic waves.

One can see that the width of the front of the phase transition wave Δx is the principal parameter of this problem that determines both the velocity of this wave and the rates of transport processes. But the value of this parameter does not emerge from the analysis of traditional growth of a new phase because it takes its place in the growth of nuclei for that new phase [133]. This means that this parameter does not result from the character of void transport, but is determined by other parameters of the total system, in particular, by its geometry. Next, according to the character of propagation of the phase transition wave, the transient region is not a uniform region in a transverse direction, but consists of individual elements, and Δx is the curvature of these elements. The solid–liquid and liquid–solid wave transition in the form of a propagating wave was demonstrated [214, 362] for a dusty plasma.

Thus, the phase transition wave propagated in particle systems may be realized under conditions when the heat of the phase transition is relatively small, allowing the wave to generate a stable new phase. This criterion is not fulfilled for classical particles with short-range interaction, in particular, for condensed inert gases near their triple point. On the contrary, for inert gases under high pressure, this form of the phase transition is possible. This general concept was demonstrated by experiments for a dusty plasma [214, 362] in which this form of the phase transition was realized.

13

Conclusion and Summary

In this book, we have examined the characteristics of phase transitions, from the viewpoints of both thermodynamics and kinetics. We have focused on homogeneous systems composed of atoms that interact by relatively short-range forces such as van der Waals forces, so that the rare gas liquids and solids are the systems that best represent what we have studied. The interpretation used throughout is based deeply in the concept of voids in an otherwise dense system, whether ordered or disordered. We have put much emphasis on the relations between bulk systems and small systems, on the differences, similarities and connections between these two forms of matter. The motivation for this approach is the way that small, readily-analyzed systems give insights into their bulk counterparts that do not emerge from looking only at large systems.

The interpretation used throughout rests on the assumption that we can neglect electronic excitation altogether, and consider only the behavior of aggregates of atoms in their ground electronic states. This behavior can then be described in terms of two kinds of excitation and of the corresponding kinds of motion: the local, small-amplitude vibrations and the configurational excitations that lead to changes of the geometric structure of the system. For almost all the phenomena discussed here, these two are different enough in amplitude and frequency that we can consider them quite separately. The vibrational motions equilibrate rapidly enough that we can assign a vibrational temperature to a system while it resides in the region of a single local minimum on its multidimensional potential energy surface. Configurational changes then correspond to passage from the region of one local minimum to another. Hence we envision configurational changes in terms of motion of the system on its potential energy surface (PES). We can describe those configurational changes in terms of the motion of either the real particles or the voids, the "empty spaces" that make such motions possible.

In this approach, a liquid has a significantly higher density of voids than a solid, higher enough to allow the fluidity and lack of specific structure that characterize liquids universally. Hence the liquid has a much higher configu-

rational entropy than the solid. However that is only part of the picture; the vibrational entropy of the liquid is also significantly higher than that of the solid. Both the vibrational and configurational parts contribute to the entropic increase that makes liquids more stable than solids at high temperatures.

The void concept is useful, based as it is on thermodynamic parameters, for describing equilibrium states and passage between them. However it also proves to be a useful device to interpret behavior of metastable and unstable forms, notably glassy states of large systems. The evolution of such systems lends itself to description in term of the formation, decay and transport of voids.

Applying the void concept to systems of identical particles exhibits a variety of their properties despite the relative simplicity of the model. In particular, the labile liquid state ceases to exist below some temperature, the freezing limit. If the liquid state is cooled below this temperature, it need not even be truly metastable, in a thermodynamic sense. In general, the simple systems of interacting identical particles, especially small systems consisting of particles with only nearest neighbors interacting, have a variety of properties that surprise, even amaze us when we first encounter them. But the laws of thermodynamics and kinetics govern them just as validly as they do for our familiar bulk systems. We just have to be prepared to think a little harder about what those laws really tell us, and what conditions and constraints each system presents, in order to understand the surprises.

References

1. R. Brout. *Phase Transitions.* New York, Benjamin, 1965
2. D. Ter Haar, H. Wergeland. *Elements of Thermodynamics.* Reading, Addison-Wesley, 1967
3. C. Kittel, H. Kroemer. *Thermal Physics.* New York, Wiley, 1980
4. L.D. Landau and E.M. Lifshitz. *Statistical Physics.* Vol 1. Oxford, Pergamon Press, 1980
5. K. Stowe. *Introduction to Statistical Physics and Thermodynamics.* New York, Wiley, 1984
6. D. Ter Haar. *Elements of Thermostatics.* New York, Addison-Wesley, 1966
7. R. Kubo. *Thermodynamics.* Amsterdam, North Holland, 1968
8. H. Callen. *Thermodynamics and Intoduction to Thermostatics.* New York, Wiley, 1984
9. J.C Dyre, *Rev. Mod. Phys.* **78**, 953 (2006)
10. O.V. Mazurin. *J. Non-Cryst. Sol.* **25**, 129 (1977)
11. G.W. Scherer. *J. Non-Cryst. Sol.* **123**, 75 (1990)
12. H. Vogel. *Phys. Zs.* **22**, 645 (1921)
13. G.S. Fulcher. *J. Am. Ceram. Soc.* **8**, 339 (1925)
14. G. Tammann, W. Hesse. *Zs. Anorg. All. Chem.* **156**, 245 (1926)
15. G. Tammann. *Der Glaszustand.* (Leipzig, Wiley, Leopold Voss, 1933)
16. R.A. Aziz, M.J. Slaman. *Chem. Phys.* **130**, 187 (1989)
17. R.A. Aziz, M.J. Slaman. *J. Chem. Phys.* **92**, 1030 (1990)
18. A.K. Dham , A.R. Allnatt, W.J. Meath, R.A. Aziz. *Mol. Phys.* **67**, 1291 (1989)
19. A.K. Dham, W.J. Meath, A.R. Allnatt, R.A. Aziz, M.J. Slaman. *Chem. Phys.* **142**, 173 (1990).
20. V.B. Leonas. *Sov. Phys. Usp.* **15**, 266 (1972)
21. R. Eisenschitz, F. London. *Zs. Phys.* **60**, 491 (1930)
22. F. London. *Zs. Phys.* **63**, 245 (1930)
23. F. London. *Zs. Phys. Chem.* **11B**, 222 (1930)
24. F. London. *Trans. Far. Soc.* **33**, 8 (1937)
25. B.M. Smirnov. *Asymptotic Methods in Theory of Atomic Collisions.* Moscow, Atomizdat, 1972
26. B.M. Smirnov. *Physics of Atoms and Ions.* (New York, Springer, 2003)
27. L.A. Sena *Units of Physical Values and Their Dimensionalities* (Moscow, Nauka, 1977)

28. L.I. Sedov. *Methods of Similarity and Dimensionalities.* (Moscow, Nauka, 1972)
29. L.B. Okun'. *Physics of Elementary Particles.* (Moscow, Nauka, 1984)
30. L.D. Landau, E.M. Lifshitz. *Fluid Mechanics* (Oxford, Pergamon Press, 1986)
31. V.P. Krainov. *Qualitative Methods in Physical Kinetics and Gasdynamics* (New York, American Institute of Physics, 1992)
32. B.M. Smirnov. *Phys. Uspekhi* **44**, 1229 (2001)
33. M.R. Hoare, P. Pal. *Adv. Phys.* **20**, 161 (1971); **24**, 645 (1975)
34. M.R. Hoare. *Adv. Chem. Phys.* **40**, 49 (1979)
35. F.H. Stillinger, T.A. Weber. *Phys. Rev.* **25A**, 978 (1982)
36. D.S. Corti, P.G. Debenedetti, S. Sastry, F.H. Stillinger. *Phys. Rev.* **55E**, 5522 (1997)
37. F.H. Stillinger, T.A. Weber. *Phys. Rev.* **28A**, 2408 (1983)
38. D.J. Wales. *Energy Landscapes.* (Cambridge: Cambr. Univ. Press, 2003)
39. K.D. Ball, R.S. Berry. *J. Chem. Phys.* **111**, 2060 (1999)
40. R.S. Berry. In: *Theory of Atomic and Molecular Clusters.*, ed. J. Jellinek (Berlin, Springer, 1999), p. 1–26
41. T. Komatsuzaki, R.S. Berry. *J. Chem. Phys.* **110**, 9160 (1999)
42. D.J. Wales, J.P.K. Doye, M.A. Miller, P.N. Mortenson, T.R. Walsh. *Adv. Chem. Phys.* **115**, 1 (2000)
43. B. Vekhter, K.D. Ball, J. Rose, R.S. Berry. *J. Chem. Phys.* **106**, 4644 (1997)
44. O.M. Becker, M. Karplus, *J. Chem. Phys.* **106**, 1495 (1997)
45. H. Reiss, H.L. Frisch, J.L. Lebowitz. *J. Chem. Phys.* **31**, 369 (1959)
46. B.M. Smirnov. *JETP* **85**, 1010 (1997)
47. B.M. Smirnov. *Phys. Scripta* **58**, 595 (1998)
48. B.M. Smirnov. *Clusters and Small Particles in Gases and Plasmas.* (New York: Springer N.Y., 1999)
49. B.M. Smirnov. *Inorg. Mater.* **35**, 562 (1999)
50. J. Jellinek, T.L. Beck, R.S. Berry. *J. Chem. Phys.* **84**, 2783 (1986)
51. D.J. Wales, R.S. Berry. *J. Chem. Phys.* **92**, 4283 (1990)
52. Ch. Bunn. *Crystals* (New York, Acad. Press, 1964)
53. G. Leibfried. *Gittertheory der Mechanischen und Thermischen Eigenschaften der Kristalle* (Berlin, Springer, 1965) Handbuch VII, Teil 2
54. N.M. Ashcroft, N.D. Mermin. *Solid State Physics.* (New York, Hort, Rinehart and Wilson, 1976)
55. Ch. Kittel. *Introduction to Solid State Physics.* (New York, Wiley, 1986)
56. B.M. Smirnov. *Phys. Uspekhi* **35**, 1052 (1992)
57. L.D. Landau, E.M. Lifshits. *Quantum Mechanics.* (Oxford: Pergamon Press, 1980)
58. B.M. Smirnov. *Phys. Uspekhi* **35**, 37 (1992)
59. B.M. Smirnov. *Phys. Scripta* **52**, 710 (1995)
60. B.M. Smirnov. *High Temp.* **33**, 700 (1995)
61. B.M. Smirnov. *Sov. Phys. Uspekhi* **36**, 933 (1993)
62. J.E. Lennard-Jones. *Proc. Roy. Soc.* **106A**, 636 (1925)
63. J.E. Lennard-Jones, A.E. Ingham. *Proc. Roy. Soc.* **107A**, 463 (1924)
64. U. Fano, L. Fano. *Physics of Atoms and Molecules.* (Chicago, Univ. Chicago Press 1972)
65. P.K. Doye, D.J. Wales, R.S. Berry. *J. Chem. Phys.* **103**, 4234 (1995)
66. T. Kihara, S. Koba. *J. Phys. Soc. Jap.* **7**, 348 (1952)
67. P.M. Morse. *Phys. Rev.* **34**, 57 (1929)

68. R.S. Berry, B.M. Smirnov, A. Yu. Strizhev. *JETF* **85**, 588 (1997)
69. B.M. Smirnov, A. Yu. Strizhev, R.S. Berry. *J. Chem. Phys.* **110**, 7412 (1999)
70. E. Schuberth, M. Creuzburg, W. Müller-Lierheim. *Phys. Stat. Sol.* **76b**, 301 (1976)
71. O. Bostanjonglo, B. Kleinschmidt. *Zs. Phys.* **21a**, 276 (1977)
72. Y. Sonnenblick, E. Alexander, Z.H. Kalman, I.T. Steinberger. *Chem. Phys. Lett.* **52**, 276 (1977)
73. *American Institute of Physics Handbook*, ed. D.E. Gray (New York, McGrow Hill, 1971)
74. A.J. Moses. *The Practicing Scientists Book.* (New York, Van Nostrand, 1978)
75. R.C. Reid, J.M. Prausnitz , B.E. Poling. *The Properties of Gases and Liquids,* 4 Edition (New York, McGraw Hill, 1987)
76. V.A. Rabinovich. *Thermophysical Properties of Neon, Argon, Krypton and Xenon* (New York, Hemishere, 1987)
77. J. Emsley. *The Elements.* 2 Edition. (Oxford, Clardon Press, 1991)
78. I. Barin. *Thermophysical Data of Pure Substances* (New York, VCH Publishers, 1993)
79. *Handbook of Chemistry and Physics*, edition 86, ed. D.R. Lide (London, CRC Press, 2003–2004)
80. B.M. Smirnov. *Phys. Uspekhi* **37**, 1079 (1994)
81. F.E. Simon, G. Glatzel. *Zs. Anorg. Allgem. Chem.* **178**, 309 (1929)
82. V.N. Zharkov, V.A. Kalinin. *The State Equatuions of Solids at High Pressures and Temperatures* (Moscow, Nauka, 1968)
83. D.A. Kofke. *J. Chem. Phys.* **98**, 4149 (1993)
84. H. Schilling. *Statistische Physik in Beispielen* (Leipzig, VEB Fachbuchverlag, 1972)
85. V.P. Skripov. *Equations of States of Gases and Liquids.* (Moscow, Nauka, 1975)
86. D.V. Sivukhin. *General Course of Physics. vol. II. Thermodynamics and Molecular Physics* (Moscow, Nauka, 1975)
87. J.P. Hansen, I.R. McDonald. *Theory of Simple Liquids.* (London, Academic Press, 1986)
88. D. Stauffer, H.E. Stanley. *From Newton to Mandelbrot* (Berlin, Springer, 1990)
89. J.O. Hirschfelder, Ch.F. Curtiss, R.B. Bird. *Molecular Theory of Gases and Liquids* (New York, Wiley, 1954)
90. G.G. Chernyi, S.A. Losev (Ed). *Physical-Chemical Processes in Gas Dynamics. Reference Book.* (Moscow, Mosc. Univ. Press, 2002)
91. T. Andrews. *Phil. Trans. Roy. Soc.* **159**, 575 (1869)
92. M.A. Leontovich. *Introduction to Thermodynamics. Statistical Physics* (Moscow, Nauka, 1983)
93. Ya.I. Frenkel. *Theory of Liquids.* (Oxford, Oxford Uni.Press, 1946)
94. I.Z. Fisher. *Statistical Theory of Liquids* (Chicago, Univ.Chicago, 1966)
95. P.A. Egelstaff. *An Introduction to the Liquid State.* (Oxford, Pergamon Press, 1967)
96. E. Stanley. *Introduction to Phase Transitions and Critical Phenomena* (New York, Oxford Univ. Press, 1971)
97. A.R. Ubbelohde. *The Molten State of Matter.* (Chicester, Wiley, 1978)
98. C. Domb. *The Critical Point* (London, Taylor and Francis, 1996)
99. J.A. Barker, D. Henderson. *Rev. Mod. Phys.* **48**, 587 (1976)
100. G.A. Martynov. *Fundamental Theory of Liquids* (Bristol, Adam Hilger, 1992)

101. R.E. Honig, H.O. Hook. *RCA Review* **21**, 360 (1960)
102. N.B. Vargaftic. *Tables of Thermophysical Properties of Liquids and Gases.* 2 Edition (New York, Wiley, 1975)
103. A.I. Rusanov. *Phase Equilibria and Surface Phenomena* (Leningrad, Khimiya, 1967)
104. J.S. Rowlinson, B. Widom. *Molecular Theory of Capillarity* (Oxford, Claredon Press, 1982)
105. V.G. Baidakov. *Reviews of Thermophysical Properties of Substances* (Moscow, IVTAN, 1988; N69)
106. V.G. Baidakov. *Interface of Simple Classical and Quantum Liquids* (Ekaterienburg, Nauka, 1994)
107. S. Ino. *J. Phys. Soc. Japan* **27** 941 (1969)
108. V.S. Vorob'ev, A.V. Eletskii. *Chem. Phys. Lett.* **254**, 263 (1996)
109. H.W. Kroto e.a. *Nature* **318**, 162 (1985)
110. H.W. Kroto. *Science* **242**, 1139 (1988)
111. O. Echt, K. Sattler, E. Recknagel. *Phys. Rev. Lett.* **94**, 54 (1981)
112. O. Echt e.a. *Ber. Bunsenges. Phys. Chem.* **86,** 860 (1982)
113. A. Ding, J. Hesslich. *Chem. Phys. Lett.* **94**, 54 (1983)
114. I.A. Harris, R.S. Kidwell, J.A. Northby. *Phys. Rev. Lett.* **53**, 2390 (1984)
115. J.C. Phillips, *Chem. Rev.* **86**, 619 (1986)
116. I.A. Harris, K.A. Norman, R.V. Mulkern, J.A. Northby. *Chem. Phys. Lett.* **130**, 316 (1986)
117. W. Miehle, O. Kandler, T. Leisner, O. Echt, *J. Chem. Phys.* **91**, 5940 (1989)
118. J. Farges, M.F. de Feraudy, B. Raoult, G. Torchet. *Surf. Sci.* **106**, 95 (1981)
119. S.S. Kim, G.D. Stein, *J. Colloid. Interface Sci.* **87**, 180 (1982)
120. J. Farges, M.F. de Feraudy, B. Raoult, G. Torchet. *J. Chem. Phys.* **78**, 5067 (1983)
121. J. Farges, M.F. de Feraudy, B. Raoult, G. Torchet. *J. Chem. Phys.* **84**, 3491 (1986)
122. J.W. Lee, G.D. Stein. *J. Phys. Chem.* **91**, 2450 (1987)
123. J. Farges, M.F. de Feraudy, B. Raoult, G. Torchet. *Adv. Chem. Phys.* **70**, 45 (1988)
124. L.S. Bartell, *Chem. Phys.* **86**, 491 (1986)
125. B.W. Van de Waal. *J. Chem. Phys.* **98**, 4909 (1993)
126. D.C. Easter, M.S. El-Shall, M.Y. Hahn, R.L. Whetten. *Chem. Phys. Lett.* **157**, 277 (1989)
127. D.C. Easter, R.L. Whetten, J.E. Wessel. *J. Chem. Phys.* **94**, 3347 (1991)
128. S.M. Beck, J.H. Hecht. *J. Chem. Phys.* **96**, 1975 (1992)
129. T.P. Martin, U.Näher, H. Schaber, U. Zimmermann. *J. Chem. Phys.* **100**, 2322 (1994)
130. T.P. Martin. *Phys. Rep.* **273**, 199 (1996)
131. T.P. Martin e.a. *Chem. Phys. Lett.* **176**, 343 (1991)
132. S.W. Wang, L.M. Falicov, W. Searcy. *Surf. Sci.* **143**, 609 (1984)
133. R.S. Berry, B.M. Smirnov. *Phys. Uspekhi* **48**, 331 (2005)
134. B.M. Smirnov. *J. Exp. Theor. Phys.* **80**, 1151 (1995)
135. B. Raoult, J. Farges, M.F. de Feraudy, G. Torchet. *Philos. Mag.* **B60**, 881 (1989)
136. B.M. Smirnov. *Phys. Scripta* **51**, 402 (1995)
137. A.L. Mackay. *Acta Crystallogr.* **15**, 916 (1962)

138. B.M. Smirnov. *Chem. Phys. Lett.* **232**, 395 (1995)
139. J.A. Northby. *J. Chem. Phys.* **87**, 6166 (1987)
140. B.W. Van de Waal. *J. Chem. Phys.* **90**, 3407 (1989)
141. J.A. Northby, J. Xie, D.L. Freeman, J.P. Doll. *Z. Phys.* **D 12**, 69 (1989)
142. J. Xie, J.A. Northby, D.L. Freeman, J.P. Doll. *J. Chem. Phys.* **91**, 612 (1989)
143. R.S. Berry, B.M. Smirnov. *JETP* **90**, 491 (2000)
144. R.S. Berry, B.M. Smirnov. *J. Chem. Phys.* **113**, 728 (2000)
145. J.D. Bryngelson, J.N. Onuchic, N.D. Socci, P.G. Wolynes. *Proteins.* **21**, 167 (1995)
146. J.P.K. Doye, D.J. Wales. *J. Phys.* **29B**, 4859 (1996)
147. D.J. Wales, H.A. Scheraga. *Science.* **285**, 1368 (1999)
148. D.R. Jennison, P.A. Schultz, M.P Sears. *J. Chem. Phys.* **106**, 1856 (1997)
149. B.W. Van de Waal. *Zs. Phys.* **20D**, 349 (1991)
150. B.J. Alder, T.E. Wainwright. *J. Chem. Phys.* **27**, 208 (1957)
151. W.G. Hoover, S.G. Gray, K.W. Johnson. *J. Chem. Phys.* **55**, 128 (1971)
152. S.M. Stishov. *Sov. Phys. Uspekhi* **17**, 625 (1974)
153. I. Gutzow, J. Schmelzer. *The Vitreous State.* (Berlin: Springer, 1995)
154. K.A. Goettel e.a. *Phys. Rev. Lett.* **62**, 665 (1989)
155. R. Reichlin e.a. *Phys. Rev. Lett.* **62**, 669 (1989)
156. M.I. Eremets. *Phys. Rev. Lett.* **85**, 2797 (2000)
157. J.D. Bernal. *Nature* **183**, 141 (1959)
158. G.D. Scott. *Nature* **178**, 908 (1960)
159. J.D. Bernal, J. Mason. *Nature* **188**, 908 (1964)
160. W.G. Hoover, F.H. Ree. *J. Chem. Phys.* **49**, 3609 (1968)
161. M.D. Rintoul, S. Torquato. *Phys. Rev. Lett.* **77**, 4198 (1996)
162. M.D. Rintoul, S. Torquato. *Phys. Rev.* **58E**, 533 (1998)
163. R. Boehler, M. Ross, P. Soderlind, D. Boercker. *Phys. Rev. Lett.* **86**, 5731 (2001)
164. A.P. Jephcoat e.a. *Phys. Rev. Lett.* **59**, 2670 (1987)
165. H. Cynn e.a. *Phys. Rev. Lett.* **86**, 4552 (2001)
166. B.M. Smirnov. *Statistical Physics and Physical Kinetics of Atomic Systems.* (Moscow: IVTRAN, 2001)
167. B.M. Smirnov. *Physics of Ionized Gases.* (New York: Wiley, 2001)
168. Z.W. Salsburg, W.W. Wood. *J. Chem. Phys.* **37**, 798 (1962)
169. W.G. Hoover, *J. Chem. Phys.* **44**, 221 (1966)
170. B.J. Alder, W.G. Hoover, D.A. Young. *J. Chem. Phys.* **49**, 3688 (1968)
171. H. Reiss, A.D. Hammerich. *J. Phys. Chem.* **90**, 6252 (1986)
172. L.V. Woodcock. *J. Chem. Soc. Faraday II* **72**, 1667 (1976)
173. L. Antl e.a. *Colloid Surf.* **17**, 67 (1986)
174. C. Pathmamanohavan, C. Slob, H.N.W. Lekkerkerker. *Colloid Polymer Sci.* **267**, 448 (1989)
175. S.E. Phan e.a. *Phys. Rev.* **54E**, 6633 (1996)
176. W.K. Kegel, A. van Blaaderen. *Science* **287**, 290 (2000)
177. P.N. Pusey e.a. *Phys. Rev. Lett.* **63**, 2753 (1989)
178. J. Zhu e.a. *Nature* **387**, 883 (1997)
179. E.R. Weeks e.a. *Science* **287**, 627 (2000)
180. U. Gasser e.a. *Science* **292**, 258 (2001)
181. P.N. Pusey, W. van Mengen. *Nature* **320**, 340 (1986)
182. P.N. Pusey, W. van Mengen. *Phys. Rev. Lett.* **59**, 2083 (1987)

183. J.K.G. Dhout, C. Smits, H.N.W. Lekkerkerker. *J. Colloid Interface Sci.* **152**, 386 (1992)
184. D.W. Marr, A.P. Gast. *Langmuir* **10**, 1348 (1994)
185. R.L. Davidchack, B.B. Laird. *Phys. Rev. Lett.* **287**, 627 (2000)
186. K. Schätzel, B. Ackerson. *Phys. Rev.* **48E**, 3766 (1993)
187. J.R. Harland, W. Van-Megen. *Phys. Rev.* **55E**, 3054 (1997)
188. S. Auer, D. Frenkel. *Nature* **409**, 1020 (2001)
189. J.G. Berryman. *Phys. Rev.* **27A**, 1053 (1983)
190. D. Frenkel, A.J.C. Ladd. *J. Chem. Phys.* **81**, 3188 (1984)
191. J.L. Colot, M. Baus. *Mol. Phys.* **56**, 807 (1985)
192. F. Ignoi. *J. Phys.* **19C**, 6907 (1986)
193. R.G. Bolhuis, D. Frenkel, S.C. Mau, D.A. Huse. *Nature* **388**, 235 (1997)
194. C. Radin, L. Sadun. *Phys. Rev. Lett.* **94**, 015502 (2005)
195. S. Pronk, D. Frenkel. *J. Chem. Phys.* **110**, 4589 (1999)
196. S.C. Mau, D.A. Huse. *Phys. Rev.* **59E**, 4396 (1999)
197. D.A. Weitz, M. Oliveria. *Phys. Rev. Lett.* **52**, 1433 (1984)
198. D.A. Weitz e.a. *Phys. Rev. Lett.* **53**, 1657 (1984)
199. D.A. Weitz e.a. *Phys. Rev. Lett.* **54**, 1416 (1985)
200. K.D. Keefer, D.W. Schaefer. *Phys. Rev. Lett.* **56**, 2376 (1986)
201. S. Aubert, D.S. Cannell. *Phys. Rev. Lett.* **56**, 738 (1986)
202. P. Dimon e.a. *Phys. Rev. Lett.* **57**, 595 (1986)
203. J.P. Wilcoxon, J.E. Martin, D.W. Schaefer. *Phys. Rev.* **39A**, 3112 (1989)
204. R.S. Berry, B.M. Smirnov. *Phys. Rev.* **71B**, 051510 (2005)
205. J.H. Chu, I. Lin. *Phys. Rev. Lett.* **72**, 4009 (1994)
206. H. Thomas, G.E. Morfill, V. Demmel, J. Goree, B. Feuerbacher, D. Möhlmann. *Phys. Rev. Lett.* **73**, 652 (1994)
207. Y. Hayashi, K. Tachibana, *Japan J. Appl. Phys.* **33**, L804 (1994)
208. A. Melzer, T. Trottenberg, A. Piel. *Phys. Lett.* **A191**, 301 (1994)
209. V.N. Tsytovich. *Phys. Uspekhi.* **40**, 53 (1997)
210. A.P. Nefedov, O.F. Petrov, V.E. Fortov. *Phys. Uspekhi* **40**, 1163 (1997)
211. G.E. Morfill, H.M. Thomas, U. Konopka, M. Zuzic. *Phys. Plasma* **6**, 1 (1999)
212. P.K. Shukla, A.A. Mamun. *Introduction to Dusty Plasma Physics.* (Bristol: IOP Publ., 2001)
213. V.E. Fortov e.a. *Phys. Uspekhi* **47**, 447 (2004)
214. G.E. Morfill e.a. *Phys. Scripta* **T107**, 59 (2004)
215. K. Ishimaru. *Phys. Rep.* **34**, 1 (1982)
216. K. Kremer, M.O. Robbins, G.J. Grest. *Phys. Rev. Lett.* **57**, 2694 (1986)
217. E.J. Meijer, D. Frenkel. *J. Chem. Phys.* **94**, 2269 (1991)
218. V.E. Fortov, I.T. Yakubov. *Nonideal Plasma.* (Moscow: Energoatomizdat, 1994)
219. S. Hamaguchi, R.T. Farouki, D.H.E. Dubin. *Phys. Rev.* **56E**, 4671 (1997)
220. O. Vaulina, S. Khrapak, G. Morfill. *Phys. Rev.* **66E**, 016404 (2002)
221. S.A. Khrapak e.a. *Phys. Rev.* **E66**, 016414 (2002)
222. A.B. Belonoshko, R. Ahuja, B. Johansson. *Phys. Rev. Lett.* **87**, 165505 (2001)
223. W. Van Vitzenburg, J.C. Stryland. *Canad. J. Phys.* **46**, 811 (1968)
224. R.K. Crawford, W.B. Daniels. *Phys. Rev. Lett.* **21**, 367 (1968)
225. S.M. Stishov, V.I. Fedosimov. *Pis'ma ZhETF* 14, 326 (1971)
226. V.M. Cheng, W.B. Daniels, R.K. Crawford. *Phys. Lett.* **43A**, 109 (1973)
227. C.S. Zha, R.S. Berry, B.M. Smirnov, *Phys. Rev.* **71B**, 144105 (2005)

228. A.P. Jephcoat, S. Beresin. *Proc. US-Japan Conf. Mineral Physics.* (Washington, 1997)
229. J.A. Barker. *Lattice Theories of the Liquid State.* (New York, Macmillan, 1963)
230. R. Kubo. *Statistical Mechanics.* (Amsterdam, North Holland, 1965)
231. R.P. Feynman. *Statistical Mechanics* (Massachusetts, Benjamin Inc., 1972)
232. J.M. Ziman. *Models of Disorder.* (Cambridge, Cambridge Univ. Press, 1979)
233. W. Bragg, H.J. Williams. *Proc. Roy. Soc.* **A145**, 699 (1934)
234. W. Bragg, H.J. Williams. *Proc. Roy. Soc.* **A150**, 552 (1935)
235. R.S. Berry, B.M. Smirnov. *J. Chem. Phys.* **114**, 6816 (2001)
236. A.I. Karasevskii, V.V. Lubashenko. *Phys. Stat. Sol.* **B194**, 483 (1996)
237. R.S. Berry, B.M. Smirnov. *J. Non-Cryst. Sol.* **351**, 1543 (2005)
238. R.S. Berry, B.M. Smirnov. In: *Nucleation Theory and Applications.* Ed. J.W.P. Schmelzer, G.Röpke and V.B. Priezzhev (Dubna, JINR, 2005). pp. 82–101
239. J.G. Kirkwood. *J. Chem. Phys.* **18**, 380 (1950)
240. W.G. Hoover, F.H. Ree. *J. Chem. Phys.* **49**, 3609 (1968)
241. C.H. Bennet, B.J. Alder. *J. Chem. Phys.* **54**, 4796 (1971)
242. K.D. Ball, R.S. Berry, R.E. Kunz, F.-Y. Lin, A. Proykova, D.J. Wales. *Science* **271** 963 (1996)
243. G. Cox, R.S. Berry, R.L. Johnston. *J. Phys. Chem. A* **110**, 11543 (2006)
244. M. Schmidt, R. Kusche, W. Kronmüller, B. von Issendorf, H. Haberland. *Phys. Rev. Lett.* **79**, 99 (1997)
245. M. Schmidt, R. Kusche, B. von Issendorf, H. Haberland. *Nature* **393**, 238 (1998)
246. R.S. Berry, J. Jellinek, G. Natanson. *Phys. Rev.* **30A**, 919 (1984)
247. R.S. Berry, T.L. Beck, H.L. Davis, J. Jellinek. *Adv. Chem. Phys.* **90**, 75 (1988)
248. R.S. Berry. *Chem. Rev.* **93**, 2379 (1993)
249. B.M. Smirnov. *Phys. Scripta* **50**, 427 (1994)
250. S.N. Khanna, P. Jena. *Phys. Rev. Lett.* **69**, 1664 (1992)
251. A. Rytkonen, S. Valkealahti, M. Manninen. *J. Chem. Phys.* **106**, 1888 (1997)
252. R.E. Kunz, R.S. Berry. *Phys. Rev. Lett.* **71**, 3987 (1993)
253. R.E. Kunz, R.S. Berry. *Phys. Rev.* **49E**, 1895 (1994)
254. J. Harms, J.P. Toennies, F. Dalfovo. *Phys. Rev.* **58B**, 3341 (1998)
255. J. Harms, J.P. Toennies. *Phys. Rev.* **63B**, 184513 (2001)
256. J.W.M. Frenken, J.F van der Veen. *Phys. Rev. Lett.* **54**, 134 (1985)
257. G. Natanson, F. Amar, R.S. Berry. *J. Chem. Phys.* **78**, 399 (1983)
258. J. Jellinek, T.L. Beck, R.S. Berry. *Chem. Phys. Lett.* **107**, 227 (1984)
259. H. Davis, J. Jellinek, R.S. Berry. *J. Chem. Phys.* **86**, 6456 (1987)
260. D.J. Wales. *Chem. Phys. Lett.* **166**, 419 (1990)
261. P.A. Braier, R.S. Berry, D.J. Wales. *J. Chem. Phys.* **93**, 8745 (1990)
262. H.-P. Cheng, R.S. Berry. *Mat. Res. Soc. Symp. Proc.* **206**, 241 (1991)
263. H.-P. Cheng, R.S. Berry. *Phys. Rev.* **A45**, 7969 (1992)
264. P. Labastie, R.L. Whetten. *Phys. Rev. Lett.* **65**, 1567 (1990)
265. J.P.K. Doye, D.J. Wales. *J. Chem. Phys.* **102**, 9659 (1995)
266. R.S. Berry, B.M. Smirnov. *JETP* **93**, 541 (2001)
267. Z.X. Cai, S.D. Mahanti, A. Antonelli, S.N. Khanna, P. Jena. *Phys. Rev.* **46B**, 7841 (1992)
268. W.N. Lipscomb. *Science.* **153**, 373 (1966)
269. R.B. King. *Inorg. Chim. Acta.* **49**, 237 (1981)

270. B.F.J. Jonston. *Chem. Soc. Chem. Comm.* 27 (1986)
271. D.J. Wales. *Phys. Chem.* **91**, 7002 (1989)
272. R.S. Berry, B.M. Smirnov. *JETP* **100**, 1129 (2005)
273. R.S. Berry, B.M. Smirnov. In: *Nucleation Theory and Applications.* Ed. J.W.P. Schmelzer, G. Röpke and V.B. Priezzhev (Dubna, JINR, 2002). pp. 340–366
274. B.M. Smirnov. In: *Nucleation Theory and Applications*, Ed. J.W.P. Schmelzer, G. Röpke and V.B. Priezzhev (Dubna, JINR, 1999). pp. 355–367
275. W. Eitel. *The Physical Properties of Silicates.* (Chicago, University of Chicago Press, 1954)
276. A. Bondi. *Physical Properties of Molecular Crystals, Liquids and Glasses.* (New York, Wiley, 1968)
277. A. Feltz. *Amorphe und Glasartige Anorganische Festkörper.* (Berlin, Akademie-Verlag, 1983)
278. M.H. Zaman, T.R. Sosnick, R.S. Berry. *Phys. Chem. Chem. Phys.* **5**, 2589 (2003)
279. V.P. Skripov. *Metastable Liquids.* (New York, Wiley, 1974)
280. P.G. Debenetti. *Metastable Liquids* (Princeton, Princ. Univ. Press, 1996)
281. T.L. Beck, J. Jellinek, R. S. Berry, *J. Chem. Phys.* **87**. 545 (1987)
282. F.A. Lindemann. *Zeit. Phys.* **11**, 609 (1910)
283. R.D. Etters, J.B. Kaelberer. *Phys. Rev. A* **11**, 1068 (1975)
284. R.D. Etters, J.B. Kaelberer. *J. Chem. Phys.* **66**, 5512 (1977)
285. J.B. Kaelberer, R.D. Etters. *J. Chem. Phys.* **66**, 3233 (1977)
286. Y. Zhou, M. Karplus, K.D. Ball, R.S. Berry. *J. Chem. Phys.* **116**, 2323 (2002)
287. T.L. Beck, J. Jellinek, R.S. Berry. *J. Chem. Phys.* **87**, 545 (1987)
288. W. Thomson. *Philos. Mag.* **42**, 448 (1871)
289. A.A. Shvartsburg, M.F. Jarrold. *Phys. Rev. Lett.* **85**, 2530 (2000)
290. G.A. Breaux, R.C. Benirschke, T. Sugai, B.S. Kinnear, M.F. Jarrold. *Phys. Rev. Lett.* **91**, 25508 (2003)
291. K. Joshi, D.G. Kanhere, S.A. Blundell. *Phys. Rev. B* **66**, 155329 (2002)
292. K. Joshi, D.G. Kanhere, S.A. Blundell. *Phys. Rev. B* **67**, 235413 (2003)
293. S. Chacko, K. Joshi, D.G. Kanhere, S.A. Blundell. *Phys. Rev. Lett.* **92**, 135506 (2004)
294. K. Joshi, S. Krishnamurty, D.G. Kanhere. *Phys. Rev. Lett.* **96**, 135703 (2006)
295. J.W. Gibbs. *Thermodynamics.* (New York, Academic Press, 1928). Vol. 1
296. V.P. Skripov, M.Z. Fazullin. In: *Nucleation Theory.* Ed. J.W.P. Schmelzer. (Berlin, Wiley-VCH, 2005). pp. 4–38
297. F.H. Stillinger. *J. Chem. Phys.* **38**, 1486 (1963)
298. D.I. Zhukhovitskii. *J. Chem. Phys.* **110**, 1770 (1999)
299. S.W. Sides, G.S. Grest, *J. Chem. Phys.* **110**, 1770 (1999)
300. D.I. Zhukhovitskii. *JETP* **94**, 336 (2002)
301. A.E. Ismail, G.S. Grest, M.J. Stevens. *J. Chem. Phys.* **125**, 014702 (2006)
302. D.I. Zhukhovitskii. *J. Chem. Phys.* **125**, 234701 (2006)
303. F.P. Buff, R.A. Lovett, F.H. Stillinger. *Phys. Rev. Lett.* **15**, 621 (1965)
304. C. Amitrano, R.S. Berry. *Phys. Rev. E* **47**, 3158 (1993)
305. V.V. Nauchitel, A.J. Pertsin. *Molec. Phys.* **40**, 1341 (1980)
306. B.M. Smirnov. *Plasma Chem. Plasma Proc.* **13**, 673 (1993); (*Phys. Uspekhi* **36**, 933 (1993)
307. B.M. Smirnov. *Phys. Uspekhi* **36**, 933 (1993)

308. B.M. Smirnov. *Principles of Statistical Physics.* (Wiley VCH, Berlin, 2006)
309. R.S. Berry, B.M. Smirnov. *JETP* **98**, 366 (2004)
310. R.S. Berry. *Isr. J. Chem.* **44**, 211 (2004)
311. J.J. Burton. *J. Chem. Phys.* **52**, 342 (1970)
312. M. Bixon, J. Jortner. *J. Chem. Phys.* **91**, 1631 (1989)
313. D.D. Franz. *J. Chem. Phys.* **115**, 6136 (2001)
314. O. Mülken, H. Stamerjohanns, P. Borrmann. *Phys. Rev.* **64E**, 047105-1 (2001)
315. D.J. Wales. *Mol. Phys.* **78**, 151 (1993)
316. D.J. Wales, R.S. Berry. *Phys. Rev. Lett.* **73**, 2875 (1994)
317. I.H. Umirzakov. *Phys. Rev.* **60E**, 7550 (1999)
318. H. Haberland. In: *Metal Clusters.* Ed. W. Ekardt (New York: Wiley, 1999)
319. H. Haberland. Proc. Les Houches 2000 Summer School on *Atomic Clusters and Nanoparticles.*
320. M. Schmidt, R. Kusche, T. Hippler e.a. *Phys. Rev. Lett.* **86**, 1191 (2001)
321. M. Schmidt, J. Donges, T. Hippler e.a. *Phys. Rev. Lett.* **87**, 203402 (2001)
322. E. Gobet, B. Farizon, M. Farizon, M.J. Gaillard, J.P. Buchet, M. Carré, P. Scheier, T.D. Märk. *Phys. Rev. Lett.* **89**, 183403 (2002)
323. J.A. Reyes-Nava, I.L. Garzón, K. Michaelian. *Phys. Rev.* **67B**, 165401 (2003)
324. A.I. Karasevskii, V.V. Lurashenko. *Phys. Rev.* **66B**, 054302 (2002)
325. B.M. Smirnov. *Sov. Phys. Uspekhi* **21**, 522 (1978)
326. J. Naghizadeh, S.A. Rice. *J. Chem. Phys.* **36**, 2710 (1962)
327. L. Bewilogua, L. Gladun, B. Kubsch. *J. Low Temp. Phys.* **4**, 299 (1971)
328. W.F. Schmidt. *Liquid State Electronics of Insulating Liquids.* (Boca Raton: CRC Press, 1997)
329. R.S. Berry, B.M. Smirnov. *JETP* **95**, 255 (2002)
330. R.S. Berry, B.M. Smirnov. *J. Chem. Phys.* **118**, 5979 (2003)
331. A. Kouchi, T. Kuroda. *Jap. J. Appl. Phys.* Part 2, **29**, L807 (1990)
332. W. van Megen, S.M. Underwood. *Phys. Rev. Lett.* **70**, 2766 (1993)
333. W. van Megen, S.M. Underwood. *Phys. Rev.* **49E**, 4206 (1994)
334. B.J. Ackerson, K. Schatzel. *Phys. Rev.* **52B**, 6460 (1995)
335. R.J. Speedy. *J. Chem. Phys.* **100**, 6684 (1994)
336. J. Yeo. *Phys. Rev.* **E52**, 853 (1995)
337. A. van Blaaderen, P. Wiltzuis. *Science* **270**, 1177 (1995)
338. P.J. Steinhardt, D.R. Nelson, M. Ronchetti. *Phys. Rev.* **28B**, 784 (1983)
339. S. Torquato, B.Lu, J. Rubinstein. *Phys. Rev.* **41A**, 2059 (1990)
340. M.H. Cohen, G.S. Grest. *Proc. N.Y. Acad. Sci.* **371**, 199 (1981)
341. T.G. Fox, P.J. Flory. *J. Appl. Phys.* **21**, 581 (1950)
342. T.G. Fox, P.J. Flory. *J. Phys. Chem.* **55**, 221 (1951)
343. R.S. Berry, B.M. Smirnov. *Phys. Rev.* **72B**, 104201 (2005)
344. Ya.B. Zeldovich. *ZhETF* **12**, 525 (1942)
345. F.F. Abraham *Homogeneous Nucleation Theory.* (Acad. Press, New York, 1974)
346. L.D. Landau, E.M. Lifshitz. *Statistical Physics. Vol. 2.* (Oxford, Pergamon Press, 1980)
347. J.W.P. Schmelzer (ed.). *Nucleation Theory.* (Wiley, Berlin, 2005)
348. W. Ostwald. *Zs. Phys. Chem.* **34**, 495 (1900)
349. L.N. Aleksandrov. *Kinetics Of Formation and Structures of Solid Layers.* (Novosibirsk, Nauka, 1972)
350. Ya.E. Geguzin, Yu.S. Kaganovskii. *Sov. Phys. Usp.* **21**, 611 (1978)

351. B. Lewis, J.C. Anderson. *Nucleation and Growth of Thin Films* (New York, Academic Press, 1978)
352. V.V. Slezov, V.V. Sagalovich. *Sov. Phys. Usp.* **30**, 23 (1987))
353. V.I. Trofimov, V.A. Osadchenko. *Growth and Morphology of Thin Films.* (Moscow, Energoatomizdat, 1993)
354. S.A. Kukushkin, V.V. Slezov. *Disperse Systems on Solid Surfaces.* (Petersburg, Nauka, 1996)
355. S.A. Kukushkin, A.V. Osipov. *Phys. Usp.* **41**, 983 (1998)
356. I.M. Lifshitz, V.V. Slezov. *JETP* **35**, 331 (1958)
357. I.M. Lifshitz, V.V. Slezov. *Fiz. Tver. Tela* **1**, 1401 (1959)
358. I.M. Lifshitz, V.V. Slezov. *J. Phys. Chem. Sol.* **19** 35 (1961)
359. E.M. Lifshitz, L.P. Pitaevskii. *Physical Kinetics.* (Oxford, Pergamon Press, 1981)
360. V.S. Vorob'ev. *Int. J. Thermophysics.* **26**, 905 (2005)
361. R.K. Crawford. In: *Rare Gas Solids.* Ed. by M.L. Klein and J.A. Venables. (Academic Press, New York, 1977). vol. 2, p. 172
362. R.S. Berry e.a. *Phys. Rev.* **B**, (2006)
363. V.G. Baidakov. *Superheating of Cryogenic Liquids.* (Ekaterinburg, Nauka, 1995)
364. V.P. Skripov, E.N. Sinitzyn, P.A. Pavlov e.a. *Thermophysical Properties of Liquids in Metastable (Superheated) State.* (London, Gordon and Breach, 1988)
365. J.P. Hansen, L. Verlet. *Phys. Rev.* **184**, 151 (1969)
366. N. Schwenther, E.E. Koch, J. Jortner. *Electronic Excitations in Condensed Rare Gases.* (Berlin, Springer, 1985)
367. K. Huang. *Statistical Mechanics* (New York, Wiley, 1963)
368. S. Valkealahti, M. Manninen. *Z. Phys.* **26D**, 255 (1993)
369. R.S. Berry. *Nature* **393**, 238 (1998)
370. B.J. Alder, T.E. Wainwright. *J. Chem. Phys.* **33**, 1439 (1960)
371. Y. Song, R.M. Stratt, E.A. Mason. *J. Chem. Phys.* **88**, 1126 (1988)
372. A. van Blaaderen, P. Wiltzius. *Science* **270**, 1177 (1995)
373. P.A. Heyney e.a. *Phys. Rev. Lett.* **66**, 2911 (1991)
374. J.S. Tse, D.D. King, D.A. Wilkinson. *Chem. Phys. Lett.* **183**, 378 (1991)
375. T.L. Beck, J.D. Doll, D.L. Freeman. *J. Chem. Phys.* **90**, 5651 (1989)
376. D.M. Leitner, J.D. Doll, R.M. Whitnell. *J. Chem. Phys.* **94**, 6644 (1991)
377. B.M. Smirnov. *Phys. Uspekhi* **43**, 453 (2000)

Index

Springer Series on

ATOMIC, OPTICAL, AND PLASMA PHYSICS

Springer Series on

ATOMIC, OPTICAL, AND PLASMA PHYSICS

10 **Film Deposition by Plasma Techniques**
By M. Konuma

11 **Resonance Phenomena in Electron–Atom Collisions**
By V.I. Lengyel, V.T. Navrotsky, and E.P. Sabad

12 **Atomic Spectra and Radiative Transitions**
2nd Edition
By I.I. Sobel'man

13 **Multiphoton Processes in Atoms**
2nd Edition
By N.B. Delone and V.P. Krainov

14 **Atoms in Plasmas**
By V.S. Lisitsa

15 **Excitation of Atoms and Broadening of Spectral Lines**
2nd Edition, By I.I. Sobel'man, L. Vainshtein, and E. Yukov

16 **Reference Data on Multicharged Ions**
By V.G. Pal'chikov and V.P. Shevelko

17 **Lectures on Non-linear Plasma Kinetics**
By V.N. Tsytovich

18 **Atoms and Their Spectroscopic Properties**
By V.P. Shevelko

19 **X-Ray Radiation of Highly Charged Ions**
By H.F. Beyer, H.-J. Kluge, and V.P. Shevelko

20 **Electron Emission in Heavy Ion–Atom Collision**
By N. Stolterfoht, R.D. DuBois, and R.D. Rivarola

21 **Molecules and Their Spectroscopic Properties**
By S.V. Khristenko, A.I. Maslov, and V.P. Shevelko

22 **Physics of Highly Excited Atoms and Ions**
By V.S. Lebedev and I.L. Beigman

23 **Atomic Multielectron Processes**
By V.P. Shevelko and H. Tawara

24 **Guided-Wave-Produced Plasmas**
By Yu.M. Aliev, H. Schlüter, and A. Shivarova

25 **Quantum Statistics of Nonideal Plasmas**
By D. Kremp, M. Schlanges, and W.-D. Kraeft

26 **Atomic Physics with Heavy Ions**
By H.F. Beyer and V.P. Shevelko

27 **Quantum Squeezing**
By P.D. Drumond and Z. Ficek

28 **Atom, Molecule, and Cluster Beams I**
Basic Theory, Production and Detection of Thermal Energy Beams
By H. Pauly

29 **Polarization, Alignment and Orientation in Atomic Collisions**
By N. Andersen and K. Bartschat

30 **Physics of Solid-State Laser Physics**
By R.C. Powell
(Published in the former Series on Atomic, Molecular, and Optical Physics)

31 **Plasma Kinetics in Atmospheric Gases**
By M. Capitelli, C.M. Ferreira, B.F. Gordiets, A.I. Osipov

32 **Atom, Molecule, and Cluster Beams II**
Cluster Beams, Fast and Slow Beams, Accessory Equipment and Applications
By H. Pauly

33 **Atom Optics**
By P. Meystre

34 **Laser Physics at Relativistic Intensities**
By A.V. Borovsky, A.L. Galkin, O.B. Shiryaev, T. Auguste

35 **Many-Particle Quantum Dynamics in Atomic and Molecular Fragmentation**
Editors: J. Ullrich and V.P. Shevelko